SYNTHESIS OF VARIOUS VALUE-ADDED PRODUCTS USING WASTE BIOMASS AND THEIR APPLICATION IN ENERGY AND ENVIRONMENT

Thesis submitted by

Subhasis Ghosh

(Registration Number: SLSBT1106722)

Doctor of Philosophy

(Science)

School of Advanced Studies in Industrial Pollution Control Engineering

Faculty of Interdisciplinary Studies, Law and Management

Jadavpur University

Kolkata, India

2025

"Research is seeing what everybody else has seen and thinking what nobody else has thought."

--- Albert Szent-Györgyi

[Nobel Prize winner (1937) for his discoveries in physiology and medicine]

This thesis is dedicated to all the minds who are contributing to enrich the scientific knowledge of humankind for the betterment of society

INDEX NUMBER: 67/22/LifeSc/27

Title of the thesis:

SYNTHESIS OF VARIOUS VALUE-ADDED PRODUCTS USING WASTE BIOMASS AND THEIR APPLICATION IN ENERGY AND ENVIRONMENT

Name, Designation & Institution of the Supervisor(s):

1. Name of Supervisor:

PROF. (DR.) PAPITA DAS

Designation and Institution of the Supervisor:

Professor, Department of Chemical Engineering, Jadavpur University, Kolkata- 700032, India.

Director, School of Advanced Studies in Industrial Pollution Control Engineering, Jadavpur University, Kolkata- 700032, India.

2. Name of Supervisor:

AVIJIT BHOWAL

Designation and Institution of the Supervisor:

Professor, Department of Chemical Engineering, Jadavpur University, Kolkata- 700032, India.

List of Publications:

1. **Ghosh, S.**, Basak, D., Manna, S., Bhowal, A., & Das, P. (2025). Removal of naphthalene utilizing synthesized silica doped PVA aerogel: removal, optimization and mechanism. *Discover Chemistry*, *2*(1), 82.
2. Samanta, A., **Ghosh, S.** & Das, P. (2025). Extraction of silica and biochar from biomass waste for the synthesis of aerogel and its application for the removal of dye. *Biomass Conv. Bioref.* https://doi.org/10.1007/s13399-025-06776-2.
3. **Ghosh, S.**, Roy, S. & Das, P. Beyond waste: waste rice husk to value-added products using sonic waves and chemical treatment and principal component analysis of extraction. *Biomass Conv. Bioref.* (2024). https://doi.org/10.1007/s13399-024-05855-0.
4. **Ghosh, S.**, Chakraborty, P., Bhowal, A. *et al.* Synthesis of polymeric aerogels with different fillers and their application for the removal of emerging pollutants: a comparative study. *Biomass Conv. Bioref.* (2024). https://doi.org/10.1007/s13399-024-05715-x.
5. **Ghosh, S.**, Sarkar, S., Mukherjee, S. *et al.* Silica-coated cellulose using *Shorea robusta* sawdust biomass and its application for methylene blue dye removal from aqueous solution. *Biomass Conv. Bioref.* (2024). https://doi.org/10.1007/s13399-024-05616-z.
6. Roy, S., Mukherjee, S., **Ghosh, S.**, & Das, P. (2024). Synthesis of rice husk-derived cellulose for efficacious removal of malachite green from aqueous solution. *Sādhanā*, *49*(1), 15.

List of Patents:

1. A method of preparation of a microbe-doped polymeric aerogel for wastewater treatment (KB ID: KBP54). (Filed)

List of Conferences:

1. **International Conference on Energy Transition: Challenges and Opportunities (IIChE-Chemcon- 2023).**

   Organized by: Indian Institute of Chemical Engineers.

   Venue: Heritage Institute of Technology, Kolkata.

   Topic: Synthesis of silane-treated aerogel for the treatment of naphthalene-containing solution.

   Date: 27-30 December 2023.

2. **3rd International Conference on Water Technologies (ICWT- 2023).**

   Organized by: Water Innovation Center: Technology, Research & Education in association with Asian Universities Alliance.

   Venue: Indian Institute of Technology Bombay.

   Topic: Bacterial Bioremediation of Acenaphthene and Phenol using Isolated Bacteria: A Promising Technology for Water Treatment.

   Date: 04-07 December 2023.

3. **International Conference on Chemical Engineering Innovation and Sustainability (ICEIS- 2023).**

   Organized by: Department of Chemical Engineering, Jadavpur University, Kolkata.

   Venue: Jadavpur University, Kolkata.

   Topic: Cellulose from acid pre-treated lignocellulosic biomass and its application in dye removal.

   Date: 26-27 February 2023.

4. **International Conference on Sustainable Resilient Remediation (ICSRR-2023).**

   Organized by: Centre for Environmental Studies (CES), Anna University, Chennai.

Venue: Anna University (Online).

Topic: Production of Biochar from Lignocellulosic Biomass and Its Application in Dye Removal.

Date: 02-03 February 2023.

5. **Himalaya Calling: Global Summit on Challenges & Opportunities in the Himalayan Region.**

   Organized by: University of Petroleum and Energy Sciences (UPES), Dehradun.

   Venue: UPES (Online).

   Topic: Preparation of silica-doped polymeric aerogel and its' application for Phenol removal from wastewater.

   Date: 10 September 2024.

6. **39th Indian Engineering Congress**

   Organized by: The Institution of Engineers (India)

   Venue: Novotel, Kolkata

   Topic: Preparation of Activated Biochar doped Polyvinyl Alcohol (PVA) Aerogel in Wastewater Treatment.

   Date: 20-22 December 2024.

PROFORMA- I

STATEMENT OF ORIGINALITY

I, Subhasis Ghosh (Reg. No. SLSBT1106722) registered on 28th February 2022 do hereby declare that this thesis entitled "**Synthesis of various value-added products using waste biomass and their application in energy and environment**" contains a literature survey and original research work done by the undersigned candidate as part of the Doctoral Studies.

All information in this thesis has been obtained and presented in accordance with existing academic rules and ethical conduct. I declare that, as required by thesis rules and conduct, I have fully cited and referred all materials and results that are not original to this work.

I also declare that I have checked this thesis as per the "Policy on Anti Plagiarism, Jadavpur University, 2019", and the level of similarity as checked by i''Thenticate software is 6%.

Certified by Supervisor(s):

(Signature with date and seal)

1. Papita Das 21/4/25

Prof. Papita Das
Director
School of Advanced Studies in
Industrial Pollution Control Engineering
Jadavpur University
Kolkata-700032, India

2. Arijit Bhowal 21/4/25

Professor
CHEMICAL ENGINEERING DEPARTMENT
JADAVPUR UNIVERSITY
Kolkata-700 032

Signature of Candidate:

Subhasis Ghosh

Subhasis Ghosh

Date: 21.04.2025

Place: Kolkata

PROFORMA-II

CERTIFICATE FROM THE SUPERVISOR(S)

This is to certify that the thesis entitled, **"Synthesis of various value-added products using waste biomass and their application in energy and environment"** submitted by **Sri Subhasis Ghosh,** who got registered (Registration no. SLSBT1106722, dated **28th February 2022**) his name under the Faculty of Interdisciplinary Studies, Law & Management for the award PhD (Science) degree of Jadavpur University is based upon his work under the supervision of **Prof. (Dr.) Papita Das** and **Prof. Avijit Bhowal,** and that neither his thesis nor any part of the thesis has been submitted for any degree/ diploma or any other academic award anywhere before.

Papita Das. 21/4/25

Prof. Papita Das

(Supervisor)

Prof. Papita Das
Director
School of Advanced Studies in
Industrial Pollution Control Engineering
Jadavpur University
Kolkata-700032, India

Avijit Bhowal 21.4.25

Prof. Avijit Bhowal

(Supervisor)

Professor
CHEMICAL ENGINEERING DEPARTMENT
JADAVPUR UNIVERSITY
Kolkata-700 032

ACKNOWLEDGEMENT

The completion of the Ph.D. degree is the beginning of a journey and not the end. Though this work bears my name as the author, this is not just a reflection of my efforts but also a testament to the unwavering support and guidance I have received along the way.

First and foremost, I would like to express my deepest gratitude to my supervisor(s), Prof. (Dr.) Papita Das and Prof. Avijit Bhowal. I consider myself fortunate to have the opportunity to work as a researcher in Prof. Das's laboratory and under her supervision. Her expertise, patience, and encouragement have been invaluable throughout this process. Her insightful feedback and constructive criticism challenged me to think critically and pushed me to refine my ideas. I am incredibly grateful for her mentorship and for believing in my potential. I am also thankful to Dr. Suvendu Manna of the University of Petroleum and Energy Studies (UPES), Dehradun for his support and advice to make this research more constructive.

I am particularly thankful to my lab mates. The camaraderie and coffee breaks I shared with Dr. Niladri Sikhar Saha, Dr. Sandipan Bhattacharya, Mr. Sayan Mukherjee, Ms. Poushali Chakraborty, Mr. Sk Aakash Hossain, Mr. Sampad Sarkar, and Ms. Debangana Bhattacharya made this journey not only bearable but enjoyable. I am thankful to the postgraduate and graduate students, Mr. Sanket Roy, Mr. Debojyoti Basak, Ms. Ashmita Samanta, and Mr. Sirsha Ganguly who came to the laboratory for their project work. I had received earnest support and assistance from them.

I would also like to recognize the administrative staff and technical staff at Jadavpur University for their assistance in navigating the various processes involved in this journey. Their efficiency and kindness made a significant difference in my experience.

To my family, words cannot fully express how thankful I am for their unconditional love and support. To my parents, thank you for instilling in me the values of perseverance and dedication. Their sacrifices have paved the way for my education, and I hope to honor that with this accomplishment.

I also like to acknowledge the SERB-Power Grant (DST No.: SPG/2021/0
that supported my research. The financial assistance allowed me to concent
my studies without the burden of financial stress.

Finally, I wish to acknowledge all the participants in my research who gener
shared their time and experiences with me. Their willingness to engage in this
made it possible for me to explore new ideas and contribute to our field.

In conclusion, I am profoundly grateful for all the support I have rece
throughout this journey. Each person mentioned here has played a crucial ro
shaping both my academic career and personal growth. Thank you all for being
of this incredible experience.

Signature of Candidate:

Subhasis Ghosh

Date: 21.04.2025

Place: Kolkata

TABLE OF CONTENTS

ABSTRACT

With the development of civilisation, industrialisation is increasing rapidly. Due to the establishment of various industries, waste is also being generated and discarded exponentially. Organic pollutants, like polyaromatic hydrocarbons (PAHs) from petrochemical industries, dyes from textile industries, heavy metals from tannery industries, and solid biotic wastes from agricultural sectors, hospitals, and residential places are generating more concerns nowadays. Rather than using a material, generating waste, and treating the waste before disposal, in the age of circular economy, the recycling and reusing waste materials of one sector as the raw material in another industry is a more accepted approach.

The current study focuses on the extraction of cellulose, hemicellulose, and lignin by the sonochemical method from rice husk and sawdust, and the synthesis of furfural and bioethanol. Also, silica and biochar were produced from the raw materials, and the biochar, cellulose, and silica were utilised to synthesise PVA aerogels for wastewater treatment was investigated. Bacteria were also doped into the PVA matrix of the aerogels to increase their efficiency, along with phytotoxicity studies were conducted to understand the environmental effects of the treated solutions. In this study, it was observed that sonication has a high influence on the cellulose content extracted from biomass. The highest cellulose content was found in the case of SD_4%_NaOH_S, and the value was 958.88 mg/g, and the lowest cellulose concentration was found to be 101.48 mg/g in the case of RH_2%_NaOH_NS. In the case of TRS, the highest TRS yield was observed in the case of SD_4%_H_2SO_4_S and was found to be 26.82 mg/g with 3 mL/ 100 mL of microbial concentration. In this study, the highest ethanol concentration was found in the case of SD_6%_H_2SO_4_NS with 1 mL microbial dose/100 mL solution, and the ethanol concentration was 3.24 mg/g of biomass. From the RSM study of bioethanol production, it was found that the model was significant with a P-value of 0.0006 (<0.05) and an F-value of 17.1 (>12). The correlation coefficient (R^2) value of the mentioned model was 0.95. The R^2 value also indicated that the predicted and observed data of this experiment were in reasonable agreement, with the value of 4.84 mg/g and 4.32 mg/g, respectively, indicating the significance of the model. In the case of furfural production, RH_4%_NaOH_S generated the highest furfural production yield, with the value of 17.35% after treating for 30 min.

From the ATR-FTIR study, it was observed that the extracted cellulose was enriched with C-H, -CCH, -CO, and C-O-C functional groups, respectively. ATR-FTIR analysis of hemicellulose revealed the presence of the xylopyranose ring, and in the case of lignin C-O, =CH, and O-H groups were found. From XRD analysis, the increase in cellulose crystallinity from 11.23 to 15.17 was found after sonication.

From a pollutant removal study in the case of naphthalene, the highest removal of naphthalene was found in the case of PVA-Si aerogel, at 313 K temperature, with the value of 96.32% removal. For phenol and acenaphthene, the highest removal was 97.44% and 94.47%, respectively, by the same aerogel. From the modelling study, it was found that the processes were endothermic and spontaneous. They were observed to follow the pseudo-2^{nd}-order kinetic model. The isotherm model, though, was found to depend on the adsorbent type. In general, the aerogels containing sawdust materials as filler followed the Langmuir isotherm model; on the other hand, the rest of the aerogels were found to better fit the Freundlich isotherm model, allowing multilayer adsorption. From the multipollutant removal study of the aerogels, it was found that the adsorbents are capable of removing multiple organic pollutants simultaneously from a mixed pollutant solution. It was also observed that the adsorbents have a higher affinity to organic pollutants and dyes compared to metal ions, as found in the selectivity study. From the RSM analysis, it was found that the adsorption experiments for all the pollutants were significant with 0.99, 0.99, and 0.98 R^2 values for naphthalene, phenol, and acenaphthene, respectively.

From the SEM analysis, it was revealed that the surface of the prepared aerogels was full of cavities and uneven structures, contributing to the adsorption efficiency of the adsorbents. Also, from the ATR-FTIR analysis, it was observed that the surface of the prepared aerogels was enriched with C=O, C-H, and Si-O-Si functional groups, respectively. The TGA analysis and XRD analysis revealed the effect of fillers on the properties of aerogels. Also, the thermal stability of the adsorbents was observed in the TGA analysis. From the physical property analysis, it was shown that the prepared aerogels were highly porous.

In the case of the bacteria, it was shown that *Bacillus sp.* showed an inhibition zone for 100 mg/L naphthalene, and *Lysinibacillus sp.* and *Pseudomonas sp.* showed the zones for 10 mg/L and 100 mg/L naphthalene concentration, confirming the tolerance of these organisms against these pollutants. During the removal of these pollutants, in the case of

naphthalene, the highest removal was achieved by *Bacillus sp.,* at 2 mL/ 100 mL dose, and the value was 99.52%. Similarly, for phenol, the highest removal achieved in this study was 84.19% by *Pseudomonas sp.* after 5 days of treatment, and for acenaphthene, the highest removal achieved in this study was 74.18% by *Lysinibacillus sp.* after 5 days of treatment.

Bacteria-doped aerogels also showed significant removal of the pollutants. For naphthalene, the highest removal was achieved by PVA-Si-*Bacillus sp.* showed the highest removal with the value of 97.39% after five days of treatment, as well as for phenol and acenaphthene, with the removal of 94.20% and 96.35%. From the GC-MS analysis of the pollutants after treatment, it was found that 2-methyl-eicosane, 3,3-dimethylhexane, and 1-iodo-tridecane were the major produced components, confirming the metabolism of the pollutants. From the toxicity analysis, it was observed that all the phytotoxicity indices improved after the remediation of the solutions by bacteria.

Keywords: *Waste valorisation, aerogels, bacteria-doped aerogels, adsorption, wastewater treatment, toxicity*.

LIST OF TABLES

LIST OF FIGURES

CHAPTER 2:

CHAPTER 4:

Chapter: 1

INTRODUCTION

Behind every research, there is a problem to solve. The problems associated with this research will be discussed in the introduction chapter of this thesis. This research work addresses three major problems, viz., the hazards associated with solid biotic waste (specifically sawdust and rice husk), water pollution, and the energy crisis, respectively. This research was performed with a multidimensional approach to contribute to the remediation of all the mentioned problems in a step-by-step manner.

1.1. Solid waste as an emerging concern:

Being a developing country, one of the main problems of India comes into focus when discussing the economy of India. The Indian economy is highly dependent on agriculture. Rice husk of *Oryza sativa*, a common cultivated cereal in India, is a by-product of its agricultural practices. Annually, India produces around 120 million tonnes of rice, and from that, 23% is rice husk. This material is difficult to break down when discarded as garbage, and due to its low density, it takes up a lot of space in landfills. While a part of rice husk is utilised for cattle feed, most is thrown away or used as animal bedding. Approximately 17.6% of the produced rice husk is burnt during October and November in India (Sahai et al., 2011). Burning of rice husk can generate aerosols, including $PM_{2.5}$ and PM_{10}. It is estimated that the burning of husk can release 627 kilotons of PM_{10} and 4677 kilotons of carbon monoxide (CO) to the atmosphere each year (Datta et al., 2020). Apart from these contaminants, burning rice husk also releases CO_2 (70%), CH_4 (0.66%), N_2O (2.09%), and ash (Pathak et al., 2021). These contaminants not only affect the surrounding air quality but also the ozone layer in the troposphere (Kumar et al., 2015).

Besides contaminating the atmosphere, these pollutants also show adverse effects on human health. The particulate matter emitted by burning the crop residue around Delhi is 17 times higher than vehicular emissions and garbage burning combined (Bhuvaneshwari et al., 2019). The volatile organic compounds (VOCs), nitrogen oxides (NO_X), and carcinogens, specifically polyaromatic hydrocarbons (PAHs), are released from this burning effect on individuals (Gheorghe and Ion, 2011). Singh (2018) reported some additional adverse effects, viz., corneal opacity, skin illnesses, and eye irritation can be

caused by the burning of crop residue. Kant et al. (2022) reported that these off-site burnings are responsible for 66,200 deaths in India in the year of 2015.

According to Gupta et al. (2011), burning the agricultural waste can elevate soil temperature to 33.8°C- 42.2°C at a soil depth of 1 cm. This increased temperature can reduce the nitrogen content by 23%-73% and disturb the C: N ratio of the soil. At the same time, carbon is emitted to the atmosphere as CO_2 and nitrogen is converted to nitrate. These processes can reduce nitrogen, phosphorus, and potassium by 824 thousand tons. The alteration in soil chemistry also affects the productivity of the soil.

On the other hand, sawdust is also gaining attention as an emerging environmental hazard. According to the FAO 2020 report, India annually produces 50.60 million cubic meters of timber and 15% of it is converted to sawdust as a by-product of the industry. Worldwide, the most common fate of the produced sawdust is being burned (Adegoke and Mohammed, 2002). Burning sawdust in the open air can cause a concerning level of environmental pollution by contributing to acid rain, releasing particulate matter, and generating greenhouse gases like CO_2. Not only air and water, but this waste also affects soil chemistry adversely. Sawdust reduces the hydrogen content significantly as well as the phosphorus content. Also, it changes the pH of the soil by increasing the acidity and contaminates it with phenolic compounds. Sawdust makes up around 10% of all waste dumped in landfills each year. From the year of 1990 to 2018, the amount of sawdust generated increased from 12,210 tons to 19.090 tons. Also, the discarded sawdust increased from 10,000 tons to 12,150 tons (Siddique et al., 2020). Butt et al. (2016) reported that USA alone produce three million tonnes of sawdust each year, most of which is used for landfills. Like rice husk, sawdust also affects the air, water, and soil chemistry of the environment, creating concerning issues in the way of sustainable development.

The main components of both rice husk and sawdust are cellulose, hemicellulose, and lignin, respectively. According to Nayak and Mishra (2016), sawdust is composed of 30.5% cellulose, 28.9% hemicellulose, and 16.4% lignin. Also, 1% of ash can be produced from sawdust according to that report. Similarly, 33% cellulose, 20% hemicellulose, 28% lignin, along with 3% silica, can be extracted from rice husk (Shen, 2017). These materials can be extracted from the biomass for their potential applications. Cellulose is a product with a diverse application spectrum; on one hand, it can be used to produce bioethanol, addressing the energy crisis, also they have the applications in

wastewater treatment. Being carbon-based components, the materials can be used to produce biochar. The extracted silica and biochar can also be used for wastewater treatment besides their multiple potential applications, and lignin and hemicellulose can gain attention for their commercial valuation.

In summary, these waste materials are creating concerning issues to the environment, but they can be investigated under the spotlight of research to address many existing problems.

1.2. Water pollution as an environmental threat:

India has access to 4% of the global water reserve and supports 18% of the world's population. Being a developing country, India is undergoing massive urbanisation. Besides that, industrialisation is also increasing rapidly. Industries like pharmaceuticals, automotive, petrochemical, chemical, and other manufacturing industries are using a humongous quantity of water for different purposes (Roshan and Kumar, 2020). However, using a huge amount of water is not the only issue. Pollutants like hospital waste, domestic waste, industrial chemicals, pharmaceuticals, textiles, and pesticides also influence the water quality. So, the amount of usable water is decreasing day by day (Amaly et al., 2022). These contaminants can harm the environment and create a substantial impact (Rathi et al., 2021).

The increasing population, industrialisation and urbanisation have created a rapid demand for synthetic dyes. It is estimated that $7x10^5$ tons of dyes are produced annually (Wan et al., 2019). In a previous study, it is reported that most of the dyes are toxic (Bani-Atta, 2022) and the industrial effluents containing dyes should be properly treated before discharge (Wang et al., 2020). Most of the dyes used in industries are reported to be carcinogenic, mutagenic, and responsible for endocrine disruption. They not only affect the microbial fauna of the environment but also affect plants and humans adversely. Also, the accumulation of dye in a water body can hinder the penetration of light and hamper the natural decontamination and photosynthesis (Chowdhury et al., 2011).

Apart from dye, another type of pollutant contributing to water pollution is organic pollutants. Organic pollutants like naphthalene exhibit carcinogenic and mutagenic activities, with acute kidney injuries and poisoning properties. Organic pollutants can introduce genetic damage, chromosomal aberrations, sister chromatid exchange, and form kinetochore-negative micronuclei. It was also found that naphthalene can delay the

fluorescence of Chlorophyll-a of the pea plant (Lankin et al., 2014). Other organic pollutants, viz., drug molecules, lipid regulators, and hormones and enter the human body from contaminated water by bioaccumulation and damage the nervous system (Frank et al., 2005). Studies have reported the presence of organic pollutants in Europe (Wen et al., 2017), Oceania (Tremblay et al., 2016), Asia (Lin et al., 2017), Africa (Edokpayi et al., 2017), and America (Gilliom, 2007).

One of the major organic pollutants, acenaphthene, is obtained by distillation from creosote oil. However, this extraction process has various drawbacks, like high energy consumption, a long production route, and strict operational conditions (Ye et al., 2016). This compound has a wide range of uses in the dye, pharmaceuticals, insecticides, and fungicides industries and causes environmental threats by settling in rivers, lakes, and ponds (Mallick, 2019). Apart from acenaphthene, another two major organic pollutants, viz., naphthalene and phenols, have been detected in water sources, sediments, and even in crustaceans (Jaward et al., 2012; Ozaki et al., 2019).

Besides dye and organic pollutants, metals also act as significant pollutants for the water system. Lead, a heavy metal dominating the water pollution, was found to be responsible for neurological damage, developmental issues, and organ damage. Mercury is a highly toxic element, causing birth defects and kidney damage. Cadmium is responsible for bone demineralisation. Arsenic, one of the most toxic pollutants, can cause skin lesions, cardiovascular disease, and neurological effects. Chromium was also found to be highly toxic, causing respiratory problems, skin irritation, and cancer (Tchounwou et al., 2012).

Water pollution is a focus of environmental research. Many techniques, viz., membrane filtration (Paredes et al., 2018), bioremediation (Torresi et al., 2019), adsorption, advanced oxidation (Altmann et al., 2015), etc., are being used over traditional methods to treat contaminated water. Among these processes, adsorption is the most cost-effective and easy to operate method at an industrial scale. But the adsorption process also has some disadvantages, like the desorption of the pollutant.

So, it can be stated that, though adsorption is an effective process, some modifications in the traditional adsorption process are much needed for the sustainable and consistent treatment of water and remediation of current problems associated with this treatment process.

1.3. Energy crisis in India:

Being the most populous country (More than 1 billion according to the 2023 report) of the world, India is facing continuous problems with the energy supply and planning for this huge and diverse population. Policymakers and the government are facing complex challenges and issues in managing the energy sector of this country. In recent years, the government of India has taken multiple steps to diversify and secure the energy future of the nation. One of the main factors influencing the increase in the Indian energy sector is the focus on renewable energy sources. The tradition of focusing on renewable energy in India was started in 1981, with the establishment of the Commission for Additional Sources of Energy (CASE), which led to the Department of Non-Conventional Energy Sources (DNES) in the year of 1982. Following that, a full-fledged ministry by the name of the Ministry of Non-Conventional Energy Sources (MNES) was established in 2006 (Singh, 2017). Being a developing country and devoid of fossil fuel reserves, India is facing a serious energy shortage. Another dimension of this problem is energy security generated from the extreme dependency on external resources. On the other hand, a continuous growth rate of the population and a rapidly growing economy ensure a steep rate of growth of energy demand over the year.

Though India has coal reserves, the quality of Indian coal is not very high due to high ash and moisture content. Also, the mining and extraction of coal is not a very eco-friendly process. More often, the coal mines are in areas with high forest cover or other environmentally sensitive zones. The mining activities can damage the ecosystems of those areas. Another issue is with the coal-fired thermal power plants. Though the coal is extracted for energy generation, the CO_2 emitted from the power plants are causing serious harm to the environment. A thermal power plant with 1000 MW gross capacity and an efficiency of about 43% can consume coal at a rate of 400 tons/hr. and cause CO_2 emission at a rate of 800 tons/hr (Mishra, 2004). Other associated issues include SO_X, NO_X, and particulate matter (PM) emissions. Further, water pollution from waste heat, acid drainage from coal, soil contamination by ash, heavy metals, and leachates from landfills are other issues associated with coal-fired thermal power plants.

A cleaner alternative to the fossil fuel family is oil and natural gas. However, its inadequate domestic reserve is the main obstacle in the way to utilising them as fuels. These reserves cannot compete with the rapidly increasing energy crisis in India, as

clarified from the reports disclosing and discussing the dependency of this country on imported crude oil.

Another conventional energy source in India is the large hydro power project. Although, as pointed out by Briscoe (2005), India has developed only about 18% of its hydroelectric potential. Also, many negative environmental impacts and social damages are associated with these large hydro projects. Two of the most significant events of modern Indian history, “Narmada Bachao movement” and “Anti-Tehri Dam movement”, are associated with the protest against building large-scale hydropower projects on Narmada and Ganges, the two largest rivers of India. A work by Pandit and Grumbine (2012) put a spotlight on the devastating floods and landslides in Uttarakhand and suspected the interference in the flow of the Ganges River as the cause.

Another factor contributing to finding the solution to the Indian energy crisis is the nuclear power plant. India's nuclear journey started in the 1960s with two units at the Tarapur Nuclear Power Plant. Since then, the nuclear power program has witnessed steady growth. The share of nuclear power in the total power consumption of this country is 3.53% (Jewell, 2011). However, after Fukushima, concerns have been raised among people about power plants under the shadow of scepticism. Keeping these issues in mind, the alternate energy sources are gaining more and more attention every day, and various sources are being investigated for energy production and optimisation.

This research investigates the integration of waste biomass through sequential extraction of lignocellulosic materials using sonochemical treatment. The extracted compounds are converted into bioethanol and furfural, while the residual biomass is pyrolysed into biochar and silica. These materials were further engineered for pollutant adsorption from aquatic systems and combined with bacterial immobilisation for enhanced remediation. Process optimisation via Response Surface Methodology (RSM) and phytotoxicity assessments ensures environmental safety and scalability.

Chapter: 2

REVIEW OF LITERATURE

Various studies are being performed in the field of energy science and environmental management. With the development of society, resource scarcity and environmental damage by anthropogenic activity are becoming more and more prominent. As discussed in Chapter 1, the conventional methods of energy generation, waste management, and wastewater treatment have some serious drawbacks. Therefore, new research has been conducted to remediate the issues. Biotic solid wastes, specifically lignocellulosic biomass, are being explored as a precursor for both energy production and wastewater treatment to solve multiple issues at the same time.

2.1. Lignocellulosic biomass to value-added products:

Bioethanol and other eco-friendly substitutes to petroleum-derived fuels are being explored to minimise the dependency on fossil fuels (Gray et al., 2006). Much research is being conducted to boost the ethanol production from lignocellulosic biomass to establish this option as economically viable and competitive with conventional fuels. On an industrial scale, maize grain (starch) and sugarcane (sucrose) are considered as the raw material for bioethanol production, but both sources compete for land and affect food production. As the world population grows, the use of these food resources will increase the already-existing food and energy crisis (de Fraiture et al. 2008). As a result, lignocellulosic waste materials are being viewed as an appealing source for future ethanol supply and the extraction of value-added products. Various products, viz., cellulose, hemicellulose, lignin, silica, etc., can be extracted from the raw biomass and used for various purposes.

2.1.1. Cellulose:

Cellulose is the most available renewable polymeric material in the world that serves as the component of the cell wall of higher plants and marine organisms (Liu et al., 2020). Chemically, cellulose is a very stable polymer due to the presence of β-1,4-glycosidic bond, which acts as the linkage between D-glucopyranosyl units. In the structure, an abundance of hydroxyl groups in C2, C3, and C6 of glucose can be observed, which helps in the formation of hydrogen linkage within and between the monomers of cellulose fibre. This bond is an important contributor to the crystalline structure, structural integrity, and

physicochemical nature of cellulose (Moon et al., 2011; Wang et al., 2020). From studying the structural properties of plant cell walls, it was concluded that no single cellulose fibre exists in nature, and the length can vary depending on the source. Furthermore, many fine-tuned structures of cellulose, viz., elementary fibrils, microfibrils, and microfibrils, were developed inside the biological organisms, and the cellulosic structures were found to be combined with hemicellulose and lignin to form a complete cell wall (Sorieul et al., 2016).

Due to the high abundance of cellulose, it is used for various purposes in the construction industry, wastewater treatment, pharmacology, and nano-material research. carboxymethyl cellulose (CMC) is a well-known compound for drilling and oil exploration (Aftab et al., 2017). The traditional fluid used in drilling causes environmental and safety hazards, hence, the usage of CMC as an additive reduces the problems and maintains the fluidity of the medium under high temperature and pressure. Another derivative of cellulose is polyanionic cellulose (PAC) with similar characteristics to CMC but high purity. From recent studies, it was found that PAC is a more efficient component for the drilling process (Bennion et al., 1998). Other than PAC and CMC, another component significant in the drilling process is hydroxyethyl cellulose (HEC). This component is not directly used in the drilling process but acts as a viscosizing agent (Caenn and Chillingar, 1996). Several studies had been conducted as well, and patents were filed about the fluid loss capacity of HEC. In the 1950s, Hurley developed a new form of cellulose, known as carboxymethyl hydroxyethyl cellulose (CMHEC) from cement slurry, that can reduce fluid loss as well as adjust the time of thickening (Hurley, 1959). Another study reported the development of a high-temperature-resistant cement slurry containing 52.5% of HEC (Frederick et al., 1964).

Apart from the application in the cement and drilling industry, the depolymerisation and treatment of cellulose opens numerous opportunities to develop new products and potential monomers. The depolymerisation of cellulose can be performed by the hydrolysis of the β-1,4-glycosidic bond and producing glucose. Various processes, viz., enzymatic degradation (Zhang et al., 2005), degradation in supercritical water (Sasaki et al., 2000) or acid-catalysed process (Climent et al., 2011) are used to break down the polymerisation of cellulose. Glucose, the most dominant monomer of cellulose, can be used for bioethanol production by fermentation (Sun et al., 2002). Furthermore, chemical

methods can be used to produce lactic acid, glucaric acid (Pamuk et al., 2001), and succinic acid (Delhomme et al., 2009).

Cellulose also has an application in bioethanol synthesis by producing total reducing sugar (TRS) and fermentation. Amaefile et al. (2023) investigated the bioethanol production from sawdust and reported that the highest TRS yield was found to be 27.8 g/100 g of biomass. Another study had reported that alkaline treatment of water hyacinth can produce cellulose up to 402 mg/g (Rezania et al., 2019). Ziaei-Rad et al. (2023) reported that 0.36 g sugar/g of biomass was observed in the case of wheat straw by treating the biomass at 130^{o}C. Timung et al. (2016) reported a comparison between sugarcane bagasse and citronella biomass and found 452.27 mg/g and 487 mg/g of TRS, respectively, while treating them at 120^{o}C. Bhattacharaya et al. (2011) reported that the removal of lignin and hemicellulose and decreasing cellulose crystallinity can improve hydrolysis yield significantly. It was observed that after sonication for 0.75% of sulphuric acid pretreatment media, wheat straw increased the TRS production by 14%, with the initial value of 38 g/kg. The effect of sonication was observed in a non-linear correlation with sonication time (Bhattacharyya et al., 2013). A study conducted by Nitayavardhana et al., (2008) reported that treating Cassava chips in an acetate buffer medium at 323K temperature and with 20 kHz sonication showed a 2.7-fold production yield compared to a non-sonicated medium. Bussemaker et al. (2013) treated wheat straw at 328K temperature with 40, 376, and 995 kHz sonication, respectively. It was found that the 40 kHz frequency favoured the delignification process, whereas at 995 kHz, carbohydrate stabilisation was observed.

Cellulose-based nanocomposites also have a wide range of uses. They are significant to replace synthetic polymers (Lavoine et al., 2012). It is also used for food packaging for its non-toxic nature and behaviour as a barrier to gas and water (Nair et al., 2014). They are also potential candidates in the electronics industry to enhance conductivity and flexibility (Razaq et al., 2012). These materials also have applications in drug and gene delivery (Sampath et al., 2017). Research has also reported that electrospun poly (e-caprolactone)/nano cellulose composites have scaffold activities that can be used for tissue engineering (Si et al., 2016).

The other two significant derivatives of cellulose are microcrystalline (MCC) and nanocrystalline (NCC) cellulose, respectively. MCC is a partially depolymerised version

of cellulose. A cellulose fibre composed of two parts, viz., the crystalline part and the amorphous part (Yang et al., 2019). The amorphous part of cellulose gets hydrolysed during acid treatment and forms the more crystalline MCC structure. This material is used as a filler, binder in the food industry, suspension stabiliser, viscosity regulator, and emulsifier (Trache et al., 2016). Various techniques, viz., physical, chemical, biological, and physico-chemical pre-treatment techniques, are used to extract MCC from the rest of the biomass (Agbor et al., 2011; Pandey et al., 2015). Also, to maintain the high purity, acid hydrolysis, neutralisation, and bleaching are conducted (Thoorens et al., 2015).

Unlike MCC, NCC has a more pure, crystalline fine structure. They are rigid, rod-like crystals with a diameter ranging from 10 to a few hundred nm (Peng et al., 2011). The process used to produce NCC is acid hydrolysis. The amorphous regions break down due to the hydrolysis, releasing individual crystals (Ranby, 1951).

2.1.2. Hemicellulose:

Hemicellulose, another component of plant cells, was a polymer with various sugars, viz., pentose (such as arabinose, xylose), hexose (such as glucose, galactose, mannose) and sugar acids. Depending on their structure, hemicellulose can be classified into four different groups, viz., mannans, xylans, xyloglucans, and mixed-linked β-glucans. As discussed in section 2.1.1, it was found that cellulose is a homogeneous polymer; on the other hand, unlike cellulose, hemicellulose's nature is highly dependent on its source. Hardwood hemicellulose mainly contains xylans; on the other hand, softwood hemicellulose is composed of glucomannans. Xylans are mainly composed of xylose monomers interlinked through β-(1,4)-linkages (Rennie and Scheller, 2014). It was also found that the compounds of the backbone are frequently accompanied by various carbohydrate monomers like glucose, xylose, glucuronic acid, and arabinose (Heinze and Liebert, 2012).

Another type of hemicellulose is xyloglucans. The backbone of xyloglucans is made with D-glucopyranosyl residues. The residues are further replaced by oligosaccharides, viz., galactosyl, arabinofuranosyl, and arabinopyranosyl. In several plant species, the xyloglucans become more complex hemicellulose by substituting additional mono- and disaccharide chains for these side chains. This structure varies depending on the different stages of plant cell growth (Pauly and Keegstra, 2016).

Mannans are another type of hemicellulose, specifically hemicellulosic heteroglycans with complex structural characteristics. Mannans are responsible for maintaining the structure and storage of the plant cell wall (Ebringerova et al., 2005) and have a hydrogen bond connection to cellulose. Mannans further have four subtypes, viz., glucomannans, galactomannans, galactoglucomannans, and homomannans, respectively. Though the mannose backbone of galactoglucomannans and glucomannans exhibits interruption due to a non-repeated glucose pattern, in the case of homomannans and galactomannans is solely composed of mannose residues linked by β-1,4-linkages. It was also observed that galactose residues connected to the mannosyl backbone residue hinder polymer self-aggregation (Qaseem et al., 2021).

Hemicellulose extracted from lignocellulosic biomass is reported to be utilised to synthesise biofuels using microbes. One study reported the use of pentose-degrading organisms such as *Pichia stipites* and *Candida shehatae* to produce bioethanol from wheat straw-derived hemicellulose (Koti et al., 2016). Alongside, sodium xylene sulfonate was used to produce biobutanol from hemicellulose (Qi et al., 2019). Another study reported that *Candida guilliermondii* has been used to produce xylitol from rice straw hemicellulose hydrolysate (Roberto et al., 1996).

2.1.3. Lignin:

Another important cell wall component is lignin, which acts as the building block of the plant cell wall. Natural lignin consists of three monomers, viz., sinapyl alcohol (S-lignin), coniferyl alcohol (G-lignin), and p-coumaryl alcohol (H-lignin). These monomers are linked by a β-O-4 ether bond to form a stable structure (Rinaldi et al., 2016; Wang et al., 2017). The % of this bond in the case of softwood is found to be 45-50%, and in the case of hardwood it increased to 60-62% (Rinaldi et al., 2016). It was found that the benzene rings of G- and H-lignin have more reactive sites, which are responsible for the reactivity of lignin in different chemical processes. Thus, softwood and grass lignin are more capable of participating in a chemical reaction (Kalami et al., 2018).

Several methods have been studied to extract lignin from raw biomass, though the most efficient process is acid-alkali treatment. It was found that the chemical extraction process can produce more types of lignin structure, called technical lignin, which lacks the characteristics of naturally available lignin structures (Karthauser et al., 2021). During pretreatment, in an alkaline environment and elevated temperature, the kraft lignin

changes its structure, which decreases the yield (Crestini et al., 2017). To enhance the yield, different solvents, viz., alkaline hydrogen peroxide, are used. It was found that this process can be performed at a relatively lower temperature (70°C) with a higher yield (Zhang et al., 2015). Acid medium is also used to treat the lignocellulosic materials under the sulphide method. This process produces lignin, called lignosulphonates and has a relatively higher molecular weight than kraft lignin. Due to sulphonation at the α-position, this lignin is soluble in water (Kai et al., 2016). For the non-wood species, the soda-pulping method is used, but no sulphur is utilised. Hence the main difference of this lignin with kraft lignin is a lower sulphur content (Wang et al., 2020; Kai et al., 2016). This structure of lignin provides an idea to cleave the lignin molecule in such a way that valuable products can be produced. This can be achieved by dissolving the lignin in organic solvents. The cleaved lignin, which is soluble in organic solvents, is known as organosolv lignin. Unlike technical lignin, whose structure is influenced by the severity of the treatment process, organosolv lignin is like natural lignin molecules (Kai et al., 2016).

Various products can be produced as by-products or derivatives from lignin. Phenolic compounds are one of the main by-products of lignin and have applications in the biopolymer, drug, and cosmetics industries. One of the most important and premium derivatives of lignin is vanillin (3-methoxy-4-hydroxybenzaldehyde), which is used as a flavouring agent. Another derivative of lignin is carbon fibre, a light and strong material which has several applications in the automotive industry (Brodin et al., 2009).

2.1.4. Silica:

Silica is one of the most important products extracted from lignocellulosic biomass. From previous studies and industrial performance, it was observed that rice husk contains about 95% silica that can be extracted by combustion and leaching. This method solves the dumping problem of agro biomass as well as mitigates soil, water, and air pollution. Furthermore, after the extraction of silica, the biomass can be used as fertiliser in agriculture or as a strengthening agent in the cement industry. To extract silica on an industrial scale, leaching is used as the most efficient technique. Leaching can be defined as the extraction process of a substance from a solid mixture using a liquid as a separation medium. By using this process, silica precipitate forms as a solid and is collected.

To extract silica from rice husk, leaching plays a significant role. Under the conventional extraction procedure, pyrolysis of raw materials is performed, and the ash is digested using NaOH to convert the silicon fraction of biomass to sodium silicate (Na_2SiO_3), also known as water glass. Following that, the silicate salt reacts with HCl to precipitate out silica as a white solid substance. The modification and structural profile of silica present in the biomass depend on the pyrolysis temperature and time. At a temperature of 550ºC-800ºC, the extracted silica consists of an amorphous structure and crystalline silica forms above this temperature (Chandrasekhar et al., 2006).

Due to the high expense of the conventional method, agro biomass can be used as a viable raw material of silica with high purity and crystallinity, which has application in battery materials. Another silica material, aminated SiO_2 ($ASiO_2$), is produced from rice husk through the reaction with aminopropylthiethoxysilane and utilised for the removal of various contaminants from the environment. It was reported that $ASiO_2$ is a great adsorbent of CO_2, CH_4, H_2, and N_2 from air. It was also seen that silica extracted from agro biomass is a great adsorbent of heavy metals.

2.2. Aerogels as an emerging research focus:

With the development of science, new and novel materials are being developed and investigated for their application potential. One of the main components to attract the attention of researchers, in recent times, is aerogel. With highly porous and open-cell structures, aerogels comprise microporous networks with interlocking nano-scale filaments with unique properties. Although considered solid materials, aerogels consist of 99.9% air by volume. The very low density (1 kg/m^3), high porosity (~99%), low thermal conductivity (~0.01 W/mK), optical transparency (~99%), low refractive index (~1.05), and low dielectric constant (~1.0-2.0) aerogels are considered as both the novel and practical material (Fricke and Emmerling, 2005; Du et al., 2013). With exceptional properties and chemistry, aerogel can morph into different structural forms, which can be utilised for numerous applications (Makeli et al., 2016).

Aerogel is produced using a sol-gel procedure and a drying technique to retain its highly porous three-dimensional network. The precursors of aerogel can be organic, inorganic, or hybrid molecules. Advanced studies have been conducted and have shown the great potential of aerogel to produce a clean environment through activities such as CO_2 adsorption and removal of contaminants from effluents. Removal of volatile organic

matter from water is an established field of aerogel research. In addition to typical aerogels, several additional forms, viz., biomass (Arboleda et al., 2013), silicon carbide (Shelmer et al., 2015), carbon, metal oxide and biopolymer aerogels have been developed. Recent applications of aerogels in space research are drawing the attention of the common people. Resorcinol formaldehyde (RF), carbonised resorcinol formaldehyde (CRF), non-silica aerogel, and aerogel composites are used for this purpose. The material was developed after 70 years the material was developed (Kistler, 1931; Pierre and Pajonk, 2002). Also, various novel non-silicon oxide aerogels, chalcogen aerogels, and gradient aerogels have been discovered as reported in previous studies (Du et al., 2013).

The drying method of the hydrogel network is one of the determining factors of the properties of the final product. Most of the characteristics of aerogels and xerogels are similar, but some differences were observed depending on how the liquid evaporates (Livage et al., 1998). Traditionally, aerogels are produced by drying the hydrogels under supercritical conditions. However, nowadays, other processes are also being used; for example, the gels produced by using lyophilisation, formerly known as cryogels, are now referred to as aerogels with about 90% porosity.

For the exceptional characteristics, these materials are being used as porous catalysts for chemical reactions, porous ceramics for filtration, and to design thermal insulators (Arboleda et al., 2013; Luyten et al., 2010; Menzel et al., 2012). The polymer aerogels, like StyrofoamTM, have applications to reduce oil spills for their sorption capacity (Korhonen et al., 2011).

S. Kistler first invented aerogels in the 1930s by using the supercritical drying method. This process was focused on a multistep reaction and considered a silica-based compound as the precursor. Due to the complexity of the production process, the aerogels were ignored for the next thirty years. But in recent times, different types of aerogels, viz., SiO_2 (Pierre and Rigacci, 2011), TiO_2 (Hirashima, 2011), Al_2O_3 (Baumann et al., 2005), and ZrO_2 (Hammouda et al., 2011) have been developed. Apart from that, organic aerogels like polyurethane, polyimide, polystyrene, and resorcinol-formaldehyde (Mulik and Sotiriou-Leventis, 2011) are also being investigated. Also, carbon aerogels, like carbon, carbon nanotubes (Worsley et al., 2008), following cellulose (Rigacci and Achard, 2011), polysaccharides, various proteins, and more recently SiC-based aerogels (Maleki, 2016) are being developed.

An aerogel state material should be able to form a macroscopic monolith; it should have a fractal and hierarchical microstructure, where the main structure coexists; it should have a gel-like structure, usually composed of nanoscale coherent skeletons with pores; and it should randomly crosslink, usually because of non-crystalline matter. Aerogel needs to have different properties from solid, gas, or regular foam. For example, it should have a high specific surface area, and very wide adjustable ranges of density and refractive index, especially for silica aerogel, with very low relative density, and very high porosity. Various techniques such as electron microscopy, pore size analysis, small-angle X-ray scattering, and others could be employed to characterise the aerogel structure. Usually, specialised devices are used to measure the qualities. For instance, a dynamic thermomechanical analyser or an accurate universal testing machine in the compression or three-point bending mode might be used for the evaluation of the mechanical characteristics of the aerogels, such as the strength, modulus, loss tangent, and stress-strain curve (Du et al., 2013).

If silica aerogels are to be used as transparent window insulation materials and thermal superinsulation, their mechanical properties must be strengthened chemically without sacrificing their primary characteristics. One significant benefit of using silica aerogels for these kinds of high-value technical applications is their transparency. A double-step procedure applied to the wet gel before the supercritical drying stage can achieve this purpose. To be utilised sustainably, silica aerogels need to have high hydrophobic characteristics that hold up over time when they are in the water (Pierre and Pajonk, 2002). A previous study proceeded with their research by hydrolysing methyltrimethoxysilane (MTMS) and tetramethyl orthosilicate (TMOS) under basic circumstances and then supercritical drying them in methanol, hydrophobic aerogels can be produced. The authors discovered that aerogels containing more than 20% MTMS were hydrophobic because they floated on water under these high-temperature drying circumstances, which resulted in a dehydrated aerogel surface. Nevertheless, the degree of silica condensation decreased with increasing MTMS content. There was a quasi-two-step gelation process since the condensation and hydrolysis rates of MTMS are substantially lower than TMOS.

The thermal conductivity of monolithic organic aerogel is like silica aerogel at room temperature. However, compared to silica aerogel, the advantages of monolithic aerogel are their properties like is less brittle, and with temperature increase, the radiation

component is minimised. Therefore, polyurethane aerogel, which is made in CH_2Cl_2, has low thermal conductivity and is non-transparent. As a result, they are regarded as novel insulators for the appliance sector, where energy standards are getting stricter (Biesmans et al., 1998). Organic precursors are even more readily able to form organic polymers on -(C-C)-covalent bonds than silica precursors. As a result, they enabled the synthesis of an intriguing new class of monolithic aerogels, comprising aerogel particles generated by the sol-gel-emulsion approach that range in size from sub-micrometres to several hundred micrometres (Lee et al., 1998). Among these materials, melamine-formaldehyde (MF) and resorcinol-formaldehyde (RF) aerogels have been investigated the most. They can be made by polycondensing melamine or resorcinol with formaldehyde in an aqueous solution that is somewhat basic. Sodium hydrogen carbonate or sodium hydroxide is frequently used as a catalyst for gelation. Phenolic-furfural (PF) combinations with poly (dimethyl siloxane) (PDMS), 2,3-didecyloxyanthracene (DDOA) with ethanol or supercritical CO_2 as the solvent, polyacrylonitrile (PAN), or polyisocyanates are other significant precursors used to create organic aerogels (Pierre and Pajonk, 2002). The latter gels have a wide range of practical applications. Under both ambient and evacuated conditions, they may be processed into novel thermal insulation materials with good insulation qualities. These substances can be processed to create polyurethane imines, polyureas, polyisocyanurate (PIR) aerogels, and extensively cross-linked polyurethanes (PUR). CH_2Cl_2 can be used as a solvent with polyurethanes and swaps directly with supercritical CO_2. The resultant organic aerogels lack transparency. They have a particular surface area of about 300 m^2/g with an overall 0.24 g/cm^3 density. It is possible to create aerogels that are optically clear by using aqueous melamine formaldehyde solutions (Biesmans et al., 1998).

One technique for producing organic aerogel, like carbon aerogel, is pyrolysis at temperatures higher than 500°C. This process can convert the organic aerogel into a carbon network that conducts electricity. The carbon aerogel that is produced from RF aerogel by the pyrolysis process maintains its high specific surface area of 400–800 m^2/g and enormous specific mesopore volume of >0.55 cm^3/g, in addition to the isotherms of its parent organic aerogel, which exhibit a hysteresis loop (Tamon et al., 1999; Zhang et al., 1999). Fractal structures were not observed in carbon aerogels until recently. A distinct type of carbon aerogel has been developed that exhibits mass fractality with a 2.5 mass fractal exponent. It was achieved by the gelation of resorcinol-formaldehyde in

acetone and perchloric acid or sodium carbonate catalysis. Furthermore, unlike all other carbon aerogels (generally mesoporous), this type of carbon aerogel has a bimodal distribution of pores with micro- and macro-pores (Pierre and Pajonk, 2002).

2.3. Adsorption technologies in wastewater treatment:

The large amount of wastewater discharge from industries and municipalities has raised a big concern amongst the aquatic ecosystem and is affecting the environment adversely, including soil and biosphere. Among all the pollutants, getting rid of organic pollutants is the trickiest part of environmental remediation. Several processes, viz., adsorption, chemical and biological treatment, photocatalysis, advanced oxidation, and membrane filtration, are being used to remediate the problems (Maleki, 2016). The removal of pollutants from wastewater has been previously studied in various research (Hessel et al., 2007; Singh and Singh, 2017). Removal of pollutants from water is important due to various reasons, viz., they are harmful to the environment and health, and they have carcinogenic and mutagenic properties. Specifically for dyes, an inhibition in photosynthesis in the aquatic environment was observed, affecting the water quality (Chikri et al., 2020; Crini, 2006).

Throughout recent years, numerous investigations have been performed to find out the most ideal process for wastewater treatment. Though many technologies were explored for this issue, only a small fraction of them are implemented by the concerned industries due to the limitations they possess (Katheresan et al., 2018). The techniques available for wastewater treatment are broadly divided into three categories, viz., physical, chemical, and biological treatment processes. Under the mentioned categories, there are many techniques for pollutant removal, such as coagulation, adsorption, chemical oxidation, membrane separation, electrochemical process, aerobic and anaerobic microbial degradation. Each of the processes has its advantages and disadvantages (Ghoreishi et al., 2003).

The term “adsorption” was first coined by the German physicist Heinrich Kayser in the year of 1881 (Choudhary, 2017). Over the past decade, a bloom was observed in the application of adsorption for wastewater treatment. This process is accepted over any other method because of its simple design, operation, cost-effectiveness, and energy efficiency (Tan and Hameed, 2017). As defined, adsorption is a mass transfer process of atoms, ions, or molecules of a gas or liquid phase to form a monolayer or multilayer on

the adsorbent surface. It indicates the preparation of bonds by the atoms or molecules sing physical or chemical forces. In practice, adsorption is performed as an operation in a batch or continuous mode in a packed bed column of porous adsorbent (Abebe et al., 2018).

Like surface tension, adsorption is a consequence of surface energy. In a bulk material, all the requirements to form a bond of an atom in a material are fulfilled by other atoms. Depending upon the nature of the bond, adsorption is divided into two categories, viz., physisorption and chemisorption. The nature of adsorption depends on the nature of pollutants.

Depending on the nature of adsorbents, it can be divided into two categories, viz., conventional and non-conventional adsorbents (Sukmana et al., 2021). Conventional adsorbents are widely used in commercial purposes, industrial sectors, and even on a laboratory scale. Activated carbon, zeolite, alumina, silica gels, and ion-exchange resins are common examples of this type of adsorbent. Activated carbon is an excellent component for pollutant removal for wastewater, and the main benefit of this type of adsorbent is that they do not produce any by-products (Crini et al., 2019). Research conducted by Feng et al. (2012) reported that ascorbic acid-coated Fe_3O_4 can remove arsenic from water. The study shows that the maximum adsorption capacity for As (III) and As (V) was 46.09 $mg.g^{-1}$ and 16.56 $mg.g^{-1}$ respectively. Another study performed by Mahmoud et al. (2016) used MgO nanoparticles and found that they can remove Remazol Red RB-133 from water solution. Wang et al. (2019) observed the use of Polyaniline/TiO_2 as an adsorbent to remove methylene blue from wastewater. This study reported that the highest removal of the dye was about 99%.

The non-conventional or natural adsorbents are produced from natural materials or industrial waste (Gupta and Suhas, 2009). For example, agricultural wastes are globally available adsorbents (Adegoke and Bello, 2015) and are rich with functional groups (da Rocha et al., 2020). The natural adsorbents are being studied to make them an alternative to conventional adsorbents (Martini et al., 2020) and are in increased demand due to their low cost and high adsorption rate (Mathurasa and Damrongsiri, 2018; Mo et al., 2018). Bellahsen et al. (2021) showed that the use of pomegranate peel powder achieved 97% removal of ammonium. On the other hand, Baby et al. (2019) used palm kernel shell as an adsorbent to remove heavy metals from water. The result showed that for Pb^{2+}, Cr^{6+},

Cd^{2+}, and Zn^{2+}, the adsorbent achieved 49.64 $mg.g^{-1}$, 49.55 $mg.g^{-1}$, 43.12 $mg.g^{-1}$, and 41.72 $mg.g^{-1}$, adsorption capacity respectively.

Zulkania et al. (2020) found the application of phosphoric acid-activated carbon produced from palm fibre waste to remove methylene blue from water solution and reported a removal of 99.84%. The modification of rice husk was investigated by Phan et al. (2019). The Triamine-activated rice husk ash was found to remove the NO_3^- ion from water and was recycled up to 10 cycles.

2.4. Aerogels in wastewater treatment:

Apart from the conventional and natural adsorbents, aerogels are also being used as an efficient adsorbent due to their unique properties. Based on studies conducted by Liu et al. (2009), hydrophobic silica aerogel can have high adsorption capacity towards organic compounds that have poor solubility, whereas hydrophilic silica aerogels have shown more efficiency towards organic molecules that are soluble in water and are adsorbed. The hydrophobic silica aerogel granule (Nanogel) was produced by Cabot Corporation by hydrophobizing silica with trimethylsilyl groups (TMS). Using an inverse fluidized setup, it was checked for the application of the aerogel for emulsified oil removal from stable oil-in-water emulsions was checked. The main factors that influence Nanogel's capacity to adsorb oil in inverse fluidised beds were bed height, fluid surface velocity, emulsifier percentage in the oil-in-water emulsion, and the nanogel granule size. The produced nanogel particles have an oil-absorbing capacity ranging up to 2.8 times more than their weight (Maleki, 2016; D. Wang et al., 2010). Recent studies have shown the potential of carbon aerogels (Worsley et al., 2008), like carbon nanotubes, carbon fibre, carbon micro belt, as well as graphene aerogel. Like silica aerogels, these materials also displayed remarkable features in the form of three-dimensional (3d) structures, including high porosity, large specific surface area, low density, and surface hydrophobicity, which made them an effective medium for oil adsorption. Aerogels made from twisted carbon fibres, for instance, have a maximum sorption capacity of around 192 times the weight of the aerogel and may absorb a significant amount of organic chemicals and oils (Bi et al., 2013). Furthermore, several organics and oils were absorbed by the CNT aerogels with a great porosity of 99%, with exceptional specificity and absorption efficiencies exceeding 180 times their weight (Gui et al., 2010). However, carbon aerogels are expensive, hazardous, and complicated, making scale production impractical. A cheap,

sustainable, and environmentally friendly alternative is developed using vegetable-derived biomass.

Research by Li et al. has shown that hydrophobic watermelon carbon aerogel (WCA) could be prepared at low density and adsorb several types of organic solvents in addition to oils. WCA can absorb organic solvents and oils up to 16–50 times its weight. Distillation was utilised to recover the pollutants and regenerate WCA. After five cycles of absorption and harvesting, WCA's capacity for absorption of organic solvents and low-boiling-point oils may recover to around 100% of its original value (Li et al., 2014). To remove dangerous organic compounds and for oil-cleaning applications, a composite aerogel with improved mechanical compressibility and hydrophobicity, because of the combined action of its constituent elements, was also taken into consideration. In the study based on Sai et al. (2013), a composite aerogel was created using an interconnected network of bacterial cellulose and silica aerogel. It showed a high contact angle of 133°, and a high surface area of 734.1 m^2 g^{-1}, with an improved modulus of elasticity of 4.15 MPa. The produced composite aerogels showed a great absorption of vegetable oil without breaking down or losing their structural integrity.

Another very concerning issue and a major burden is the contamination of water and wastewater is the presence of heavy metals that are generated from industrial effluents and discharges. Heavy metals include copper (Cu), mercury (Hg), chromium (Cr), lead (Pb), manganese (Mn), zinc (Zn), iron (Fe), nickel (Ni), etc. which are known for their toxic nature and causing serious health damages to kidney, liver, and other organs, further, they are also non-biodegradable for the environment (Li et al., 2013). Hence, it is essential to address the heavy metals in the water that are coming from contaminated water resources. Heavy metal ions have been removed from wastewater using a variety of methods, including filtering, ion exchange, membrane separation, precipitation, reverse osmosis, and other biological processes. Nevertheless, problems with high energy consumption, operating expenses, and implementation difficulties have led to comparatively subpar outcomes, such as low removal concentrations of heavy metal ions and a failure to fulfil process safety and convenience standards. Active carbon's enormous surface area and porous network make it a well-investigated material for heavy metal ion adsorption. However, regeneration is hampered by physical adsorption and low capacity (Maleki, 2016). Therefore, a novel adsorbent class is needed for effective, long-term removal from water sources.

2.5. Formation of research questions:

The following research questions were formed from the literature review and were investigated during this study:

a. How can hemicellulose, cellulose, and lignin extracted from waste biomass via sonochemical pretreatment be converted into bioethanol and furfural for energy production?

b. How can the extracted cellulose, silica, and produced biochar composites be utilised for aerogel synthesis and environmental remediation?

c. What are the ecological impacts associated with these processes?

The overall research process followed to find the answers to the mentioned research questions is presented in Fig. 2.1.

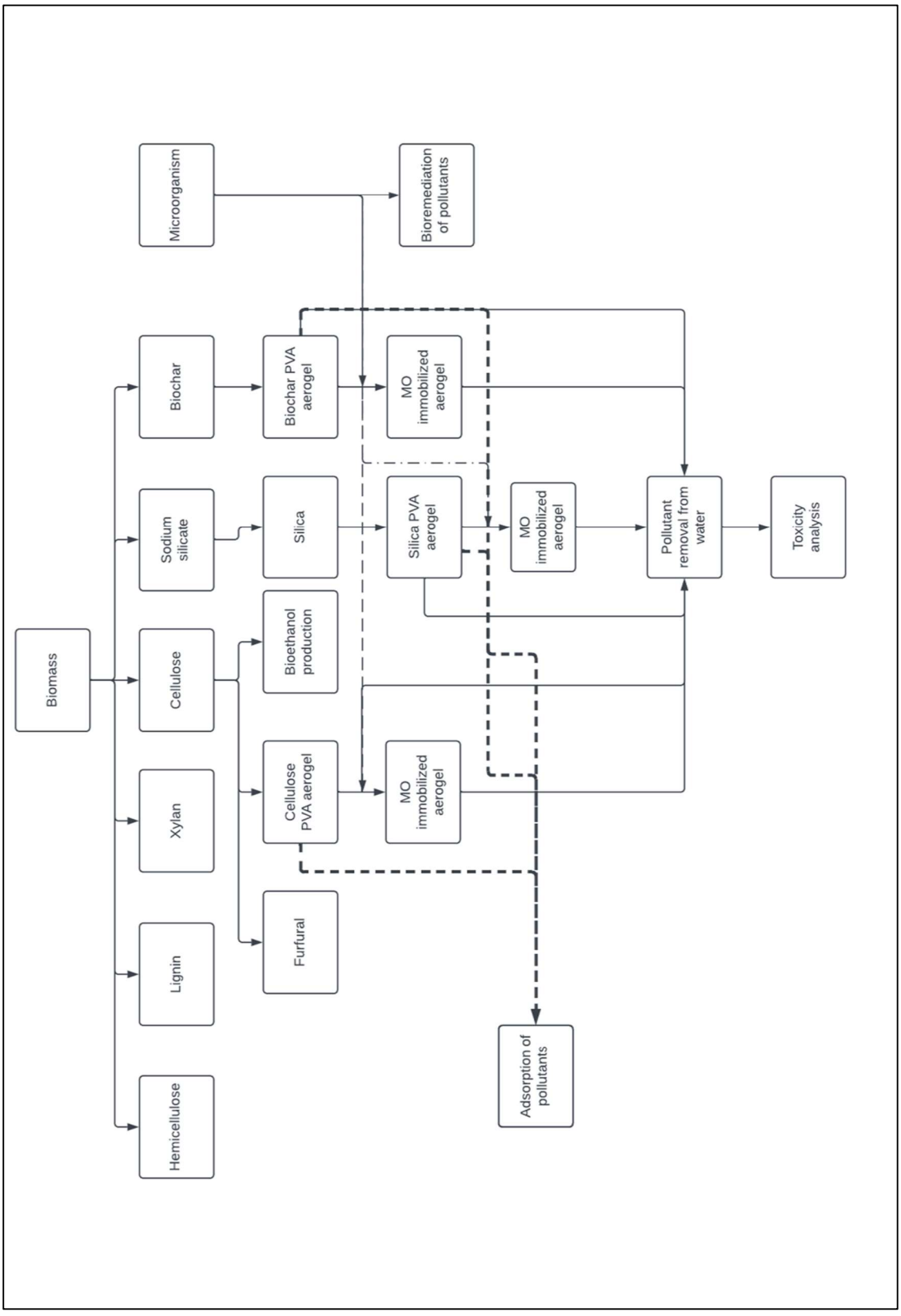

Figure 2.1: Overall workflow diagram of conducted research work

Chapter: 3

OBJECTIVE OF THE RESEARCH

3.1. Objective of the Research work: Based on the literature review (Chapter 2) and recent research trends, the objectives of this study were selected and are listed below:

1. To extract cellulose, hemicellulose, and lignin from waste biomass and characterise the extracted components.

2. To synthesise bioethanol and furfural from cellulose.

3. To produce biochar and silica from residual biomass and fabricate PVA aerogels loaded with cellulose, biochar, and silica for pollutant adsorption.

4. To immobilise pollutant-degrading bacteria in aerogels and compare remediation efficiency with a standalone system.

3.2. Novelty of the work:

The novelty of this research work has been identified and discussed below:

a. **Multi-stage valorisation:** This study combines chemical pretreatment, sonication, pyrolysis, and sol-gel methods to extract and repurpose all lignocellulosic fractions, minimising waste.

b. **Hybrid applications:** This study integrates energy production with environmental remediation, addressing both the energy crisis and water pollution.

c. **Eco-toxicology focus:** This study includes phytotoxicity assessments post-remediation, ensuring practical applicability and safety, an underexplored area in biomass-derived materials research.

Chapter: 4

PREPARATION OF VALUE-ADDED PRODUCTS FROM LIGNOCELLULOSIC BIOMASS

4.1. Introduction:

Lignocellulosic biomass is the most available raw material for biofuel production, and being a second-generation product, this biomass does not compete with food crops. Large-scale biomass processing mainly focuses on two sectors, biofuels and bioenergy (Chaturvedi et al., 2022). Though these materials significantly affect the production of cleaner energy, the production of biomass-derived value-added products faces different limitations. The derivation of a single product from a single biomass is the main scheme of biomass valorisation, but it also leads towards a contemporary biobased approach. On the other hand, processing of multiple biomass leads to multiple bio-based products, including but not limited to biofuels, biochemicals, bioenergy, and high-value by-products. Rice is India's main food crop, and rice husk (RH) production in this nation is significant. Worldwide, 50% of the total rice husk produced originates in India.

Rice husk is one of the most common by-products of rice production. After the grain is collected, the husk biomass is mainly discarded as garbage. This biomass is difficult to break down and takes up much landfill space due to its low density. A portion of this waste is used to feed domestic cattle, but most is thrown away without proper disposal. Nowadays, the majority of rice husk is burnt for energy generation (Yam and Mak, 2014), though the ash residue after burning contains a major amount of silica and poses a threat to the environment (Zhang et al., 2015). The exterior surface of rice husk comprises a significant amount of inorganic silica (2-5 wt%), and the interior layer is mostly made up of lignin (28%) and cellulose (33%) with vascular bundles that serve as a root for nutrient and water transfer. In some recent studies, rice husk has been identified as a valuable raw material to extract different products (Moayedi et al., 2019), viz., silica, silicon carbide, and permeable carbon (Shi et al., 2019).

Another waste material with high potential is sawdust (SD). In the timber processing industry, raw timber goes through a variety of stages. From ripping the wood to transportable size, cutting it to give the desired shape, mortising, and polishing produce a large amount of sawdust as waste in each stage. The industry introduces various

machinery and manual labour to achieve the desired product from raw timber. Due to the high precision of the machines and modern infrastructure, developed countries produce more sawdust than developing nations (Shigehisa et al., 2014). With the advancement of technology, sawdust is becoming a concern for the environment. Burning of this material can lead to acid rain and the production of greenhouse gases. On the other hand, without proper disposal, sawdust can affect the soil and water chemistry (Rominiyi et al., 2017).

Apart from the problems associated with rice husk and sawdust, there are many approaches to extracting different products from these materials. This approach not only remediates the environmental issues but also promotes cleaner energy production, and the derivation of different valuable products and positively affects the world economy. In this study, the potential of sawdust and rice husk to produce bio alcohol and the extraction of cellulose, lignin, and hemicellulose in a single process will be investigated. The effect of different parameters, viz., the nature and concentration of pre-treatment media, sonication, reaction time, material's dose, pH, and temperature, will also be studied. The effect of these parameters on the production of different by-products, viz., furfural and xylan, will also be investigated.

4.2. Materials and Methods:

4.2.1. Materials: Rice rusk and sawdust were considered raw materials for this study. The raw materials were collected from the local rice mill and sawmill, respectively, in Dhaniakhali, a village in Hooghly district, West Bengal, India. Sodium hydroxide (NaOH), sulphuric acid (H_2SO_4), hydrochloric acid (HCl), anthrone reagent, 3,5-dinitrosalicylic acid, Furfural, cellulose, and xylan were purchased from Merck (Germany). Dextrose, ammonium sulphate, ethanol, sodium nitrate, magnesium sulphate heptahydrate, ferrous sulphate, potassium chloride, sodium sulphite, dipotassium hydrogen phosphate, magnesium chloride, potassium dihydrogen phosphate, nutrient broth, agar, yeast extract, Czapek dox broth, and peptone were purchased from HiMedia (India) and used as received.

4.2.2. Pre-processing of biomass: The collected sawdust and rice husk were ground with a mixture grinder to reduce the particle size of the materials. After that, the ground biomass was cleaned with deionised (DI) water and dried under natural sunlight for three days. After the materials are completely dry, they are collected and stored in a dry container.

4.2.3. Pretreatment of biomass and cellulose extraction: In this study chemical pretreatment method was used to extract products from the raw materials. Two different pre-treatment media, viz., alkaline and acidic, with different concentrations, were used. For alkaline treatment, NaOH solution was used in three different concentrations, viz., 2%, 4%, and 6% (w/v). To make 100 mL of the solution, the desired weight of NaOH was measured using a weighing machine (Sartorius, Germany) and dissolved in 90 mL of DI water on a magnetic stirrer. After the solution was prepared, it was poured into a volumetric flask, and DI water was added for volume makeup. Similarly, for acid treatment, H_2SO_4 (95%) was mixed with DI water and stirred on a magnetic stirrer. Three different concentrations of H_2SO_4, viz., 2%, 4%, and 6% (v/v), were used in this study. 1 g of raw material was measured by a weighing machine (Sartorius, Germany) and mixed with 100 mL of pretreatment media into an Erlenmeyer flask. The mixture was stirred for 1 hour at 364 K on a magnetic stirrer, followed by 30 min. of sonication in a bath sonicator (LMUC-4, Labman, India) at 40 KHz. After sonication, the samples were treated on a magnetic stirrer for 30 min. After the treatment was complete, the solid residue was collected by filtration (Whatman-10), consisting of cellulose in its composition. The pretreated biomass was then washed with DI water to neutralise the pH. After neutralisation, the treated biomass was dried in a hot air oven at 334 K and collected after drying. Another set of the described experiments was conducted following the same process but without sonication. An anthrone test was used (mentioned in section 4.2.4) to estimate the cellulose content present in the pretreated biomass (Ghosh et al., 2024).

4.2.4. Anthrone test: The anthrone test was performed to estimate the cellulose content in the pre-treated biomass. In this test, the cellulose reacts with concentrated sulfuric acid and produces furfural. Following that, the produced furfural reacts with anthrone reagent, and a bluish-green complex appears in the solution. The intensity of this complex can be measured by a UV-Vis spectrophotometer.

4.2.4.1. Reagent preparation: To produce the anthrone reagent solution, 200 mg of anthrone reagent was measured on a weighing machine (Sartorius, Germany) and mixed with 100 mL of ice-cold sulphuric acid (95%) in an Erlenmeyer flask using a glass rod. This solution was prepared fresh and stored in a refrigerator for 2 hours before use. On the other hand, concentrated sulphuric acid (95%) was mixed with DI water in another Erlenmeyer flask to make the concentration 67%.

For the standard curve, commercially purchased cellulose was dissolved in DI water, and a solution of 100mg/L concentration was prepared. The stock solution was further diluted to prepare the concentrations of 1 mg/L, 10 mg/L, and 50 mg/L, respectively.

4.2.4.2. Experiment: 0.1 g of each pretreated biomass was taken, and 10 mL of 67% H_2SO_4 was added to the samples. This mixture was kept at room temperature for 1 hour. After 1 hour, 1 mL of the mentioned solution was taken and diluted to 100 mL by adding DI water. 1 mL of this newly prepared solution was added to 10 mL of anthrone reagent solution and thoroughly mixed. After mixing, the test tubes were heated in a water bath for 15 min, and the development of a bluish-green colour solution was observed. The solution was cooled down, and the absorbance was measured using a UV-Vis spectrophotometer (PerkinElmer, USA) at 630 nm (Ghosh et al., 2024).

4.2.5. Hemicellulose extraction: After the separation of cellulose (section 4.2.3), the collected hydrolysate was studied to extract hemicellulose from the media. In a storage bottle, 25 mL of hydrolysate was mixed with ethyl alcohol (70%) in a 1:1 (v/v) ratio and stored for 24 hours without agitation or stress. After 24 hours, a brown precipitate of hemicellulose was observed at the bottom of the container. The hydrolysate part was then separated by centrifugation (RM-12C, Remi, India), and the brown precipitate was dried in a hot air oven at 334 K (Ghosh et al., 2024).

4.2.6. Lignin extraction: The hydrolysate collected after hemicellulose extraction was again treated with concentrated HCl until the pH reached 3.5. The pH of the solution was monitored by a pH meter (TestR-35, Eutech, USA). After adjusting the pH, the solution was stored in a storage bottle for 24 hours. An opaque white precipitate of lignin was observed in the solution. The precipitate was separated from the liquid hydrolysate by centrifugation (RM-12C, Remi, India) and dried in a hot air oven at 334 K (Ghosh et al., 2024).

4.2.7. Estimation of xylan content: The hydrolysate after lignin extraction was analysed by a UV-Vis spectrophotometer (PerkinElmer, USA) to estimate the xylan content in the media. The standard solutions were prepared by using commercially purchased xylan. 100 mg of the xylan was measured by using a weighing machine (Sartorius, Germany) and dissolved in 500 mL of water. After the solution was prepared, it was poured into a volumetric flask, and water was added to make the volume 1 L. Other standard solutions,

viz., 10 mg/L and 1 mg/L, are made by diluting the stock solution. The xylan content present in the sample was measured at 275 nm absorption spectra (Ghosh et al., 2024).

4.2.8. Production of bioethanol: The previously extracted cellulose (mentioned in section 4.2.3) from biomass was considered as the raw material for bioethanol production. The method of ethanol production followed in this study was microbial fermentation. Microbial strains, *Saccharomyces cerevisiae* (MTCC 170) and *Aspergillus sp.* (Genebank: MH119104), were used in this experiment.

4.2.8.1. Saccharification of biomass: Saccharification is the breaking down of complex carbohydrate structures (i.e. cellulose) to simpler reducing sugars (i.e. dextrose). In this experiment, living *Aspergillus sp.* fungus was used to break down cellulose by its cellulase enzyme, which is present in the fungal cell and is important for its biochemical pathways. The detailed process of the mentioned experiment is described below.

4.2.8.1.1. Preparation of microbial culture: The Czapek Dox broth media was prepared by dissolving 3.5 g of Czapek Dox media powder in 100 mL of DI water in an Erlenmeyer flask and the pH of the media was measured by using a pH meter (TestR-35, Eutech, USA) and adjusted at 7.2 using 0.1 (M) NaOH and 0.1 (M) HCl buffer solutions. The media were sterilised using an autoclave at 394 K temperature and 15 psi pressure. After sterilisation, the media were cooled down to room temperature and placed inside a laminar airflow chamber. 0.1 mL of the previously isolated *Aspergillus sp.* strain was used to inoculate 100 mL of broth. The inoculated media was incubated for 7 days in a BOD shaker incubator (Remi) at 303 K temperature. On the other hand, Czapek Dox agar media was prepared by dissolving purchased Czapek Dox powder and agar powder (20 g/L) in 100 mL of DI water. pH of the media was measured by using a pH meter (TestR-35, Eutech, USA) and adjusted to 7.2 using 0.1 (M) NaOH and 0.1 (M) HCl buffer solutions. The media were also sterilised following the previously mentioned conditions. After sterilisation, the Czapek Dox agar plate was prepared with the sterilised agar media and sterilised Petri plates. The plates were placed inside a laminar airflow chamber for solidification and to avoid any contamination. After the plates were ready, 0.1 mL of the previously incubated *Aspergillus sp.* culture was used to inoculate the plates by the spread plate method. This plate was incubated for seven days in a BOD shaker incubator (Remi, India) at 303 K. After the incubation of the plates, another Czepek Dox broth media was prepared and sterilised while maintaining pH. A single *Aspergillus sp.* colony was

collected from the incubated plate, and the freshly prepared broth media was inoculated and incubated under the same conditions. This broth medium was used for the saccharification of biomass.

4.2.8.1.2. Minimal media preparation: Sodium nitrate (0.2 g/ 100 mL), potassium chloride (0.05 g/ 100 mL), magnesium sulphate (0.05 g/ 100 mL), ferrous sulphate (0.001 g/ 100 mL), dipotassium hydrogen phosphate (0.1 g/ 100 mL), and peptone (2 g/ 100 mL) was measured in a weighing machine (Sartorius, Germany) and mixed with 90 mL DI water in an Erlenmeyer flask to prepare the minimal media. After the solution was prepared, water was added to make the volume 100 mL. 1 g of pretreated biomass was added to the media. While adjusting the pH to 7 stirred on a magnetic stirrer for 15 min and sterilised at 394 K under 15 psi pressure using an autoclave. After sterilisation, the flask was placed in a laminar airflow chamber to avoid any contamination.

4.2.8.1.3. Microbial inoculation and experiment: The prepared fresh culture was used to inoculate the minimal media. 1 mL of the *Aspergillus sp.* culture was pipetted out by using a micropipette and added to the minimal media containing treated biomass. This culture was also incubated for seven days in a BOD shaker incubator (Remi, India) at 303 K temperature. After the incubation period, the flasks with microbe culture were sterilised at 394 K under 15 psi pressure using an autoclave and cooled down to room temperature. Different experimental parameters, viz., inoculation time (5 days- 10 days), pH of the medium (4-10), temperature (298 K- 313 K), microbial dose (1 mL/100 mL- 3 mL/100 mL), and substrate concentration (1 g/100 mL -3 g/100 mL) were varied to study their effect on the reducing sugar production. Total reducing sugar (TRS) content analysis was performed by the DNS method to estimate the concentration of reducing sugar after saccharification (mentioned in section 4.2.8.2).

4.2.8.2. Total reducing sugar (TRS) content estimation: The TRS content in the saccharified media was estimated by the 3,5-Dinitrosalicylic acid (DNS) method. Because of their structure, DNS can detect the presence of a free carbonyl group present in the reducing sugar molecule and take part in a redox reaction. In this reaction, oxidation of the ketone functional group (in the case of fructose) and aldehyde functional group (in the case of glucose) occurred, and the DNSA molecule was reduced to 3-amino-5-nitrosalicylic acid (ANS) that developed a reddish-brown colour in the solution. The

maximum absorbance of this solution was found at a wavelength of 540 nm in a UV-Vis spectrophotometer (PerkinElmer, USA) (Ghosh et al., 2024).

4.2.8.2.1. Reagent preparation: To prepare the DNS solution, 1 g of DNS, 200 mg of crystalline phenol, and 50 mg of sodium sulphite were measured on a weighing machine (Sartorius, Germany) and mixed with 100 mL of 1% NaOH solution under continuous stirring.

Sodium-potassium tartrate solution was prepared by dissolving 40 g of sodium-potassium tartrate in 100 mL of DI water.

4.2.8.2.2. Experiment: After the saccharification was complete, 1 mL of the hydrolysate was collected in a test tube, and 2 mL of DI water was added to it. Following that, 3 mL of DNS solution was added to each sample and mixed thoroughly. After mixing, the test tubes were heated for 10 min. As the heating was complete, the solutions were cooled down to room temperature, and 1 mL of 40% sodium-potassium tartrate solution was added to each test tube. As the reddish-brown colour developed, the absorbance was recorded by a UV-Vis spectrophotometer (PerkinElmer, USA) at 540 nm (Ghosh et al., 2024).

4.2.8.3. Fermentation: Fermentation is the last step of bioethanol production from lignocellulosic biomass. In this process, a microbe (in this study, *Saccharomyces cerevisiae*) is used to break down the produced reducing sugar into ethanol under anaerobic conditions. A detailed description of this study is given below.

4.2.8.3.1. Preparation of microbial culture: For the preparation of *Saccharomyces cerevisiae* culture, which was purchased from MTCC, Yeast Extract-Peptone-Dextrose (YEPD) media was used. To prepare this media, yeast extract (10 g/L), peptone (20 g/L), and dextrose (15 g/L) were mixed with 100 mL of DI water inside an Erlenmeyer flask and stirred for 15 min. pH of the media was adjusted at 7 by using a pH meter (TestR-35, Eutech, USA) and 0.1 (M) NaOH and HCl buffer solutions respectively. After the solution was prepared, it was sterilised at 393 K under 15 psi pressure along with 100 mL of DI water using an autoclave. After sterilisation, the media were cooled down to room temperature and inoculated with the *Saccharomyces cerevisiae* strain. For this inoculation, the powdered bacterial sample was dissolved in the sterilised water, and 1 mL of the water was collected with a sterilised micropipette. This collected DI water, containing bacteria, was used for the inoculation of the YEPD media. This inoculated

media was incubated in a BOD shaker incubator (Remi, India) for five days at 303 K temperature. After incubation, another YEPD medium was prepared with the same composition mentioned previously and bacterial agar (20 g/L). These chemicals were mixed in an Erlenmeyer flask and stirred on a magnetic stirrer to prepare the solution. pH of the media was maintained by using a pH meter (TestR-35, Eutech, USA) and adjusted to 7 using 0.1 (M) NaOH and 0.1 (M) HCl buffer solutions and buffer solutions. Following that, the YEPD media was sterilised at 394 K under 15 psi pressure. After sterilisation, agar plates were prepared by pouring the media into sterilised petri plates under laminar airflow and solidifying them. As the media solidified, it was inoculated using 0.1 mL of the previously prepared culture by the spread plate method. These plates were also incubated for five days at 303 K. After the incubation period, another 100 mL of YEPD broth was prepared and sterilised. The freshly prepared broth was inoculated with a single colony collected from the cultured Petri plates and incubated for five days in a BOD shaker incubator (Remi, India) at 303 K.

4.2.8.3.2. Microbial inoculation and experiment: The previously prepared saccharified media (mentioned in section 4.2.8.1.3) were sterilised and inoculated with 1 mL of *Saccharomyces cerevisiae* culture. Following that, the system was incubated for five days at 303 K in a BOD shaker incubator (Remi, India). After incubation, the culture was sterilised, and the hydrolysate was collected by filtration (Watman-10). The whole process was conducted in a laminar airflow chamber to eliminate any contamination. Different parameters, viz., inoculation time (3 days- 7 days), pH of the medium (4-10), temperature (298 K-313 K), microbial dose (1 mL/ 100 mL- 3 mL/ 100 mL), and substrate concentration (1 g- 5 g) were varied to study their effect on the bio-ethanol production.

4.2.8.4. Estimation of bioethanol in the media: A dichromate titration test was used to estimate the concentration of produced bioethanol. The titration method involves the oxidation of ethanol (C_2H_5OH) to acetic acid (CH_3COOH) using acidified potassium dichromate ($K_2Cr_2O_7$). The excess dichromate is then reacted with potassium iodide (KI) solution producing iodine (I_2). This iodine is subsequently titrated with sodium thiosulphate ($Na_2S_2O_3$). The detailed process is described below.

4.2.8.4.1. Reagent preparation: The first reagent in this experiment is an acid dichromate solution. To prepare this solution, 125 mL of DI water was taken in an Erlenmeyer flask and 70 mL of sulphuric acid (98%) was added. The reagents were mixed

and cooled under tap water. After cooling, 0.75 g of potassium dichromate was added to it. Further DI water was mixed in the solution to make the volume 250 mL. The solution was mixed well and stored.

The indicator of this titration was starch indicator solution. To make the solution 1 g of starch was dissolved in 100 mL of recently boiled water. The mixture was stirred on a magnetic stirrer for homogeneous mixing and stored for future use.

Sodium thiosulphate solution was prepared by adding 7.44 g of sodium thiosulphate to 900 mL of DI water and mixed well on a magnetic stirrer. After that, the volume was made up to l lit. by adding DI water.

To prepare the potassium iodide solution, 5 g of potassium iodide (KI) was dissolved in 25 mL of water and mixed well.

4.2.8.4.2. Experiment: 1 mL of the fermentation broth was added with 25 mL of $K_2Cr_2O_7$ solution in an Erlenmeyer flask and 9 mL of distilled water to make up the volume to 35 mL. Followed by this step, the mixture was heated at 338 K for 25 min. in a water bath. After that, the solution was cooled down to room temperature, and DI water was added to make the volume 50 mL. After incubation, 5 mL of KI solution was added to the mixture. This mixture was titrated against sodium thiosulfate in the presence of a 1 mL starch indicator. The endpoint of the titration was determined by observing the colour change of the indicator from blue to colourless. This reaction is a three-step process. In the first step, the ethanol is oxidised to acetic acid by acidified dichromate solution as shown in equation (4.1). In the second step, as stated by equation (4.2), the excess dichromate ions react with the KI solution, and in the final step, the produced iodine molecules are titrated with thiosulfate solution as stated in equation (4.3).

$$2Cr_2O_7{}^{2-} + 16H^+ + 3C_2H_5OH = 4Cr^{3+} + 11H_2O + 3CH_3COOH \ldots\ldots\ldots \text{(4.1)}$$

$$Cr_2O_7{}^{2-} + 14H^+ + 6I^- = 2Cr^{3+} + 3I_2 + 7H_2O \ldots\ldots\ldots\ldots \text{(4.2)}$$

$$2S_2O_3{}^{2-} + I_2 = S_4O_6{}^{2-} + 2I^- \ldots\ldots\ldots\ldots\ldots\ldots\ldots \text{(4.3)}$$

4.2.8.4.3. Calculation: The data of the dichromate titration was analysed by the stochiometric method. For calculating the concentration of produced ethanol, first, the mol and the molarity of thiosulfate used were calculated by equations (4.4) and (4.5), respectively.

$$Moles\ of\ thiosulphate = \frac{Mass\ of\ thiosulphat\ \ (g)}{molar\ mass\ of\ thiosulphate\ (g\ mol)} \ldots\ldots\ldots\ldots (4.4)$$

$$Molarity\ of\ thiosulphate\ (M) = \frac{Moles\ of\ thiosulphate}{Volume\ of\ solution\ (L)} \ldots\ldots\ldots\ldots (4.5)$$

From equations (4.2) and (4.3), it can be stated that 6 mol of thiosulfate is equivalent to 1 mol of dichromate. Similarly, from equation (4.1), it can be shown that 2 mol of dichromate is equivalent to 3 mol of ethanol. So, 1 mol of thiosulfate is equivalent to 0.25 mol of ethanol. From the experiment, the volume of reacted thiosulfate can be observed, and by applying the stoichiometric equivalence rule, the concentration of ethanol was calculated.

4.2.8.4.4. Optimisation of fermentation: To optimise the fermentation process, response surface methodology (RSM) was performed. The experimental model was created by using the Box-Behnken design and a second-order system. Being a second-order system, the model followed a quadratic equation that was validated by varying different experimental parameters, viz., time (3-7 days), substrate concentration (1g -5g), and microbial dose (1 mL- 3 mL). Design Expert-13 (Version- 7) software was used for this purpose, and a total of seventeen unique combinations of the experimental conditions were investigated. For the ANOVA analysis, all the data of the mentioned seventeen runs were collected and fitted by using the quadratic equation. From the result of this analysis, the validity of the design was established.

4.2.8.5. Furfural production: The previously extracted cellulose (mentioned in section 4.2.3) was considered the raw material of furfural synthesis. To synthesise furfural, 10 mL of 1.5% H_2SO_4 was taken in a hydrothermal reactor, and 1 g of extracted cellulose was added to it. The system was treated under 459 K for 10 min. After the reaction ended, the solution was cooled down, and the supernatant was collected.

To quantify the produced furfural, a High-Performance Liquid Chromatography (HPLC) machine (Waters model- 2489) with a manual injector (model- U6K), and a Waters binary HPLC pump (model- 1525) was used. A UV-Vis detector (model- 2489) was used to detect the quantity of produced furfural. To prepare the sample for HPLC analysis, the collected hydrolysate was passed through a syringe filter with 2% methanol to eliminate any particles present in the media. For analysis, 0.20 mL of the filtered sample was injected manually, and the acetonitrile-water solution was used isocratically as the mobile

phase at a 2 mL/min flow rate. A Sunfire C18 column was used to separate the components. The retention time and peaks were analysed using Breeze software.

To optimise the process of furfural synthesis, eight cellulose samples, one from each parametric combination group, were selected. The parameters, viz., time (10 min.- 30 min.), dose of cellulose (1g/L-3g/L), and concentration of sulphuric acid (1%-2%) were varied to study their effect on furfural synthesis.

4.2.9. Characterisation: Characterisation is a vital step for research to understand the structure and properties of any substance. The proximate analysis, one of the main characterisation processes of the biomass, focuses on the moisture content, volatile matter, ash content, and fixed carbon content, respectively, for sawdust and rice husk. Also, the crystallographic profiling, functional group analysis, elemental composition, and surface morphology of extracted cellulose, hemicellulose, and lignin were studied.

4.2.9.1. Proximate analysis: Proximate analysis of biomass can bring the spotlight on the energy content, combustion characteristics and help in feedstock selection. Thus, this characteristic study is an important part of alternate energy production and value-added product extraction.

4.2.9.1.1. Moisture content: To measure the amount of water present in the biomass, moisture content was analysed. 1 g of biomass was measured using a weighing machine (Sartorius, Germany) and placed inside a hot-air oven at 358 K for two hours. After the sample was completely dried, the final weight was measured. The moisture content was analysed using equation (4.6).

$$Moisture\ content\ (MC) = \frac{Initial\ weight - Fina\ \ weight}{Initial\ weigh}\ x\ 100 \ldots\ldots\ldots\ldots \quad (4.6)$$

4.2.9.1.2. Volatile matter content: 1 g of biomass was packed tightly in an enamel crucible and heated inside a muffle furnace in an anaerobic condition at 1073 K temperature for 2 hours. After the complete combustion of biomass, the leftover was collected, and the weight was recorded. Volatile matter content was measured by equation (4.7).

$$Volatile\ matter\ content\ (VMC) = \frac{Initial\ weight - Final\ weig}{Initial\ weigh}\ x\ 100 \ldots\ldots\ldots\ldots \quad (4.7)$$

4.2.9.1.3. Ash content: Ash is the inorganic content in biomass and primarily consists of silica, calcium, and potassium. To measure the ash content of biomass, the biomass was

dried in a hot air oven at 334 K until it was completely dried. Following that, 1 g of the dried biomass was taken in an enamel crucible and combusted at 1073 K for two hours in the presence of oxygen. After the biomass was completely converted to ash, the residue was collected, and the weight was measured. The ash content of a biomass was calculated by equation (4.8).

$$Ash\ content\ (AC) = \frac{Weight\ of\ ash\ residue\ after\ combustion}{Weight\ of\ dried\ biomass} x\ 100 \ldots\ldots\ldots\ldots \quad (4.8)$$

4.2.9.1.4. Fixed carbon content: The fixed carbon content represents the solid carbon content that remains after combustion and is a key indicator of the energy potential of biomass. The fixed carbon content was calculated by using equation (4.9).

$$Fixed\ carbon\ content\ (FCC) = \{100 - (MC + VMC + AC)\}\% \ldots\ldots\ldots\ldots \quad (4.9)$$

4.2.9.2. Crystallographic characteristics: To analyse the crystallographic structure of extracted products X-ray diffraction (XRD) study was conducted using an X-ray diffractometer (Bruker D-8 advanced, USA). For this analysis, a point detector was used with a scan rate of 2º /min. and a range from 10º to 80º (2Θ). During the sample analysis, the wavelength used was 1.5481 x 10^{-10} m with an operating voltage of 40 kV and a current flow of 40 mA. The data was analysed, and characteristic peaks were detected by using Origin (2018) software. The crystallinity% % was determined by using equation (4.10).

$$\%\ Crystallinity = \frac{Area\ under\ the\ crystallinity\ curve}{Total\ area\ under\ the\ curve}\ x\ 100 \ldots\ldots\ldots \quad (4.10)$$

From the peaks identified in the XRD graph, Miller's indices were calculated by WinplotR software. Also, the d_{hkl} value was calculated using Bragg's law as presented in equation (4.11) to understand the crystal properties.

$$\lambda = 2.\mathrm{dhlk.Sin}\theta \ldots\ldots\ldots\ldots\ldots\ldots\ldots\ldots\ldots \quad (4.11)$$

Here, λ= wavelength of X-Ray (1.5481 x 10^{-10} m), and θ= half of the diffraction angle.

4.2.9.3. Functional group analysis: To analyse the functional groups present on the surface of extracted products, ATR-FTIR (PerkinElmer, Spectrum-2, USA) was performed. A wavelength range of 500-4000 cm^{-1} with a transmission rate of 4 cm/sec was considered. The data was analysed and functional groups were detected by using Origin (2018) software.

4.2.9.4. Surface morphology analysis: The surface morphology of extracted products was analysed by scanning electron microscopy (SEM) (ZEISS EVO MA-10, Germany). As a step of sample preparation, the samples were coated with gold (Au) under high vacuum conditions. This analysis was performed at an acceleration voltage of 20 kV

4.2.9.5. Elemental analysis: To study the elemental composition of the surface, energy dispersive X-ray analysis (EDAX) was performed. EDAX is a technique that analyses the elements present on the surface of any substance. For this study, the samples were coated with gold (Au) under high vacuum conditions and conducted at an acceleration voltage of 20 kV. The detector position for this analysis was tilt (deg) at 0.0, elevation (deg) at 35.0, and azimuth (deg) at 0.0, respectively.

To understand the total elemental nature of the components, CHNS analysis was performed. In this analysis, the main interest was to study the total chemical composition of the material and not only the surface, as this composition has a high influence on fuel production. For the sample preparation, the materials were measured by a weighing machine (Sartorius, Germany) and placed on an aluminium tray. These trays were placed inside the analyser (Elemental, model- Vario micro). The instrument pyrolyses the sample, and the detector detects different oxides produced during pyrolysis and calculates the % of carbon, hydrogen, nitrogen, and sulphur, respectively.

4.3. Result:

4.3.1. Moisture content: The moisture content of raw materials was measured by heating the materials at 358 K for two hours. From the observation, it was stated that the moisture content of rice husk and sawdust was 4% and 3%, respectively. Ahn et al. (2016) reported that the maximum moisture content in sawdust was 16.4% and rice husk was 8.7%, respectively. Another study reported that the moisture content of rice husk was found to be 12%-16%. In this study, the comparatively low moisture content led to more efficiency in these materials for energy generation. As biomass with more moisture content was found to demand more energy for combustion and decreased the efficiency of reactors. Also, moisture significantly decreased biomass's calorific value, making it less effective as a fuel source. Effective moisture content not only enhances combustion efficiency but also improves fuel quality.

4.3.2. Volatile matter content: In this experiment, the volatile matter content of rice husk and sawdust was found to be 47% and 73%, respectively. This result, with a high volatile

matter content, showed their tendency to be easily ignited and burn rapidly. These characteristics made them more suitable for various energy applications. The enhanced combustibility of these materials due to their high volatile matter content made them advantageous for industrial applications for cleaner combustion processes and reduced smoke emission compared to traditional fuels (Andrew and Gbabo, 2015). A previously conducted study reported that the volatile matter content of rice husk can be 62.2% to 68.2% (Mutuku, 2019). Ahn et al. (2016) reported that the volatile matter content of sawdust can be up to 75%. These previously reported results confirmed that the raw materials of this experiment were suitable for energy production.

4.3.3. Ash content: In this experiment, the ash content was 15% and 7% for rice husk and sawdust, respectively. Biomass with low ash content was found to be potentially able to enhance cleaner combustion and higher calorific value. This result could be explained by the spatial distribution in the combustion chamber. High ash content was found to occupy more space in the chamber, making the combustible material less available for burning, resulting in incomplete combustion and increased pollutant emission (Andrew and Gbabo, 2015). Also, higher ash content was reported to cause slagging, fouling, and corrosion within the combustion system. Alkali metals present in the ash stimulated these problems by forming sticky deposits in the chamber (Puri et al., 2024).

4.3.4. Fixed carbon content: The fixed carbon content in this experiment was found to be 34% and 17% in the case of rice husk and sawdust, respectively. Banta and Leon (2018) reported that fixed carbon content could be increased by changing processing methods. The study also reported that the fixed carbon content of sawdust could increase to 26.6%. Fixed carbon content is a vital parameter to understand the suitability of biomass for fuel generation. It was also observed that fixed carbon could influence the combustion temperature of biomass. Biomass containing higher amounts of fixed carbon could be burnt at higher temperatures, making the combustion more efficient and higher heat generation (Jia et al., 2021). It was also reported that fuels with higher fixed carbon content could reduce the emission of pollutants into the atmosphere. As these materials were pyrolysed at a higher temperature, it led to the complete burning of the biomass and reduced the release of incomplete burnt particles (Dalkhsuren et al., 2023).

4.3.5. Extraction of cellulose: After pretreatment, filtration, and washing, the collected solid residue, which contains most of the cellulose of lignocellulosic raw materials, was

dried in a hot air oven at 60°C. After drying, the final weight was measured and recorded. From 1 g of raw material, the maximum collected cellulose was 98%, in the case of 2% NaOH-treated rice husk with sonication. The lowest recovery rate was observed in the case of 6% NaOH-treated non-sonicated sawdust. For each pretreatment, the weight of collected cellulose varied and is represented in Fig. 4.1. This data signified the minimum sample loss in the pre-treatment process and enhanced the acceptance in industrial sectors. In this study, several parameters, viz., type of pretreatment media, the concentration of pretreatment media, type of raw materials, and application of sonic waves were considered. Based on these variations, all the extracted cellulose was categorised into eight different groups and designated with unique codes. All the categories and codes are represented in Table 4.1.

Table 4.1: Cellulose samples prepared by the pretreatment process

Group	**Raw material**	**Treatment process**	**Code**
A	Rice husk	2% NaOH with sonication	RH_2%_NaOH_S
	Rice husk	4% NaOH with sonication	RH_4%_NaOH_S
	Rice husk	6% NaOH with sonication	RH_6%_NaOH_S
B	Rice husk	2% NaOH without sonication	RH_2%_NaOH_NS
	Rice husk	4% NaOH without sonication	RH_4%_NaOH_NS
	Rice husk	6% NaOH without sonication	RH_6%_NaOH_NS
C	Rice husk	2% H_2SO_4 with sonication	RH_2%_H_2SO_4_S
	Rice husk	4% H_2SO_4 with sonication	RH_4%_H_2SO_4_S
	Rice husk	6% H_2SO_4 with sonication	RH_6%_H_2SO_4_S

D	Rice husk	2% H_2SO_4 without sonication	RH_2%_H_2SO_4_NS
	Rice husk	4% H_2SO_4 without sonication	RH_4%_H_2SO_4_NS
	Rice husk	6% H_2SO_4 without sonication	RH_6%_H_2SO_4_NS
E	Sawdust	2% NaOH with sonication	SD_2%_NaOH_S
	Sawdust	4% NaOH with sonication	SD_4%_NaOH_S
	Sawdust	6% NaOH with sonication	SD_6%_NaOH_S
F	Sawdust	2% NaOH without sonication	SD_2%_NaOH_NS
	Sawdust	4% NaOH without sonication	SD_4%_NaOH_NS
	Sawdust	6% NaOH without sonication	SD_6%_NaOH_NS
G	Sawdust	2% H_2SO_4 with sonication	SD_2%_H_2SO_4_S
	Sawdust	4% H_2SO_4 with sonication	SD_4%_H_2SO_4_S
	Sawdust	6% H_2SO_4 with sonication	SD_6%_H_2SO_4_S
H	Sawdust	2% H_2SO_4 without sonication	SD_2%_H_2SO_4_NS
	Sawdust	4% H_2SO_4 without sonication	SD_4%_H_2SO_4_NS
	Sawdust	6% H_2SO_4 without sonication	SD_6%_H_2SO_4_NS

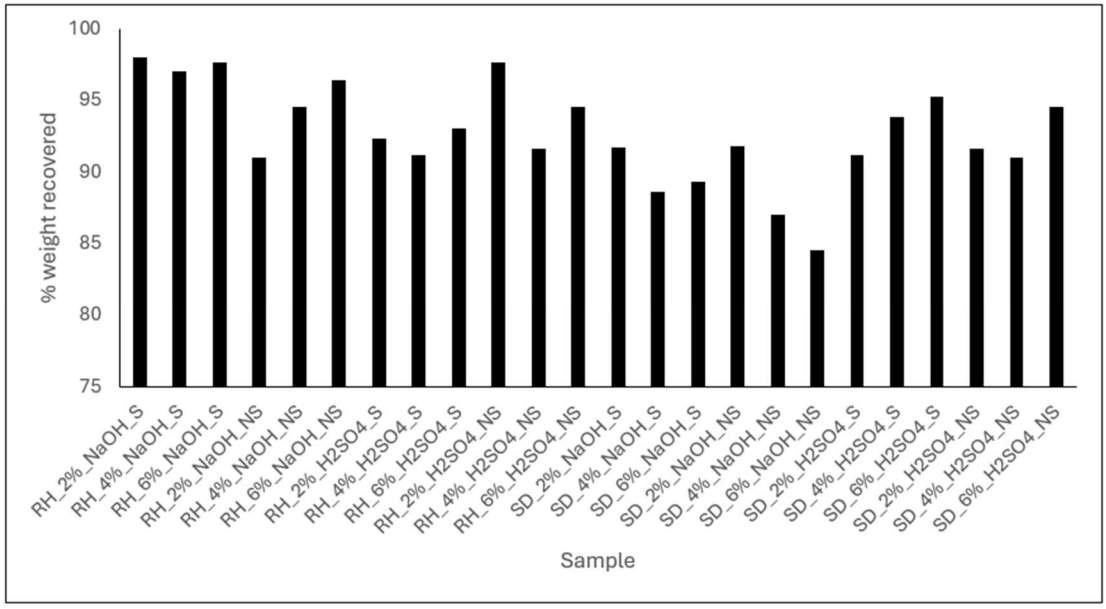

Figure 4.2: Percentage of biomass recovery for each pre-treated biomass

4.3.6. Cellulose content analysis: To analyse the cellulose content in the pretreated biomass, the anthrone test was performed. As shown in Fig. 4.2, it could be stated that in every condition of pre-treatment, the content of cellulose increased after sonication. Because of the vibrational frequency of the sonication process, the chemical bonds present in the biomass ruptured and became exposed to the chemicals of the pre-treatment media. A study reported that before ultrasonic treatment, rice straw showed a cellulose yield of 27.19%, which increased to 63.84% after sonication (Ratnakumar et al., 2022). One of the main effects of ultrasonication is the enhancement of chemical reactions or the choice of certain reaction pathways (Bussemaker and Zhang, 2013). In the presence of ultrasound, water performed a sonochemical process and the H-O bond was cleaved, resulting in a hydroxyl radical and hydrogen. These radicals then initiated reactions to produce hydrogen gas, hydrogen peroxide, and oxygen gas, or recombined to produce water (Mason, 2002; Adewuyi, 2005). In this experiment, the highest cellulose yield was found in the case of SD_4%_NaOH_S, and the value was 958.88 mg/g, and the lowest cellulose concentration was found to be 101.48 mg/g in the case of RH_2%_NaOH_NS. As sonication broke the chemical bonds present in the biomass, the materials became easily accessible for delignification. Also, as mentioned before, the sonochemical reaction of water produces hydroxyl ions and caused a right shift of reaction equilibrium in NaOH-containing pre-treatment media and a greater yield of cellulose. Like alkali-treated biomass, acid treatment with sonication also showed a higher yield compared to a sample without sonication. Though the cellulose yield of acid-treated sonicated biomass

was less than alkali-treated sonicated biomass, which could be explained by the reaction of -OH ions produced during the sonochemical reaction of water, and the proton released from acid, this medium also affected the yield for cellulose production. During sonication, as water molecules broke into hydroxyl ions, they reacted with the proton released by the sulfuric acid present in the media. Unlike alkaline media, this condition caused a left shift of the reaction equilibrium and slowed down the chemical process. From Fig. 4.2, it could be stated that for the acid-treated biomass, cellulose yield increased significantly after sonication, representing the importance of this process in pre-treatment.

Another trend shown in the mentioned figure was the relationship between the cellulose concentration and the increasing concentration of pre-treatment media. Initially, the yield of cellulose increased due to the separation of lignin and hemicellulose from the biomass. This could be explained by the reaction kinetics. As the media concentration increased, the equilibrium of the reaction underwent a right shift, enhancing the product formation. But, after a point of concentration, the yield slightly decreased. The most appropriate explanation is that with 6% media concentration, the reagent degraded cellulose by breaking the chemical bonds.

From this analysis, the pretreated biomass with the highest cellulose yield, viz., RH_4%_H_2SO_4_NS (436.29 mg/g), RH_6%_H_2SO_4_NS (332.96 mg/g), RH_4%_H_2SO_4_S (823.7 mg/g), RH_6%_H_2SO_4_S (832.96 mg/g), RH_4%_NaOH_NS (438.51 mg/g), RH_6%_NaOH_NS (447.77 mg/g), RH_2%_NaOH_S (851.48 mg/g), RH_4%_NaOH_S (899.63 mg/g), SD_4%_H_2SO_4_NS (342.22 mg/g), SD_6%_H_2SO_4_NS (353.33 mg/g), SD_4%_H_2SO_4_S (923.7 mg/g), SD_6%_H_2SO_4_S (892.22 mg/g), SD_4%_NaOH_NS (751.48 mg/g), SD_6%_NaOH_NS (740.37 mg/g), SD_2%_NaOH_S (958.51 mg/g), and SD_4%_NaOH_S (958.88 mg/g) respectively was selected for saccharification.

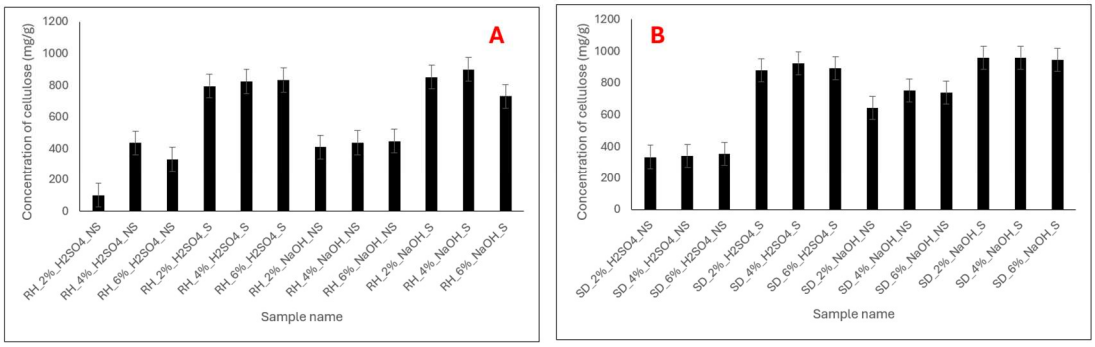

Figure 4.3: Cellulose content of pre-treated (A) rice husk, and (B) sawdust determined by anthrone test.

4.3.7. Total reducing sugar (TRS) content analysis: The pretreated biomass was treated with *Aspergillus sp.* previously isolated in the laboratory, and reducing sugar was produced from the extracted cellulose. The total reducing sugar content of the biomass was estimated by the DNS (di-nitro salicylic acid) method, and the change in TRS production with the change of different experimental parameters was investigated.

4.3.7.1. Effect of biomass type: As shown in Fig. 4.3 (A) and (B), the nature of biomass influenced the total reducing sugar content. It was found that SD_4%_H_2SO_4_S had the highest TRS yield, with a value of 24.84 mg/g. A previous study reported that 88 mg/ml sugar production from sawdust, which was treated with 2.5% (V/V) H_2O_2 (Rubaay and Ali, 2022). In the case of rice husk, the highest TRS yield was found to be 20.02 mg/g for RH_2%_NaOH_S. A study reported 47.34% of TRS from rice husk hydrolysate treated with the alkaline solution at 394 K for 3 hours (Lin et al., 2022). This variation of TRS output could be explained by considering the composition of raw biomass. Depending on the biomass type, the chemical composition of the raw material differed. Cellulose, the main carbohydrate backbone of biomass, is surrounded by a sheet of lignin, and hemicellulose plays a role in binding the cellulose backbone to lignin. This binding strength differs depending on the nature of the raw materials, and the degree of TRS production differs for this reason.

4.3.7.2. Effect of sonication: Another parameter influencing the TRS content was sonication. As mentioned in the previous paragraph, Fig. 4.3(A) and (B) show that the application of sonic waves increased the TRS yield of biomass. Sonication significantly improved biomass delignification. Ziaei-Rad et al. (2023) reported that ultrasound at frequencies between 20 kHz and 50 kHz could improve the removal of lignin from raw materials. Another study reported that after applying sonication, the sugar extraction rate

from potato peels increased significantly (Bhattacharyya et al., 2013). In the current study, the highest TRS yield before sonication was 17.26 mg/g from SD_6%_NaOH_NS. On the other hand, after sonication, it was increased to 24.84 mg/g. Gul et al., (2023) reported that sonication caused a more uniform distribution and smaller particle size of the biomass and affected the production of various derivatives.

4.3.7.3. Effect of treatment time: In this current study, the saccharified media were collected in 5, 7, and 10-day intervals. It was observed that initially, with the increase in saccharification time duration, the yield of TRS also increased. The highest TRS content was observed in the case of SD_2%_NaOH_S, and the value was 20.89 mg/g after 7 days of saccharification. In every scenario, it was observed that from 7 to 10 days, the production of reducing sugar slightly declined. As reported by Sivamani et al. (2022), with the increasing treatment time, several inhibitory complexes, viz., furfural and hydroxymethylfurfural (HMF), could be synthesised in the reaction media, resulting in a decline in the rate of TRS production. The change in TRS production rate with respect to treatment time is represented in Fig. 4.3 (C) and (D). Timung et al. (2016) reported a study using sugarcane bagasse and observed similar results, supporting the findings of the current study. The mentioned study reported that the highest TRS yield was found to be 296.64 mg/g from sugarcane bagasse.

4.3.7.4. Effect of pH: As shown in Fig. 4.3 (E) and (F), the pH of the media affected the TRS yield significantly. As reported by Lin et al. (2022), β-glucosidase is an enzyme responsible for reducing sugar production functions at a pH of 5 to 7. Another enzyme, called cellulase, is present in *Aspergillus sp*. and was reported to have an optimal pH of 5 to 6.5 (Prasetyo et al., 2009). According to the figures, the highest TRS yield was observed at the neutral pH. Both in acidic and alkaline conditions, the yield declined, which was explained by the denaturation of the cellulase enzyme at extreme pH. In the case of SD_4%_H_2SO_4_S, the highest TRS yield was observed during this study. At pH 7, it showed 24.84 mg/g TRS production. Evate et al. (2023) reported that at pH 6.11, pineapple peel biomass showed the highest TRS production after 48.88 hours.

4.3.7.5. Effect of temperature: Temperature showed a significant effect on TRS production from cellulose. As shown in Fig. 4.3 (G) and (H), the highest TRS yield was found at 30^{o}C. Being a biological process, the TRS yield of the substrate was highly dependent on the growth of microbes (*Aspergillus sp.*) and enzymatic activity (Lin et al.,

2022). In both extreme temperatures (298 K and 313 K), the TRS yield decreased significantly, and the highest yield was observed at 30ºC. In the case of this study, the highest TRS yield at 303 K was observed for SD_4%_H_2SO_4_S with a value of 24.84 mg/g. For the same biomass, 6.47 mg/g, 13.79 m/g, and 7.38 mg/g TRS yield was observed at 398 K, 308 K, and 313 K temperatures, respectively. This observation can be explained by the enzymatic activity under different temperatures. At very high and low temperatures, microbial growth ceased, and the activity of the enzyme declined either due to inactivity or denaturation, resulting in a decreased yield of TRS production (Nashiruddin et al., 2022). Mannaa and Kim (2018) reported that although the cellulase enzyme showed the highest activity at 45ºC, prolonged exposure to the enzyme at this temperature can cause thermal inactivation of the biochemical process.

4.3.7.6. Effect of biomass concentration: The increase in substrate concentration also affected TRS production. In every scenario, it was observed that the increase in substrate concentration increased TRS yield. The effect of substrate concentration on TRS yield is shown in Fig. 4.3 (I) and (J). As mentioned in the figure, the highest TRS was produced in the case of SD_4%_H_2SO_4_S, with the value of 35.38 mg/g from 3g/ 100 mL biomass concentration. For the same sample, 24.84 mg/g and 27.53 mg/g TRS yield were observed for 1g/100 mL and 2g/100 mL substrate concentration.

A previously conducted study used Pennisetum grass and saccharified the biomass using *Aspergillus fumigatus.* It was found that with increasing biomass concentration, the TRS yield increased significantly up to 396 mg/g (Mohapatra et al., 2018). Mrudula and Murugammal (2011) reported that the enzymatic activity of cellulase extracted from *Aspergillus sp.* increased with the increasing concentration of substrate till 1:10 (w/v) dilution. Another study conducted by Agabo-Garcia et al. (2023) used *Aspergillus awamori* for the valorisation of *Rugulopteryx okamurae,* a brown alga, and found a maximum of 240 g/kg TRS yield from the mentioned biomass. This phenomenon can be explained by the availability of more active sites with increasing substrate concentration. As the biomass concentration increased, more active sites present on the biomass surface became exposed to the enzyme for enzymatic reactions. Thus, the production of TRS also increased.

4.3.7.7. Effect of microbial dose: The effect of microbial dose on TRS production is shown in Fig. 4.3 (K) and (L). From the graphical representation, it could be stated that

the TRS yield with increasing microorganisms initially increased and then slightly declined. The highest TRS yield was observed in the case of SD_4%_H_2SO_4_S and was found to be 26.82 mg/g with 3 mL/ 100 mL of microbial concentration. For the same substrate, 24.84 mg/g and 24.75 mg/g TRS yield were found in the case of 1 mL/ 100 mL and 5 mL/ 100 mL microbial concentration. On the other hand, RH_4%_NaOH_NS showed the lowest TRS yield with a value of 7.77 mg/g while treated with 5 mL/ 100 mL microbial concentration. As the microbial concentration increased in the medium, the availability of cellulase also increased, increasing TRS yield. But in higher concentrations, the competition of microorganisms increased, resulting in a decline in the TRS content.

From the TRS analysis, a total of eight cellulose samples, viz., RH_6%_H2SO4_NS, RH_4%_H2SO4_S, RH_6%_NaOH_NS, RH_2%_NaOH_S, SD_6%_H2SO4_NS, SD_4%_H2SO4_S, SD_6%_NaOH_NS, and SD_2%_NaOH_S, were selected for fermentation and further studies.

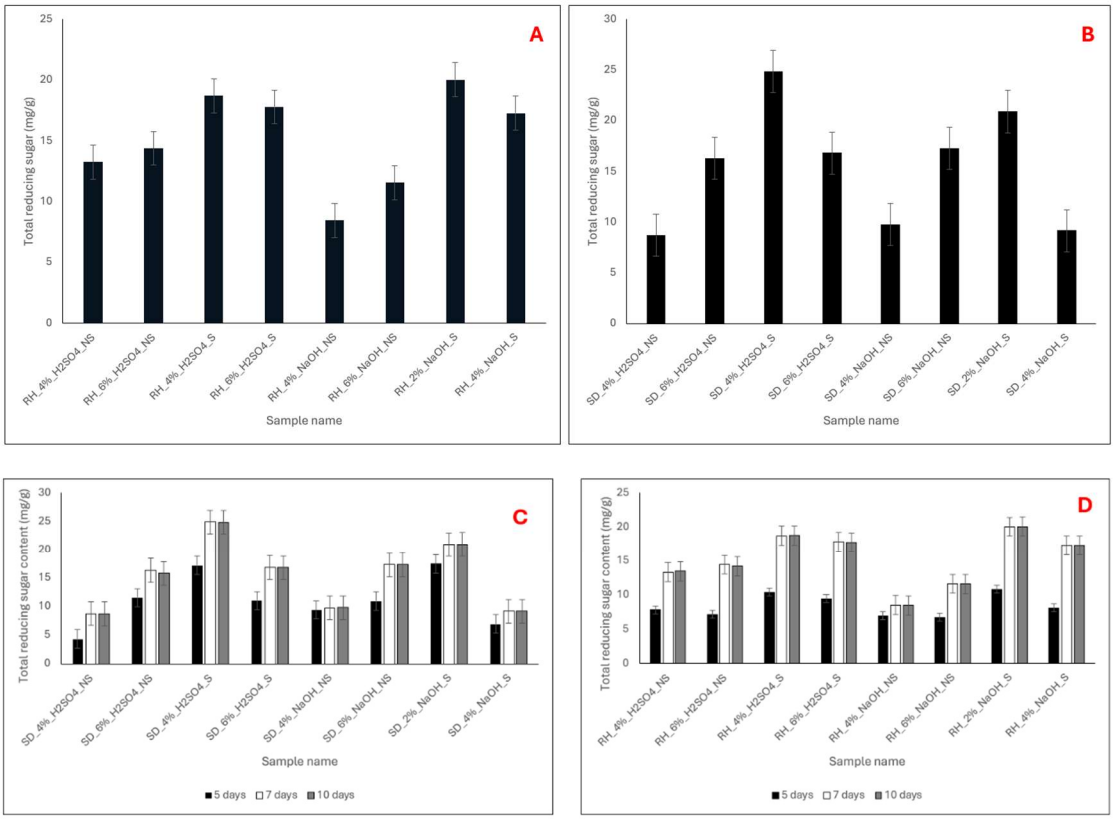

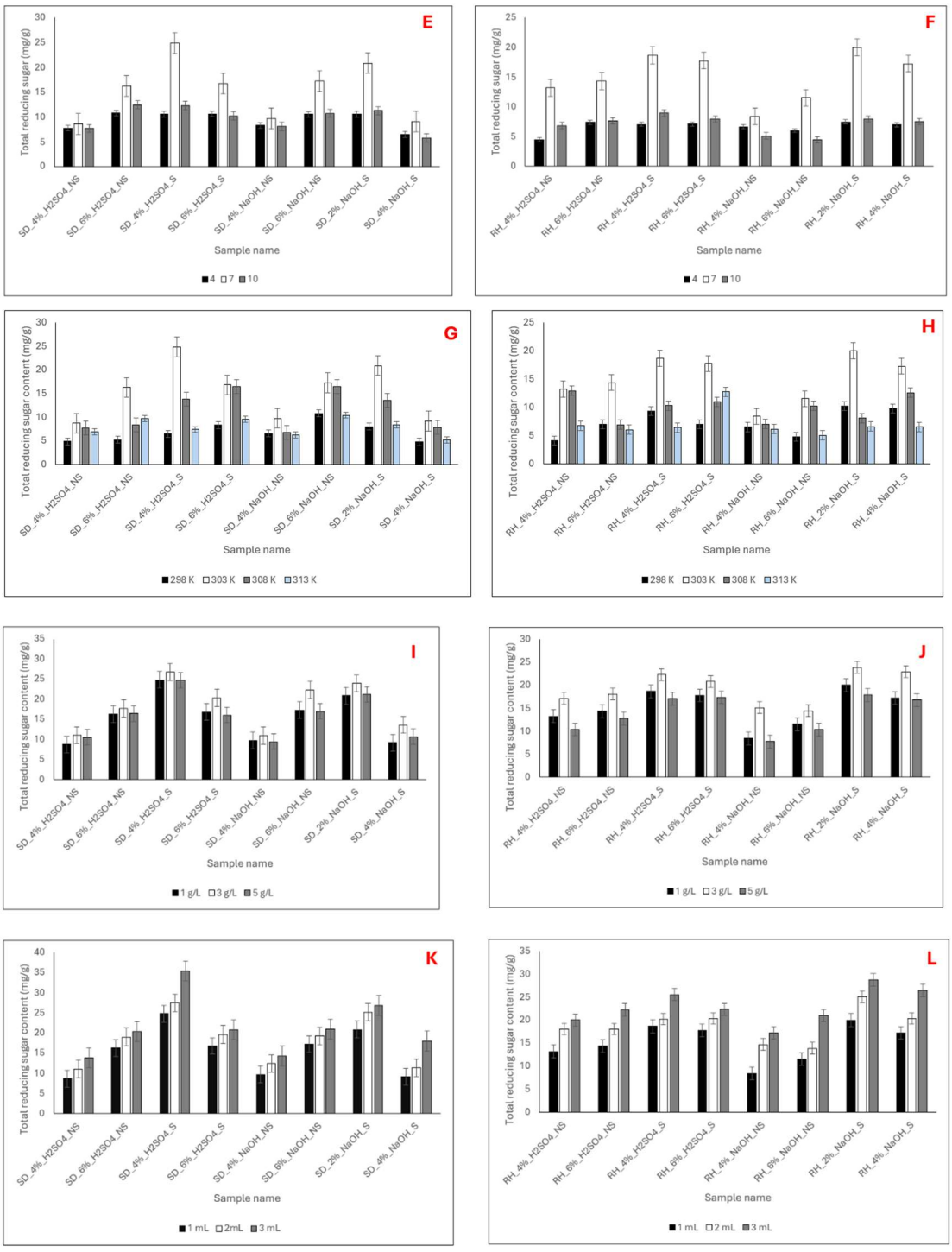

Figure 4.3: Effect of biomass type and sonication (A and B), treatment time (C and D), pH of media (E and F), temperature (G and H), biomass dose (I and J), and microbial concentration (K and L) on TRS production by saccharification.

4.3.8. Bioethanol content analysis: After saccharification, the media were sterilised at 15psi pressure and 120ºC. The saccharified hydrolysate was separated from the solid biomass by filtration and collected in a sterilised Erlenmeyer flask. *Saccharomyces cerevisiae* culture was added to the hydrolysate for bioethanol production by fermentation. Different parameters were varied to investigate their effect on the

bioethanol yield. The dichromate titration method was used to quantify the produced ethanol.

4.3.8.1. Effect of reaction time: Fig. 4.4 (A) represents the effect of reaction time on bioethanol production. As shown in the figure, the ethanol content increased from 3 to 5 days of treatment but decreased on day 7. Dimos et al. (2019) investigated the effect of various experimental parameters on bioethanol production from cotton stalks and reported that after 80 hours of treatment, the ethanol production reached a saturation point. Another study performed by Siregar and Amraini (2019) reported that the production of bioethanol from empty fruit bunches can reach equilibrium after 5 days of treatment with *Saccharomyces cerevisiae*.

After 7 days of fermentation, some dead fungal biomass was observed in the medium, resulting in a decline in the bioethanol production yield. A similar result was reported by Suleman et al. (2016) while producing bioethanol from sugarcane juice. Apart from the life cycle of the fungus, another limiting factor for bioethanol production was the presence of inhibitory compounds. Compounds like hemicellulose and HMF present in the media inhibited ethanol production. In the current study, the highest ethanol was produced from SD_6%_H_2SO_4_NS with a value of 3.24 mg/g of biomass after five days of fermentation. Also, the lowest yield was found in the case of RH_4%_H_2SO_4_S after three days of fermentation.

4.3.8.2. Effect of pH: Fig. 4.4 (B) showed the effect of different pH on the fermentation process and the yield of bioethanol. In every scenario, it was found that the highest ethanol content was observed at pH 7. In this study, the highest ethanol was found to be produced from SD_6%_H_2SO_4_NS, with the value of 3.24 mg/g of biomass. On the other hand, the lowest bioethanol content was found in the case of RH_4%_H_2SO_4_S with a value of 0.27 mg/g of biomass. Being a biological process, pH had a great impact on the fermentation process. Bajpai and Margaritis (1987) produced ethanol from Jerusalem artichoke extract using *Kluyveromyces marxianus* and found pH 5 as the optimum pH for the process. At extreme pH, viz., 4 and 10, the enzymatic activity of *Saccharomyces cerevisiae* ceased and caused a decline in ethanol production. In the neutral environment Wang et al., (2021) reported that at lower pH, the free H^+ ions present in the media inhibited the necessary enzymes required for fermentation. Conversely, it was found that

at higher pH, the environment inhibited the growth of *Saccharomyces cerevisiae,* causing a decline in bioethanol production (Bajpai and Margaritis, 1987).

4.3.8.3. Effect of biomass concentration: The effect of biomass concentration on ethanol production is represented in Fig. 4.4 (C). From the figure, it was stated that with the increasing biomass, in every scenario, the ethanol content increased. Increasing biomass concentration enhanced bioethanol yield, but at extremely high concentrations, microbial cells were exposed to competition for space and decreased the ethanol production (Shukla et al., 2023). El-Mekkawi et al. (2019) explained the interaction between bioethanol production kinetics and substrate concentration. According to the mentioned study, longer fermentation time resulted in a higher bioethanol yield at optimal biomass concentration, but with excessive biomass, the rest of the parameters should be optimised to maintain ethanol production. This study also reported that, by using algal biomass as the raw material, 18.57 g/L ethanol was produced for 98.7 g/L biomass concentration. But with a 100 g/L concentration of algal biomass, the production declined to 11.46 g/L. In the current study, the highest production of ethanol was found at 3 g/100 mL biomass concentrations among all scenarios. The highest amount of ethanol was produced from RH_6%_NaOH_NS with a value of 4.76 mg/g of biomass. The lowest yield was observed in the case of the RH_4%_H_2SO_4_S sample, and the yield was 1.62 mg/g of biomass.

4.3.8.4. Effect of microbial dose: Being a biological process, the dose of microorganisms had a great impact on the final output of fermentation. Fig. 4.4 (D) showed the effect of *Saccharomyces cerevisiae* on the bioethanol production. From the figures, it could be stated that the yield of bioethanol increased initially with the increase of microbial dose but declined at a higher dose. From the research conducted before, it was found that lower microbial concentration could lead to lower ethanol yield due to inadequate conversion of sugar and insufficient fermentation activity. Conversely, a very high dosage could initiate competition among the cells and result in competitive inhibition. The limitations of space and resources could cause stress inside the cell and decrease ethanol production (El-Mekkawi et al., 2019). Another study reported that for a long-time duration of fermentation, higher microbial dosage could decline ethanol production as initially produced ethanol inhibited the microbial biomass from performing further fermentation (Hackmann and Firkins, 2015). In this study, the highest ethanol

concentration was found in the case of SD_6%_H_2SO_4_NS with 1 mL microbial dose/100 mL solution, and the ethanol concentration was 3.24 mg/g of biomass.

4.3.8.5. Effect of temperature: Temperature played a very important role in the fermentation process. As microbial growth kinetics is dependent on environmental temperature, the optimised temperature is important to get the maximum ethanol yield. From previous research, it could be found that the optimum temperature range for *Saccharomyces cerevisiae* to produce ethanol was between 303 K to 307 K. Bajpai and Margaritis (1987) reported that above 307 K, the ethanol production yield started to decline due to increased glycerol production and environmental stress. Abarca-Rivas et al. (2023) reported that at lower temperatures, the growth of *Saccharomyces cerevisiae* could be ceased and took a long time to complete the fermentation. For the current study, the effect of temperature on ethanol production is shown in Fig. 4.4 (E). From the figure, it was observed that for every cellulose sample, 303 K temperature was the optimum to produce ethanol. The maximum ethanol concentration was found to be 5.84 mg/g of biomass in the case of RH_6%_NaOH_NS.

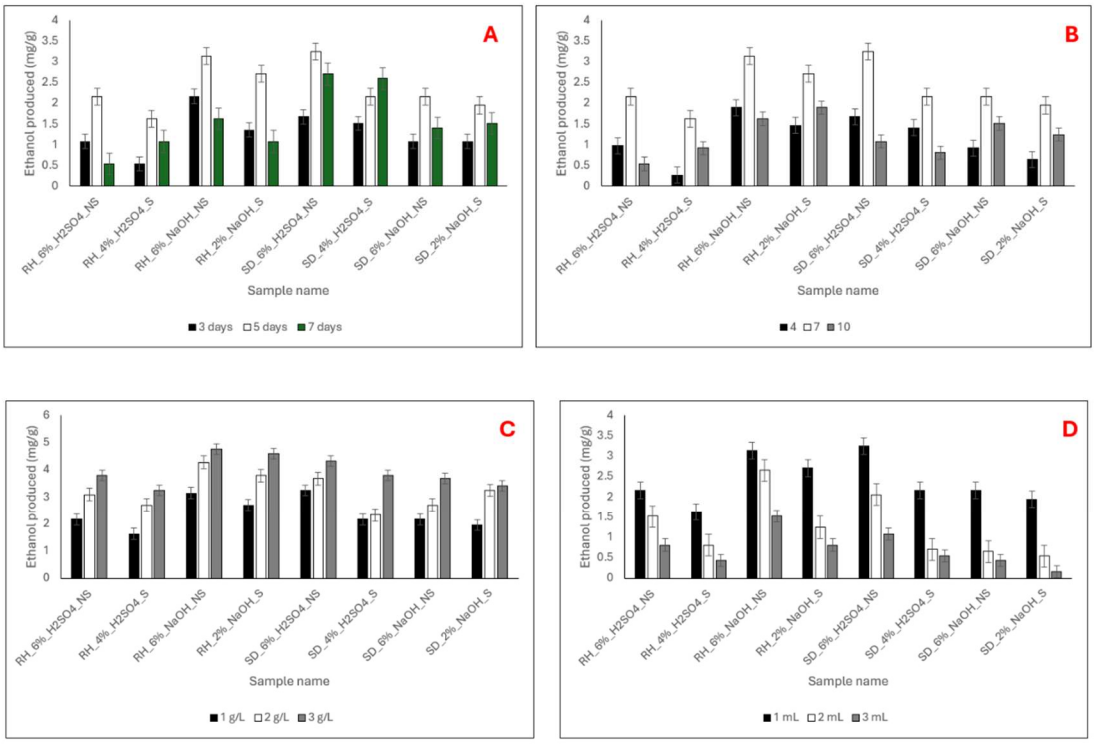

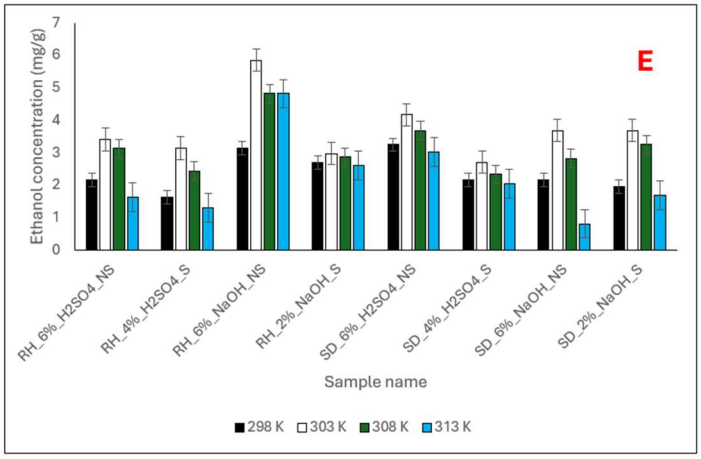

Figure 4.4: Effect of treatment time (A), pH of media (B), biomass dose (C), microbial concentration (D), and temperature (E) on bioethanol production by fermentation.

4.3.8.6. Optimisation of fermentation: To optimise the bioethanol production by fermentation, a Response Surface Methodology (RSM) study was performed (Aydar, 2018). A quadratic equation, presented as equation (4.12), was used to analyse and validate the experimental design.

$$R = 2.5 + 0.1 * A + 0.2875 * B + 0.3125 * C + 0.175 * AB - 0.0325 * AC + 0.1 * BC - 1.08 * A^2 - 0.3 * B^2 - 0.1 * C^2 \quad \text{(4.12)}$$

Here, A, B, C, and R are reaction time (days), microbial dose (mL/100 mL), substrate concentration (g/100mL), and bioethanol concentration (mg/g of biomass), respectively.

4.3.8.6.1. Validation of the model: From the ANOVA analysis, it was observed that this model was significant with a P-value of 0.0006 (<0.05) and an F-value of 17.1 (>12). The correlation coefficient (R^2) value of the mentioned model was 0.95. The R^2 value also indicated that the predicted and observed data of this experiment were in reasonable agreement, with the value of 4.84 mg/g and 4.32 mg/g, respectively, indicating the significance of the model.

Fig. 4.5 (A) represents the residual plot confirming the model of fit for this design. Residuals are the difference between the experimental and predicted values of a model. From the mentioned figure, it could be stated that all the residual values were evenly distributed on both sides of the straight line, signifying the probability distribution of the residual values from the trend line. This result further confirmed the acceptability of the model. As stated in Fig. 4.5 (B), the predicted and actual values exhibited the minimum deviation from the trend line (Altınışık et al., 2024). The interaction of predicted and experimental values was represented in Fig. 4.5 (C). From the graph, it could be stated

that the experimental values were almost evenly distributed throughout the straight line, increasing the acceptance of this model.

4.3.8.6.2. Response of time and microbial dosage: The response of time and microbial dosage is presented in Fig. 4.5 (D). The graph showed that the optimum bioethanol yield was observed at 2 mL /100 mL microbial dosage after 5 days of fermentation. The maximum yield of ethanol under these conditions was found to be 2.57 mg/g of biomass. Being a biological process, fermentation showed a maximum yield at a mid-point of the parameter's range, rather than in extreme limits (Kamal et al., 2021).

4.3.8.6.3. Response of microbial dosage and biomass concentration: In Fig. 4.5 (E), the response of microbial dosage and biomass concentration is presented. From the figure, it could be stated that at the microbial dose of 2 mL/ 100 mL and 2 g/100 mL biomass concentration, the optimum ethanol output was achieved. The optimum amount of bioethanol produced in these conditions was 2.85 mg/g of biomass. This result was observed as the yeast cells were in close contact with sufficient nutrients, which ignored the competition but inhibited any adverse effect. (Kopsahelis et al., 2007).

4.3.8.6.4. Response of biomass concentration and time: The crosstalk between biomass concentration and incubation time is represented in Fig. 4.5 (F). From the figure, it was observed that at an incubation time of 5 days and 2 g/100mL biomass concentration, the highest ethanol yield was achieved. The optimum bioethanol concentration in this experiment was 2.37 mg/g of biomass. Like the previously described conditions, this condition also showed the optimum value at the mid-point of the parameter's range for the same reason (Azhar et al., 2017).

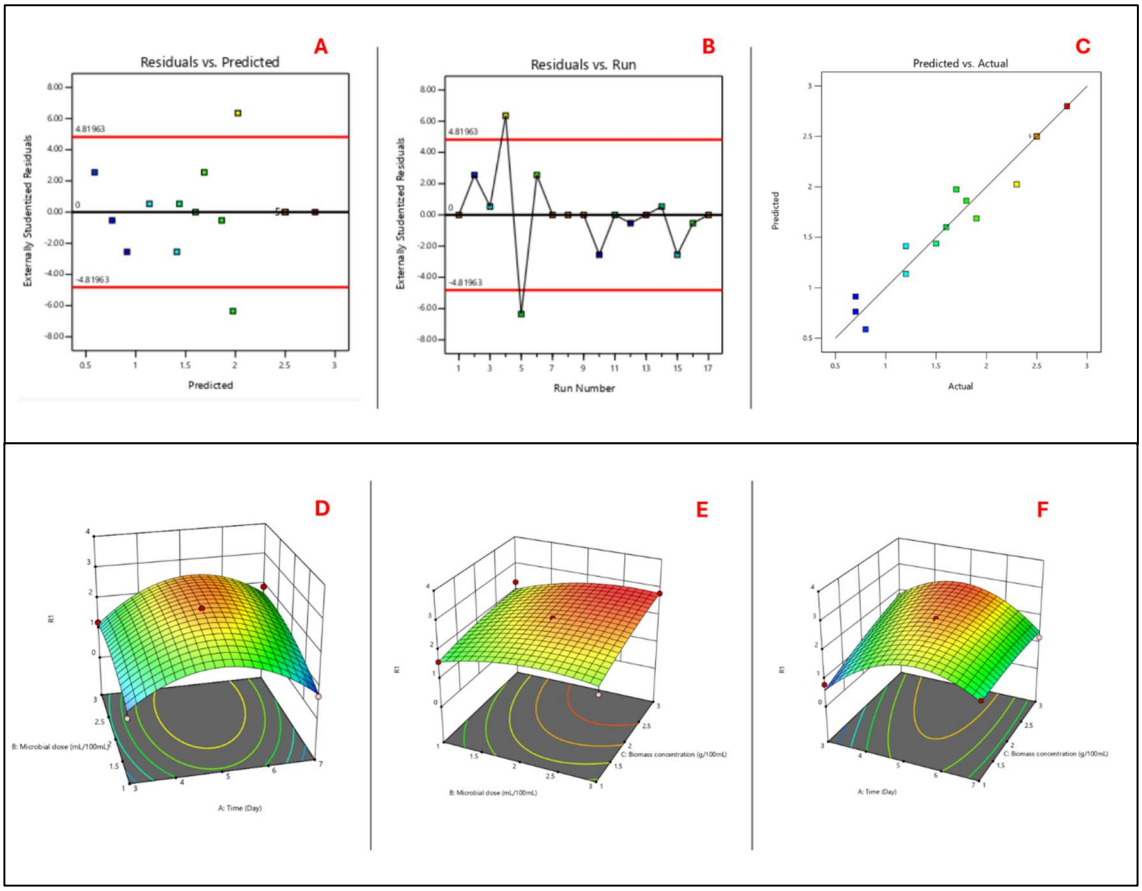

Figure 4.5: Optimization of bioethanol production by fermentation process using Response Surface Methodology representing (A and B) The model fit of the design, (C) comparison of actual and predicted result, (D) response of time and microbial dose, (E) response of microbial dose and biomass concentration, (F) response of time and biomass concentration.

4.3.9. Production of Furfural from extracted cellulose: In this study, hydrothermal treatment of cellulose was performed with sulphuric acid to produce furfural. Under high temperature and pressure, sulphuric acid oxidised cellulose and the dark brown hydrolysate was collected, which contained furfural. The furfural concentration was measured by high-performance liquid chromatography (HPLC) as shown in Fig. 4.6 (A). The effect of different parameters on furfural production was investigated.

4.3.9.1. Effect of biomass type: Four different cellulose samples with the highest cellulose concentration (section 4.3.6), viz., RH_4%_H_2SO_4_NS, RH_6%_H_2SO_4_S, RH_6%_NaOH_NS, RH_4%_NaOH_S, SD_6%_H_2SO_4_NS, SD_4%_H_2SO_4_S, SD_4%NaOH_NS, and SD_4%_NaOH_S, were used in this study. Fig. 4.6 (B) represents the effect of biomass type on furfural production. From the figure, it could be stated that the highest furfural yield in this experiment was observed in the case of the RH_4%_NaOH_S sample with a value of 15.12%. Binder et al. (2010) reported furfural production from xylan and xylose, respectively. It was found that 24% of furfural was

produced from xylose after 2 hours of treatment while using $CrCl_2$ as a catalyst at 373 K temperature. On the other hand, in the case of xylan, a 4% yield was reported while using $CrCl_3$ as a catalyst at 393 K. Another study had investigated the conversion of microcrystalline cellulose to furfural using sonic waves. It was found that with 4 mol/L HNO_3 media at 303 K temperature, a sonication of 60 min resulted in a 78% conversion yield (Santos et al., 2018). The structure and cellulose distribution, as well as the purity of extracted cellulose, depend on the type of raw materials. Hence, depending on the cellulose concentration present in the sample, the furfural content varied.

4.3.9.2. Effect of treatment time: Three different time durations, viz., 10 min., 20 min., and 30 min., were considered for this experiment, and the effect of treatment time is represented in Fig. 4.6 (C). From the figure, it was observed that in every scenario, the yield of furfural increased with increasing treatment time. For RH_6%_H_2SO_4_S cellulose, the least furfural production yield was observed with the value of 3.95% after 10 min. of treatment. Maintaining the same conditions, RH_4%_NaOH_S generated the highest furfural production yield with the value of 17.35% after treating for 30 min. Jiang et al. (2021) reported that a furfural production yield of 85% was achieved by treating the biomass under 454 K temperature for 1 hour. Ong and Sashikala (2007) reported that acid hydrolysis of rice husk with 10% sulphuric acid at 498 K showed a furfural yield of 15g/kg. This observation could be explained by the reaction kinetics of the process. With the increasing time duration, the substrate got enough time to reach the equilibrium and complete the reaction. So, with the increasing time, the concentration of furfural also increased.

4.3.9.3. Effect of cellulose concentration: Fig. 4.6 (D) represents the furfural production in different cellulose concentrations. Three concentrations, viz., 1g/L, 2g/L, and 3g/L are considered the concentration of interest. From the figure, it can be stated that in every scenario, the concentration of furfural increased with increasing cellulose concentration. This observation can be explained by the increasing concentration of cellulose makes more substrate available for the reaction, shifting the reaction equilibrium to the left, and increasing the product concentration. The highest furfural concentration in this experiment was 13.87% from 3g/L RH_4%_H_2SO_4_NS. For comparison, Lacerda et al. (2015) reported the highest furfural yield to be 9.96% from cellulose as a raw material and using ChCl/oxalic acid and TiO_2 as media and catalyst, respectively.

4.3.9.3. Effect of acid concentration: The effect of acid concentration on furfural production is presented in Fig. 4.6 (E). 1%, 1.5%, and 2% (v/v) sulphuric acid solutions were used to study the effect of the mentioned parameter, respectively. With the increasing concentration, it was observed that initially, the furfural% increased and then slightly decreased at 2% sulphuric acid concentration. This observation can be explained by the reaction of furfural with excess acid reagent. As a previously conducted study reported, furfural can be converted to furoic acid and maleic acid by oxidation (Zhang et al., 2021). In the current study, it was observed that the highest furfural concentration achieved was 15.74% from RH_4%_NaOH_S with 1.5% acid concentration. The lowest concentration was found to be 3.51% from RH_6%_H_2SO_4_S while treating it with a 2% sulphuric acid solution.

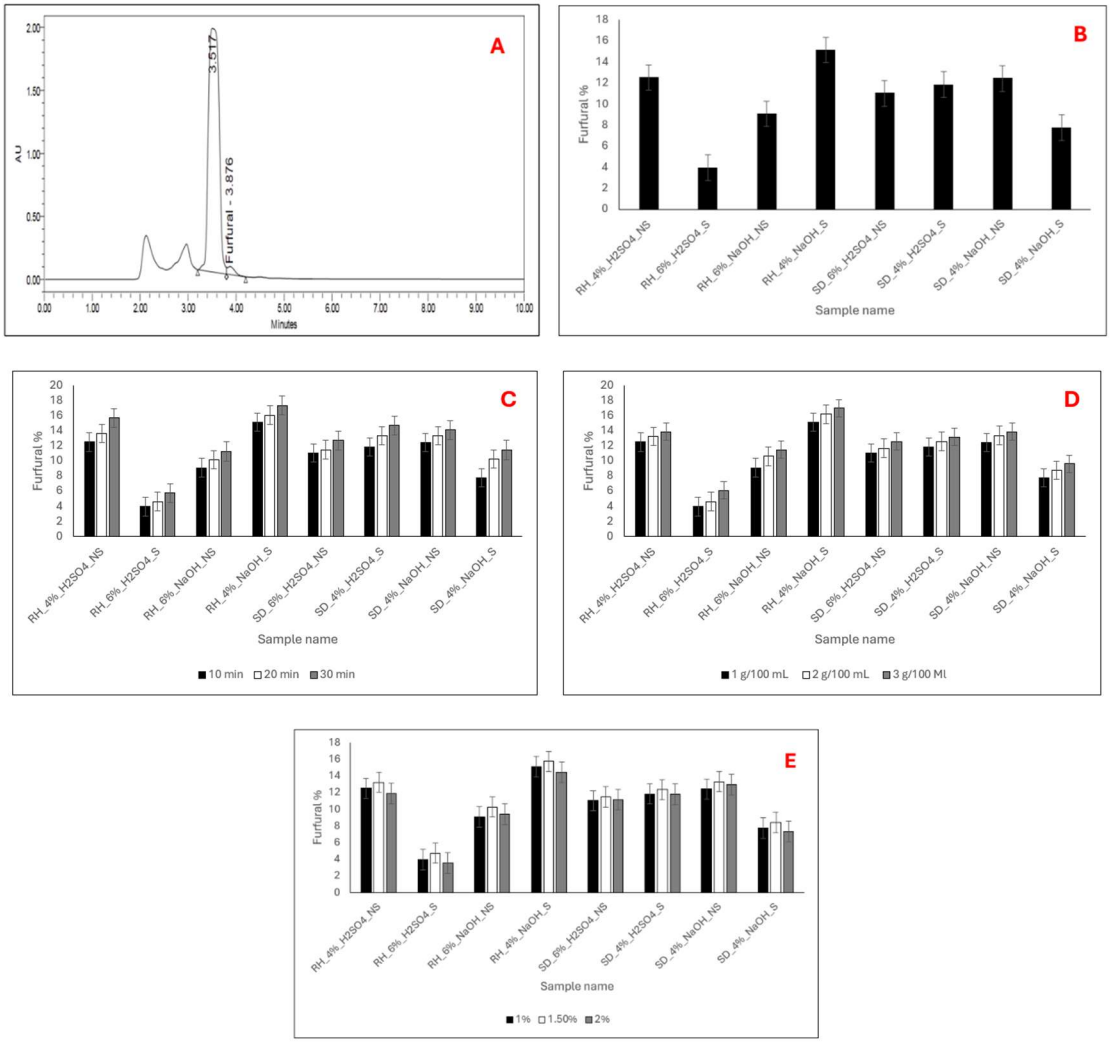

Figure 4.6: (A) HPLC graph of furfural detection. Effect of (B) sample type, (C) treatment time, (D) biomass concentration, (E) acid concentration on furfural production from cellulose by acid pre-treatment method.

4.3.10. Estimation of Xylan content in the hydrolysate: From Fig. 4.7, it was observed that xylan was present in the hydrolysate in every pre-treatment scenario. It was also observed that in sulphuric acid-containing media, the xylan concentration was higher compared to sodium hydroxide media. The best explanation that fits with this result is that the acidic or alkaline pre-treatment media help in the extraction of xylan from biomass. Xylan is a component that can be synthesised from hemicellulose, and due to the oxidative property of sulphuric acid, a higher concentration was observed in the acidic media. It was reported that oxidising agents target carbon 2 and 3 atoms of the carbohydrate backbone and convert them to aldehyde groups. This reaction results in the production of dialdehyde xylan, and further converted into xylan molecules (Amer et al., 2016).

The effect of sonication on the xylan quantity is visible in the figure, and it can be stated that with the application of sonication, the xylan quantity increased. The effect of raw material on xylan quantity can also be observed from the figure. It can be stated that rice husk showed a higher xylan concentration compared to sawdust. This result can be explained by the structure of the raw materials. With a stronger bonding and a rigid structure, the extraction of different materials, like xylan, showed a lower yield compared to rice husk. The highest concentration of xylan was observed in the case of RH_2%_H_2SO_4_NS with a value of 8.24%. On the other hand, the lowest concentration was 3.17% in the case of SD_6%_NaOH_NS.

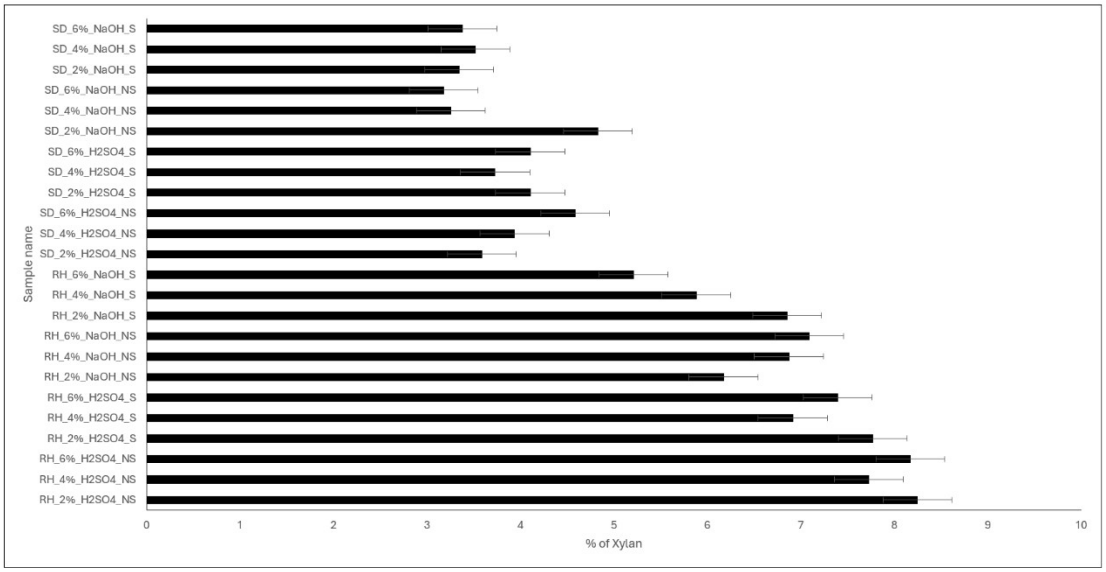

Figure 4.7: Quantification of xylan in different pre-treatment media

4.3.11. Functional group analysis: ATR-FTIR analysis was performed to analyse the functional groups and chemical bonds on the surface of extracted components. Fig. 4.8 (A) represents the ATR-FTIR analysis of cellulose extracted from rice husk and sawdust, respectively. In the figure, major peaks were observed at 3343 cm^{-1}, 2892 cm^{-1}, 1588 cm^{-1}, 1419 cm^{-1}, 1158 cm^{-1}, 1031 cm^{-1}, and 874 $cm^{-1,}$ respectively. According to Kondo (2005), the peak at 3343 cm^{-1} represents OH stretching on the cellulose surface. Another peak at 2892 cm^{-1} confirms C-H_n stretching because of alkyl, aliphatic, and aromatic groups (Yang et al., 2007). Another major peak was found at 1419 cm^{-1} assigned as CH_2 wagging (Cao and Tan, 2004). Also, Chen and Yokochi. (2000) reported the peak at 1158 cm^{-1} assigned γ C-O-C group at the β-glucosidic linkage. The peak at 1031 cm^{-1} confirms the presence of the γ-CO group at C-6 carbon (Kacˇura´kova´ et al., 2000). Another peak at 874 cm^{-1} represents the presence of the γ-CCH group at C-5 and C-6 carbon (Cao and Tan, 2004). Another distinct peak was observed in the case of cellulose extracted from rice husk at 1100 cm^{-1}, representing the dominance of γ ring in plane (Liang and Marchessault, 1959).

Fig. 4.8 (B) shows FTIR analysis of cellulose extracted in different pre-treatment media. Similar peaks were observed for the pre-treatment media, and no significant difference was found. The presence of OH stretching (3343 cm^{-1}), C-H_n stretching (2889 cm^{-1}), the γ C-O-C group at the β-glucosidic linkage (1158 cm^{-1}), and the γ-CO group at C-6 carbon (1026 cm^{-1}) was confirmed by analysing the wavelength of peaks observed in this analysis. The peak at 1620 cm^{-1} is assigned to the C=C stretching on the cellulose surface (Nandiyanto et al., 2019).

Fig. 4.8 (C) represents the effect of different concentrations of pre-treatment media on the FTIR analysis. In this case, no significant difference was found in the position of peaks, but the percentage of transmittance changed with the increasing reagent concentration (NaOH or H_2SO_4). With the increasing concentration of pre-treatment media, the intensity of the peak increased, signifying a proper delignification of the biomass.

The effect of sonication on biomass chemistry was also investigated by the FTIR study. In Fig. 4.8 (D). A significant increase in the intensity was observed after the sonication of biomass. From this observation, it can be interpreted that sonication significantly affects the delignification process.

The extracted hemicellulose was analysed by ATR-FTIR analysis to determine the functional groups present on the surface. As shown in Fig. 4.8 (E), the comparative FTIR graph of hemicellulose extracted from sawdust and rice husk is presented respectively. From the figure, it can be stated that both the hemicellulose samples represent peaks at 3362 cm^{-1}, 2933 cm^{-1}, 1636 cm^{-1}, and 1376 cm^{-1}. Shen et al. (2010) reported similar results for FTIR analysis of hemicellulose. According to this study, the peak at 3362 cm^{-1} is assigned to the C-H stretching. Another peak at 1636 cm^{-1} represents C=O stretching, and the peaks at 2933 cm^{-1} and 1376 cm^{-1} show the presence of C-H stretching and C-C skeleton in R-CO-R' form, respectively. Exclusive peaks such as 1069 cm^{-1}, 1041 cm^{-1}, and 900 cm^{-1} were found in the case of hemicellulose extracted from rice husk. A recent study reported that the peaks represent the presence of the bending vibration of crystalline water, the stretching vibration of the xylopyranose ring (Kostryukov et al., 2023), C-O stretching in R-OH form, and C=O dactyl-zone in CO_2 form, respectively (Shen et al., 2010). This result confirmed the dominance of symmetric and asymmetric C-H stretching vibration in CH, CH_2, and CH_3 groups along with the C-H bending vibration of the xylopyranose ring.

Fig. 4.8 (F) shows the comparative ATR-FTIR analysis of hemicellulose extracted using different pre-treatment media. From the figure, it can be stated that in the case of H_2SO_4 pre-treated hemicellulose, a distinct peak was observed at 1099 cm^{-1}, signifying the stretching vibration of the xylopyranose ring (Kastryukov et al., 2023). It was observed that the intensity of the peaks was not changed with different media, and also, the loss of any existing peak or peak shifting was not found.

No significant difference in the peaks of hemicellulose was found before and after sonication, as shown in Fig. 4.8 (G). Peaks at 3352 cm^{-1}, 1636 cm^{-1}, 1071 cm^{-1}, and 1041 cm^{-1} respectively. These peaks represent the presence of O-H stretching vibration, bending vibration of crystalline water, and stretching vibration of xylopyranose ring, respectively (Kastryukov et al., 2023).

Fig. 4.8 (H) represents the ATR-FTIR analysis of lignin extracted from sawdust and rice husk, respectively. From the figure, it can be stated that peaks at 3349 cm^{-1}, 2969 cm^{-1}, 2905 cm^{-1}, 1639 cm^{-1}, 1452 cm^{-1}, 1041 cm^{-1}, and 878 cm^{-1} were observed, respectively. The peaks at 2905 cm^{-1} and 1452 cm^{-1} indicate the presence of stretching and bending vibrations of a methylene group ($-CH_2-$) (Gupta et al., 2015). According to Reyes-Rivera

and Terrazas (2017), the peaks at 3449 cm^{-1}, 2969 cm^{-1}, and 1639 cm^{-1} represent the presence of O-H stretching, CH_2 asymmetric vibration, and conjugated C-O, respectively. It was also reported that C-H asymmetric deformation was detected at a peak of 1452 cm^{-1} (Xu et al., 2006). Other peaks observed at 1041 cm^{-1} referred to the presence of C-O stretching (Pandey and Pitman, 2003), and 878 cm^{-1} indicates C-H deformation (Chen et al., 2010). Other than these peaks, another distinct peak was found at 954 cm^{-1} in the case of lignin extracted from rice husk. This peak represents =CH out-of-plane deformation (Reyes-Rivera and Terrazas, 2017). Another peak at 1085 cm^{-1} found in lignin extracted from sawdust indicates the presence of C-O stretching vibrations.

Another observation made from Fig. 4.8 (I) was the effect of pre-treatment media on the properties of extracted lignin. In the case of acid-treated lignin, two distinct peaks at 1188 cm^{-1} and 1082 cm^{-1} were found, respectively. As reported by Casas et al. (2011), the peak at 1082 cm^{-1} represents C-O deformation in secondary alcohols and aliphatic esters. On the other hand, the peak at 1188 cm^{-1} occurred due to the presence of C-O-C vibration (Pandey and Pitman, 2003). For alkali-treated lignin, another two distinct peaks were found at 1044 cm^{-1} and 876 cm^{-1}, respectively. The peak at 1044 cm^{-1} represents the C-O stretching of alcohol (Ma et al., 2016), and in the case of 876 cm^{-1}, the presence of *p*-hydroxyphenyl unit (Ying et al., 2018).

In Fig. 4.8 (J), the effect of sonication on the properties of extracted lignin is presented. From the figure, it can be stated that no significant sonication effect was observed on the surface functional groups of lignin.

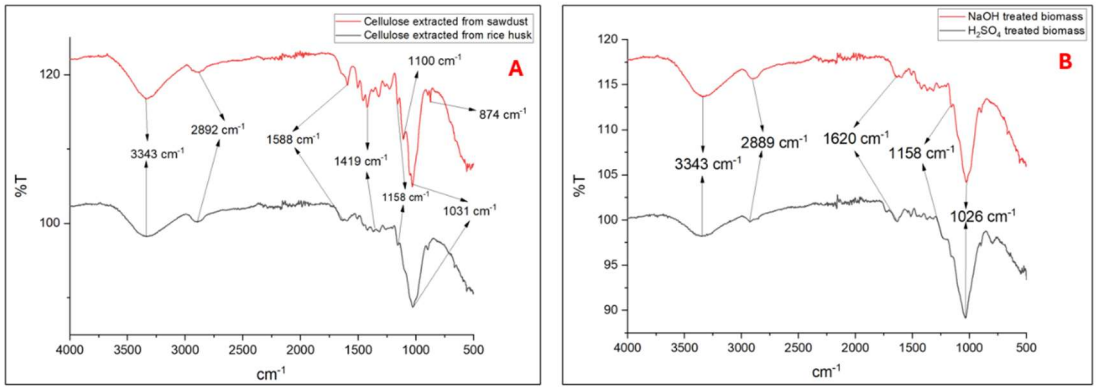

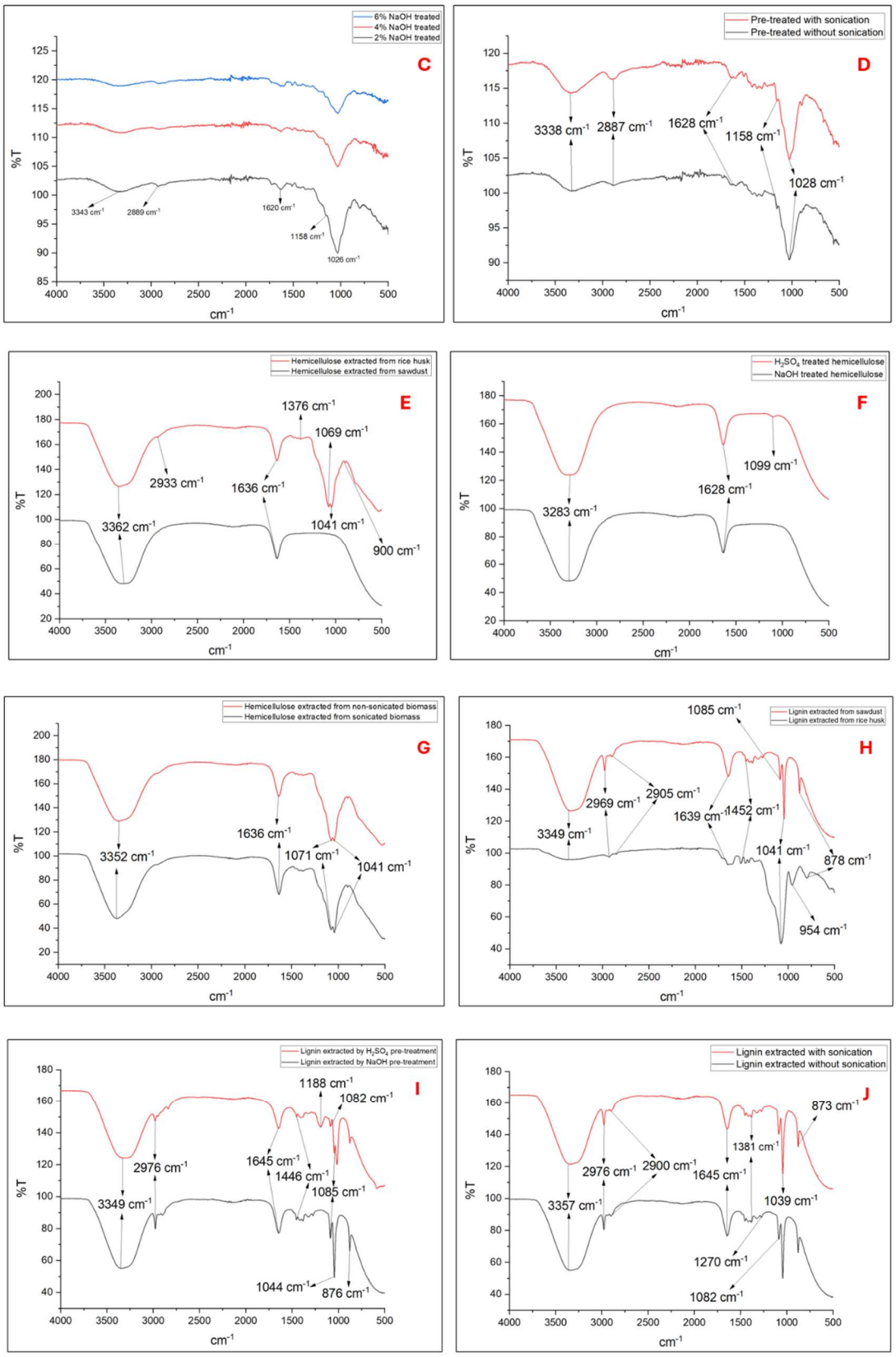

Figure 4.8: Comparative ATR-FTIR analysis of cellulose extracted (A) from different biomass, (B) by different pre-treatment media, (C) by pre-treatment media of different concentrations, (D) applying sonication, hemicellulose extracted (E) from different biomass, (F) by different pre-treatment media, (G) applying sonication, lignin extracted (H) from different biomass, (I) by different pre-treatment media, (J) applying sonication.

4.3.12. Crystallographic structure analysis: The crystallographic structure analysis of extracted products was studied by XRD analysis. Fig. 4.9 (A) presents the comparative XRD pattern of cellulose extracted from sawdust and rice husk. In both the cellulose samples, a prominent major peak was observed at 2Θ= 22.29º. Two independent studies reported similar peaks of cellulose at 2Θ= 22º (Zhao et al., 2007) and 20º (Louis and Venkatachalam, 2020), respectively. Another study conducted by Kim et al. (2013) also reported that Iβ cellulose exhibited a peak at 2Θ= 22º. The mentioned studies reported that these peaks represent the crystallographic plane of cellulose. From Fig. 4.9 (A), it can also be stated that the intensity of crystallinity is highly influenced by the nature of raw materials. In the case of cellulose extracted from sawdust shows other peaks are observed at 2Θ= 14.91º, 24.50º, 30.10º, and 45.84º, respectively. Foner and Adan (1983), reported the peak at 2Θ= 14.91º is a secondary peak that can disappear as the major peak become a hump after proper degradation of cellulose. This explanation supports the XRD pattern of cellulose extraction from sawdust. Escobar et al. (2022) reported the presence of an amorphous halo at 2Θ= 30.10º detected by the XRD detector. This study also reported that another peak at 2Θ= 45.84º is associated with the (200) plane of cellulose I crystal structure and is part of a broader amorphous background in the cellulose XRD pattern.

From Fig. 4.9 (B), the effect of pre-treatment media on the crystallinity of cellulose is presented. From the figure, it can be stated that the cellulose extracted from the alkaline pre-treatment process shows more prominent peaks at 2Θ= 14.91º and 30.10º respectively compared to the cellulose extracted from the acidic pre-treatment method. This observation signifies the amorphous nature of cellulose increased after the alkaline pretreatment, indicating a more promising delignification process. This observation also supports the data of the anthrone test of this work, as explained in section 4.3.6. Another Fig. 4.9 (C) represents the effect of sonication on the crystallinity of extracted cellulose. From the figure, it can be stated that though the quantity has increased after the sonication of biomass, no significant change in the crystallographic profile was observed.

Fig. 4.9 (D) presents the XRD pattern of hemicellulose extracted from biomass. From the figure, several peaks, viz., 2Θ= 13.73º, 15.19º, 24.55º, 38.21º, 47.31º, and 52.94º, were observed. The characteristic peak of hemicellulose was reported to be at 2Θ= 18.9º (Louis and Venkatachalam, 2020). In this study, the peak was found at 2Θ= 15.19º, signifying the presence of hemicellulose in the extracted sample. Liang and Wang (2017) reported

that the peaks at 2Θ= 13.73° and 15.19° represent the amorphous nature of hemicellulose. The peak at 2Θ= 24.55° signifies the scattering from the amorphous region of hemicellulose, which can be associated with chain packing distances. Another peak at 2Θ= 38.21°, 47.31°, and 52.94° is associated with the partial crystallisation of the sample.

In the case of lignin, the crystalline characterisation is presented in Fig. 4.9 (E). This figure shows the promising peaks of lignin at 2Θ= 27.23°, 31.68°, 45.16°, 56.25°, and 75.04°, respectively. Goudarzi et al. (2014) reported that the peaks at 2Θ= 27.23°, 31.68° typically represent the amorphous nature of the sample. According to the same study, the peaks at 2Θ= 45.16° and 56.25° are associated with the semicrystalline region of lignin. Also, the peak at 2Θ= 75.04° represents the highly ordered structure present in the lignin sample. Overall, from the XRD analysis of lignin, it can be stated that the sample is amorphous with some highly ordered domains present inside the substrate.

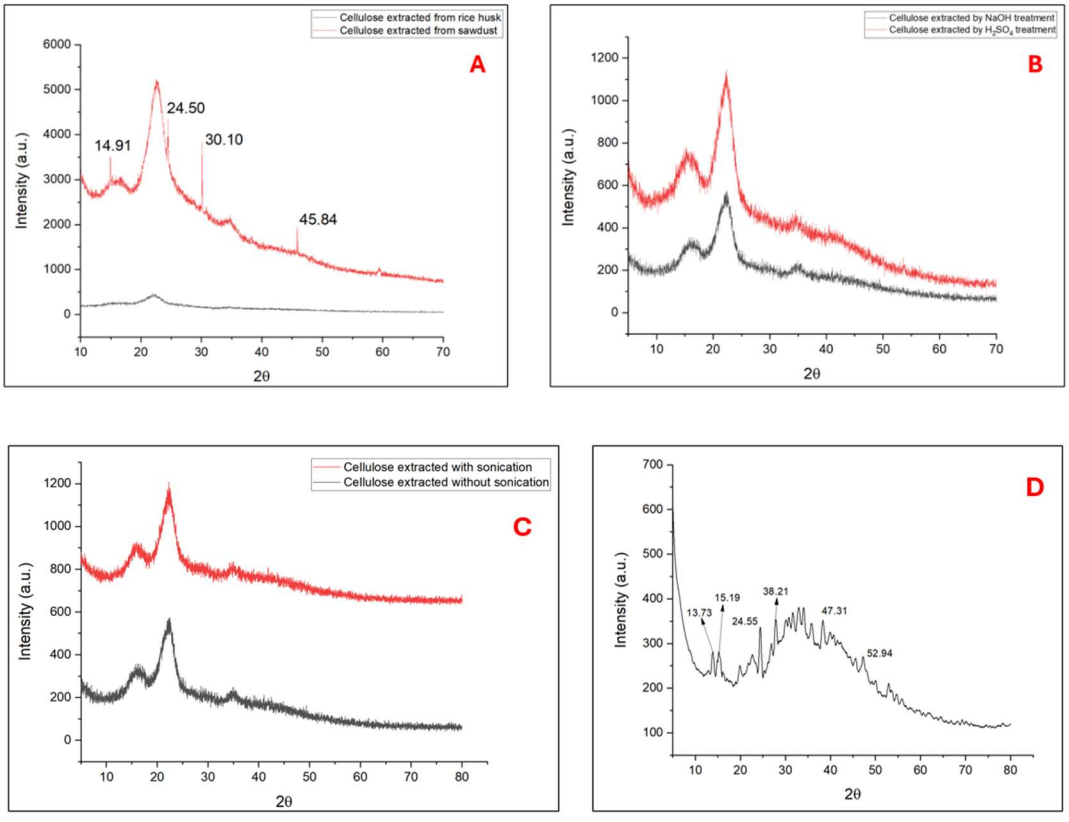

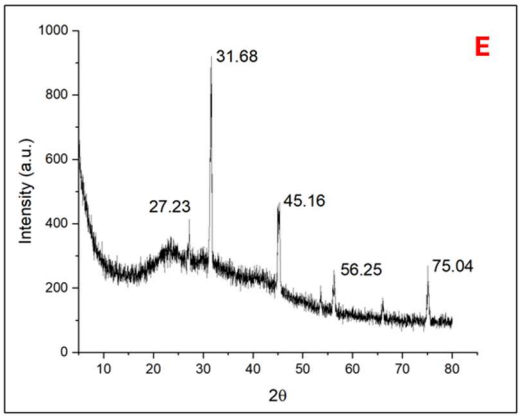

Figure 4.9: XRD analysis of cellulose extracted (A) from different biomass, (B) by different pre-treatment media, (C) applying sonication, (D) extracted hemicellulose, and (E) extracted lignin from biomass.

The % of crystallinity was also calculated in the case of all the samples and is presented in Table 4.2.

Table 4.2: Crystallinity percentage of extracted samples

Sample	Crystallinity %
Rice husk cellulose	19.37
Sawdust cellulose	25.56
Acid-treated cellulose	24.01
Alkali-treated cellulose	13.10
Non sonicated cellulose	11.23
Sonicated cellulose	15.17
Hemicellulose	11.06
Lignin	9.58

From the table, it can be stated that the crystallinity % of cellulose is dependent on the nature of the raw biomass. For cellulose extracted from sawdust, the crystallinity was observed to be 25.56%, which is comparatively higher than the cellulose extracted from

rice husk with a crystallinity of 19.37%. It was also observed that for acid-treated cellulose, the crystallinity% was 24.01%, significantly compared than alkali-treated cellulose with a crystallinity% of 13.10. These observations also match the data observed from the XRD curve of the components. The effect of sonication on the crystallinity of cellulose was also observed. By applying sonication, the crystallinity% increased from 11.23% to 15.17%. The increase in the crystallinity% indicates a more efficient delignification of raw biomass. The crystallinity% of hemicellulose and lignin was found to be 11.06% and 9.58%, respectively.

The orientation of the plane inside the crystalline lattice and interplanar distance were calculated from Bragg's equation. The Miller's indices of extracted products and the interplanar distance (d) are presented in Table 4.3.

Table. 4.3: Orientation of crystalline plane and interplanar distance

Sample	**λ (Å)**	**2Θ**	**Θ**	**Sin(Θ)**	**d_{hkl} (Å)**	**(h k l)**
Cellulose	1.5481	21.752	10.876	0.188859	4.098563	(1 1 1)
Hemicellulose	1.5481	38.151	19.0755	0.32688	2.367997	(2 2 0)
Lignin	1.5481	45.16	22.58	0.383885	2.016359	(2 2 2)

From the table, it can be stated that in cellulose, the orientation plane cuts the X, Y, and Z axes in 1, 1 and 1 positions, respectively. For hemicellulose, the orientation plane is parallel with the Z-axis, and the X and Y axes were cut by the plane in $\frac{1}{2}$, and $\frac{1}{2}$ position. In the case of lignin, the plane cuts the X, Y and Z axes in $\frac{1}{2}, \frac{1}{2}$ and $\frac{1}{2}$ position. From this data, it can be observed that only the crystal lattice of cellulose intercepts one of the coordinates on the negative side with the interplanar distance of 4.09 Å. Following that, the interplanar distance of hemicellulose and lignin was found to be 2.36 Å and 2.01 Å, respectively.

4.3.13. Scanning Electron Microscopy (SEM): The scanning electron microscopy (SEM) analysis was performed to understand the surface morphology of extracted products. From Fig. 4.10 (A) and (B), the sonication's effect on cellulose's surface morphology can be observed. As presented in the figures, it can be stated that the surface morphology of cellulose changes significantly after the application of sonication. Rosli et al. (2013) reported that chemical treatment affects the surface morphology of cellulose.

In that study, it was observed that before any treatment of the raw materials, a bundle of fibres appeared bonded together by non-cellulosic components. On the other hand, SEM analysis of pre-treated biomass displayed a rougher cellulose structure and delignification by the removal of non-cellulosic materials (Mtibe et al., 2014). In the current study, it was observed that after sonication, further modification of the cellulose surface appeared. In Fig. 4.10 (B), more ruptures and roughness on the cellulose surface were observed compared to Fig. 4.10 (A), which represents cellulose without sonication treatment. Krishnamachari et al. (2011) reported that the SEM analysis of cellulose extracted from softwood exhibits a fibrillar structure, also supported by the observation of this study. It was also reported that the shape of these cellulose particles has a non-isometric structure (Das et al., 2010).

Figure 4.10 (C) presents the SEM image of hemicellulose. From the image, it can be stated that the extracted hemicellulose exhibits a crystal-like structure with a rough surface. In a previous study, it has been reported that the structure of hemicellulose depends on the type (Haimer et al., 2010). Also, Peng et al. (2012) reported that the presence of Xylan backbone can result in a tightly resembled structure. From the observation of this study, it can be stated that the Xylan removal by the pre-treatment was significant, as no tightly packed structure was observed. In Fig. 4.10 (D), the SEM image of extracted lignin is presented. From the figure, it can be stated that the extracted lignin exhibits an irregular structure with an uneven structure. Koo et al. (2012) reported the SEM analysis of lignin droplets, representing similar results to this study. The uneven and rough surface has resulted from the release of gaseous materials trapped in the lignin process during drying (Sharma et al., 2004). Ibrahim et al. (2010) reported a similar structure of lignin extracted from biomass by steam-explosion.

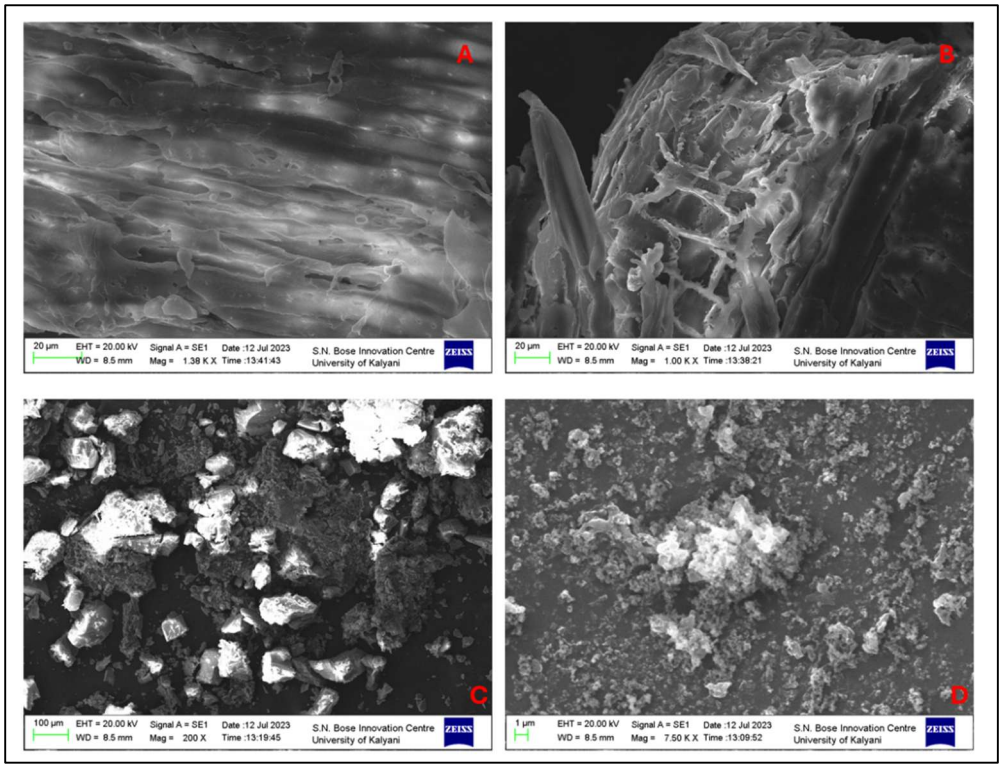

Figure 4.10: SEM images of extracted (A) cellulose without sonication, (B) cellulose with sonication, (C) hemicellulose, and (D) lignin.

4.3.14. Elemental composition analysis: The elemental analysis of the extracted products was performed using CHNS and energy-dispersive X-ray spectroscopy (EDAX) analysis, respectively.

4.3.14.1. Surface elemental composition: The elemental composition of the surface of extracted products was detected by EDAX analysis. The result of this study is presented in Table 4.3. As a supplementary to the analysis, Fig. 4.11 represents the EDAX graph of the mentioned components. From the data gathered by EDAX analysis, it can be stated that the surface of the extracted products is mainly composed of carbon and hydrogen, an efficient raw material for different secondary product synthesis.

Table 4.4: EDAX analysis of extracted products

Extracted Products	Carbon atomic %	Oxygen atomic %	Silica atomic %
Cellulose	63.45	36.55	-
Hemicellulose	57.38	42.63	-
Lignin	77.07	21.95	0.98

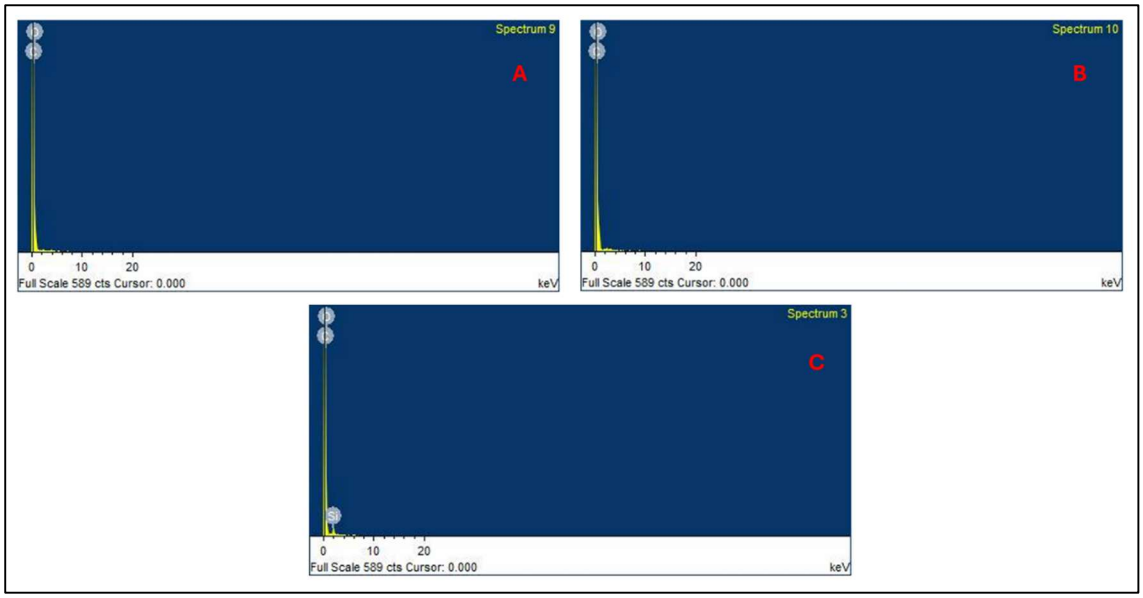

Figure 4.11: EDAX analysis of (A) cellulose (B) hemicellulose, and (C) lignin.

4.3.14.2. Total elemental composition: The total elemental composition of the extracted products is analysed by a CHNS analyser. As presented in Fig. 4.12, it can be stated that the majority % of the products are carbon with 45.46%, 33.19%, and 29.14% in the case of cellulose, hemicellulose, and lignin, respectively. The second highest component was hydrogen, with 3.9%, 4.37%, and 5.71% respectively for the products mentioned above. In the case of nitrogen, the highest weight% was found in the case of cellulose, to be 1.7%, and for sulphur, the weight% is negligible at less than 1%. Hence, from the elemental analysis, it can be stated that these materials are capable of biofuel synthesis and the production of different derivatives as secondary value-added products.

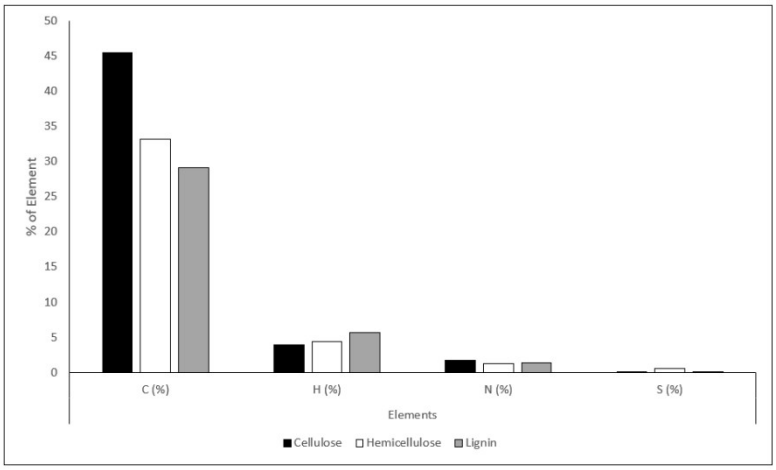

Figure 4.12: CHNS analysis of different extracted compounds.

4.4. Conclusion:

Several studies have been performed before that focused on the usage of lignocellulosic biomass for different value-added product extraction. This study mainly focuses on the usage of sawdust and rice husk to extract cellulose, hemicellulose, and lignin, respectively, by chemical pre-treatment method as well as sonication in a single pathway. Furthermore, the production of different derivatives, viz., furfural, xylan, and bioethanol, was also investigated in this work. From the result, it was found that treating the raw material with acid and alkaline solutions effectively separates the products from the raw material, and sonication significantly affects the process. From the anthrone test, it was observed that for rice husk, the highest yield of cellulose was found in the RH_4%_NaOH_S sample with a value of 899.62 mg/g. For sawdust, the cellulose yield was 958.88 mg/g from an SD_4%_NaOH_S sample. After saccharification, it was found that 24.84 mg/g of TRS content was produced from SD_4%_H_2SO_4_S. In the case of rice husk, the highest TRS yield was observed in the RH_2%_NaOH_S sample with a value of 20.02 mg/g. The highest ethanol content in this study was observed to be 3.24 mg/g synthesised from an SD_6%_ H_2SO_4_NS sample. The highest furfural was synthesised from 16.98 % from 3g/100 mL RH_4%_NaOH_S after 20 min. of hydrothermal treatment. From this study, it was observed that different value-added products can be extracted effectively from biomass by the physicochemical pre-treatment method. However, the extraction yield is low compared to conventional energy sources and is under research by the scientific community. The potential of the biotic waste materials is not only bound by the value-added product extraction but also extends its spectrum towards wastewater treatment. The application of these materials in wastewater treatment is investigated in the later chapters of this thesis.

Chapter: 5

PREPARATION OF POLYVINYL ALCOHOL AEROGEL AND ITS APPLICATION IN WASTEWATER TREATMENT

5.1. Introduction:

With the advancement of technology and the spontaneous growth of industry, the consumption of environmental resources is increasing. Apart from the consumption, the exploitation of these resources is making it a serious issue. From the governments of different nations, international bodies, and the research community to the common people, these issues are highlighting themselves and demanding a sustainable solution. Over the decades, among these problems, one of the main problems human societies have faced is water pollution. Using water for different purposes and disposing of it without proper treatment is causing rapid degradation of the environment.

To treat this wastewater, several studies have been conducted using adsorption (Rashid et al., 2021), bioremediation (Saeed et al., 2022), membrane filtration (Hube et al., 2020), ion exchange (Swanckaert et al., 2022), and coagulation-flocculation (Zhao et al., 2021). However, being the most conventional method, adsorption has been investigated extensively in recent times. Different types of adsorbents, viz., biochar (Wang et al., 2020), cellulose-based materials (Peng et al., 2020), silica (Silva et al., 2021), metal-organic framework (Liu et al., 2023), nanomaterials and nanocomposites (Tripathy et al., 2024), and polymeric materials (Otero and Coimbra, 2025). Another emerging adsorbent, being utilised for wastewater treatment, is aerogel.

Being a material with exclusive properties, aerogel has a wide range of applications. In 1931, S. Kistler first developed silica aerogel by extracting liquid from silica gel and converting it to a solid material with high porosity (Kistler, 1931). From then, different types of aerogels, viz., SiO_2-based aerogel, carbon-based aerogel (Maleki, 2016), and organic-based aerogel (Tao et al., 2008) were developed and explored. Despite this extensive research, the production of aerogel is facing several challenges like, its fragile nature and high cost. One of the main responsible processes for these problems is the critical drying of aerogel to extract the liquid.

In this study, polyvinyl alcohol (PVA) based aerogels were developed without solution substitution and critical drying, and biomass was used to prepare different fillers for the

aerogels. The efficiency of these gels for wastewater treatment was investigated, and the effect of the presence of different fillers was also observed. Different physical properties of the prepared aerogels were also identified in detail, along with their selectivity for pollutants, to understand the detailed profile of wastewater treatment.

5.2. Materials and Methods:

5.2.1. Materials: Polyvinyl alcohol (PVA), glutaraldehyde, hydrochloric acid (HCl), sodium hydroxide (NaOH), nitric acid (HNO_3), acetone, and hydrogen peroxide (H_2O_2) were purchased from Merck (Germany). Methanol, naphthalene, acenaphthene, phenol, phenanthrene, pyrene, anthracene, lead nitrate ($Pb(NO_3)_2$), potassium dichromate ($K_2Cr_2O_7$), hydrogen fluoride (HF), methylene blue, aniline blue, and congo red were purchased from Loba chamie (India). Kerosene oil was purchased from the local market of Jadavpur, India and all the materials were used as received.

5.2.2. Preparation of fillers: Three different components, viz., cellulose, biochar, and silica, were extracted from sawdust and rice husk. These materials were considered as the filler of PVA aerogels.

5.2.2.1. Preparation of cellulose: Cellulose was extracted using the process as described in section 4.2.3, and the cellulose content was analysed by performing an anthrone test as described in section 4.2.4 of chapter 4. One type of cellulose from each raw material with the highest cellulose concentration was selected for further modification. For further modification of cellulose, 50% (v/v) H_2O_2 was used.

To prepare the solution, 50 mL of H_2O_2 was poured into an Erlenmeyer flask, and water was mixed into it in a 1:1 (v/v) ratio. The solution was stirred on a magnetic stirrer for 15 min. Following that, the previously extracted cellulose was poured into the solution in a 10 g/ 100 mL concentration and again mixed on a magnetic stirrer for 1 hr. After the cellulose particles were properly suspended, the mixture was again stirred for 30 min. at 363 K. In this step, bleaching of cellulose was observed as the colour converter from brown to white. As the bleaching was completed, the solution was cooled down to room temperature, and the solid biomass was collected. The biomass was washed with DI water and dried in a hot air oven at 333 K.

5.2.2.2. Preparation of biochar: To prepare biochar from the waste biomass, the biomass was placed tightly inside an enamel crucible. The crucible was then placed inside

a muffle furnace and heated at 874 K for 3 hr. to pyrolyse the sample. After the pyrolysis was completed, the carbonaceous biochar was collected and treated with 4% (w/v) NaOH solution for 2 hr. at 363 K.

For this treatment, 4 g of NaOH beads were measured using a weighing machine (Sartorius, Germany) and dissolved in 90 mL of DI water on a magnetic stirrer. After the solution was prepared, it was poured into a volumetric flask, and DI water was added to make the volume 100 mL. Following that, 5 g of biochar was measured using a weighing machine (Sartorius, Germany) and mixed with the NaOH solution inside an Erlenmeyer flask. The mixture was placed on a magnetic stirrer and stirred for 2 hr. at 90^{o}C. After the treatment was completed, the mixture was cooled down to room temperature, and the solid biochar was collected. Following that, the biochar was washed with DI water to make the pH neutral and dried in a hot air oven at 334 K.

5.2.2.3. Extraction of silica: To extract silica from biomass, the raw biomass was placed inside an enamel crucible and burnt in a muffle furnace at 1073 K for 2 hr in the presence of oxygen. After it was completely converted to ash, the burnt biomass was collected and treated with 12% (w/v) NaOH solution at 363 K.

For this treatment, 12 g of NaOH beads were measured using a weighing machine (Sartorius, Germany) and dissolved in 90 mL of DI water on a magnetic stirrer. After the solution was prepared, it was poured into a volumetric flask, and DI water was added to make the volume 100 mL. The burnt biomass was added to the solution inside an Erlenmeyer flask, maintaining the ratio of ash and NaOH solution in a 1:7 (w/v) ratio. The mixture was placed on a magnetic stirrer and stirred at 363 K till the solution became transparent. In this step, the silicon, present in the ash, reacts with NaOH and produces sodium silicate (Na_2SiO_3), also known as water glass. After the treatment was completed, the solution was cooled down to room temperature and filtered using a filter paper (Whatman 41) with a diameter of 110 mm. The clear filtrate was collected and again placed on a magnetic stirrer. While stirring, concentrated HCl was added to the solution by a dropper. The sodium silicate reacted with the acid and created a white precipitate of silicon dioxide or silica. After precipitation, the solution was again filtered using a filter paper (Whatman 41) with a diameter of 110 mm and the silica was collected. Following that, it was washed with DI water and dried in a hot air oven at 60^{o}C.

5.2.3. Preparation of aerogel: The aerogels were prepared by using PVA as the gel matrix. 5 g of PVA powder was measured using a weighing machine (Sartorius, Germany) and dissolved in 100 mL of DI water, taken in a beaker on a magnetic stirrer at 90^{o}C. After the PVA was completely dissolved, the solution was cooled down to room temperature and 1 mL of glutaraldehyde was added to it. The solution was again mixed on a magnetic stirrer for 15 min. After proper mixing of glutaraldehyde, 1 mL of concentrated HCl was added to the solution. The solution was again stirred on a magnetic stirrer for 15 min. at room temperature and then at 363 K till the PVA solution was converted to a hydrogel. As the hydrogel was prepared, it was cooled down to room temperature and stored inside a refrigerator (Cell Frost) at 278 K for 24 hr. After 24 hr., the hydrogel was placed inside a lyophilisation chamber, and the lyophilizer (EYELA, FDU-1200) was used to extract the water and convert the hydrogel to aerogel. After the aerogels were prepared, they were collected and stored inside a dry container for further use.

For preparing PVA aerogels with immobilised filler, the same protocol was used, but before adding glutaraldehyde to the solution, 1 g of filler material, viz., cellulose, silica, or biochar, was measured using a weighing machine (Sartorius, Germany) and added to the solution. The mixture was stirred on a magnetic stirrer for 30 min. for proper mixing of the filler material.

In this process total of six aerogels, viz., PVA, PVA-rice husk cellulose (PVA-RHC), PVA-sawdust cellulose (PVA-SDC), PVA-rice husk biochar (PVA-RHBC), PVA-sawdust biochar (PVA-SDBC), PVA-silica (PVA-Si), were prepared.

5.2.4. Characterization of aerogels: Characterization is a vital step for research to understand the structure and properties of any substance. The crystallographic profiling, functional group analysis, elemental composition, thermal profiling, and surface morphology of the extracted fillers and prepared aerogels were studied. Also, different physical characteristics, viz., porosity, density, moisture content, swelling property, and the effect of temperature, salinity, and pH were investigated.

5.2.4.1. Crystallographic structure analysis: The crystallographic structure of the prepared aerogels was analysed by X-Ray Diffraction (XRD) study as described in section 4.2.9.2 of chapter 4.

5.2.4.2. Functional group analysis: To analyse the functional groups present on the surface of aerogels, ATR-FTIR was performed as described in section 4.2.9.3 of chapter 4.

5.2.4.3. Surface morphology analysis: The surface morphology of aerogels was analysed by scanning electron microscopy (SEM), as described in section 4.2.9.4 of chapter 4.

5.2.4.4. Elemental analysis: To study the elemental composition of the surface, energy dispersive X-ray analysis (EDAX) was performed as described in section 4.2.9.5 of chapter 4.

5.2.4.5. Thermal profiling: To study the thermal profile of prepared samples, thermogravimetric analysis (TGA), differential scanning calorimetry (DSC), and differential thermal analysis (DTA) were performed. These analyses were conducted using a TGA analyser (PerkinElmer, TGA-4000, USA). The TGA analysis was performed using an Argon (Ar) atmosphere in an alumina crucible. The temperature range of 40^{o}C to 800^{o}C was considered in this study with a ramping rate of 20^{o}C/ min. The data was analysed by using Origin (2018) software.

5.2.4.6. Microscopic analysis: Apart from SEM, the microscopic analysis of aerogels was performed to understand the surface morphology of aerogels. A fluorescent microscope (Dewinter, Fluorex-LED) was used to observe the microscopic structure of the prepared aerogels. The small pieces of aerogels were placed on the stage of the microscope and were magnified at 40x to study the evenness of the surface, and the presence of pores and filler particles.

5.2.4.7. Physical properties analysis: To understand the physical properties of prepared aerogels, density, porosity, moisture content, swelling property, and the effect of temperature, salinity, and pH on the aerogel were studied.

5.2.4.7.1. Density analysis: To measure the density of the prepared aerogels, 50 mL of DI water was taken into a measuring cylinder. 1 g of each aerogel was measured using a weighing machine (Sartorius, Germany) and submerged in water. When the aerogel was submerged in the water, with submerged aerogel the final volume of the water was calculated. The density of the prepared aerogel was calculated using equation (5.1).

$$Density\ of\ aerogel = \frac{Mass\ of\ aerogel}{Final\ volume\ of\ water - Initial\ volume\ of\ water} \ldots\ldots\ldots\ldots\ldots (5.1)$$

5.2.4.7.2. Porosity analysis: To calculate the skeletal density of the aerogels, the skeletal density of PVA and the fillers was calculated. 1 g of each component was measured using a weighing machine (Sartorius, Germany). The gap between the particles was decreased by applying pressure, and the volume was calculated. From the volume and weight, the skeletal density of the component was calculated.

The density of the aerogels was calculated as mentioned in section 5.2.4.7.1. To calculate the porosity, equation (5.2) was used (Ferrero, 2007).

$$Porosity\ of\ aerogel = 1 - \frac{Density\ of\ aerogel}{Skeletal\ density\ of\ fillers} \ldots\ldots\ldots\ldots\ldots\ldots (5.2)$$

5.2.4.7.3. Swelling test: To study the swelling behaviour of the prepared aerogel, 1 g of aerogel was measured using a weighing machine (Sartorius, Germany) and submerged in 100 mL of DI water in an Erlenmeyer flask. The submerged aerogels were left for 2 hr. in the water, and following that, they were collected, and the final weight was measured. The water uptake by the aerogels was calculated by equation (5.3).

$$\%\ of\ water\ uptake = \frac{Weight\ difference}{Initial\ weight} x100 \ldots\ldots\ldots\ldots\ldots\ldots (5.3)$$

5.2.4.7.4. Moisture content: The moisture content of the aerogels was also investigated in this study. To determine the moisture content, 1 g of the aerogel was measured using a weighing machine (Sartorius, Germany) and placed inside a hot air oven for 1 hr. at 60ºC. After the heat treatment, the aerogels were collected, and the final weight was measured. The water content was calculated using equation (5.4).

$$Moisture\ content = \frac{Weight\ before\ heating - Weight\ after\ heati}{Initial\ weigh} x100 \ldots\ldots\ldots\ldots\ldots (5.4)$$

5.2.4.7.5. Effect of temperature: The effect of temperature on the surface chemistry of aerogels was studied by treating the aerogels with heat. 1 g of the aerogel was measured using a weighing machine (Sartorius, Germany) and placed inside a hot air oven for 1 hr. at 60ºC. After the heat treatment, the aerogels were collected and characterised by ATR-FTIR analysis (PerkinElmer, Spectrum-2, USA). A wavelength range of 500-4000 cm^{-1} with a transmission rate of 4 cm/sec was considered. The data was analysed and functional groups were detected by using Origin (2018) software.

5.2.4.7.6. Effect of salinity: To study the effect of salinity on the aerogel surface, the prepared aerogels were treated with 10% (w/v) NaCl solution. To prepare the solution, 10 g of NaCl was measured using a weighing machine (Sartorius, Germany) and taken in an Erlenmeyer flask. 90 mL of DI water was added to it and mixed on a magnetic stirrer. After the solution was prepared, 1 g of aerogel was added to the solution and treated for 1 hr. Following that step, the treated aerogels were collected and dried in open air at room temperature. The change in the aerogel surface was monitored by analysing it with an ATR-FTIR (PerkinElmer, Spectrum-2, USA). A wavelength range of 500-4000 cm^{-1} with a transmission rate of 4 cm/sec was considered. The data was analysed, and functional groups were detected by using Origin (2018) software. Also, the % weight loss of the aerogels was calculated using equation (5.5) after treating them with 10% (w/v) NaCl solution.

$$\%\ of\ weight\ difference = \frac{Weigh\ \ difference}{Initial\ weight} x100 \ldots\ldots\ldots\ldots\ldots\ldots \quad (5.5)$$

5.2.4.7.7. Effect of pH: Five different pH solutions, viz., 2,4,6,8, and 10, were prepared by adjusting the pH of DI water. pH of the water was maintained by using a pH meter (TestR-35, Eutech, USA) and adjusted at the desired pH using 0.1 (M) NaOH and 0.1 (M) HCl buffer solutions. 1 g of the prepared aerogels was submerged in the 100 mL solution and treated for 2 hr. After treatment, the aerogels were collected and dried in the open air at room temperature. The final weight of the treated aerogels was measured using a weighing machine (Sartorius, Germany), and the % of weight loss was calculated using equation (5.7) as mentioned in section 5.2.5.12. The change in the aerogel surface was examined by using an ATR-FTIR (PerkinElmer, Spectrum-2, USA). A wavelength range of 500-4000 cm^{-1} with a transmission rate of 4 cm/sec was considered. The data was analysed and functional groups were detected by using Origin (2018) software.

5.2.4.7.8. The oil absorption capacity of the aerogel: To understand the oil absorption capacity of the prepared aerogels, 100 mL of kerosene oil was measured by a measuring flask and transferred into an Erlenmeyer flask. The aerogel was measured by a weighing balance (Sartorius, Germany) and added to the oil in a 1 g/L dose. The flask was placed on a table at room temperature and the time was monitored, that was required to absorb the oil by the aerogel. Also, oil was added to the system continuously to understand the maximum absorption capacity of aerogels.

5.2.5. Adsorption of pollutants from aqueous system by aerogel: The adsorption of pollutants from the water solution by aerogel was performed with a batch study. Different parameters in this experiment were optimised to study their effect on the adsorption process. Response Surface Methodology (RSM) was utilised to optimise the adsorption process, and modelling of the data was performed to understand the underlying phenomena of the adsorption.

5.2.5.1. Preparation of pollutant solution: In this study, three organic pollutants, naphthalene, acenaphthene, and phenol, were used as the pollutants of interest.

5.2.5.1.1. Preparation of naphthalene solution: 10 mg of naphthalene was measured using a weighing machine (Sartorius, Germany) and taken into an Erlenmeyer flask. 5 mL of acetone was added to the naphthalene and stirred on a magnetic stirrer to completely dissolve the naphthalene in acetone. After the solution was prepared, 900 mL of DI water was added to the solution and again stirred for 30 min. at 333 K to eliminate the acetone from the solution. After the acetone was removed, the solution was cooled down to room temperature and poured into a measuring cylinder. DI water was added to it to make the volume 1 L. This 10 mg/L naphthalene solution was used as the stock solution, and the rest of the desired concentrations were made by diluting it.

5.2.5.1.2. Preparation of acenaphthene solution: The acenaphthene solution was prepared following the same process as the naphthalene solution, described in section 5.2.4.1.

5.2.5.1.3. Preparation of phenol solution: 10 mg of crystalline phenol was measured using a weighing machine (Sartorius, Germany) and taken into an Erlenmeyer flask. 900 mL of DI water was added to it and stirred on a magnetic stirrer until the phenol was completely dissolved. After preparing the solution, it was poured into a volumetric flask, and DI water was added to make the volume 1 L. This 10 mg/L phenol solution was used as the stock solution, and the rest of the desired concentrations were made by diluting it.

5.2.5.2. Experimental Procedure: The previously prepared pollutant solutions (mentioned in section 5.2.5.1**)** were used for the batch study in this research. To perform the batch study, 100 mL of each solution was taken into an Erlenmeyer flask, and the aerogels of the desired weight were measured using a weighing machine (Sartorius, Germany). The aerogel was added to the solution and treated inside a BOB shaker incubator for 180 min. Samples were collected in a pre-determined interval and analysed

by a UV-Vis spectrophotometer (PerkinElmer, USA) as well as an HPLC machine (Waters model- 2489). The detailed specification of the analysis is mentioned in section 5.2.5.2. For the baseline study, the pollutant concentration was 5 mg/L, and the dose of adsorbent, pH, and temperature were maintained at 1 g/L, 7, and 303 K, respectively. For the detailed batch study, the pollutant concentration (1 mg/L- 10 mg/L), dose of adsorbents (0.5 g/L- 1.5 g/L), pH (2-10), and temperature (298 K- 313 K) were varied to study their effect on the adsorption process.

The percentage removal of the pollutants was calculated by equation (5.6)

$$Removal\ \% = \frac{C_0 - C_t}{C_0} x100 \ldots\ldots\ldots\ldots\ldots \text{(5.6)}$$

Where C_0 is the initial concentration (mg/L) of pollutant in aqueous solution, C_t is the concentration (mg/L) of pollutant after the adsorption performed for time t.

5.2.5.3. Isotherm analysis of adsorption process: The adsorption isotherm model was performed to understand the equilibrium performance of the adsorbents when the temperature was constant. The result of this batch study, conducted over the variable conventions and constant temperature, was utilised to analyse the isotherm of the process. Two isotherm models, namely Langmuir and the Freundlich models, were explored to understand the behaviour of the process. In this study and during the model analysis, it was assumed that the whole surface of the aerogel with or without fillers acted as an adsorbent.

5.2.5.3.1. Langmuir isotherm model: The Langmuir isotherm model assumes that during adsorption, the adsorbate molecules form a single layer on the adsorbent particles to get attached. This layer formation is known as monolayer adsorption. As per the assumptions, the adsorption occurs at identical sites, and each molecule contributes a homogeneous and equal activation energy and constant enthalpy. To analyse the Langmuir isotherm model, the linear form of the equation was considered and presented as equation (5.7).

$$\frac{C_e}{q_e} = \frac{1}{Q_0 b} + \frac{C_e}{Q_0} \ldots\ldots\ldots \text{(5.7)}$$

Where C_e (mg/L) is the equilibrium concentration of adsorbate, q_e (mg/g) is the theoretical maximum adsorption capacity, Q_o (mg/g) is the maximum monolayer coverage capacity, and b (L/mg) is the Langmuir coefficient.

5.2.5.3.2. Freundlich isotherm model: In the case of this model, a multilayered adsorption process and an exponential distribution of the active site and active site energy are considered. According to the Freundlich isotherm, the adsorption heat and affinities are not considered to be evenly distributed throughout the heterogeneous surface of the adsorbent. The non-linear form of the adsorption model is presented as equation (5.8).

$$\ln(q_e) = \frac{1}{nf}\ln(C_e) + \ln(k_f) \ldots\ldots\ldots\ldots \quad (5.8)$$

Where n_f is the adsorption intensity and k_f (mg/g) is the Freundlich coefficient of adsorption capacity. C_e and q_e are the same as mentioned in equation (5.7).

5.2.5.4. Kinetics analysis of adsorption process: Adsorption kinetics analysis is significant to understand the time required for the adsorption to reach equilibrium and information about the adsorption pathway and mechanism. The adsorption process is divided into four steps:

a. Bulk diffusion: In this step, the adsorbate molecule enters from the solution to a liquid film surrounding the adsorbent surface.

b. External diffusion: During this process, the adsorbate molecule diffuses throughout the thin liquid film.

c. Internal diffusion/ Intraparticle diffusion: In this process, the adsorbate molecule is transferred from the liquid film to the surface of the adsorbent. This process involves two mechanisms, viz., pore diffusion and surface diffusion.

d. Interaction of adsorbate particles and adsorbent surface, either by physisorption or chemisorption. Desorption (reverse adsorption) is also included in this step.

The first and fourth steps are fast, whereas the second and third steps are slow. The overall rate of reaction is determined by the slowest of the four steps. To analyse the kinetics of the adsorption process, two kinetic models, viz., the pseudo-first-order model and the pseudo-second-order model, were adopted.

5.2.5.4.1. Pseudo-first-order kinetic model: The main assumption of this kinetic model is that the rate of change of solute uptake with time is directly proportional to the difference in saturation concentration and the amount of solid uptake with time. This model also assumes that the sorption only occurs on the localised site and there is no interaction between the adsorbed molecules, the concentration of adsorbate is constant

during the reaction, surface coverage does not affect the adsorption energy, and adsorption is a monolayer process. The linear form of the pseudo-first-order kinetic model is presented as equation (5.9).

$$\log(q_e - q_t) = [\log q_e - \frac{k_1}{2.303} t] \text{ ..... (5.9)}$$

Where k_1 is the Pseudo-first-order rate constant, q_e (mg/g) is the quantity of adsorbate adsorbed at equilibrium, and q_t is the quantity of adsorbate adsorbed at time t.

5.2.5.4.2. Pseudo-second-order kinetic model: The Pseudo-second-order kinetic model assumes that the rate-limiting step of the adsorption process is the chemisorption, and the adsorption rate is dependent on the adsorption capacity of the adsorbent. The linear equation of the Pseudo-second-order kinetic model is presented as equation (5.10).

$$\frac{t}{q_t} = \frac{1}{k_2 \, q_e^2} + \frac{t}{q_e} \text{ ..... (5.10)}$$

Where k_2 is the Pseudo-second-order rate constant, q_e and q_t are the same as mentioned in equation (5.10).

5.2.5.5. Thermodynamics analysis of the adsorption process: The thermodynamics of the adsorption process was studied by the changes of the Gibbs free energy (ΔG; kJ/mol), enthalpy (ΔH; kJ/mol), and entropy (ΔG; $J^{-1}mol^{-1}K^{-1}$). The thermodynamic variables were calculated by using the following equations.

$$K_c = \frac{C_a}{C_e} \text{ ..... (5.11)}$$

$$\Delta G = RT \ln K_c \text{ ..... (5.12)}$$

$$lnK_c = -\left(\frac{\Delta H}{\Delta R}\right)\left(\frac{1}{T}\right) + \left(\frac{\Delta s}{R}\right) \text{ ..... (5.13)}$$

Where K_c, C_a and T are the distribution coefficient of adsorption, the quantity of pollutant adsorbed by a unit mass of adsorbent, and the operational temperature is Kelvin, respectively.

5.2.5.6. Optimisation of adsorption process by Response Surface Methodology (RSM): To optimise the adsorption process, response surface methodology (RSM) was performed. The experimental model was created by using the Box-Behnken design and a second-order system. Being a second-order system, the model followed a quadratic equation that was validated by varying different experimental parameters, viz., time (5-

180 min.), adsorbent dose (0.5g/L -1.5g/L), and pollutant concentration (1 mg/L- 10 mg/L). Design Expert-13 (Version- 7) software was used for this purpose, and a total of seventeen unique combinations of the experimental conditions were investigated. For the ANOVA analysis, all the data of the mentioned seventeen runs were collected and fitted by using the quadratic equation. From the result of this analysis, the validity of the design was established.

5.2.6. Selectivity study of aerogels: To analyse the selectivity of the aerogel towards different types of pollutants eleven adsorbates viz., naphthalene (Naph), phenol (Phe), acenaphthene (Ace), anthracene (Ant), pyrene (Pyr), phenanthrene (Phen), congo red (CR), methylene blue (MB), aniline blue (AB), chromium (Cr), lead (Pb), and Fluoride (F) were chosen respectively.

5.2.6.1. Preparation of adsorbate solution: As the chosen adsorbates cover a wide spectrum of compounds, the solution preparation process varies depending on the pollutant. However, each solution was prepared with a concentration of 5 mg/L.

5.2.6.1.1. Preparation of naphthalene solution: The naphthalene solution was prepared following the process described in section 5.2.5.1.1.

5.2.6.1.2. Preparation of acenaphthene solution: The acenaphthene solution was prepared following the process described in section 5.2.5.1.2.

5.2.6.1.3. Preparation of phenol solution: The phenol solution was prepared following the process described in section 5.2.5.1.3.

5.2.6.1.4. Preparation of anthracene solution: The anthracene solution was prepared following the same process as naphthalene described in section 5.2.5.1.1.

5.2.6.1.5. Preparation of pyrene solution: The pyrene solution was prepared following the same process as naphthalene described in section 5.2.5.1.1.

5.2.6.1.6. Preparation of phenanthrene solution: The phenanthrene solution was prepared following the same process as naphthalene described in section 5.2.5.1.1.

5.2.6.1.7. Preparation of congo red solution: To prepare the congo red solution, 5 mg of congo red dye was measured using a weighing machine (Sartorius, Germany) and taken into an Erlenmeyer flask. 900 mL of DI water was measured by a measuring cylinder and added to it. The flask was placed on a magnetic stirrer under constant

rotation to make the dye solution homogenous. After the solution was prepared, it was poured into a measuring cylinder, and DI water was added to make the volume 1 L.

5.2.6.1.8. Preparation of methylene blue solution: The methylene blue solution was prepared following the same process as congo red described in section 5.2.6.1.7.

5.2.6.1.9. Preparation of aniline blue solution: The aniline blue solution was prepared following the same process as congo red described in section 5.2.6.1.7.

5.2.6.1.10. Preparation of chromium solution: 7.07 mg of $K_2Cr_2O_7$ salt was measured using a weighing machine (Sartorius, Germany) and taken into an Erlenmeyer flask. 40 mL of DI water was added to it and stirred on a magnetic stirrer to make the solution homogeneous. After the solution was prepared, taken in a measuring cylinder, and 10 mL of DI water was added to make the volume 50 mL.

To prepare 50 mL of 5 mg/L chromium solution from the previously prepared solution, 5 mL of the solution was taken, and DI water was added to make the volume 50 mL.

5.2.6.1.11. Preparation of fluoride solution: 2.63 mg of HF salt was measured using a weighing machine (Sartorius, Germany) and taken into an Erlenmeyer flask. 40 mL of DI water was added to it and stirred on a magnetic stirrer to make the solution homogeneous. After the solution was prepared, taken in a measuring cylinder, and 10 mL of DI water was added to make the volume 50 mL.

To prepare 50 mL of 5 mg/L fluoride solution from the previously prepared solution, 5 mL of the solution was taken, and DI water was added to make the volume 50 mL.

5.2.6.1.12. Preparation of lead solution: 3.99 mg of $Pb(NO_3)_2$ salt was measured using a weighing machine (Sartorius, Germany) and taken into an Erlenmeyer flask. 40 mL of DI water was added to it and stirred on a magnetic stirrer to make the solution homogeneous. After the solution was prepared, taken in a measuring cylinder, and 10 mL of DI water was added to make the volume 50 mL.

To prepare 50 mL of 5 mg/L lead solution from the previously prepared solution, 5 mL of the solution was taken, and DI water was added to make the volume 50 mL.

5.2.6.2. Experimental Procedure: 50 mL of prepared pollutant solutions (described in section 5.2.6.1) with a 5 mg/L concentration were taken in an Erlenmeyer flask. The desired weight of aerogel was measured using a weighing balance (Sartorius, Germany)

and added to the solutions at a 1 g/L dose. The flasks were placed into a BOD shaker incubator (Remi) and treated for 180 min. while keeping pH at 7, and temperature at 30^{o}C. The samples were collected after the adsorption was completed and analysed to determine the final concentration of pollutants in the solutions.

5.2.6.3. Analysis: The organic pollutants used in this study were analysed by an HPLC machine (Waters model- 2489). The final concentration of dyes was measured by a UV-Viz spectrophotometer (PerkinElmer, USA), and the chromium and lead ions were analysed by an ICP-OES (PerkinElmer, USA, Model- 8000). The fluoride concentration was measured by a fluoride meter (Orion Star A-214).

5.2.6.3.1. Analysis of dye: The analysis of dye concentration by using a UV-Viz spectrophotometer (PerkinElmer, USA) was performed following the same procedure as described in section 5.2.5.2.1. The maximum wavelength (λ_{max}) was 603 nm, 665 nm, and 497 nm in the case of aniline blue, methylene blue, and congo red, respectively.

5.2.6.3.2. Analysis of organic pollutants: The analysis of the final concentration of organic pollutants was performed using an HPLC (Waters model- 2489) machine and following the process described in section 5.2.5.2.2.

5.2.6.3.3. Analysis of metal ions: The standard solutions of metal for ICP-OES analysis were prepared by diluting the solutions previously prepared (As mentioned in sections 5.2.6.1.10 and 5.2.6.1.12). Four standard solutions of concentrations 0.1 mg/L, 1 mg/L, 3 mg/L, and 4 mg/L were prepared, respectively, and passed through a syringe filter before analysis by the ICP-OES (PerkinElmer, USA, Model- 8000). A 2% HNO_3 solution was used as the blank solution for this analysis. Syngistix software was used to determine the unknown concentrations from the standard solutions.

For fluoride analysis, a fluoride meter (Orion Star A-214) was used. Three standard solutions with a concentration of 0.1 mg/L, 1 mg/L, and 10 mg/L were prepared by dissolving the stock solution previously prepared (mentioned in section 5.2.6.1.11). An Orion ion plus filling solution was used as the charge carrier of the detection probe. The instrument was calibrated using the standard solutions, and the unknown concentration was detected from the calibration curve by submerging the probe in the solution. A TISAB-II adjustment buffer was used with a concentration of 1 mL/ 10 mL solution to maintain the equal distribution of fluoride ions in the solution.

5.2.7. Multipollutant removal study by the aerogels: To study the multipollutant removal capacity of the prepared aerogel, naphthalene, acenaphthene, and phenol were considered as the pollutants of interest.

5.2.7.1. Preparation of solutions: To prepare the solutions of naphthalene, acenaphthene, and phenol with 5 mg/L concentrations, the same process as described in sections 5.2.5.1.1, 5.2.5.1.2, and 5.2.5.1.3. respectively were followed. A total of four mixed pollutant solutions, 100 mL each, were prepared by mixing equal volumes of the single pollutant solutions into Erlenmeyer flasks. Four solutions, viz., naphthalene-phenol (N-P), naphthalene-acenaphthene (N-A), acenaphthene-phenol (A-P), and naphthalene-acenaphthene-phenol (N-A-P), were prepared to check the removal of these pollutants.

5.2.7.2. Experiment: The prepared aerogel was measured using a weighing balance (Sartorius, Germany) and added to the pollutant solution with a 1 g/L dose, which was taken inside an Erlenmeyer flask. The solutions were treated inside a BOD shaker incubator (Remi) for 180 min. under constant agitation, while other parameters were kept constant (pH 7, temperature 303 K). After the treatment was completed, the samples were collected and analysed using an HPLC machine (Waters model- 2489).

5.2.7.3. Analysis: The analysis of the final concentration was performed by following the process described in section 5.2.5.2.2.

5.3. Result:

5.3.1. Crystallographic profiling: The crystallographic profiling of the filler materials, viz., cellulose, silica, and biochar, was performed by XRD analysis and is presented in Fig. 5.1 (A), (B), and (C), respectively. From Fig. 5.1 (A), it was observed that two distinct peaks were found at 2Θ= 22.36°, and 35.22°. Two independent studies reported similar peaks of cellulose at 2Θ= 22° (Zhao et al., 2007) and 20° (Louis and Venkatachalam, 2020), respectively. Another study conducted by Kim et al. (2013) also reported that Iβ cellulose exhibited a peak at 2Θ= 22°. The mentioned studies reported that these peaks represent the crystallographic plane of cellulose. Escobar et al. (2022) reported the presence of an amorphous halo at 2Θ= 30.10° detected by the XRD detector. This study also reported that another peak at 2Θ= 45.84° is associated with the (200) plane of cellulose I crystal structure and is part of a broader amorphous background in the cellulose XRD pattern.

From Fig. 5.1 (B), it was observed that in the case of biochar, four peaks at 2Θ= 8.85°, 17.87°, 28.91°, and 33.72° were found respectively. Xin et al., 2015 reported that a peak at 2Θ= 16° was found in the case of biochar, representing the 101 spacing of the biomasses. Another study reported that, for rice husk biochar, a peak at 2Θ= 41° was observed (Burachevskaya et al., 2023). The peak at 2Θ= 28.91° and 33.72° represents the (220) and (311) crystal planes, respectively, as reported by Santhosh et al. (2020). Another peak at 2Θ= 8.85° signifies the amorphous characteristics of the prepared biochar (Han et al., 2021).

Fig. 5.1 (C) represents the XRD analysis of silica. Three significant peaks were observed at 2Θ= 22.27°, 34.34°, and 40.51°, respectively. According to Nguyen et al. (2022), the peak at 2Θ= 22.27° indicates the amorphous structure of extracted silica. The peak at 2Θ= 34.34° represents the trace of silicate quartz in the sample. This peak is typically associated with the (101) plane of the quartz. On the other hand, the peak at 2Θ= 40.51° is attributed to the (200) plane of crystalline silica. This peak typically characterises cristobalite, a high-temperature SiO_2 polymorph.

The crystallographic profiling of the prepared aerogels was performed by XRD analysis. Fig. 5.1 (D) shows the result of the XRD analysis of the prepared aerogel. From the figure, for all the aerogel samples, a peak at 2Θ= 19.3° was observed. Hema et al. (2009) reported that this peak is a characteristic peak of the PVA component. From Fig., a change in the XRD peak was also observed after adding fillers into the aerogel network. In case of PVA-BC aerogel, a new peak was observed at 2Θ= 27° was observed, confirming the presence of biochar inside the matrix (Santhosh et al., 2020). In the case of PVA-C aerogel, the characteristic peak of cellulose was observed 2Θ= 21.90° (Zhao et al., 2007). From the XRD analysis of PVA-Si aerogel, a peak at 2Θ= 26.73° was observed, confirming the presence of silica inside the PVA network (Nguyen et al. 2022).

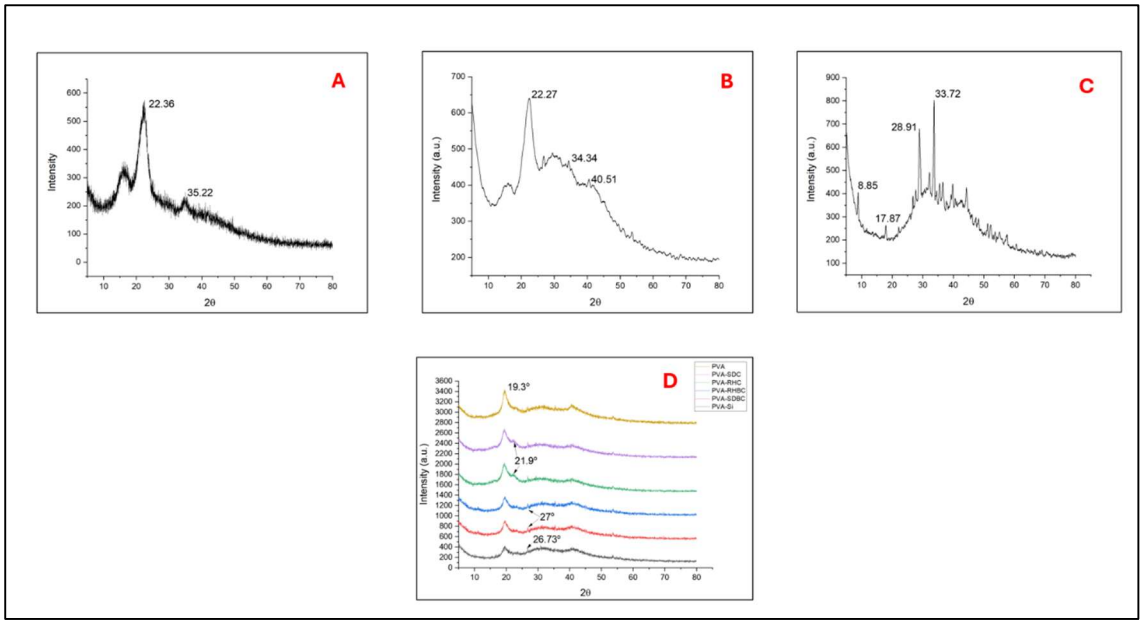

Figure 5.1: XRD analysis of (A) cellulose, (B) biochar, (C) silica, (D) aerogels

The degree of crystallinity of the filler material and the prepared aerogels was calculated. From the data presented in Table 5.1, it was observed that the % of crystallinity changed significantly after the addition of fillers. From the table, it was observed that both type of biochar and silica plays a significant role in increasing the crystallinity of the prepared PVA aerogel. In case of normal aerogel, where the % of crystallinity was found to be 18.40%, in case of biochar, it increased to 37.75% and 41.17% by adding SDBC and RHBC, respectively. As a contribution of silica, the % of crystallinity was found to be 23.45%. On the other hand, being a softer material, cellulose slightly decreased the crystallinity % of aerogel after adding it to the network. The crystallinity% % of PVA-SDC and PVA-RHC aerogels were found to be 16.81% and 17.23%, respectively.

Table 5.1: Crystallinity percentage of prepared aerogels

Aerogel	**% of Crystallinity**
PVA	18.40
PVA-SDBC	37.75
PVA-RHBC	41.17
PVA-SDC	16.81
PVA-RHC	17.23
PVA-Si	23.45

The orientation of the plane inside the crystalline lattice and the interplanar distance were calculated from Bragg's equation. The Miller's indices of prepared aerogels and the interplanar distance (d) are presented in Table 5.2.

Table. 5.2: Orientation of crystalline plane and interplanar distance

Aerogels	λ (Å)	2Θ	Θ	Sin(Θ)	h, k, l	d_{hkl} (Å)
PVA	1.5481	19.3	9.65	0.167545	(1 1 1)	4.619954
PVA-SDBC	1.5481	27	13.5	0.233329	(1 2 0)	3.317416
PVA-RHBC	1.5481	27.62	13.81	0.238584	(1 2 1)	3.244346
PVA-SDC	1.5481	21.9	10.95	0.189857	(1 1 1)	4.077012
PVA-RHC	1.5481	22.03	11.015	0.19097	(1 1 1)	4.053248
PVA-Si	1.5481	26.73	13.365	0.231039	(2 1 0)	3.350306

The table shows that PVA aerogel intersects the X, Y, and Z axes at 1, 1, and 1 position, as do both PVA-cellulose aerogels. For PVA-SDBC and PVA-Si aerogels, the unit cells are parallel to the Z axis and intersect X and Y axes at 1 and $\frac{1}{2}$ positions. For PVA-RHBC aerogel, the unit cell intersects the X, Y, and Z axes at 1, $\frac{1}{2}$, and 1 position. From this observation, it can be interpreted that the filler material has a high influence on the aerogels' crystalline structure and unit cell orientation.

The interplanar distance was observed not to vary significantly. As represented in the table, the d-value varied from 3.24 Å to 4.61 Å.

5.3.2. Functional group analysis: The functional groups present on cellulose, biochar, and silica surface are presented in Fig. 5.2 (A), (B), and (C), respectively. From Fig. 5.2 (A), it can be observed that in the case of cellulose, peaks at 3324 cm^{-1}, 2931 cm^{-1}, 2858 cm^{-1}, 1732 cm^{-1}, 1628 cm^{-1}, 1510 cm^{-1}, 1159 cm^{-1}, 1030 cm^{-1}, 897 cm^{-1}, and 791 cm^{-1} are present. Tsalagkas (2015) reported that the peaks at 3324 cm^{-1} and 2931 cm^{-1} represent the inter and intra H-bonds and CH stretching vibration, respectively. The peak at 1732 cm^{-1} is responsible for the C=O group (Garside and Wyeth, 2003). Also, it was found that the peaks at 1628 cm^{-1} and 1510 cm^{-1} are attributed to the C=O stretching and N-H bending, respectively (Zhang et al., 2012). The peaks at 1159 cm^{-1} and 1030 cm^{-1} represent the C=C group and Si-O-Si group, respectively (Yang et al., 2007; Daffalla et al., 2020). Another study conducted by Vârban et al. (2021) reported that the peaks at 897

cm^{-1} and 791 cm^{-1} represent the presence of the C-O-C stretching vibration of β-glycosidic linkages and out-of-plane bending vibrations of C-H bonds, respectively.

As presented in Fig. 5.2 (B), the ATR-FTIR analysis of biochar shows the presence of transmittance peaks at 3738 cm^{-1}, 1990 cm^{-1}, 1599 cm^{-1}, 1088 cm^{-1}, and 788 cm^{-1}, respectively. Krivoshein et al. (2022) reported that the peak at 3738 cm^{-1} is attributed to the Si-O-H bond in the biochar, which is a common functional group present in agricultural waste. Another peak at 1990 cm^{-1} represents the Si-O-Si bond (Liu et al., 2015). Another study reported that the peak at 1599 cm^{-1} represents the COO^- group (Ray et al., 2020). Also, it was found that the peak at 1088 cm^{-1} is attributed to the C-O stretching in polysaccharides. Also, the peak at 788 cm^{-1} is associated with the aromatic C-H out-of-plane bending (Krivoshein et al., 2022).

The ATR-FTIR analysis of silica is presented in Fig. 5.2 (C). From the figure, five peaks, viz., 3392 cm^{-1}, 1638 cm^{-1}, 1044 cm^{-1}, 784 cm^{-1}, and 606 cm^{-1}, were observed respectively. Chuan-Chao et al. (2014) reported that the peak at 3391 cm^{-1} is attributed to -SiOH stretching vibrations. The other peaks at 1638 cm^{-1}, 1044 cm^{-1} and 784 cm^{-1} represent the H-O-H bending vibration and Si-O-Si bridge, respectively (Chuan-Chao et al., 2014). Another peak, 606 cm^{-1} attributed to the Si-O-Si vibration or lattice modes in silica.

Fig. 5.2 (D) presents the ATR-FTIR analysis of prepared aerogels. From the figure, four major peaks were seen at 3373 cm^{-1}, 2914 cm^{-1}, 1645 cm^{-1}, and 1091 cm^{-1}, respectively. The presence of an aldehyde group in the aerogel was observed at 3373 cm^{-1} due to the usage of glutaraldehyde in the production process. Peaks at 2914 cm^{-1} and 1645 cm^{-1} are attributed to the C-H of alkyl groups and C=O groups, respectively (Mansur et al., 2004). The presence of C-O stretching of acetyl groups is represented by 1091 cm^{-1} (Nafee et al., 2017). As the PVA, biochar, and cellulose contain almost the same functional group compositions on their surface, no significant difference in the ATR-FTIR analysis was observed. However, in the case of PVA-Si aerogel, a distinct peak at 606 cm^{-1} was observed representing Si-O-Si vibration (Chuan-Chao et al., 2014).

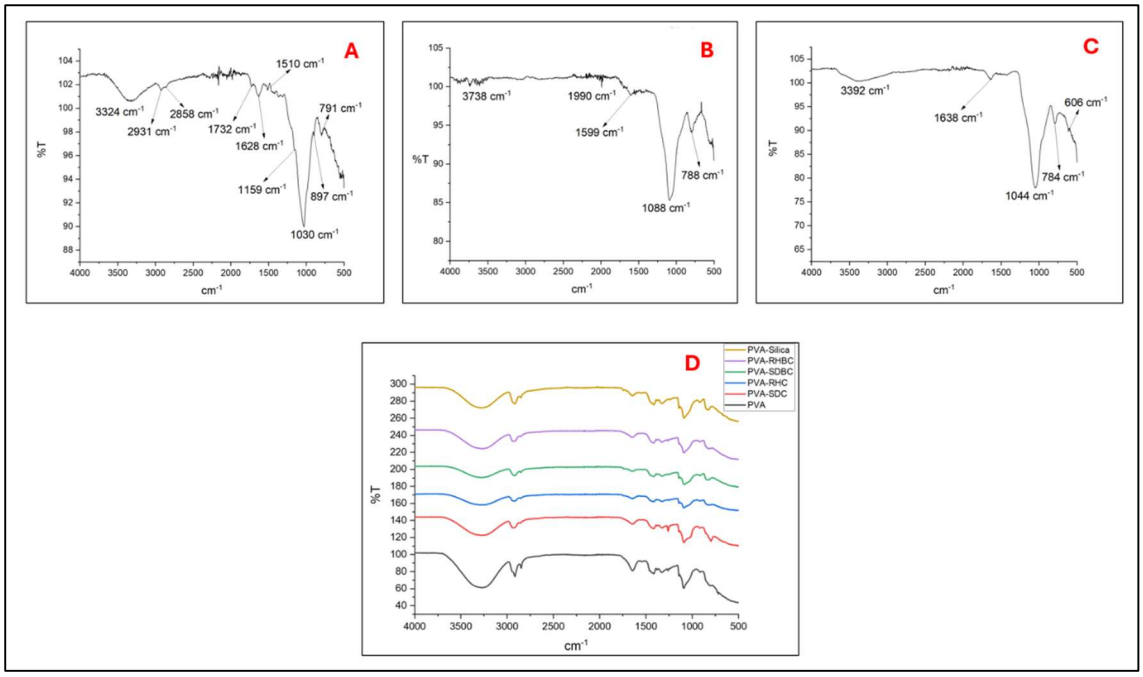

Figure 5.2: ATR-FTIR analysis of (A) cellulose, (B) biochar, (C) silica, (D) aerogels

5.3.3. Scanning electron microscopy: To understand the surface morphology of the fillers and prepared aerogels, SEM analysis was performed. Fig. 5.3 presents the SEM images of different components. From Fig. 5.3 (A), the SEM image of cellulose was observed. In the image, the uneven surface of extracted cellulose is visible, which contributes to its high surface area. Krishnamachari et al. (2011) reported similar results, and Das et al. (2010) concluded the particle shapes were not isomeric. In case of biochar, as shown in Fig. 5.3 (B), the individual particles are clearly visible. The particles are different in size, with uneven surfaces and varied shapes. Gondim et al. (2018) reported a similar result for SEM images of biochar and concluded that these substrates contain a high volume of pores, which makes them favourable for adsorption. In Fig. 5.3 (C), the SEM image of silica is presented. The amorphous nature of the silica surface can be observed from the image. This amorphous nature contributes to the mesoporous characteristics of the extracted silica and ensures its ability to adsorb pollutants.

The SEM images of prepared aerogels are presented in Fig. 5.3 (D)- 5.3 (I). In Fig. 5.3 (D), the surface of PVA aerogel is presented. Compared to that, the rest of the aerogel surfaces are showing uneven structures with the presence of pores. In the case of every aerogel, the surface morphology changed significantly after adding fillers to the PVA network. The presence of these cavities on the surface contributes to the high adsorption efficiency of the aerogels. In a previous study from the SEM image analysis, it was

reported that the aerogels prepared by freeze-drying depend on the H-bond for their structures (Chen et al., 2011).

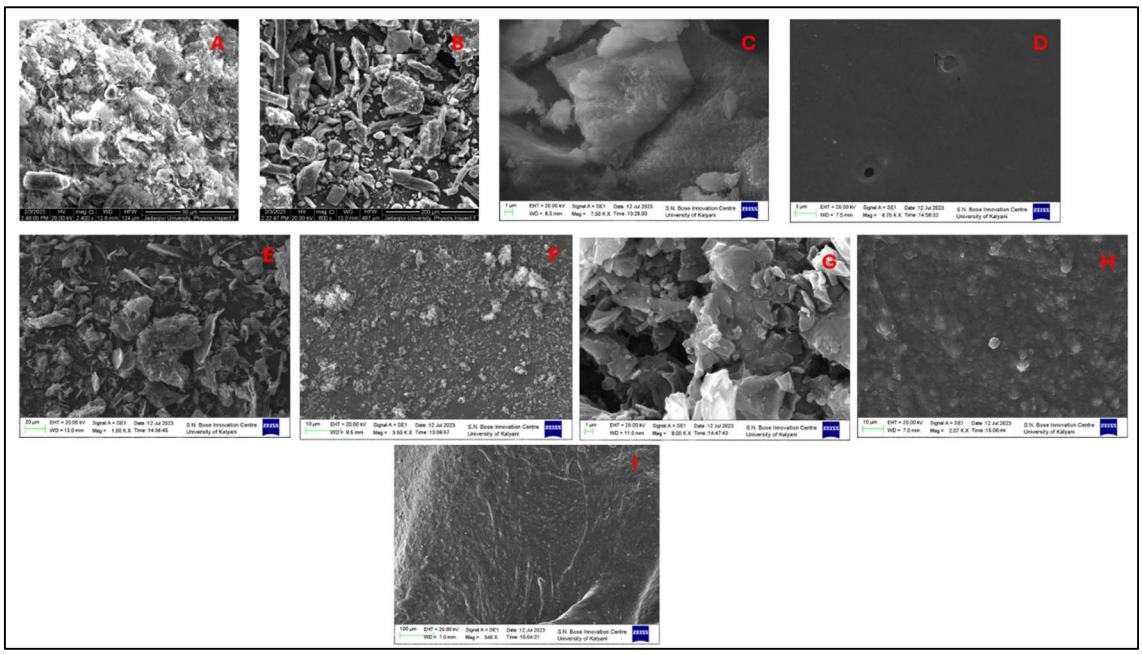

Figure 5.3: Scanning electron microscopy (SEM) analysis of (A) cellulose, (B) biochar, (C) silica, (D) PVA aerogels, (E) PVA-SDC aerogel, (F) PVA-RHC aerogel, (G) PVA—PVA-RHBC aerogel, (H)PVA-Si aerogel, (I) PVA-SDBC aerogel.

5.3.4. Elemental analysis: The surface elemental composition of the aerogels was studied by EDAX analysis. The EDAX analysis reported a uniform distribution of the fillers inside the aerogel network. A previous study reported a similar distribution of nanoparticles inside aerogels (Bigall et al., 2009). Table 5.3 represents % of different materials present in the synthesised aerogels. From the study, it was found that PVA aerogel contains 100% carbon, and PVA-Si aerogel contains the least carbon, with the value of 51.13%. Also, the presence of silica was detected in the PVA-Si aerogel network at 8.78%. The rest of the aerogels contain carbon and oxygen with different %. The results of EDAX analysis are presented in Fig. 5.4 (A)- 5.4 (F).

Table 5.3: EDAX analysis of synthesized aerogels

Aerogels	Carbon atomic %	Oxygen atomic %	Silica atomic %
PVA	100	-	-

PVA-SDC	62.04	37.96	-
PVA-RHC	64.77	35.23	-
PVA-SDBC	57.68	42.32	-
PVA-RHBC	57.58	42.42	-
PVA-Si	51.13	40.10	8.78

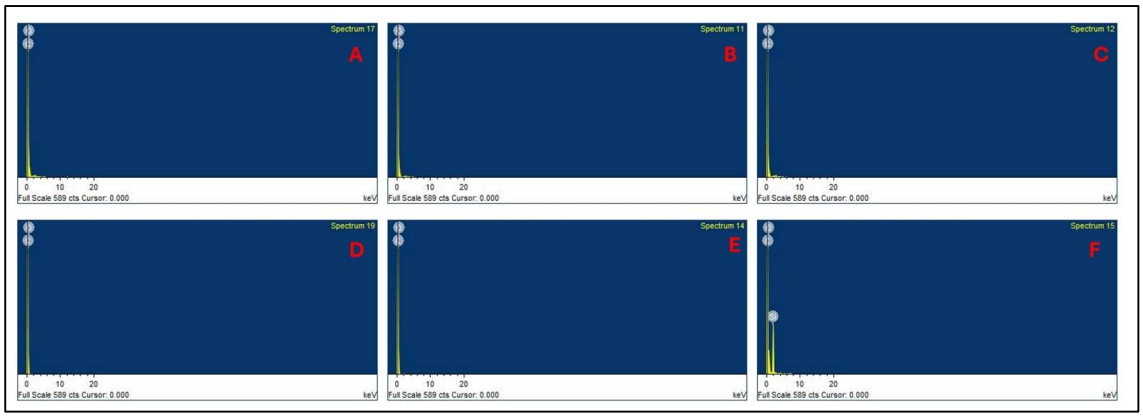

Figure 5.4: EDAX analysis of (A) PVA aerogel, (B) PVA-SDC aerogel, (C)PVA-RHC aerogel, (D) PVA-SDBC aerogels, (E) PVA-RHBC aerogel, (F) PVA-Si aerogel.

5.3.5. Microscopic analysis: The microscopic structure of prepared aerogels was studied by a light microscope (Dewinter, Fluorex-LED). The surface observed under the microscope is presented in Fig. 5.5 (A)- 5.5 (F). The figures show that the aerogels consist of an uneven surface that plays a significant role in the adsorption efficiency of the prepared aerogels. From the result of this analysis, it was also observed that the fillers distributed themselves inside the aerogel network and affected the distribution, number, and size of the pores present on the surface.

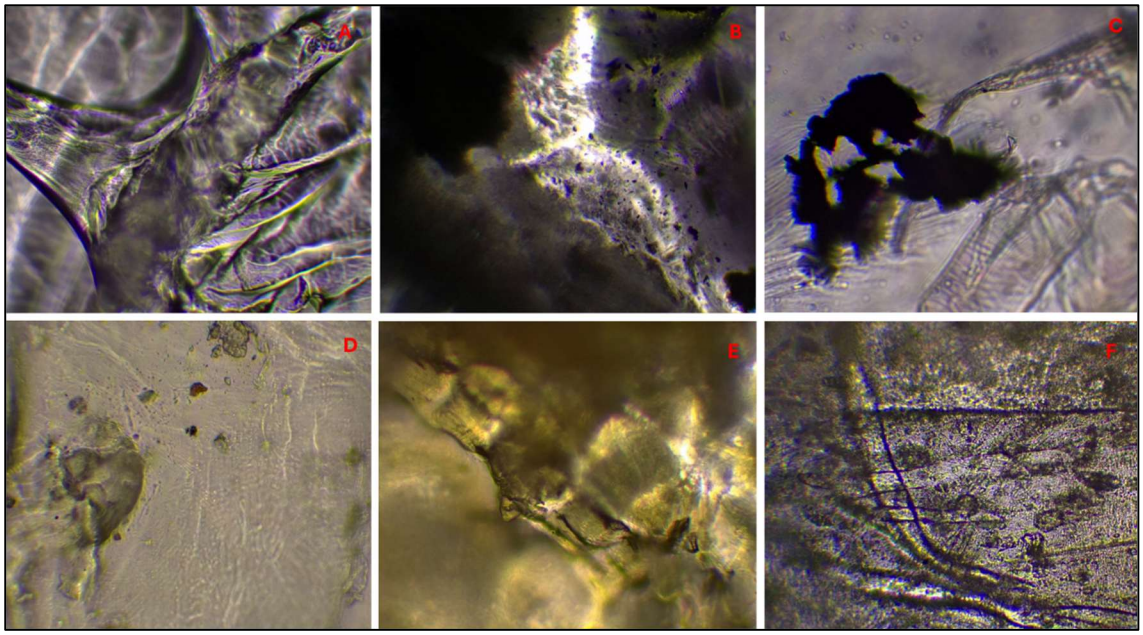

Figure 5.5: Microscopic images of (A) PVA aerogel, (B) PVA-SDBC aerogel, (C) PVA-RHBC aerogel, (D) PVA-RHC aerogels, (E) PVA-SDC aerogel, (F) PVA-Si aerogel.

5.3.6. Thermal profiling: Fig. 5.6 (A) shows the thermogravimetric analysis (TGA) of the prepared aerogels. From this figure, a difference in the change in percentage of weight for temperature was observed. For PVA aerogel, the weight% % decreased to 87.97% at the temperature 176 ºC, and then it rapidly degraded to 0%. For the rest of the aerogels, the first stage of sample degradation was found in the range of 40ºC to 269.24 ºC. The weight loss in this stage signifies the degradation of PVA. The second stage of aerogel was continued till 481.86 ºC. This stage is attributed to the degradation of the crosslinking of the PVA network. From 481.86 ºC to 800ºC, carbonation of the samples was observed (Yang, 2007). From the result of TGA analysis, it can be stated that, despite the presence of different fillers, the aerogels showed a similar type of TGA curve, indicating that the degradation behaviour of the aerogels depends more on the properties of PVA than the fillers. On the other hand, it was also observed that the degradation behaviour of the aerogels changed after adding the fillers. From this observation, it can be stated that the fillers have a significant role in the thermal stability of the aerogels.

Fig. 5.6 (B) shows the differential thermal analysis (DTA) of the prepared aerogels. In the figure, in the first step of the reaction, upward peaks are visible for PVA-Si, PVA-SDC, and PVA-RHC aerogels at 144.48 °C, 506.63 ºC, and 493.12 ºC, respectively. These peaks signify an exothermic event during the sample degradation. In this stage, for PVA, PVA-SDBC, and PVA-RHBC aerogels, a downward peak was observed at 181.56 ºC,

106.75 ºC, and 106.71 ºC, respectively. These peaks represent an endothermic event during this analysis. In the second step of the reaction, PVA-Si, PVA-SDC, and PVA-RHC showed an endothermic event till the end of the experiment and for PVA-SDBC and PVA-RHBC, an exothermic shift was observed. In the case of PVA aerogel, a sudden exothermic reaction was observed till 255.73 ºC, and after that, no significant change was observed. This observation explains the sudden degradation of PVA aerogel as shown in Fig. 5.6 (A).

Fig. 5.6 (C) shows the differential scanning calorimetry (DSC) analysis of the prepared aerogels. In that figure, a distinct endothermic peak for PVA aerogel was observed at 176 ºC supports the TGA data and rapid degradation of the PVA aerogel. The gradual increase of heat flow for all the samples suggests the continuous decomposition of the samples with increasing temperature. At a higher temperature, a divergence in the thermal curves was observed for different samples, explaining their different thermal stability and behaviour. It was also observed that the PVA-Si aerogel is showing a distinct characteristic compared to other aerogels with a lower heat flow and smooth profile due to the exceptional thermal properties of silica. The observations of DSC analysis support the conclusions made from the TGA analysis of the aerogels as presented in Fig. 5.6 (A).

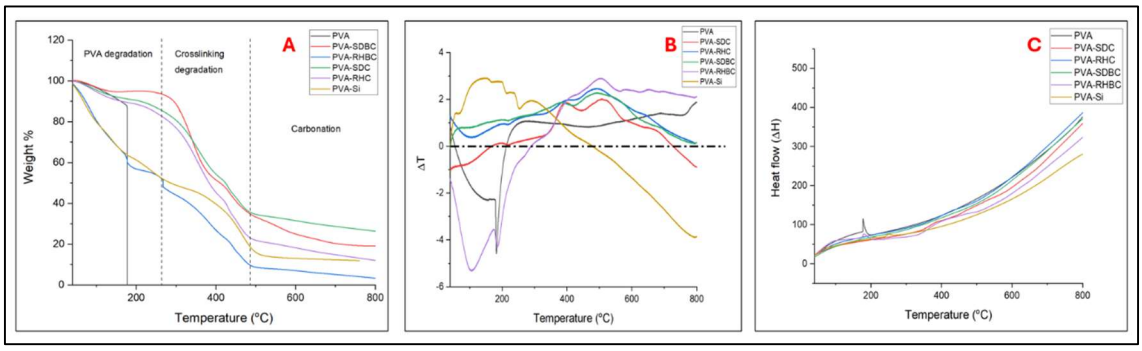

Figure 5.6: (A) TGA, (B) DTA, (C) DSC analysis of aerogels.

5.3.7. Physical properties of aerogel: From analysing different physical properties of the prepared aerogels, it was observed that fillers have a significant effect on the physical properties of the substances. The detailed analysis result is described below.

5.3.7.1. Density analysis: Fig. 5.7 (A) shows the density of different aerogels. From the figure, it was observed that the PVA-Si aerogel has the lowest density among all the prepared aerogels, with the value of 0.1091 g/cm^3. Another independent study reported that the density of PVA-Si aerogel with 5% volume of fibres was 0.11 g/cm^3 that also

supports the finding of this study (Linhares et al., 2019). It was also reported that the density of silica aerogel was 0.140 g/cm^3, and the density of PVA-RHBC was observed to be 0.2629 g/cm^3 (Kim et al., 2008). This result can be explained by considering the particle size of the fillers. The small particle is responsible for the blockage of pores and for increasing the density of aerogels. According to another study, the density of aerogel was found to be between 0.0081 g/cm^3 and 0.02 g/cm^{3,} which also supports the finding of this study, as the aerogels prepared in this experiment show a density less than or equal to 0.02 g/cm^3 (Ferrero, 2007).

5.3.7.2. Porosity analysis: The mechanical, thermal, and optical properties of a substance are highly dependent on the porosity. Fig. 5.7 (B) shows the porosity of different aerogels prepared in this study. From the figure, it can be stated that the PVA-RHBC aerogel has the least porosity, with a value of 83.56%. On the other hand, the highest porosity was found in the case of PVA-Si aerogel with the value of 97.05%. Another study reported that the porosity of aerogel after freeze-drying was between 80%-97% (Hossen et al., 2020). This result also supports the findings of this study.

5.3.7.3. Moisture content analysis: The result of moisture content analysis is shown in Fig. 5.7 (C). From the figure, it was shown that PVA-Si aerogel had the lowest moisture content among all the aerogels, with the value of 8.12%. This behaviour of the prepared aerogel can be explained by the hydrophobic nature of silica. A similar result was reported in a previous study conducted with TEOS and TMOS aerogel (Ingale et al., 2011). The highest moisture content was observed in the case of PVA aerogel, with the value of 16%.

5.3.7.4. Swelling test: The swelling test was conducted to understand the water uptake capacity of the prepared aerogels to understand their water uptake capacity. From the experiment, it was observed that all the aerogels absorb water, and the highest water uptake was observed in the case of PVA-SDBC aerogel. The least water uptake was observed in the case of PVA-SDC aerogel. The result of the swelling test is presented in Fig. 5.7 (D). A similar result was observed in a previous study conducted by PVA-chitosan aerogel (Xu et al., 2021). This result can be explained by the presence of -OH groups on the PVA surface (Javadi et al., 2013). The PVA-SDBC aerogel showed the highest absorption among all the samples due to its highly porous structure as observed in the microscopic analysis. The swelling of PVA-Si aerogel could be explained by the

hydrophobic property of silica (He et al., 2019; Yokogawa and Yokoyama, 1995; Malfait et al., 2015).

5.3.7.5. Effect of temperature: Fig. 5.7 (E) shows the effect of temperature on the aerogels. As stated in the figure, changes in four major peaks are visible at 3277 cm^{-1}, 1649 cm^{-1}, 1416 cm^{-1}, and 1084 $cm^{-1,}$ respectively, after heating the aerogel at 60^{o}C. As reported in a previous study, the peak at 3277 cm^{-1} represents the aldehyde group present in the aerogel network (Mansur et al., 2004). Other peaks at 1649 cm^{-1} and 1084 cm^{-1} show that the C=O group and C-O stretching, respectively, are also affected by temperature (Nafee et al., 2017). All the mentioned functional groups play an important role in the crosslinking of PVA aerogel. So, temperature is an important parameter for affecting the crosslinking of the aerogel network.

5.3.7.6. Effect of salinity: A difference in weight% was observed after the aerogels were treated with 10% NaCl (w/v) solution. As presented in Fig. 5.7 (F), PVA-Si aerogel was observed to be affected the most and lost 27% of its initial weight after 1 hr of salinity treatment. For the rest of the aerogels, an increase in the weight% % was found. After salinity treatment of the aerogels, they were analysed by ATR-FTIR analysis and changes in peaks at 2914 cm^{-1}, 2846 cm^{-1}, 914 cm^{-1}, and 827 cm^{-1} were detected, respectively, as presented in Fig. 5.7 (G). It was reported that the peak at 2914 cm^{-1} represents the C-H bond of alkyl groups (Mansur et al., 2004). Another peak at 2846 cm^{-1} appeared due to the presence of C-H stretching (Xu et al., 2021). A depletion of the peak after salt treatment represents the C-H bond breaking due to the reaction with NaCl. The peak at 2846 cm^{-1} represents the -CONH stretching vibration (Costa-Junior et al., 2009). Another peak at 1646 cm^{-1} represents the N-H bending stretching. Also, two peaks at 914 cm^{-1} and 827 cm^{-1}, respectively, became more prominent after salt treatment, confirming the reaction between the PVA network and NaCl.

5.3.7.7. Effect of pH: Fig. 5.7 (H) shows the effect of different pH on the prepared aerogels after treating them for 2 hr. Five different pH values, viz., 2, 4, 6, 8, and 10, were considered for this experiment. From the figure, it was observed that no significant weight difference was found under the influence of pH, except for the PVA aerogel. It was also found that the degradation of aerogels increased in an alkaline environment. In the preparation process of aerogel, HCl was used as the catalyst, which indicates the crosslinking reaction is favourable at lower pH. This explains the degradation of the PVA

network at higher pH. The least degradation was found in the case of PVA-Si aerogel, and the highest value of the degradation of PVA-Si aerogel was found to be 3.4% at pH 10. On the other hand, for PVA aerogel, the degradation was found to be 11%. This observation signifies that the presence of fillers significantly increases the stability of the PVA network.

5.3.7.8. Oil absorption study: Fig. 5.7 (I) shows the oil absorption property of aerogels. From the figure, it can be stated that all the prepared aerogels tend to absorb oil from the media. PVA-Si was found to be the most efficient among all aerogels to absorb the oil in 6 min. This result can be explained by the hydrophobic property of silica. PVA aerogel took the longest time, 20 min. to absorb the same volume of oil, which indicates that the addition of fillers to the PVA network significantly increases the oil absorption capacity of the aerogels.

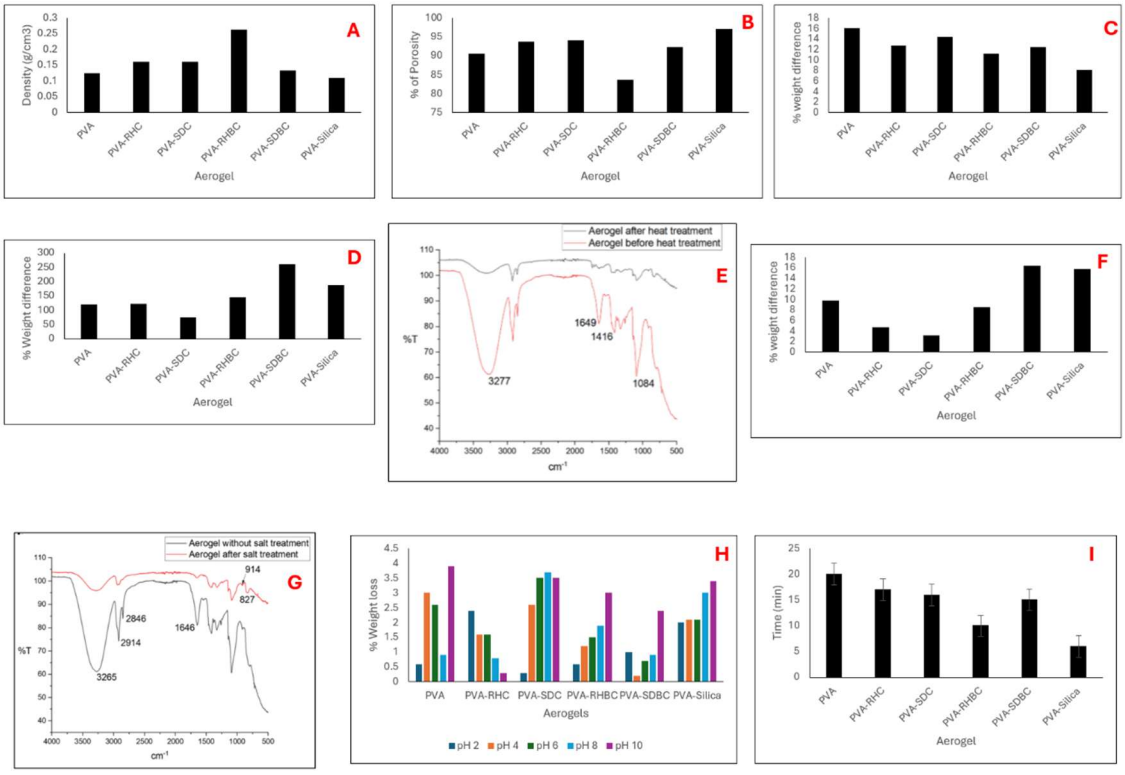

Figure 5.7: Physical characteristics of aerogels (A) density, (B) porosity, (C) moisture content, (D) swelling property, (E) effect of temperature, (F) effect of salinity, (G) effect of salinity on surface functional groups, (H) effect of pH, (I) oil absorption property.

5.3.8. Removal of pollutants by fillers: In this study, three contaminants of interest, naphthalene, phenol, and acenaphthene, were considered, and their removal was investigated using the fillers cellulose, silica, and biochar.

5.3.8.1. Removal of naphthalene: In the case of naphthalene, the highest removal% found was 84.03% in the case of rice husk cellulose after 3 hr. of treatment. The least removal was observed with sawdust biochar, with the value of 64.55%. The result is presented in Fig. 5.8 (A). A similar result was reported by Pathak et al. (2023), where naphthalene was removed by biochar produced from sugarcane bagasse. Another study reported that by using pinewood sawdust biochar, 90% of naphthalene removal was achieved (Rashad et al., 2022). This phenomenon can be explained by considering the contact time and morphology of the adsorbent. All the adsorbents, viz., cellulose, silica, and biochar, had a highly porous structure that can adhere the pollutant molecules to their surface. On the other hand, a long duration of treatment time increased the interaction probability of pollutant molecules with the adsorbent surface increased the removal of the contaminants.

5.3.8.2. Removal of phenol: The results of phenol removal by different fillers are presented in Fig. 5.8 (B). Same as naphthalene, for phenol, rice husk cellulose showed the highest removal of 67.70% and the least removal was found by sawdust biochar with the value of 56.37%. Khoj (2024) reported that by using silica-calcium alginate nanocomposite, phenol removal was achieved with 100.55 mg. g^{-1} adsorption capacity. This phenomenon can be explained by considering the contact time and morphology of the adsorbent. All the adsorbents, viz., cellulose, silica, and biochar, had a highly porous structure that can adhere the pollutant molecules to their surface. On the other hand, a long duration of treatment time increased the interaction probability of pollutant molecules with the adsorbent surface increased the removal of the contaminants.

5.3.8.3. Removal of acenaphthene: The result of acenaphthene removal is presented in Fig. 5.8 (C). From the figure, it can be stated that silica showed the highest acenaphthene removal, with the value of 77.96%. On the other hand, sawdust biochar showed the least acenaphthene removal, and the value was 62.13%. This phenomenon can be explained by considering the contact time and morphology of the adsorbent. All the adsorbents, viz., cellulose, silica, and biochar, had a highly porous structure that can adhere the pollutant molecules to their surface. On the other hand, a long duration of treatment time increased the interaction probability of pollutant molecules with the adsorbent surface increased the removal of the contaminants.

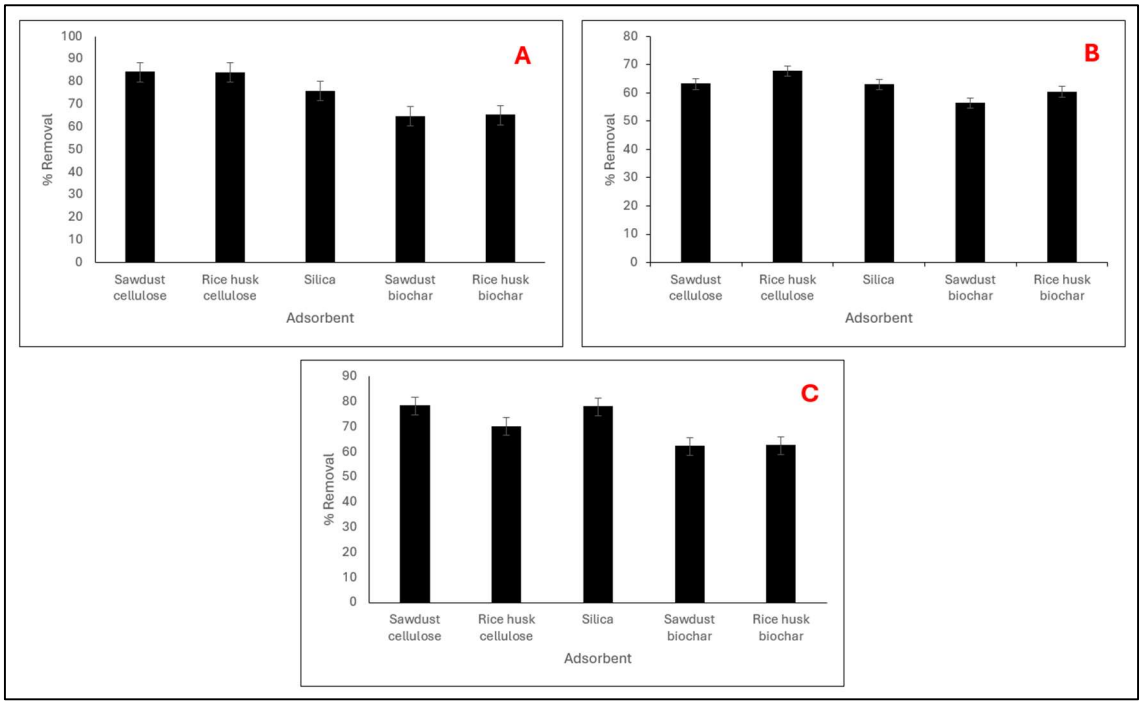

Figure 5.8: Adsorption of (A) naphthalene, (B) phenol, and (C) acenaphthene by fillers.

5.3.9. Removal of naphthalene by aerogel: In this study, a total of six aerogels were prepared, and the removal of naphthalene by these aerogels was studied. To understand the detailed nature of the adsorption process, different parameters, viz., time, dose of aerogel, concentration of pollutant, pH, and temperature, were varied. The detailed result is explained below.

5.3.9.1. Effect of contact time: The effect of contact time on the adsorption of naphthalene is shown in Fig. 5.9 (A). As represented in the figure, the removal of naphthalene increased with time, and the highest removal achieved in this study was 87.97% by PVA-SDBC aerogel after 3 hr. of treatment while the other parameters were constant (pH 7, dose 1g/L, concentration 5mg/L, and temperature at 303 K). For comparison, under the same conditions, for PVA-Si, PVA-SDC, and PVA-RHBC. PVA-RHC and PVA aerogel showed 82.20%, 80.03%, 79.35%, 79.12%, and 64.23%, respectively. After 180 min. of treatment, no significant change was observed in the concentration of naphthalene, indicating that the adsorption equilibrium was achieved. A previous study showed that for PVA-Si aerogel, the naphthalene removal reached up to 70.5% (Ghosh et al., 2024). This observation can be explained by considering the available surface area on the adsorbent surface and the interaction time of the adsorbent with adsorbate molecules. Before achieving the adsorption equilibrium, a large surface area and many pores on the adsorbent surface were available that contributed to the

significant removal of the contaminant. But after 3 hr., the active sites on the aerogel surface eventually got saturated, which ceased the rapid increase of the removal% (Gao et al., 2019). From this observation, it can also be stated that fillers have a significant effect on the removal efficiency of aerogels, which causes the difference in removal using different aerogels.

5.3.9.2. Effect of adsorbent dose: The dosage of adsorbent is a crucial parameter and affects the adsorption process significantly by the quantitative ratio of adsorbate and adsorbent (Şentürk and Alzein, 2020). According to Kroeker's rule, for a constant initial concentration, the specific adsorbed volume decreases with increasing adsorbent mass (Pernyeszi et al., 2019). Thus, the adsorbent dose is positively correlated with the removal of the contaminant. This study considered three different dosages of aerogels, viz., 0.5 g/L, 1 g/L, and 1.5 g/L, respectively. The effect of adsorbent dose on the removal of naphthalene is shown in Fig. 5.9 (B). As represented in the figure, with the increasing dose of aerogel, the removal also increased. It was observed that for PVA, PVA-SDC, PCA-RHC, PVA-SDBC, PVA-RHBC, and PVA-Si, the removal increased from 47.55% to 76%, 48.62% to 81.13%, 46.72% to 82.76%, 48.40% to 86.48%, 54.60% to 87.12%, and 48.40% to 87.55%, respectively. With the increasing adsorbent dosage, at a constant concentration of pollutant, more active surface area is available to interact with the pollutant molecules and increase the adsorption of the pollutant (Ma et al., 2020). From the result, it was also observed that, from 0.5 g/L to 1 g/L aerogel dosage, the adsorption increased rapidly, whereas from 1 g/L dosage to 1.5 g/L, the increase in the removal% was not significant. This observation can be explained as after a specific adsorbent dosage, maximum adsorption is reached, and the availability of additional active sites does not affect the saturation point (Rápó et al., 2020; Rápó et al., 2019; Hamza et al., 2018).

5.3.9.3. Effect of naphthalene concentration: Initial pollutant concentration is one of the key parameters to affect the adsorption process. The pollutant concentration has a significant role in the interaction rate between contaminant molecules and adsorption sites. The initial concentration of the solute acts as a driving force of the adsorption process, favouring diffusion and mass transfer from the solution. In such water treatment systems, the efficiency of the pollutant removal and the maximum concentration of pollutant adsorbed on the adsorbent's surface are directly related to initial dye concentration (Terangpi and Chakraborty, 2017). In this study, four naphthalene

concentrations, viz., 1 mg/L, 5 mg/L, 7 mg/L, and 10 mg/L, respectively, were considered. As shown in Fig. 5.9 (C), the maximum removal of naphthalene was observed in the case of PVA-Si aerogel, at 1 mg/L concentration. The removal was 97.64%. Being an efficient adsorbent, PVA-Si shows higher removal of naphthalene compared to other aerogels. It was also observed that with the increasing initial concentration, the removal decreased. In the case of PVA-Si aerogel, the removal% dropped to 70.35% at 10 mg/L initial concentration and showed the highest removal among all the aerogels at the specific initial concentration. This observation can be explained by the saturation of adsorption sites on the adsorbent surface. At low pollutant concentration, the active site and contaminant molecule's ratio is larger, allowing the molecules to rapidly interact with the active site and to be removed from the solution. As the concentration increased, the trend slowed down due to the increased competition (de Farias Silva and da Gama, 2020).

5.3.9.4. Effect of temperature: Temperature is an important physicochemical parameter to influences the adsorption process as it can shift the nature of the process from endothermic to exothermic and vice versa (Yeow et al., 2020). Moreover, it can also affect the process by increasing and decreasing the removal (Badwy et al., 2020). The temperature can also affect the adsorption process depending on the nature of adsorption, adsorbent and pollutant. Szende et al. (2020) reported that if the adsorption process is physical adsorption ($\Delta H_{physisorption}$= -20 kJ/mol), the higher temperature will negatively affect the adsorption process. On the other hand, if the process is chemical adsorption ($\Delta H_{chemisorption}$= -200 kJ/mol), the increasing temperature will also increase the sorption rate. Fig. 5.9 (D) represents the effect of temperature on the adsorption of naphthalene by prepared aerogels. For this study, a total of four temperatures, viz., 298 K, 303 K, 308 K, and 313 K, were considered. From the result of the batch study, it was observed that with the increase in temperature, the removal of naphthalene also increased. The highest removal of naphthalene was found in the case of PVA-Si aerogel, at 313 K temperature, with the value of 96.32% removal. For the same aerogel, the removal at 298 K was 79.42%. This phenomenon can be explained by the increase in kinetic energy of the samples. As the kinetic energy increased, the diffusivity of the molecules in the water also increased, causing their increased movement towards the aerogel pores.

5.3.9.5. Effect of pH: pH is an important parameter of the adsorption process, influencing the capacity of the adsorbent and affecting the efficiency of this process. pH affects the process in various ways, viz., the chemistry of pollutants, the coexisting ions of the

solution, the functional groups and surface charge of the adsorbent surface (Khasri et al., 2021). pH also affects the adsorption mechanism and degree of ionisation of the adsorbed ions. The effect of pH on the adsorption of naphthalene by the prepared aerogels is shown in Fig. 5.9 (E). For this study, six different pH values, viz., 2,4,6,7,8, and 10, were considered respectively. From the figure, it can be stated that with the increasing pH, the adsorption of naphthalene decreased. The highest removal of naphthalene was found to be 94.84% in the case of PVA-Si aerogel at pH 2 and pH 10, the value decreased to 64.87%. This observation can be explained by the surface charge of the adsorbent. During the preparation of the aerogels, HCl was used as a catalyst; the surface of the aerogels is highly protonated. This protonated nature is important to maintain the crosslinking and the pore structures of the aerogels. Exposing them to an alkaline environment can weaken the chemical bonds and disrupt the pores. A similar result was found when the aerogels were treated with DI water at different pH, as described in section 5.3.7.7. The disruption of the pores and crosslinking networks causes a decline in the removal of pollutants at a higher pH level.

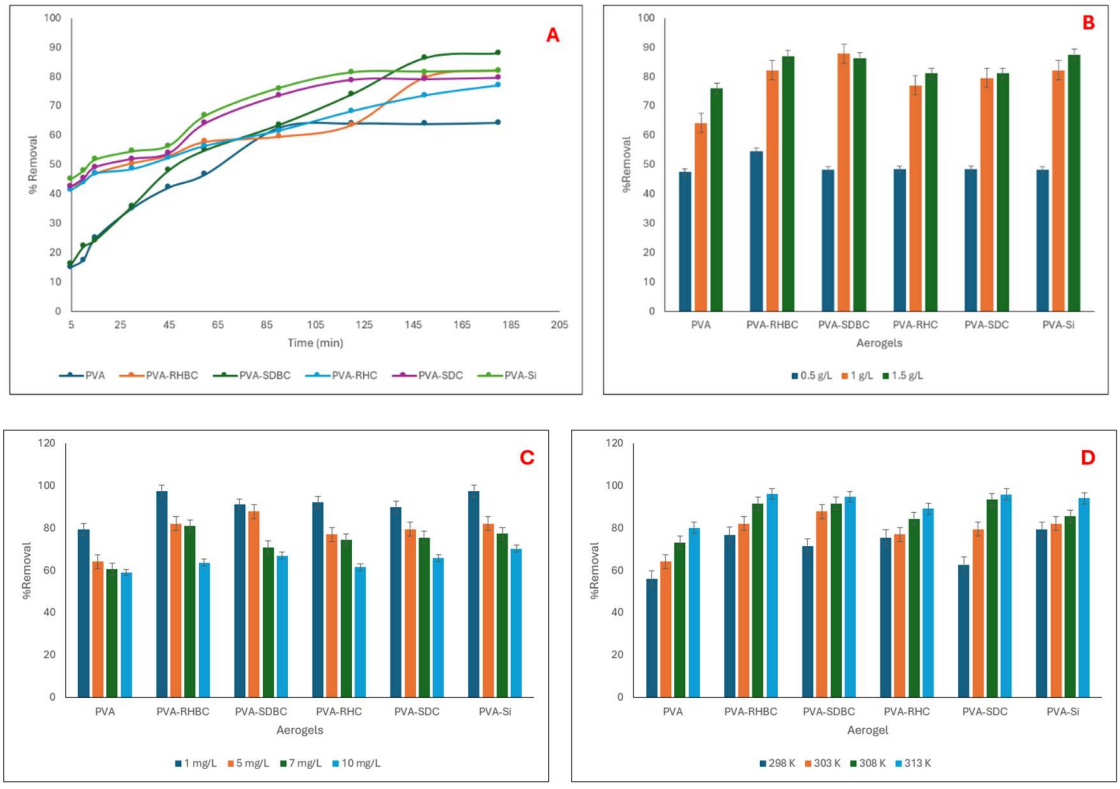

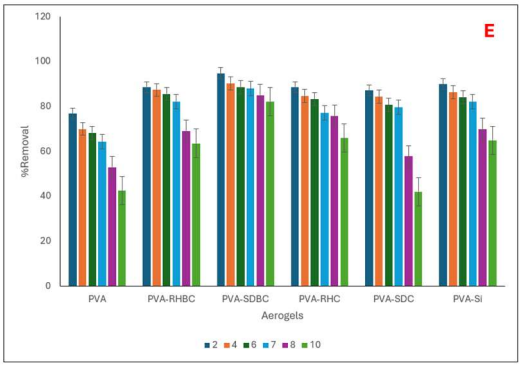

Figure 5.9: Adsorption of naphthalene by prepared aerogels under the influence of (A) contact time, (B) aerogel dose, (C) pollutant concentration, (D) reaction temperature, and (E) pH of media.

5.3.9.6. Adsorption isotherm analysis: In this study, the Langmuir and the Freundlich isotherm models were analysed by plotting $\frac{1}{q_e}$ vs $\frac{1}{C_e}$ and ln C_e vs ln q_e curves, respectively. From Table 5.4, it was observed that PVA-SDBC and PVA-SDC aerogels follow the Langmuir model, and the rest of the aerogels follow the Freundlich isotherm model, respectively. Hence, it was suspected that PVA-SDBC and PVA-SDC aerogels prefer a single-layer adsorption on the other side; the rest of the aerogels exhibited multilayered adsorption characteristics with heterogeneous pore distribution (Das et al., 2021).

Table 5.4: Isotherm modelling of naphthalene removal by aerogels

Adsorbent	Langmuir isotherm			Freundlich isotherm		
	q_m	K_L	R^2	n	K_F	R^2
PVA	8.9	0.38	0.88	1.51	2.23	**0.99**
PVA-RHBC	7.00	2.29	0.94	2.61	4.10	**0.99**
PVA-SDBC	7.30	2.08	**0.99**	1.83	4.19	0.89
PVA-RHC	7.98	1.14	0.96	1.89	3.60	**0.99**
PVA-SDC	7.33	1.23	**0.99**	1.85	3.35	0.98
PVA-Si	7.69	2.13	0.94	2.45	4.45	**0.99**

5.3.9.7. Adsorption kinetics analysis: The pseudo-1st order and pseudo-2nd order kinetic model was analysed by plotting log (q_e-q_t) vs time (t) and $\frac{t}{q_t}$ vs time (t) respectively. The

equilibrium adsorption capacity (q_e) and kinetic constant (K) were calculated from the slope and intercept. As shown in Table 5.5, all the aerogels follow the pseudo 2nd order kinetic model for naphthalene removal with a significantly higher R^2 value.

Table 5.5: Kinetic modelling of naphthalene removal by aerogels

Adsorbent	Pseudo 1st order				Pseudo 2nd order			
	q_e (mg/g)	q_t (mg/g)	K_1 (min^{-1})	R^2	q_e (mg/g)	q_t (mg/g)	K_1 (min^{-1})	R^2
PVA	3.62	3.21	0.03	0.94	3.84	3.21	0.008	**0.98**
PVA-RHBC	3.66	1.11	0.02	0.74	4.15	4.11	0.01	**0.95**
PVA-SDBC	8.73	4.39	0.03	0.77	5.42	4.39	0.003	**0.96**
PVA-RHC	3.15	3.85	0.02	0.77	3.96	3.85	0.01	**0.98**
PVA-SDC	3.21	3.98	0.03	0.95	4.27	3.98	0.01	**0.99**
PVA-Si	3.13	4.11	0.03	0.96	4.39	4.11	0.01	**0.99**

5.3.9.8. Adsorption thermodynamics analysis: For the thermodynamic study of the aerogels, thermodynamic parameters, viz., Gibbs free energy (ΔG), enthalpy (ΔH), and entropy (ΔS), were calculated respectively in four different temperature conditions. As represented in Table 5.6, the adsorption process with all the aerogels in every temperature condition is endothermic, as the ΔH value in every scenario is positive. It was also observed that the absolute value of ΔG increased with increasing temperature, signifying that the removal process is more efficient at higher temperatures. This observation also supports the result of temperature temperature-dependent batch study. From the positive value of ΔS, it can be stated that the adsorption process is spontaneous (Das et al., 2021). Also, it was observed that the absolute value of ΔG is higher for every aerogel, compared to the normal PVA aerogel, showing the significant effect of filler materials on the adsorption process.

Table 5.6: Thermodynamic modelling of naphthalene removal by aerogels

Adsorbent	Parameter	Temperature (K)

		298	303	308	313
PVA	ΔH	60135.99			
	ΔS	203.68			
	ΔG	-562.043	-1580.47	-2598.89	-3617.31
PVA-SDBC	ΔH	101464.05			
	ΔS	349.45			
	ΔG	-2673.25	-4420.52	-6167.79	-7915.06
PVA-RHBC	ΔH	109129.56			
	ΔS	374.77			
	ΔG	-2554.43	-4428.32	-6302.21	-8176.1
PVA-SDC	ΔH	145378.60			
	ΔS	492.15			
	ΔG	-1283.75	-3744.53	-6205.3	-8666.08
PVA-RHC	ΔH	53378.37			
	ΔS	187.58			
	ΔG	-2523.08	-3461.03	-4398.97	-5336.91
PVA-Si	ΔH	70225.86			
	ΔS	245.42			
	ΔG	-2912.06	-4139.21	-5366.35	-6593.5

5.3.9.9. Optimization of naphthalene removal: To optimize the naphthalene adsorption process, a Response Surface Methodology (RSM) study was performed (Aydar, 2018). A quadratic equation, presented as equation (5.15), was used to analyse and validate the experimental design. From the batch adsorption study, PVA-Si was selected as the most

suitable aerogel for the process, and the RSM study was conducted with that adsorbent only.

$$R = 75.63 + 35.98 * A + 1.73 * B - 10.75 * C + 0.5225 * AB + 1.52 * AC - 3.64 * BC - 26.99 * A^2 - 0.7813 * B^2 + 2.77 * C^2 \quad \text{(5.15)}$$

Here, A, B, C, and R are reaction time (min), adsorbent dose (g/L), pollutant concentration (mg/L), and removal%, respectively.

5.3.9.9.1. Validation of the model: From the ANOVA analysis, it was observed that this model is significant with a P-value of 0.0001 (<0.05) and an F-value of 149.57 (>12). The correlation coefficient (R^2) value of the mentioned model was 0.99. The R^2 value also indicates that the predicted and observed data of this experiment are in reasonable agreement, indicating the significance of the model. Fig. 5.10 (A) shows the distribution of predicted and experimental values satisfying the validity of this model.

5.3.9.9.2. Response of time and adsorbent dosage: The response of time and adsorbent dosage is presented in Fig. 5.10 (B). The graph shows that the optimum removal% was observed at 1.5g/ /L adsorbent dosage after 180 min. of adsorption. The maximum pollutant removal under these conditions was found to be 96.45%.

5.3.9.9.3. Response of adsorbent dosage and pollutant concentration: In Fig. 5.10 (C), the response of adsorbent dosage and pollutant concentration is presented. From the figure, it can be stated that at the adsorbent dose of 1.5g/L and 1mg/L pollutant concentration, the optimum removal was achieved. The optimum removal in these conditions was 95.28%.

5.3.9.9.4. Response of pollutant concentration and time: The crosstalk between pollutant concentration and treatment time is represented in Fig. 5.10 (D). From the figure, it was observed that at a treatment time of 180 min. and 1 mg/L pollutant concentration, the highest removal was achieved. The optimum removal in this experiment was 98.2%.

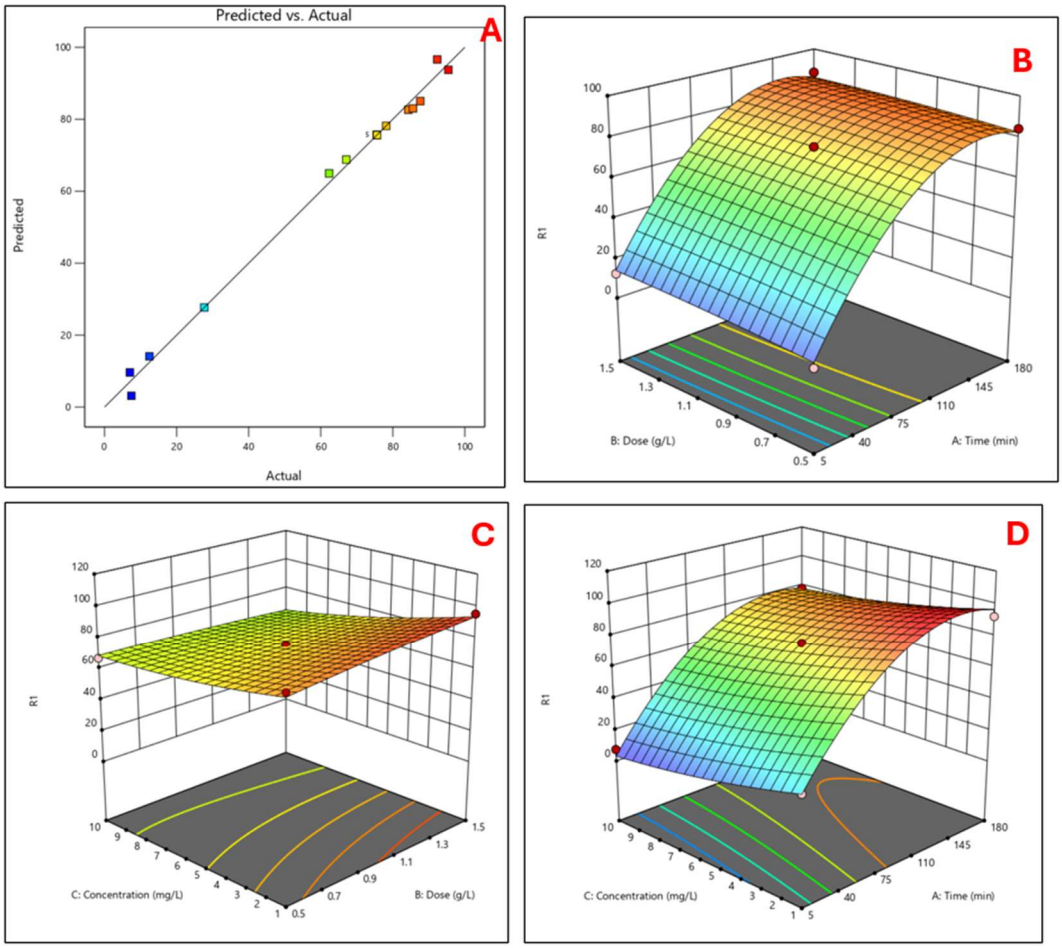

Figure 5.10: Optimization of naphthalene removal by PVA-Si aerogel using Response Surface Methodology, representing (A) comparison of actual and predicted results, (B) response of time and aerogel dose, (C) response of aerogel dose and pollutant concentration, (D) response of time and pollutant concentration.

5.3.10. Removal of phenol by aerogel: In this study, a total of six aerogels were prepared, and the removal of phenol by these aerogels was studied. To understand the detailed nature of the adsorption process, different parameters, viz., time, dose of aerogel, concentration of pollutant, pH, and temperature, were varied. The detailed result is explained below.

5.3.10.1. Effect of contact time: The effect of contact time on the adsorption of phenol is shown in Fig. 5.11 (A). As represented in the figure, the removal of phenol increased with time, and the highest removal achieved in this study was 96.67% by PVA-Si aerogel after 3 hr. of treatment while the other parameters were constant (pH 7, dose 1g/L, concentration 5mg/L, and temperature at 303 K). For comparison, under the same conditions, PVA-SDBC, PVA-SDC, PVA-RHBC, PVA-RHC, and PVA aerogel showed 93.71%, 88.70%, 90.24%, 87.15%, and 79.44%, respectively. After 180 min. of treatment, no significant change was observed in the concentration of naphthalene,

indicating that the adsorption equilibrium was achieved. A previous study showed that for PVA-Si aerogel, the phenol removal reached up to 67.12% (Ghosh et al., 2024). This observation can be explained by considering the available surface area on the adsorbent surface and the interaction time of the adsorbent with adsorbate molecules. Before achieving the adsorption equilibrium, a large surface area and many pores on the adsorbent surface were available that contributed to the significant removal of the contaminant. But after 3 hr., the active sites on the aerogel surface eventually got saturated, which ceased the rapid increase of the removal% (Gao et al., 2019). From this observation, it can also be stated that fillers have a significant effect on the removal efficiency of aerogels, which causes the difference in removal% using different aerogels.

5.3.10.2. Effect of adsorbent dose: The dosage of adsorbent is a crucial parameter and affects the adsorption process significantly by the quantitative ratio of adsorbate and adsorbent (Şentürk and Alzein, 2020). According to Kroeker's rule, for a constant initial concentration, the specific adsorbed volume decreases with increasing adsorbent mass (Pernyeszi et al., 2019). Thus, the adsorbent dose is positively correlated with the removal of the contaminant. This study considered three different dosages of aerogels, viz., 0.5 g/L, 1 g/L, and 1.5 g/L, respectively. The effect of adsorbent dose on the removal of phenol is shown in Fig. 5.11 (B). As represented in the figure, with the increasing dose of aerogel, the removal also increased. It was observed that for PVA, PVA-SDC, PCA-RHC, PVA-SDBC, PVA-RHBC, and PVA-Si, the removal increased from 69.42% to 86.51%, 70.06% to 89.60%, 76.72% to 92.76%, 69.93% to 92.81%, 73.66% to 93.20%, and 69.93% to 94.45%, respectively. With the increasing adsorbent dosage, at a constant concentration of pollutant, more active surface area is available to interact with the pollutant molecules and increase the adsorption of the pollutant (Ma et al., 2020). From the result, it was also observed that, from 0.5 g/L to 1 g/L aerogel dosage, the adsorption increased rapidly, whereas from 1 g/L dosage to 1.5 g/L, the increase in the removal% was not significant. This observation can be explained as after a specific adsorbent dosage, maximum adsorption is reached, and the availability of additional active sites does not affect the saturation point (Rápó et al., 2020; Rápó et al., 2019; Hamza et al., 2018).

5.3.10.3. Effect of phenol concentration: Initial pollutant concentration is one of the key parameters to affect the adsorption process. The pollutant concentration has a significant role in the interaction rate between contaminant molecules and adsorption

sites. The initial concentration of the solute acts as a driving force of the adsorption process, favouring diffusion and mass transfer from the solution. In such water treatment systems, the efficiency of the pollutant removal and the maximum concentration of pollutant adsorbed on the adsorbent's surface are directly related to initial dye concentration (Terangpi and Chakraborty, 2017). In this study, four phenol concentrations, viz., 1 mg/L, 5 mg/L, 7 mg/L, and 10 mg/L, respectively, were considered. As shown in Fig. 5.11 (C), the maximum removal of phenol was observed in the case of PVA-Si aerogel, at 1 mg/L concentration. The removal was 97.49%. Being an efficient adsorbent, PVA-Si shows higher removal of phenol compared to other aerogels. It was also observed that with the increasing initial concentration, the removal decreased. In the case of PVA-Si aerogel, the removal% dropped to 82.65% at 10 mg/L initial concentration and showed the highest removal among all the aerogels at the specific initial concentration. This observation can be explained by the saturation of adsorption sites on the adsorbent surface. At low pollutant concentration, the active site and contaminant molecule's ratio is larger, allowing the molecules to rapidly interact with the active site and to be removed from the solution. As the concentration increased, the trend slowed down due to the increased competition (de Farias Silva and da Gama, 2020).

5.3.10.4. Effect of temperature: Temperature is an important physicochemical parameter to influences the adsorption process as it can shift the nature of the process from endothermic to exothermic and vice versa (Yeow et al., 2020). Moreover, it can also affect the process by increasing and decreasing the removal (Badwy et al., 2020). The temperature can also affect the adsorption process depending on the nature of adsorption, adsorbent and pollutant. Szende et al (2020) reported that if the adsorption process is physical adsorption ($\Delta H_{physisorption}$= -20 kJ/mol), the higher temperature will negatively affect the adsorption process. On the other hand, if the process is chemical adsorption ($\Delta H_{chemisorption}$= -200 kJ/mol), the increasing temperature will also increase the sorption rate. Fig. 5.11 (D) represents the effect of temperature on the adsorption of phenol by prepared aerogels. For this study, a total of four temperatures, viz., 298 K, 303 K, 308 K, and 313 K were considered respectively. From the result of the batch study, it was observed that with the increase in temperature, the removal of phenol also increased. The highest removal of phenol was found in the case of PVA-Si aerogel, at 313 K temperature with the value of 97.44% removal. For the same aerogel, the removal at 298 K was 88.57%. This phenomenon can be explained by the increase in kinetic energy of the

samples. As the kinetic energy increased, the diffusivity of the molecules in the water also increased, causing their increased movement towards the aerogel pores.

5.3.10.5. Effect of pH: pH is an important parameter of the adsorption process, influencing the capacity of the adsorbent and affecting the efficiency of this process. pH affects the process in various ways, viz., the chemistry of pollutants, the coexisting ions of the solution, the functional groups and surface charge of the adsorbent surface (Khasri et al., 2021). pH also affects the adsorption mechanism and degree of ionization of the adsorbed ions. The effect of pH on the adsorption of phenol by the prepared aerogels is shown in Fig. 5.11 (E). For this study, six different pH values, viz., 2,4,6,7,8, and 10, were considered respectively. From the figure, it can be stated that with the increasing pH, the adsorption of phenol decreased. The highest removal of phenol was found to be 94.87% in the case of PVA-Si aerogel at pH 2 and pH 10, the value decreased to 79.83%. This observation can be explained by the surface charge of the adsorbent. During the preparation of the aerogels, HCl was used as a catalyst; the surface of the aerogels is highly protonated. This protonated nature is important to maintain the crosslinking and the pore structures of the aerogels. Exposing them to an alkaline environment can weaken the chemical bonds and disrupt the pores. A similar result was found when the aerogels were treated with DI water at different pH, as described in section 5.3.7.7. The disruption of the pores and crosslinking networks causes a decline in the removal of pollutants at a higher pH level.

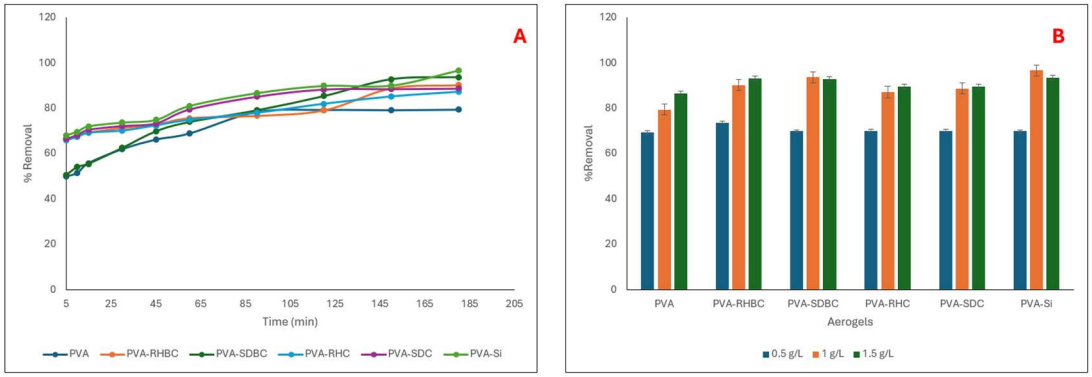

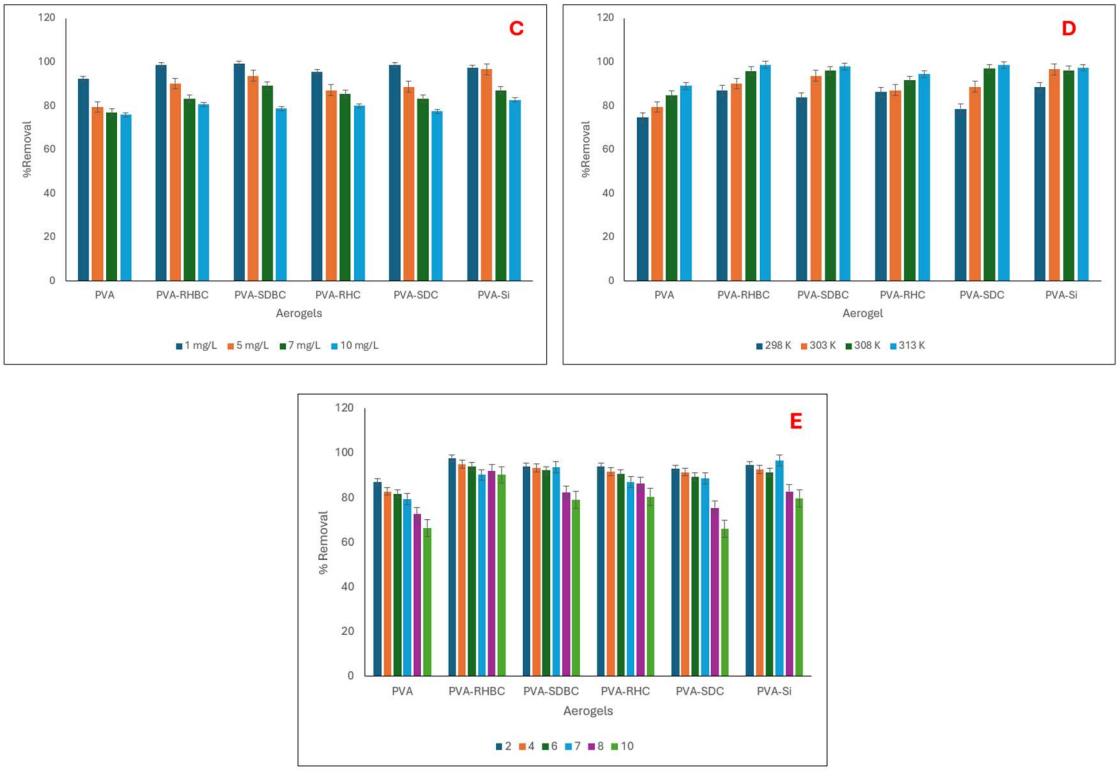

Figure 5.11: Adsorption of phenol by prepared aerogels under the influence of (A) contact time, (B) aerogel dose, (C) pollutant concentration, (D) reaction temperature, and (E) pH of media.

5.3.10.6. Adsorption isotherm analysis: In this study, the Langmuir and the Freundlich isotherm models were analyzed by plotting $\frac{1}{q_e}$ vs $\frac{1}{C_e}$ and ln C_e vs ln q_e curves, respectively. From Table 5.7, it was observed that PVA-SDBC and PVA-SDC aerogels follow the Langmuir model, and the rest of the aerogels follow the Freundlich isotherm model, respectively. Hence, it was suspected that PVA-SDBC and PVA-SDC aerogels prefer a single-layer adsorption on the other side; the rest of the aerogels exhibited multilayered adsorption characteristics with heterogeneous pore distribution (Das et al., 2021).

Table 5.7: Isotherm modelling of phenol removal by aerogels

Adsorbent	Langmuir isotherm			Freundlich isotherm		
	q_m	K_L	R^2	n	K_F	R^2
PVA	8.7	0.37	0.82	1.43	2.21	**0.99**
PVA-RHBC	7.06	2.25	0.93	2.51	4.18	**0.98**
PVA-SDBC	7.37	2.06	**0.96**	1.85	4.17	0.82

PVA-RHC	7.92	1.17	0.95	1.87	3.63	**0.98**
PVA-SDC	7.35	1.21	**0.96**	1.84	3.31	0.88
PVA-Si	7.68	2.16	0.91	2.41	4.47	**0.98**

5.3.10.7. Adsorption kinetics analysis: The pseudo-1st order and pseudo-2nd order kinetic model was analyzed by plotting log (q_e-q_t) vs time (t) and $\frac{t}{q_t}$ vs time (t) respectively. The equilibrium adsorption capacity (q_e) and kinetic constant (K) were calculated from the slope and intercept. As shown in Table 5.8, all the aerogels follow the pseudo-2nd-order kinetic model for phenol removal with a significantly higher R^2 value.

Table 5.8: Kinetic modelling of phenol removal by aerogels

Adsorbent	Pseudo 1st order				Pseudo 2nd order			
	q_e (mg/g)	q_t (mg/g)	K_1 (min^{-1})	R^2	q_e (mg/g)	q_t (mg/g)	K_1 (min^{-1})	R^2
PVA	3.61	3.24	0.02	0.94	3.81	3.23	0.007	**0.98**
PVA-RHBC	3.63	1.13	0.03	0.74	4.13	4.14	0.02	**0.99**
PVA-SDBC	8.72	4.32	0.02	0.77	5.44	4.34	0.004	**0.99**
PVA-RHC	3.14	3.87	0.02	0.77	3.91	3.87	0.01	**0.99**
PVA-SDC	3.20	3.94	0.03	0.92	4.22	3.95	0.06	**0.96**
PVA-Si	3.15	4.15	0.02	0.96	4.35	4.13	0.03	**0.98**

5.3.10.8. Adsorption thermodynamics analysis: For the thermodynamic study of the aerogels, thermodynamic parameters, viz., Gibbs free energy (ΔG), enthalpy (ΔH), and entropy (ΔS), were calculated respectively in four different temperature conditions. As represented in Table 5.9, the adsorption process with all the aerogels in every temperature condition is endothermic in nature, as the ΔH value at every scenario is positive. It was also observed that the absolute value of ΔG increased with increasing temperature, signifying that the removal process is more efficient at higher temperatures. This

observation also supports the result of temperature temperature-dependent batch study. From the positive value of ΔS, it can be stated that the adsorption process is spontaneous in nature (Das et al., 2021). Also, it was observed that the absolute value of ΔG is higher for every aerogel, compared to the normal PVA aerogel, showing the significant effect of filler materials on the adsorption process.

Table 5.9: Thermodynamic modelling of phenol removal by aerogels

Adsorbent	Parameter	Temperature (K)			
		298	303	308	313
PVA	ΔH	61035.99			
	ΔS	213.68			
	ΔG	-572.043	-1682.47	-2698.89	-3627.31
PVA-SDBC	ΔH	102464.05			
	ΔS	329.45			
	ΔG	-2773.25	-4410.52	-6157.79	-7905.06
PVA-RHBC	ΔH	107329.56			
	ΔS	384.77			
	ΔG	-2554.43	-4428.32	-6302.21	-8176.1
PVA-SDC	ΔH	145378.60			
	ΔS	492.15			
	ΔG	-1283.75	-3744.53	-6105.3	-8666.08
PVA-RHC	ΔH	53378.37			
	ΔS	187.58			
	ΔG	-2523.08	-3461.03	-4388.97	-5336.91
PVA-Si	ΔH	72225.86			
	ΔS	245.42			

	ΔG	-2912.06	-4139.21	-5366.35	-6593.5

5.3.10.9. Optimization of phenol removal: To optimize the phenol adsorption process, a Response Surface Methodology (RSM) study was performed (Aydar, 2018). A quadratic equation, presented as equation (5.16), was used to analyze and validate the experimental design. From the batch adsorption study, PVA-Si was selected as the most suitable aerogel for the process, and the RSM study was conducted with that adsorbent only.

$$R = 73.46 + 33.05 * A + 3.24 * B - 6.84 * C - 1.55 * AB - 1.89 * AC - 10.61 * BC - 24.37 * A^2 - 3.57 * B^2 - 5.67 * C^2 \quad \text{(5.16)}$$

Here, A, B, C, and R are reaction time (min), adsorbent dose (g/L), pollutant concentration (mg/L), and removal%, respectively.

5.3.10.9.1. Validation of the model: From the ANOVA analysis, it was observed that this model is significant with a P-value of <0.0001 and an F-value of 107.70 (>12). The correlation coefficient (R^2) value of the mentioned model was 0.99. The R^2 value also indicates that the predicted and observed data of this experiment are in reasonable agreement, indicating the significance of the model. Fig. 5.12 (A) shows the distribution of predicted and experimental values satisfying the validity of this model.

5.3.10.9.2. Response of time and adsorbent dosage: The response of time and adsorbent dosage is presented in Fig. 5.12 (B). The graph shows that the optimum removal% was observed at 1.5g/ /L adsorbent dosage after 180 min. of adsorption. The maximum pollutant removal under these conditions was found to be 97.25%.

5.3.10.9.3. Response of adsorbent dosage and pollutant concentration: In Fig. 5.12 (C), the response of adsorbent dosage and pollutant concentration is presented. From the figure, it can be stated that at the adsorbent dose of 1.5g/L and 1mg/L pollutant concentration, the optimum removal was achieved. The optimum removal in these conditions was 97.28%.

5.3.10.9.4. Response of pollutant concentration and time: The crosstalk between pollutant concentration and treatment time is represented in Fig. 5.12 (D). From the figure, it was observed that at a treatment time of 180 min. and 1 mg/L pollutant

concentration, the highest removal was achieved. The optimum removal in this experiment was 97.5%.

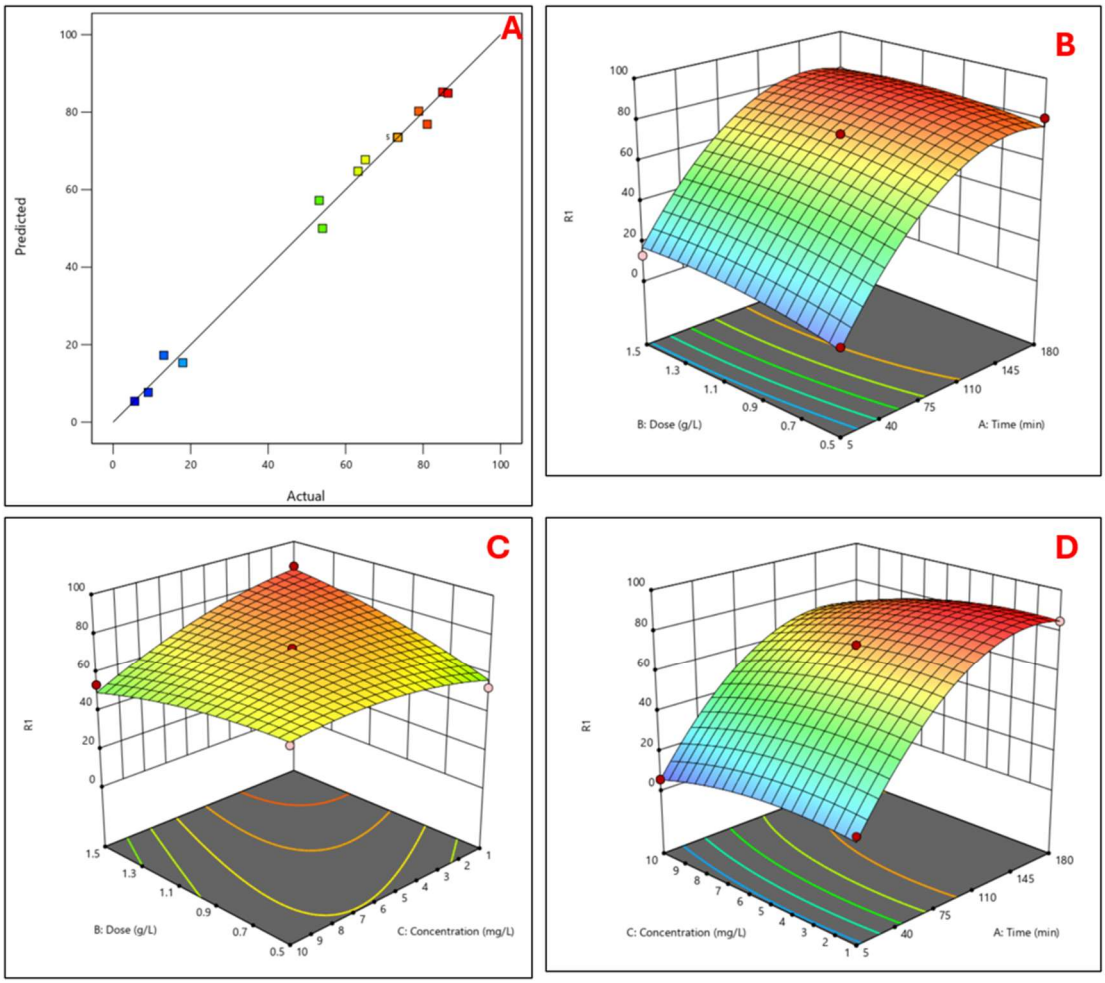

Figure 5.12: Optimization of phenol removal by PVA-Si aerogel using Response Surface Methodology, representing (A) comparison of actual and predicted results, (B) response of time and aerogel dose, (C) response of aerogel dose and pollutant concentration, (D) response of time and pollutant concentration.

5.3.11. Removal of acenaphthene by aerogel: In this study, a total of six aerogels were prepared, and the removal of acenaphthene by these aerogels was studied. To understand the detailed nature of the adsorption process, different parameters, viz., time, dose of aerogel, concentration of pollutant, pH, and temperature, were varied. The detailed result is explained below.

5.3.11.1. Effect of contact time: The effect of contact time on the adsorption of acenaphthene is shown in Fig. 5.13 (A). As represented in the figure, the removal of acenaphthene increased with time, and the highest removal achieved in this study was 93.48% by PVA-Si aerogel after 3 hr. of treatment while the other parameters were constant (pH 7, dose 1g/L, concentration 5mg/L, and temperature at 303 K). For

comparison, under the same conditions, for PVA-SDBC, PVA-SDC, and PVA-RHBC. PVA-RHC and PVA aerogel showed 89.68%, 83.23%, 85.22%, 81.25%, and 71.33%, respectively. After 180 min. of treatment, no significant change was observed in the concentration of acenaphthene, indicating that the adsorption equilibrium was achieved. A previous study showed that for PVA-Si aerogel, the acenaphthene removal reached up to 72.54% (Ghosh et al., 2024). This observation can be explained by considering the available surface area on the adsorbent surface and the interaction time of the adsorbent with adsorbate molecules. Before achieving the adsorption equilibrium, a large surface area and many pores on the adsorbent surface were available that contributed to the significant removal of the contaminant. But after 3 hr., the active sites on the aerogel surface eventually got saturated, which ceased the rapid increase of the removal% (Gao et al., 2019). From this observation, it can also be stated that fillers have a significant effect on the removal efficiency of aerogels, which causes the difference in removal using different aerogels.

5.3.11.2. Effect of adsorbent dose: The dosage of adsorbent is a crucial parameter and affects the adsorption process significantly by the quantitative ratio of adsorbate and adsorbent (Şentürk and Alzein, 2020). According to Kroeker's rule, for a constant initial concentration, the specific adsorbed volume decreases with increasing adsorbent mass (Pernyeszi et al., 2019). Thus, the adsorbent dose is positively correlated with the removal of the contaminant. This study considered three different dosages of aerogels, viz., 0.5 g/L, 1 g/L, and 1.5 g/L, respectively. The effect of adsorbent dose on the removal of acenaphthene is shown in Fig. 5.13 (B). As represented in the figure, with the increasing dose of aerogel, the removal also increased. With the increasing adsorbent dosage, at a constant concentration of pollutant, more active surface area is available to interact with the pollutant molecules and increase the adsorption of the pollutant (Ma et al., 2020). From the result, it was also observed that, from 0.5 g/L to 1 g/L aerogel dosage, the adsorption increased rapidly, whereas from 1 g/L dosage to 1.5 g/L, the increase in the removal% % was not significant. This observation can be explained as after a specific adsorbent dosage, maximum adsorption is reached, and the availability of additional active sites does not affect the saturation point (Rápó et al., 2020; Rápó et al., 2019; Hamza et al., 2018).

5.3.11.3. Effect of acenaphthene concentration: Initial pollutant concentration is one of the key parameters to affect the adsorption process. The pollutant concentration has a

significant role in the interaction rate between contaminant molecules and adsorption sites. The initial concentration of the solute acts as a driving force of the adsorption process, favouring diffusion and mass transfer from the solution. In such water treatment systems, the efficiency of the pollutant removal and the maximum concentration of pollutant adsorbed on the adsorbent's surface are directly related to initial dye concentration (Terangpi and Chakraborty, 2017). In this study, four acenaphthene concentrations, viz., 1 mg/L, 5 mg/L, 7 mg/L, and 10 mg/L, respectively, were considered. As shown in Fig. 5.13 (C), the maximum removal of acenaphthene was observed in the case of PVA-Si aerogel, at 1 mg/L concentration. The removal was 93.48%. Being an efficient adsorbent, PVA-Si shows higher removal of naphthalene compared to other aerogels. It was also observed that with the increasing initial concentration, the removal decreased. In the case of PVA-Si aerogel, the removal% dropped to 76.90% at 10 mg/L initial concentration and showed the highest removal among all the aerogels at the specific initial concentration. This observation can be explained by the saturation of adsorption sites on the adsorbent surface. At low pollutant concentration, the active site and contaminant molecule's ratio is larger, allowing the molecules to rapidly interact with the active site and to be removed from the solution. As the concentration increased, the trend slowed down due to the increased competition (de Farias Silva and da Gama, 2020).

5.3.11.4. Effect of temperature: Temperature is an important physicochemical parameter to influences the adsorption process as it can shift the nature of the process from endothermic to exothermic and vice versa (Yeow et al., 2020). Moreover, it can also affect the process by increasing and decreasing the removal (Badwy et al., 2020). The temperature can also affect the adsorption process depending on the nature of adsorption, adsorbent and pollutant. Szende et al (2020) reported that if the adsorption process is physical adsorption ($\Delta H_{physisorption}$= -20 kJ/mol), the higher temperature will negatively affect the adsorption process. On the other hand, if the process is chemical adsorption ($\Delta H_{chemisorption}$= -200 kJ/mol), the increasing temperature will also increase the sorption rate. Fig. 5.13 (D) represents the effect of temperature on the adsorption of acenaphthene by prepared aerogels. For this study, a total of four temperatures, viz., 298 K, 303 K, 308 K, and 313 K, were considered. From the result of the batch study, it was observed that with the increase in temperature, the removal of acenaphthene also increased. The highest removal of acenaphthene was found in the case of PVA-Si aerogel, at 313 K temperature

with the value of 94.47% removal. For the same aerogel, the removal at 298 K was 83.07%. This phenomenon can be explained by the increase in kinetic energy of the samples. As the kinetic energy increased, the diffusivity of the molecules in the water also increased, causing their increased movement towards the aerogel pores.

5.3.11.5. Effect of pH: pH is an important parameter of the adsorption process, influencing the capacity of the adsorbent and affecting the efficiency of this process. pH affects the process in various ways, viz., the chemistry of pollutants, the coexisting ions of the solution, the functional groups and surface charge of the adsorbent surface (Khasri et al., 2021). pH also affects the adsorption mechanism and degree of ionization of the adsorbed ions. The effect of pH on the adsorption of acenaphthene by the prepared aerogels is shown in Fig. 5.13 (E). For this study, six different pH values, viz., 2,4,6,7,8, and 10, were considered respectively. From the figure, it can be stated that with the increasing pH, the adsorption of acenaphthene decreased. The highest removal of acenaphthene was found to be 91.17% in the case of PVA-Si aerogel at pH 2 and pH 10, the value decreased to 71.83%. This observation can be explained by the surface charge of the adsorbent. During the preparation of the aerogels, HCl was used as a catalyst; the surface of the aerogels is highly protonated. This protonated nature is important to maintain the crosslinking and the pore structures of the aerogels. Exposing them to an alkaline environment can weaken the chemical bonds and disrupt the pores. A similar result was found when the aerogels were treated with DI water at different pH, as described in section 5.3.7.7. The disruption of the pores and crosslinking networks causes a decline in the removal of pollutants at a higher pH level.

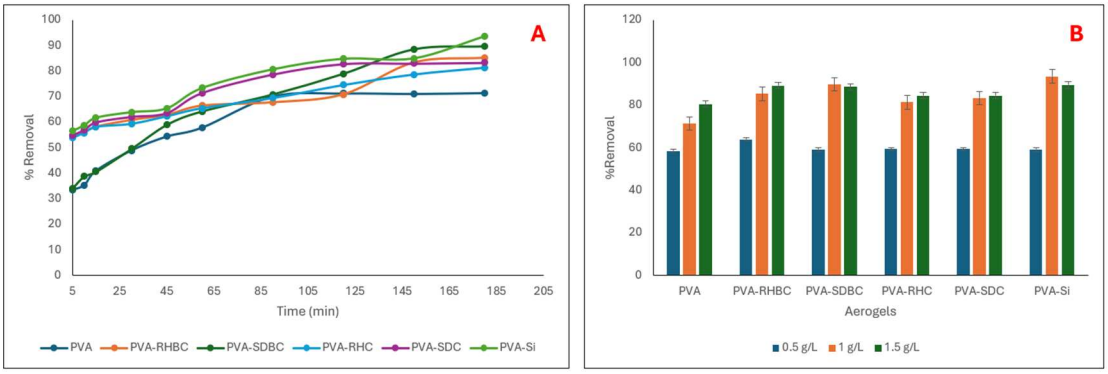

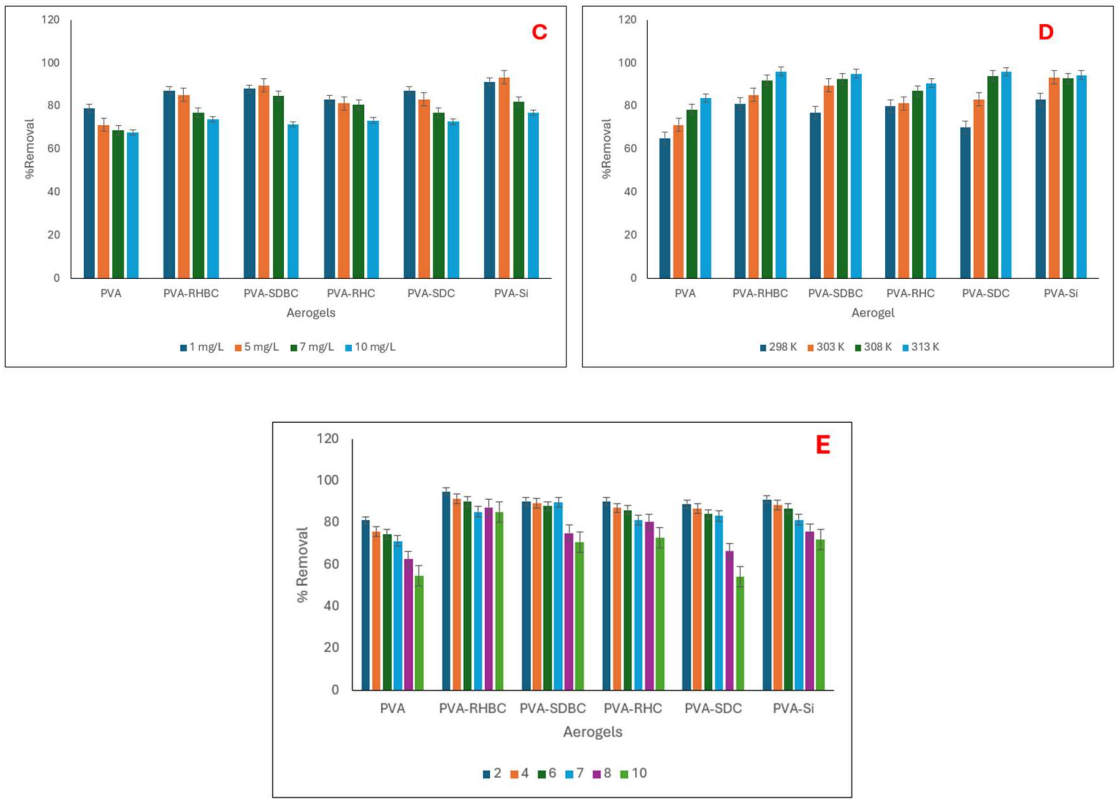

Figure 5.13: Adsorption of acenaphthene by prepared aerogels under the influence of (A) contact time, (B) aerogel dose, (C) pollutant concentration, (D) reaction temperature, and (E) pH of media.

5.3.11.6. Adsorption isotherm analysis: In this study, the Langmuir and the Freundlich isotherm models were analyzed by plotting $\frac{1}{q_e}$ vs $\frac{1}{C_e}$ and ln C_e vs ln q_e curves, respectively. From Table 5.10, it was observed that PVA-SDBC and PVA-SDC aerogels follow the Langmuir model, and the rest of the aerogels follow the Freundlich isotherm model, respectively. Hence, it was suspected that PVA-SDBC and PVA-SDC aerogels prefer a single-layer adsorption on the other side; the rest of the aerogels exhibited multilayered adsorption characteristics with heterogeneous pore distribution (Das et al., 2021).

Table 5.10: Isotherm modelling of acenaphthene removal by aerogels

Adsorbent	Langmuir isotherm			Freundlich isotherm		
	q_m	K_L	R^2	n	K_F	R^2
PVA	8.9	0.38	0.88	1.51	2.23	**0.98**
PVA-RHBC	7.00	2.29	0.94	2.61	4.10	**0.99**
PVA-SDBC	7.30	2.08	**0.99**	1.83	4.19	0.89

PVA-RHC	7.98	1.14	0.96	1.89	3.60	**0.99**
PVA-SDC	7.33	1.23	**0.96**	1.85	3.35	0.89
PVA-Si	7.69	2.13	0.94	2.45	4.45	**0.98**

5.3.11.7. Adsorption kinetics analysis: The pseudo-1st order and pseudo-2nd order kinetic model was analyzed by plotting log (q_e-q_t) vs time (t) and $\frac{t}{q_t}$ vs time (t) respectively. The equilibrium adsorption capacity (q_e) and kinetic constant (K) were calculated from the slope and intercept. As shown in Table 5.11, all the aerogels follow the pseudo 2nd order kinetic model for acenaphthene removal with a significantly higher R^2 value.

Table 5.11: Kinetic modelling of acenaphthene removal by aerogels

Adsorbent	Pseudo 1st order				Pseudo 2nd order			
	q_e (mg/g)	q_t (mg/g)	K_1 (min^{-1})	R^2	q_e (mg/g)	q_t (mg/g)	K_1 (min^{-1})	R^2
PVA	3.62	3.21	0.03	0.94	3.84	3.21	0.008	**0.96**
PVA-RHBC	3.66	1.11	0.02	0.74	4.15	4.11	0.01	**0.95**
PVA-SDBC	8.73	4.39	0.03	0.77	5.42	4.39	0.003	**0.98**
PVA-RHC	3.15	3.85	0.02	0.77	3.96	3.85	0.01	**0.99**
PVA-SDC	3.21	3.98	0.03	0.95	4.27	3.98	0.01	**0.98**
PVA-Si	3.13	4.11	0.03	0.96	4.39	4.11	0.01	**0.96**

5.3.11.8. Adsorption thermodynamics analysis: For the thermodynamic study of the aerogels, thermodynamic parameters, viz., Gibbs free energy (ΔG), enthalpy (ΔH), and entropy (ΔS), were calculated respectively in four different temperature conditions. As represented in Table 5.12, the adsorption process with all the aerogels in every temperature condition is endothermic in nature, as the ΔH value at every scenario is positive. It was also observed that the absolute value of ΔG increased with increasing

temperature, signifying that the removal process is more efficient at higher temperatures. This observation also supports the result of temperature temperature-dependent batch study. From the positive value of ΔS, it can be stated that the adsorption process is spontaneous in nature (Das et al., 2021). Also, it was observed that the absolute value of ΔG is higher for every aerogel, compared to the normal PVA aerogel, showing the significant effect of filler materials on the adsorption process.

Table 5.12: Thermodynamic modelling of acenaphthene removal by aerogels

Adsorbent	Parameter	Temperature (K)			
		298	303	308	313
PVA	ΔH	60135.99			
	ΔS	203.68			
	ΔG	-552.043	-1280.47	-2591.89	-3627.31
PVA-SDBC	ΔH	101464.05			
	ΔS	349.45			
	ΔG	-2663.25	-4430.52	-6157.79	-7815.06
PVA-RHBC	ΔH	109129.56			
	ΔS	374.77			
	ΔG	-2554.43	-4428.32	-6302.21	-8176.1
PVA-SDC	ΔH	145378.60			
	ΔS	492.15			
	ΔG	-1283.75	-3744.53	-6215.3	-8652.08
PVA-RHC	ΔH	53378.37			
	ΔS	187.58			
	ΔG	-2523.08	-3761.03	-4698.97	-5336.91
PVA-Si	ΔH	70225.86			

	ΔS	245.42			
	ΔG	-2912.06	-4139.21	-5386.35	-6593.5

5.3.11.9. Optimization of acenaphthene removal: To optimize the acenaphthene adsorption process, a Response Surface Methodology (RSM) study was performed (Aydar, 2018). A quadratic equation, presented as equation (5.17), was used to analyse and validate the experimental design. From the batch adsorption study, PVA-Si was selected as the most suitable aerogel for the process, and the RSM study was conducted with that adsorbent only.

$$R = 64.76 + 33.14 * A + 1.92 * B - 11.11 * C + 0.2725 * AB - 0.9325 * AC - 4.23 * BC - 22.82 * A^2 - 0.8787 * B^2 + 1.61 * C^2 \quad (5.17)$$

Here, A, B, C, and R are reaction time (min), adsorbent dose (g/L), pollutant concentration (mg/L), and removal%, respectively.

5.3.11.9.1. Validation of the model: From the ANOVA analysis, it was observed that this model is significant with a P-value of <0.0001 and an F-value of 49.20 (>12). The correlation coefficient (R^2) value of the mentioned model was 0.98. The R^2 value also indicates that the predicted and observed data of this experiment are in reasonable agreement, indicating the significance of the model. Fig. 5.14 (A) shows the distribution of predicted and experimental values satisfying the validity of this model.

5.3.11.9.2. Response of time and adsorbent dosage: The response of time and adsorbent dosage is presented in Fig. 5.14 (B). The graph shows that the optimum removal% was observed at 1.5g/ /L adsorbent dosage after 180 min. of adsorption. The maximum pollutant removal under these conditions was found to be 97.45%.

5.3.11.9.3. Response of adsorbent dosage and pollutant concentration: In Fig. 5.14 (C), the response of adsorbent dosage and pollutant concentration is presented. From the figure, it can be stated that at the adsorbent dose of 1.5g/L and 1mg/L aerogel concentration, the optimum removal was achieved. The optimum removal in these conditions was 96.28%.

5.3.11.9.4. Response of pollutant concentration and time: The crosstalk between pollutant concentration and treatment time is represented in Fig. 5.14 (D). From the

figure, it was observed that at a treatment time of 180 min. and 1 mg/L pollutant concentration, the highest removal was achieved. The optimum removal in this experiment was 98.7%.

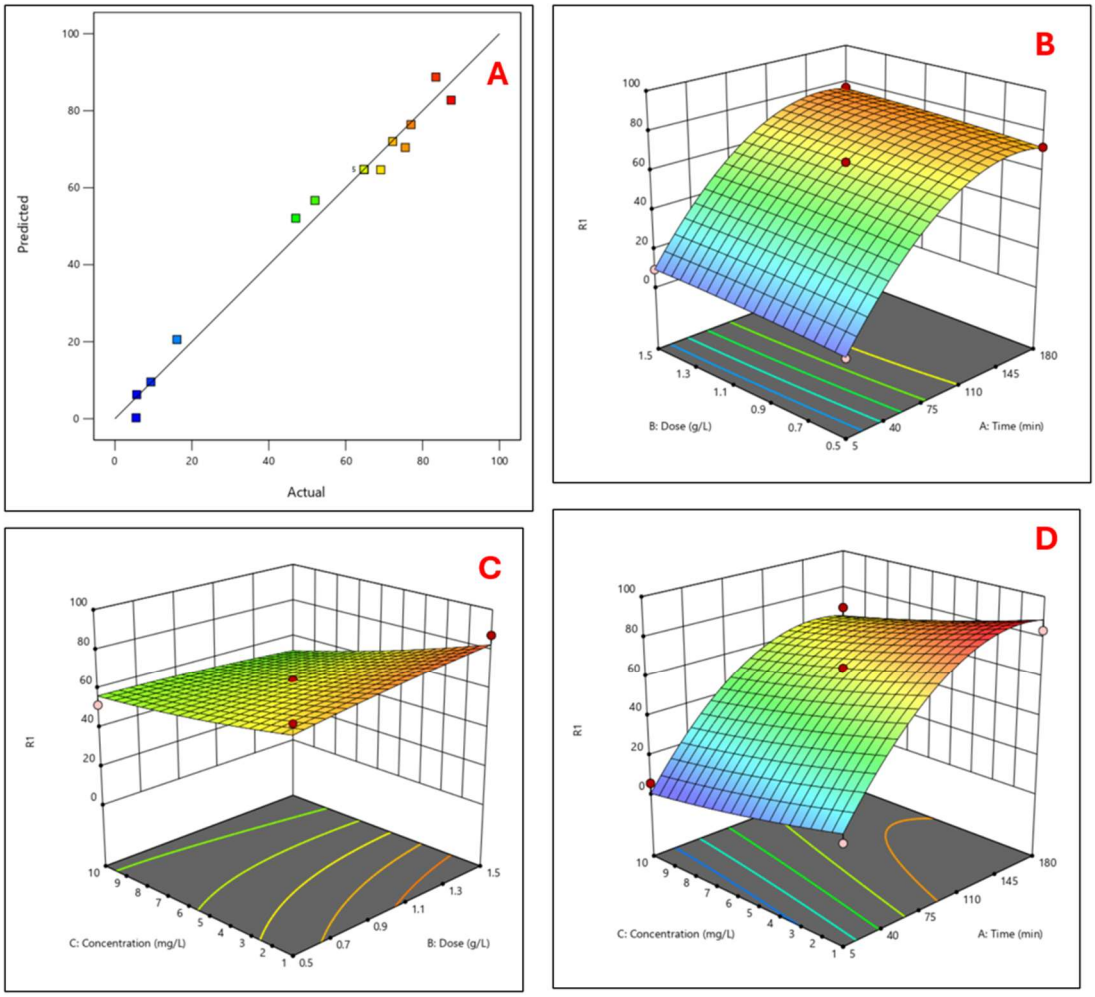

Figure 5.14: Optimization of acenaphthene removal by PVA-Si aerogel using Response Surface Methodology, representing (A) comparison of actual and predicted results, (B) response of time and aerogel dose, (C) response of aerogel dose and pollutant concentration, (D) response of time and pollutant concentration.

5.3.12. Multipollutant removal study of aerogels: For the multipollutant removal study, three different mixed pollutant solutions, viz., N-P, N-A, A-P, and N-P-A, were prepared and used. This experiment was conducted using PVA-Si aerogel, as it showed the highest efficiency in removing the pollutants from the solution. The result of this experiment is presented in Fig. 5.15. As shown in the figure, the removal of all the pollutants decreased compared to the single-pollutant solution. This phenomenon can be explained by the intermolecular competition of the contaminants. In the batch study, it was observed that all the pollutants show high efficiency for removal by these prepared aerogels. As another pollutant is introduced into the media, a competition is started between the molecules that

decrease the removal. As shown in Fig. 5.15 (A), the removal of naphthalene and phenol was observed to be 24.68% and 50.57%, respectively. As the molecular size of naphthalene is larger compared to phenol, the phenol molecules can easily cross the hindrance barrier caused by the naphthalene molecule and bind to the surface of the aerogel. On the other hand, for the same reason, the naphthalene molecule faced difficulty to reach to the adsorbent surface. Fig. 5.15 (B) and 5.15 (C) represent the result of adsorption in A-P and N-A solutions, respectively. In the case of the A-P solution, a similar result to the N-P solution was observed and can be explained by the same phenomenon. In this solution, the removal of acenaphthene and phenol was found to be 17.85% and 57.00%, respectively. On the other hand, in the case of N-A solution, removal of both pollutants was found to be closer due to the similarity of their structure. The removal of naphthalene and acenaphthene was 15.29% and 22.80%, respectively. Fig. 5.15 (D) shows the removal of the pollutants in N-P-A solution, and it was observed that naphthalene showed the least removal with the value of 8.87%. For phenol and acenaphthene, the removal was 29.37% and 29.42%. From this study, it was inferred that the molecular size of the pollutants played a vital role in their removal during this experiment.

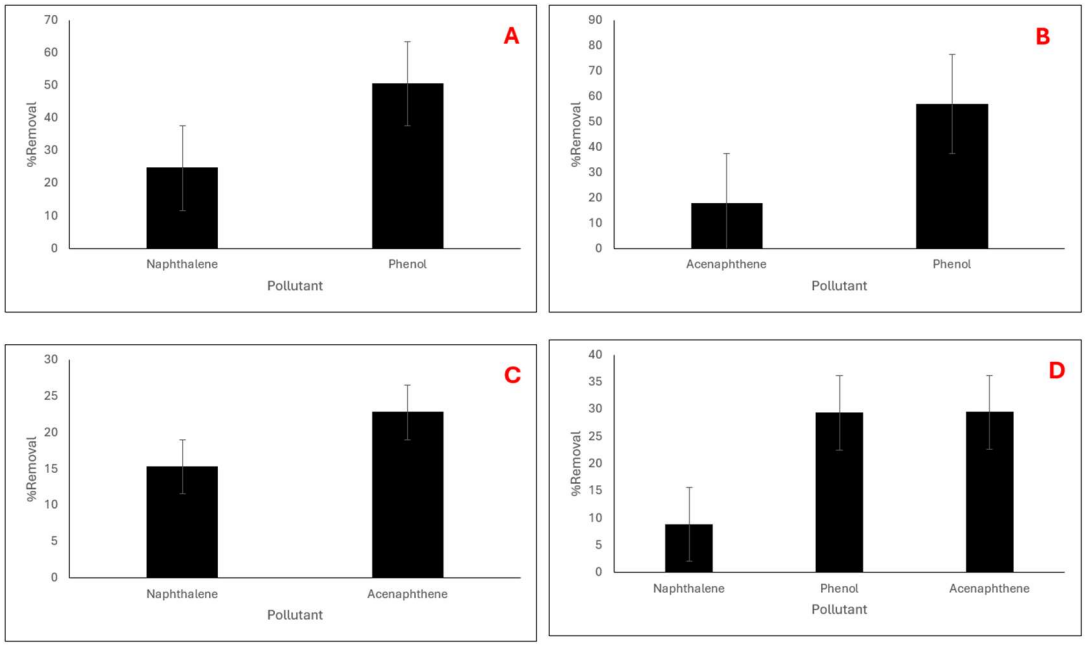

Figure 5.15: Multipollutant removal study of PVA-Si aerogel using (A) N-P, (B) A-P, (C) N-A, and (D) N-A-P solutions.

5.3.13. Selectivity study of aerogels: For the selectivity study of the aerogel, a total of 12 pollutants were used. Six organic pollutants (naphthalene, phenol, acenaphthene,

anthracene, pyrene, phenanthrene), three dyes (methylene blue, aniline blue, congo red), and three metal ions (chromium, fluoride, lead) were used in this experiment. PVA-Si aerogel was used in this study, being the most efficient adsorbent throughout the experiment. The result of this experiment is presented in Fig. 5.16. From the figure, it was shown that the prepared adsorbents have an affinity towards organic pollutants and dyes, compared to metals. The lowest adsorption by these aerogels was found in the case of lead, with a removal of 9.24%. On the other hand, the highest removal was found in the case of phenanthrene, with 98.23% of removal. This phenomenon can be explained by the adsorption mechanism of the aerogels. The functional groups attached to the surface of the adsorbent promote the attachment of organic pollutants and dyes over metal.

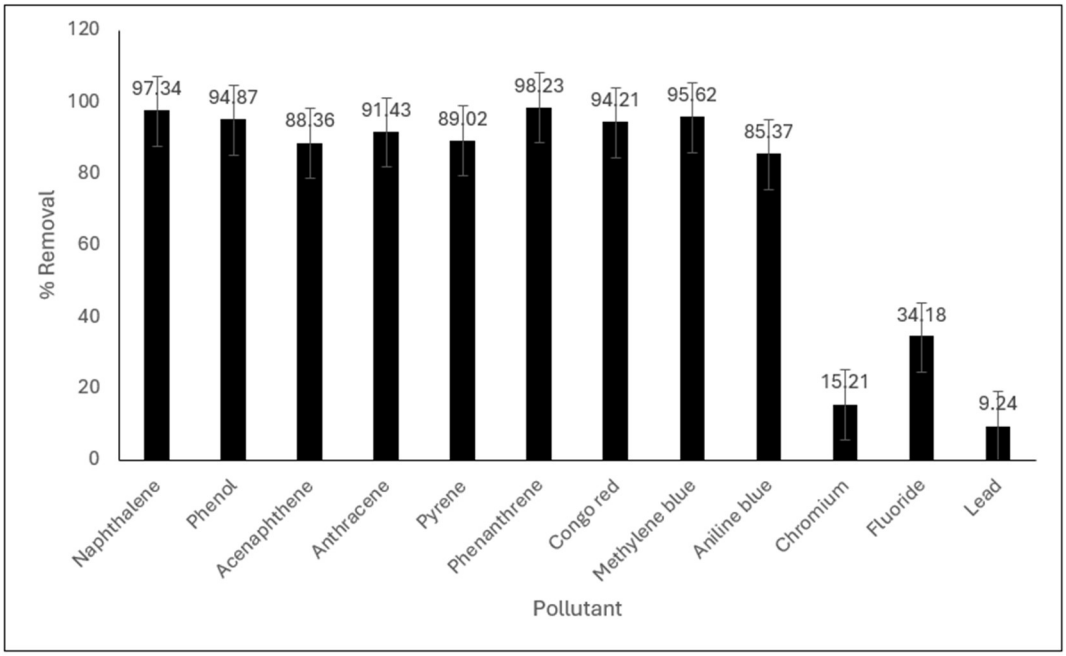

Figure 5.16: Selectivity study of PVA-Si aerogel.

5.4. Conclusion:

This chapter of this thesis mainly focuses on the preparation of PVA aerogel by a novel method, along with investigating the effect of filler materials on wastewater treatment. It was found that the prepared aerogels are showing significant removal of organic pollutants (viz., naphthalene, phenol, and acenaphthene) from aqueous solution, and the filler materials incorporated into the aerogel network are affecting the removal capacity. From the batch study, it was found that the PVA-Si aerogel is the most efficient one for wastewater treatment. From the modelling of the adsorption study, it was found that in

the case of all the pollutants, the process followed the pseudo-2nd-order kinetic model. It was also observed that the process was endothermic and spontaneous at all temperatures. From isotherm modelling, it can be stated that the process followed the Freundlich isotherm model for every pollutant and aerogel, but for PVA-SDC and PVA-SDBC, the best-fitted model was the Langmuir isotherm model. From the selectivity and multipollutant removal study, it was observed that the aerogels have an affinity towards organic pollutants and dyes compared to metal ions. Though the prepared aerogels showed significant adsorption for all the pollutants throughout the batch study, the adsorption process has some drawbacks of its own. To overcome them, bioremediation can be an effective process. This process was used to further investigate the research problems and is described in the next chapter.

Chapter: 6

PREPARATION OF BACTERIA-DOPED AEROGEL AND ITS APPLICATION IN WASTEWATER TREATMENT

6.1. Introduction:

Aerogels, known for their unique properties, can provide an ideal matrix for bacterial doping depending on the building materials of the matrix. According to a previous study, wrapping bacteria isolated from the environment on a graphene nanosheet can enhance the dye removal activity by encapsulating two processes into the mechanism of one adsorbent. Also, selective biodegradation of oil in the wastewater treatment process was observed using microorganism-immobilised hydroxyethyl cellulose composite. Chen et al. (2024) reported that the degradation was improved after immobilising microorganisms on cellulose compared to their suspension stage. Ongoing advanced studies in material science and microbiology continue to refine the design and performance of the bacteria-immobilised components, paving the way for widespread adsorption in environmental remediation and beyond.

This chapter of the thesis, a study will be discussed focusing on the synthesis of bacteria-doped PVA aerogel and its applications in organic pollutant removal from wastewater.

6.2. Materials and Methods:

6.2.1. Materials: Nutrient broth and nutrient agar were purchased from Himedia (India). Dipotassium hydrogen phosphate (K_2HPO_4), potassium dihydrogen phosphate (KH_2PO_4), magnesium sulphate ($MgSO_4$), ammonium sulphate ($(NH_4)_2SO_4$), disodium hydrogen phosphate (Na_2HPO_4), naphthalene, acenaphthene, and phenol were purchased from Loba Chemie (India). Hydrochloric acid (HCl), sodium hydroxide (NaOH), methanol, sodium chloride (NaCl), potassium chloride (KCl) and n-hexane ($CH_3(CH_2)_4CH_3$) were purchased from Merck (Germany).

6.2.2. Isolation of bacteria: To isolate the bacteria used in this study, soil was collected from Dhapa, East Kolkata Wetland, Kolkata. Also, a multistep process was followed to prepare a pure culture of the bacterium of interest.

6.2.2.1. Serial dilution: A total of six test tubes were taken, and each was filled with 9 mL of DI water. The test tubes were cotton-plugged and sterilized at 394 K temperature

under 15 psi pressure. After the sterilization was complete, 1g of the collected soil was measured using a weighing machine (Sartorius, Germany) and taken in a sterilized test tube. The test tube was shaken, and the soil with the water was mixed thoroughly. After the mixture was prepared, 1 mL of the mixture was taken with a sterilized micropipette and transferred to the next test tube. The process was repeated in the case of the 2^{nd} test tube, and 1 mL of the mixture was again transferred to the 3^{rd} one. By repeating this process, the initial mixture was diluted up to 10^{-6} concentration of the initial concentration.

6.2.2.2. Preparation of bacterial culture: 100 mL of DI water was measured using a measuring cylinder and taken in an Erlenmeyer flask. The nutrient agar media was measured using a weighing machine (Sartorius, Germany) and mixed with water at a 13 g/L concentration. The mixture was stirred on a magnetic stirrer to make it homogeneous. After the nutrient agar media was properly mixed, it was sterilized at 394 K temperature and under 15 psi pressure. The sterilized agar media were placed inside a laminar airflow chamber and poured into sterilized Petri dishes. After the solidification of the agar, 0.1 mL of previously prepared soil mixture with a 10^{-6} dilution was taken and spread on the agar medium using the spread plate method. The plates were incubated inside a BOD shaker incubator (Remi, India) at 303 K for 72 hr.

6.2.2.3. Pure culture preparation: After 72 hr., the Petri plates were observed, and bacterial colonies were found with distinct colour and texture. In an Erlenmeyer flask, 100 mL of DI water was poured, and a sterilized nutrient broth media was prepared as described in section 6.2.2.2. From the cultured petri plates, one single colony was collected with a culture loop, and the nutrient broth was inoculated with the colony. The broth media was incubated in a BOD shaker incubator (Remi, India) at 303 K under constant rotation for 72 hr.

After the incubation period, bacterial growth was observed in the nutrient media. One set of nutrient agar culture plates was prepared following the process described in section 6.2.2.2, and 0.1 mL of the cultured broth was used to inoculate the Petri plates. Again, the plates were incubated in a BOD shaker incubator under conditions as mentioned previously. This process was repeated until a single type of colony was isolated.

In this study, this isolated microorganism was named as SMO or soil isolated microorganism, till it was identified by RT-PCR. Rest on the microorganisms used in this

study were *Bacillus sp.* and *Pseudomonas sp.,* were purchased from MTCC. Another organism *Lysinibacillus sp.* was isolated previously in the laboratory.

6.2.3. Behaviour of bacteria under stress: To understand the behaviour of the bacteria under different stress conditions, parameters like pH (2-10), salinity (2%-5%), and temperature (298 K-313 K) were varied. Also, the growth pattern of bacteria in the presence of pollutants, viz., naphthalene, acenaphthene, and phenol, was observed compared to the growth in the nutrient broth.

6.2.3.1. Preparation of nutrient media for analysis of physical stress: The behaviour of bacteria under different pH, salinity, and temperature conditions was observed by growing the microbes in a nutrient broth. The nutrient broth was prepared as described in section 6.2.2.2. To adjust the salinity of the solution, NaCl was measured by using a weighing machine (Sartorius, Germany) and mixed with the nutrient broth media. In the case of pH, 0.1 (N) NaOH and 0.1 (N) HCl buffer solutions were used to adjust the pH. A pH meter (TestR-35, Eutech) was used to measure the pH. Also, in the case of temperature stress, the temperature was controlled by using BOD shaker incubators (Remi).

6.2.3.2. Preparation of media to study the effect of pollutants: On the other hand, to analyze the stress effect of contaminants, viz., naphthalene, phenol, and acenaphthene, minimal media was used.

6.2.3.2.1. Preparation of pollutant solution: To make the solutions of naphthalene, acenaphthene, and phenol, with a 5mg/L concentration, the process was followed as described in sections 5.2.5.1.1, 5.2.5.1.2, and 5.2.5.1.3. respectively.

6.2.3.2.2. Preparation of minimal media: 500 mL of the prepared pollutant solutions were measured in a measuring cylinder and taken into an Erlenmeyer flask. 3.5 g of di-potassium hydrogen phosphate, 1 g potassium di-hydrogen phosphate, 0.05 g of magnesium sulphate, and 0.5 g ammonium sulphate were measured using a weighing machine (Sartorius, Germany) and added to the DI water. The solution was stirred on a magnetic stirrer to make the distribution of solute homogeneous.

6.2.3.3. Inoculation of bacteria: To sterilize the prepared nutrient media, it was treated inside an autoclave at 394 K temperature and 15 psi pressure. The minimal media was sterilized in a laminar airflow cabinet using UV exposure. After the sterilization is

complete, 1 mL of previously prepared bacterial culture is added to the media and incubated in a BOD shaker incubator (Remi) for five days at 303 K under constant rotation. The samples were collected in a specific time interval.

6.2.3.4. Measuring the bacterial growth: The bacterial growth in the collected samples was measured using a UV-Viz spectrophotometer (PerkinElmer, USA) at a wavelength (λ_{max}) of 600 nm. All the data was analyzed using Microsoft Excel 365.

6.2.4. Minimal inhibitory concentration (MIC) analysis: Minimal inhibitory concentration is an important parameter in a microbiology experiment. This test determines the minimum concentration of any substance that induces an inhibitory effect on the growth of a microorganism. In this study, three pollutants of interest, viz., naphthalene, acenaphthene, and phenol, were investigated for their minimal inhibitory concentration on microorganisms, viz., *Bacillus sp.*, *Lysinibacillus sp.*, *Pseudomonas sp.*, and SMO, respectively.

6.2.4.1. Preparation of solution: For this study, the pollutant solutions were prepared with a 100 mg/L concentration following the processes as described in sections 5.2.5.1.1, 5.2.5.1.2, and 5.2.5.1.3. respectively. These solutions were stored as stock solutions. A further dilution of the stock solutions to three different concentrations, viz., 10 mg/L, 1 mg/L, and 0.1 mg/L, respectively, was performed.

6.2.4.2. Preparation of microbial culture media: To culture the microorganisms, nutrient agar media were used in this experiment. The nutrient agar Petri plates were prepared by following the process described in section 6.2.2.3. On the other hand, filter papers (Whatman 41) were cut into small circles and submerged in the prepared pollutant solutions and sterilized in a laminar chamber under UV exposure. After sterilization, the filter papers were treated with the solutions for 24 hr. Following that, four of the filter papers with four different concentrations were placed on the four corners of the Petri plates.

6.2.4.3. Inoculation of microbial media and measuring of MIC: 0.1 mL of previously prepared microorganisms was used to inoculate the plates with the spread plate method and incubated inside an incubator for 5 days at 30^{o}C. After the incubation was completed, the plates were collected, and rings were observed surrounding the filter papers. The diameter of the rings was measured.

6.2.5. Bioremediation of pollutants by bacteria: The bioremediation of pollutants from the water solution by bacteria was performed with a batch study. Different parameters in this experiment were optimized to study their effect on the adsorption process.

6.2.5.1. Preparation of pollutant solution: In this study, three organic pollutants, naphthalene, acenaphthene, and phenol, were used as the pollutants of interest. The solutions were prepared as mentioned in section 6.2.3.2.2.

6.2.5.2. Experimental Procedure: The previously prepared pollutant solutions (mentioned in section 6.2.5.1) were used for the batch study in this research. To perform the batch study, 100 mL of each solution was taken into an Erlenmeyer flask, and 1 mL of the microorganisms was added to the solution and treated inside a BOB shaker incubator for 5 days. Samples were collected in a pre-determined interval and analysed by a UV-Vis spectrophotometer (PerkinElmer, USA) and an HPLC machine (Waters model- 2489). The detailed specification of the analysis is mentioned in section 5.2.5.2. For the baseline study, the pollutant concentration was 5 mg/L, and the dose of microbes, pH, and temperature were maintained at 1 mL/100 mL, 7, and 303 K respectively. For the detailed batch study, the pollutant concentration (1 mg/L- 10 mg/L), dose of microbe (0.5 mL/100 mL- 3 mL/100 mL), pH (2-10), salinity (1%-3%) and temperature (298 K-313 K) were varied to study their effect on the adsorption process.

The percentage removal of the pollutants was calculated by equation (6.1)

$$Removal\ \% = \frac{C_0 - C_t}{C_0} x100 \ldots\ldots\ldots\ldots \quad (6.1)$$

Where C_0 is the initial concentration (mg/L) of pollutant in aqueous solution, C_t is the concentration (mg/L) of pollutant after the adsorption performed for time t.

6.2.5.3. Modelling of bioremediation using the Monod model: The Monod model is the fundamental kinetic framework used to analyse microbial growth and substrate utilization in the bioremediation process. It describes the relationship between the specific growth rate of microorganisms (μ) and the concentration of a limiting substrate (S). The relationship is expressed as equation (6.2).

$$\mu = \mu_{max} \frac{S}{K_S + S} \ldots\ldots\ldots\ldots\ldots\ldots\ldots\ldots \quad (6.2)$$

Here, μ_{max} is the maximum specific growth rate, and K_s is the half-saturation constant.

6.2.6. Doping of microorganisms into aerogel matrix: From the bioremediation study, three different microbial strains were selected with the highest removal efficiency and doped into the aerogel network. Aerogels were prepared following the process as described in section 5.2.3. The nutrient broth medium was prepared and inoculated using the microorganisms as described in section 6.2.2.3. Following that, the aerogels were submerged in the media and incubated in a BOD shaker incubator (Remi) for seven days at 303 K temperature and under constant rotation. After the incubation period, the aerogels were collected and lyophilized using a freeze-drier (EYELA, FDU-1200).

6.2.7. Removal of organic pollutants using bacteria-doped aerogel: The bioremediation of pollutants from the water solution by bacteria-doped aerogels was performed with a batch study. Different parameters in this experiment were optimized to study their effect on the adsorption process. Response Surface Methodology (RSM) was utilized to optimize the removal process, and modelling of the data was performed to understand the underlying phenomena.

6.2.7.1. Preparation of pollutant solution: In this study, three organic pollutants, naphthalene, acenaphthene, and phenol, were used as the pollutants of interest. The solutions were prepared as mentioned in section 6.2.3.2.2.

6.2.7.2. Experimental procedure: The batch study of this experiment was conducted according to the process as described in section 6.2.5.2.

6.2.7.3. Optimization of removal using Response Surface Methodology: To optimize the removal process, response surface methodology (RSM) was performed. The experimental model was created by using the Box-Behnken design and a second-order system. Being a second-order system, the model followed a quadratic equation that was validated by varying different experimental parameters, viz., time (5-8640 min.), adsorbent dose (0.5g/L -1.5g/L), and pollutant concentration (1 mg/L- 10 mg/L). Design Expert-13 (Version- 7) software was used for this purpose, and a total of seventeen unique combinations of the experimental conditions were investigated. For the ANOVA analysis, all the data of the mentioned seventeen runs were collected and fitted by using the quadratic equation. From the result of this analysis, the validity of the design was established.

6.2.7.4. Gas chromatography mass spectroscopy (GC-MS) analysis of solution after removal: GC-MS analysis was performed to identify the compounds produced after

bioremediation of the pollutants. For this analysis, a GC-MS machine (Thermo Trace-1300) was used with a TG-5MS column. To prepare the samples, 0.1 mL of each solution was taken and diluted with n-Hexane in a 1:10 ratio. Following that, the samples were shaken vigorously and left for 10 min. to form separate layers. The upper layer (hexane) was collected using a micropipette and passed through a syringe filter. 0.1 mL of the sample was taken in a syringe and injected into the inlet of the GC-MS analyzer. Xcalibur software and the MS library were used to identify the products.

6.2.8. Characterization study: The characterization of bacteria, as well as bacteria-doped aerogels, was performed to better understand their interaction with the pollutants.

6.2.8.1. Gram staining of bacteria: The Gram staining process was used to determine if the used bacteria were Gram-positive or Gram-negative. For this experiment, a glass slide was cleaned with 70% ethanol, and 2 loopfuls of bacterial culture were added to the slide. The slide was dried using the heat-fix technique by the flames of a spirit lamp. For primary staining, crystal violet stain was used. The slide was flooded with crystal violet solution and left for 60 seconds. As a mordant, in this experiment, the stained slide was treated with Gram's iodine for 1 min. Following that, it was washed for 30 seconds with ethanol. In the next step, also known as counterstaining, the slide was flooded with Safranin stain and left for another 30 seconds. After the staining was complete, it slides were blotted dry and sealed using a cover slip. The prepared slides were then observed under a light microscope (Dewinter, Fluorex-LED).

6.2.8.2. Inverted microscopy of bacteria: For the inverted microscopy, the slides were prepared by the heat-fix method as described in section 6.2.8.2. After that, a cover slip was used to seal the glass slide. The prepared slide was used to observe under an inverted microscope (Zeiss, Germany).

6.2.8.3. Identification of bacteria: The identification of isolated soil microorganism (SMO) was performed by RT-PCR techniques along with gel electrophoresis and matching FASTA sequence. This analysis was performed by Biokart India Pvt. Ltd.

6.2.8.4. Gram staining of bacteria-doped aerogel: For gram staining of the bacteria-doped aerogel, the aerogels were cut into small pieces and placed on a glass slide. For the rest of the experiment, the process described in section 6.2.8.1 was followed.

6.2.8.5. Crystallographic profiling of bacteria-doped aerogel: The crystallographic profiling of the bacteria-doped aerogel was performed by following the process described in section 4.2.9.2 of chapter 4.

6.2.8.6. Functional group analysis of bacteria-doped aerogel: To analyze the functional groups present on the surface of bacteria-aerogels, ATR-FTIR was performed as described in section 4.2.9.3 of chapter 4.

6.2.8.7. Surface morphology analysis of bacteria-doped aerogel: The surface morphology of bacteria-aerogels was analyzed by scanning electron microscopy (SEM), as described in section 4.2.9.4 of chapter 4.

6.2.8.8. Thermal profiling of bacteria-doped aerogel: To study the thermal profile of prepared samples, thermogravimetric analysis (TGA), differential scanning calorimetry (DSC), and differential thermal analysis (DTA) were performed as described in section 5.2.4.5 of chapter 5.

6.2.8.9. Elemental analysis of bacteria-doped aerogel: To study the elemental composition of the surface, energy dispersive X-ray analysis (EDAX) was performed as described in section 4.2.9.5 of chapter 4.

6.2.8.10. AO/EB alternate staining of bacteria-doped aerogel: For the AO/EB alternate staining method, two stains, viz., ethidium bromide (EB) and acridine orange (AO), were used respectively. This method was performed to understand the survival of bacteria inside the aerogel network.

6.2.8.10.1. Preparation of phosphate buffer solution (PBS) and bacterial suspension: To stain the bacterial colony, the bacteria were released from the aerogel network by treating it with phosphate buffer. To prepare the PBS solution, 8 g of NaCl, 0.2 g of KCl, 1.44 g of Na_2HPO_4, and 0.24 g of KH_2PO_4 were measured using a weighing balance (Sartorius, Germany) and mixed with 1 L of DI water in an Erlenmeyer flask on a magnetic stirrer. The PBS solution was sterilized under 15 psi pressure and at 394 K temperature. The sterilized PBS media was then inoculated with 1 g of bacteria-doped aerogel and incubated for 3 days in a BOD shaker incubator (Remi) under constant agitation and at 303 K temperature.

6.2.8.10.2. Preparation of staining solutions: To make the stain stock solution, 50 mg and 30 mg of AO and EB stains were measured, respectively, using a weighing machine

(Sartorius, Germany) and diluted in 10 mL of ethanol to make separate solutions. Following that, 0.1 mL of AO and EB stock solutions were taken and mixed with 1 mL of PBS solution.

6.2.8.10.2. Staining of microorganism: 0.2 mL of each stain solution was taken and mixed. 0.1 mL of the phosphate buffer was mixed with the staining mixture and incubated for 10 min. 2 loopfuls of bacteria inoculated stain solution were placed on a sterilized glass slide and sealed with a cover slip. The prepared slide was observed under the fluorescent microscope (Dewinter, Fluorex-LED) at 460 nm.

6.3. Result:

6.3.1. MIC: The MIC analysis was performed to understand the minimum inhibitory concentration of each pollutant for every bacterium. From Fig. 6.1, it can be stated that *Bacillus sp., Lysinibacillus sp.,* and *Pseudomonas sp.* have shown inhibition in the case of naphthalene at a 100 mg/L concentration. From *Lysinibacillus sp.* and *Pseudomonas sp.,* inhibition at 10 mg/L was also observed. The diameters of the inhibition zones are presented in Table 6.1.

Table 6.1: The diameter of inhibition zones

Bacteria	Pollutant	Concentration (mg/L)	Diameter of inhibition zones (cm)
Bacillus sp.	Naphthalene	0.1	-
		1	-
		10	-
		100	2.0
	Phenol	0.1	-
		1	-
		10	-
		100	-
	Acenaphthene	0.1	-
		1	-
		10	-
		100	-

Lysinibacillus sp.	Naphthalene	0.1	-
		1	-
		10	1.5
		100	2.3
	Phenol	0.1	-
		1	-
		10	-
		100	-
	Acenaphthene	0.1	-
		1	-
		10	-
		100	-
Pseudomonas sp.	Naphthalene	0.1	-
		1	-
		10	1.7
		100	2.5
	Phenol	0.1	-
		1	-
		10	-
		100	-
	Acenaphthene	0.1	-
		1	-
		10	-
		100	-
SMO	Naphthalene	0.1	-
		1	-
		10	-
		100	-
	Phenol	0.1	-
		1	-
		10	-
		100	-

	Acenaphthene	0.1	-
		1	-
		10	-
		100	-

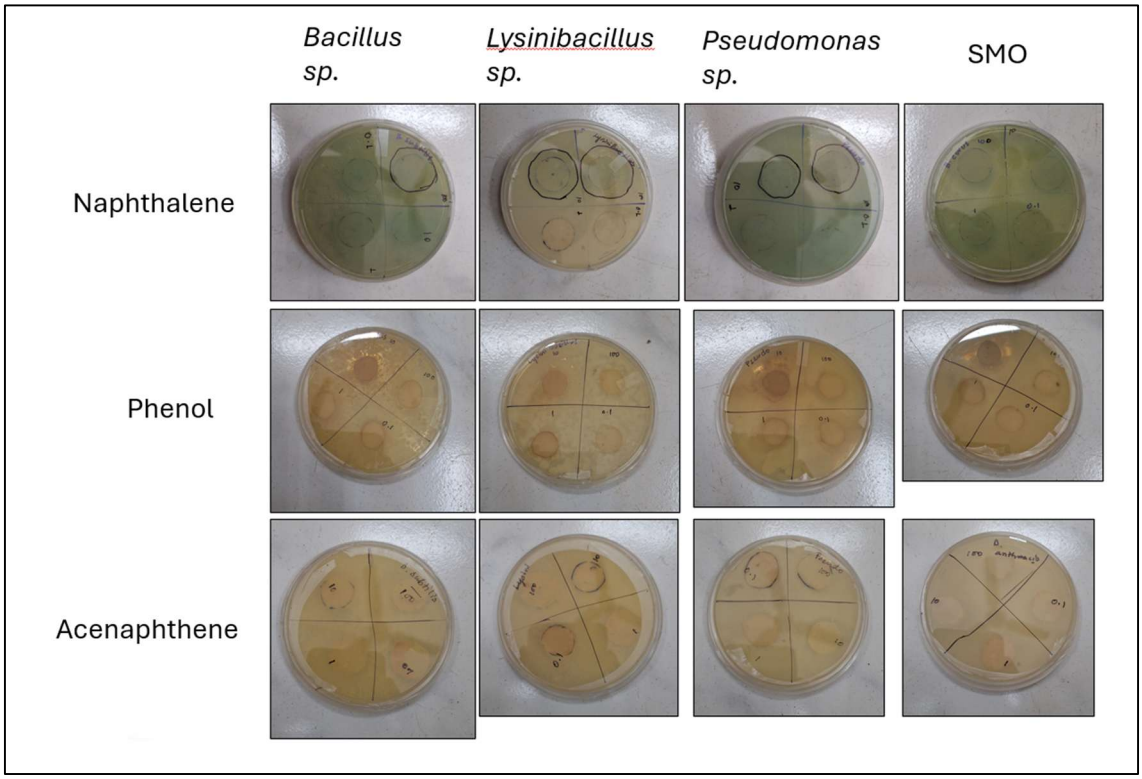

Figure 6.1: MIC analysis of bacteria

From the data, it was observed that Phenol and acenaphthene did not show any inhibitory effect on the microbes even at a higher concentration, showing their resistance towards the inhibitory effect. In the case of naphthalene, inhibitory zones were found, but the diameter in minimal. From this data, the selection of these microorganisms to remediate the pollutants of interest can be explained.

6.3.2. Identification of bacteria: Using RT-PCR, gel electrophoresis, and FASTA sequence matching, the identification of SMO was performed. From the data, it was concluded that the bacterium isolated from soil was *Bacillus anthracis* (Also presented as *B. anthracis*); GeneBank: PP159024.1. The picture of gel electrophoresis and phylogenetic tree of the bacteria is presented as Fig. 6.2 (A) and (B), respectively.

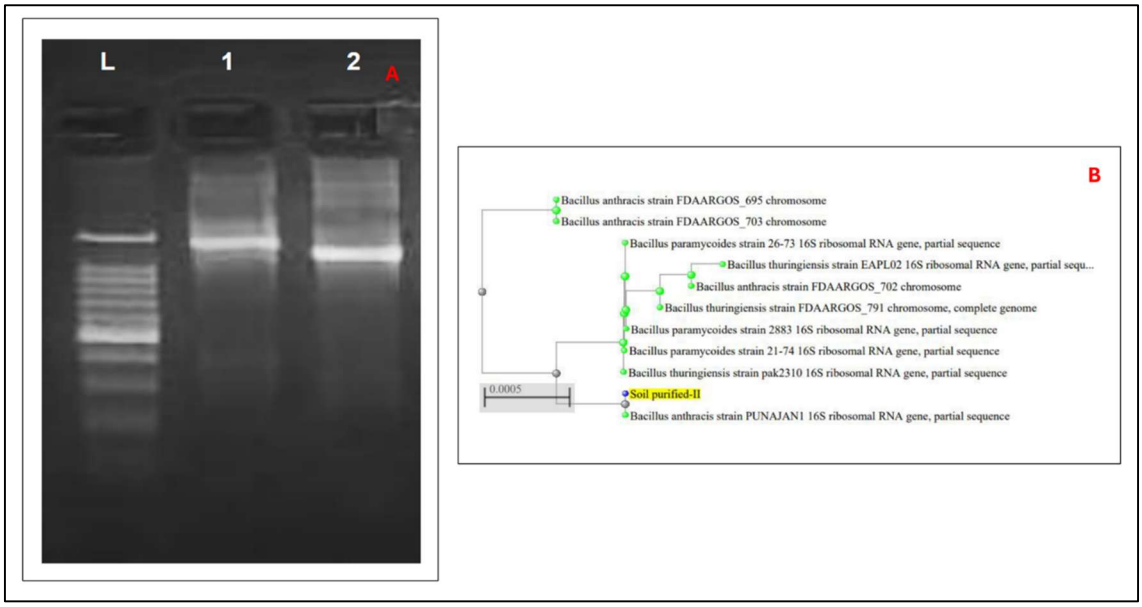

Figure 6.2: Identification of SMO (A) gel electrophoresis, and (B) phylogenetic tree

6.3.3. Stress response of bacteria: To understand the response of the bacteria under different stress conditions, the conditions were simulated in the laboratory, and the growth kinetics of the bacteria were observed.

6.3.3.1. Effect of pollutant: The pollutants can have a significant influence on the growth of bacteria. As shown in Fig. 6.3 (A), the growth curve of the bacteria in the nutrient broth is stable. The effect of naphthalene, phenol, and acenaphthene is presented in Fig. 6.3 (B), (C), and (D), respectively. From the figure, it can be stated that the pollutant, present in the media, can act as a nutrient source for the bacteria to grow, but it also inhibits the bacterial growth compared to the nutrient media. As shown in Figure 6.3 (A), all the bacteria reach the saturation phase after five days of inoculation, but no saturation was observed in the case of naphthalene. Also, the maximum optical density value of the bacterial culture in the nutrient broth was found to be 0.78, whereas for naphthalene-treated media, the optical density value was 0.39. From this observation, it can be stated that naphthalene shifts the bacterial growth curve to the right side of the time axis by delaying the growth.

In the presence of both acenaphthene and phenol, as shown in Fig. 6.3 (C) and (D) respectively, the death phase of the growth curve was observed. Also, the maximum optical density values observed in this study, compared to Fig. 6.3 (A), were very less. This result indicates the effect of phenol and acenaphthene slow down the growth of bacteria.

6.3.3.2. Effect of pH: The growth of the microorganisms was observed under different pH conditions. As shown in Fig. 6.3 (E), it was observed that the shift of pH to the acidic or alkaline side inhibits the growth of bacteria. For all the organisms, the maximum growth was found at pH 8. Sánchez-Clemente et al. (2018) reported that, at extreme pH, the ATP production of cells is affected. The synthesis of ATP is highly dependent on the proton gradient of the cell. At extreme pH, the gradient gets disrupted, hence affecting the ATP synthesis and the survival of bacteria. Another factor to inhibit bacterial growth at extreme pH is the alteration of protein structure. Also, at high pH, hydrogen bonds become vulnerable, causing damage to DNA and protein structures.

6.3.3.3. Effect of temperature: The effect of temperature on the growth of bacteria is shown in Fig. 6.3 (F). From the figure, it was observed that the maximum bacterial growth was observed at 303 K temperature. A previous study reported similar results for *E. coli,* explaining the reason for the growth inhibition. According to this study, extreme temperatures can alter enzymatic activity, affect membrane integrity and nucleic acid stability, causing permanent cellular damage (Nguyen, 2006).

6.3.3.4. Effect of salinity: Salinity was also an important parameter affecting bacterial growth. As presented in Fig. 6.3 (G), with the increasing salinity, bacterial growth is inhibited. Zhang et al. (2014) reported that with the increasing salinity, osmotic stress also increased, causing disruption of cells. Ion toxicity and metabolic disruption are also responsible for the inhibition of bacterial growth (Rath et al., 2018).

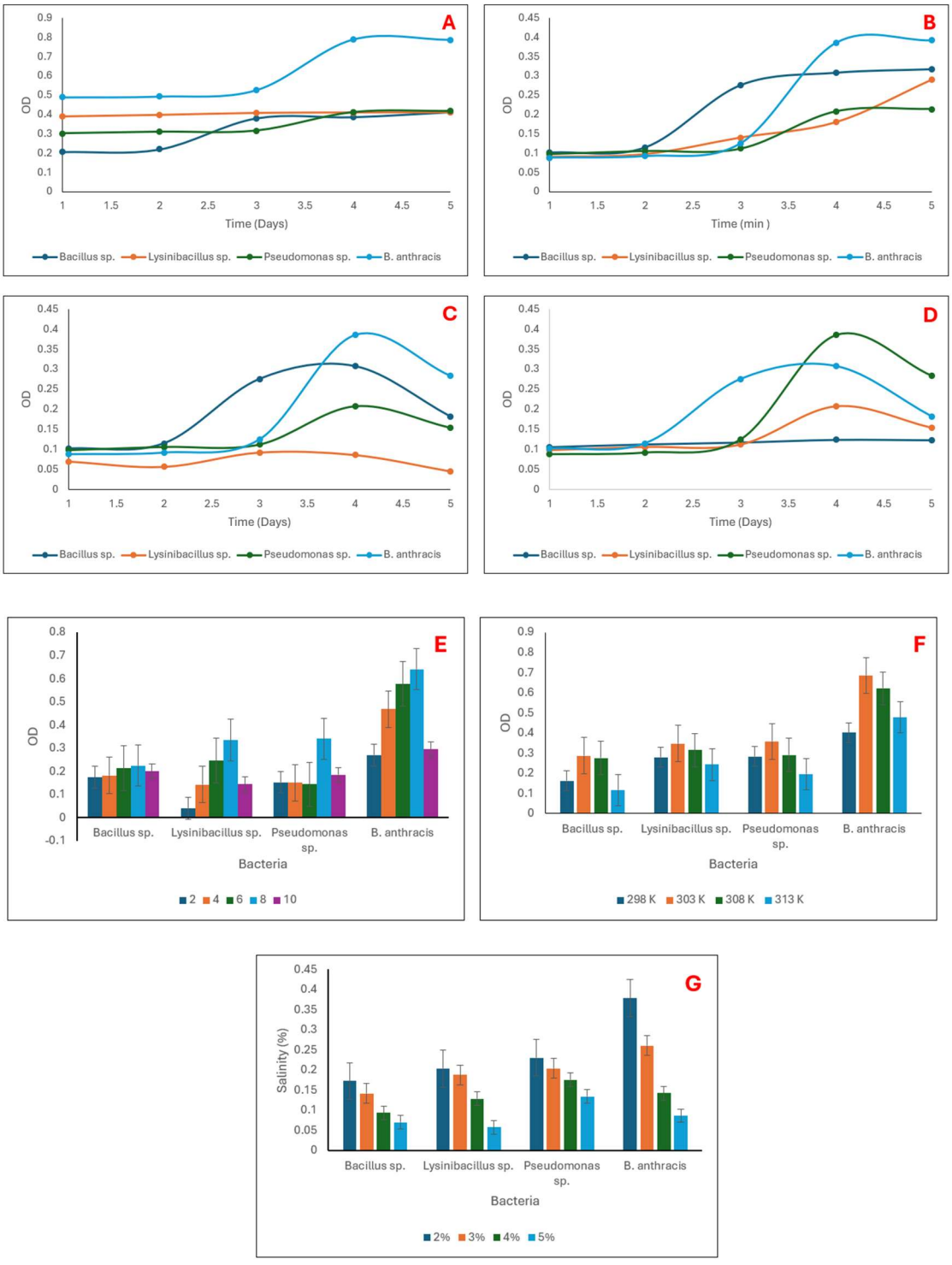

Figure 6.3: Response of bacteria in (A) nutrient broth, (B) naphthalene media, (C) phenol media, (D) acenaphthene media, (E) under different pH, (F) under different temperature, (G) under different salinity.

6.3.4. Microscopy: The microscopic images of *Bacillus sp., Lysinibacillus sp., Pseudomonas sp.,* and *B. anthracis* after Gram staining are presented in Fig. 6.4 (A), (B), (C), and (D), respectively. From the figures, it can be observed that all the microorganisms used in this study, but *Pseudomonas sp.,* are Gram-positive. The *Pseudomonas* strain was found to be Gram-negative.

The inverted microscopic images of *Bacillus sp., Lysinibacillus sp., Pseudomonas sp.,* and *B. anthracis* are presented in Fig. 6.4 (E), (F), (G), and (H). From the figure, it was observed that all the microorganisms are rod-shaped.

Fig. 6.4 (I) presents the bacterial colony inside the aerogel network (marked with a black circle). This observation assures the proper doping and growth of microorganisms inside the gel matrix.

Fig. 6.4 (J) and (K) show the result of AO/EB staining. In Figure 6.4 (J), the presence of a green colony indicates the survival of bacteria inside gel matrix. On the other hand, figure 6.5 (K) represents red colony, indicating the dead microorganisms. The dominance of the green colony over red colony signifies the inside environment of the prepared aerogels are suitable for the bacteria to survive.

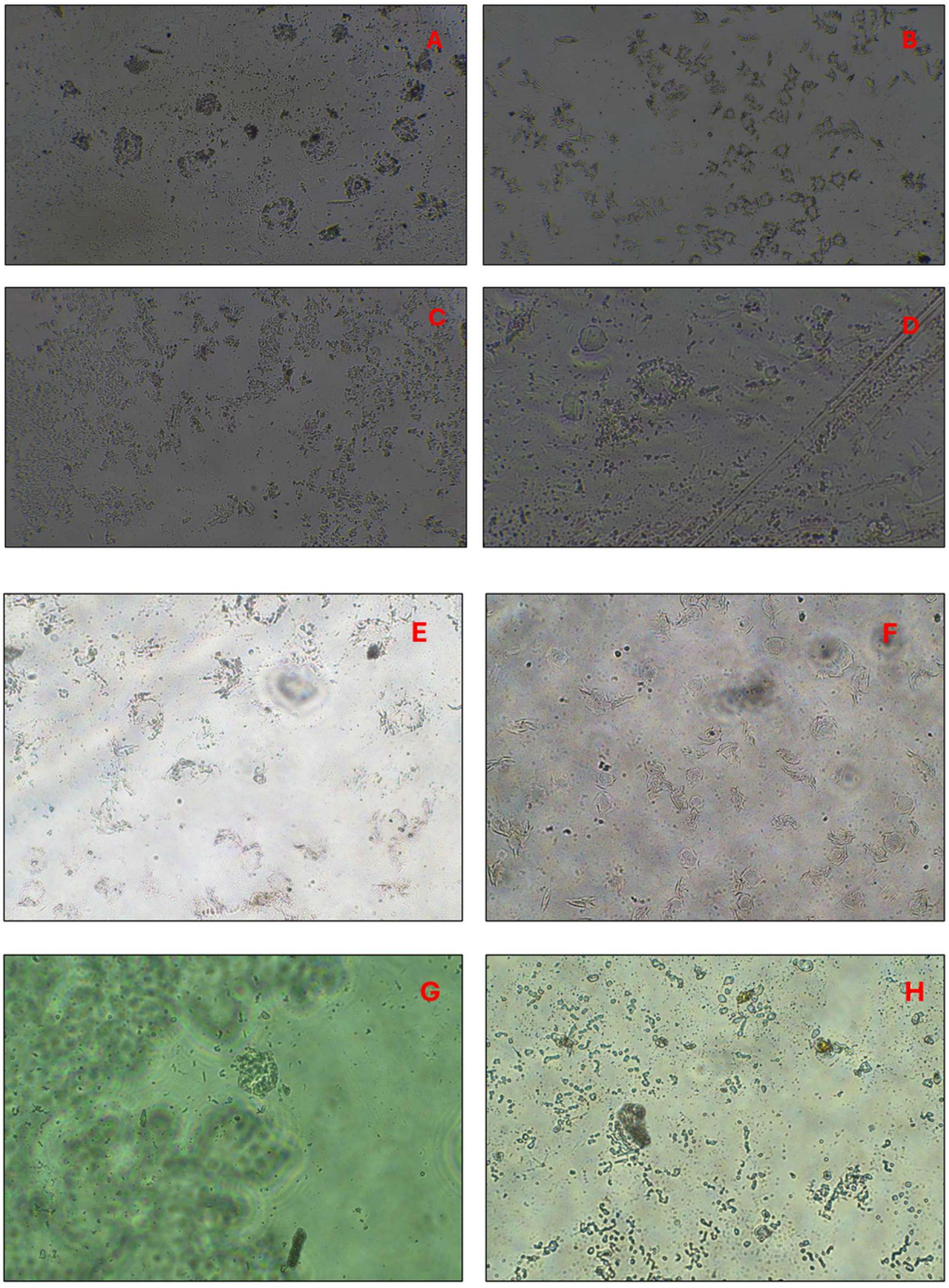
A
B
C
D
E
F
G
H

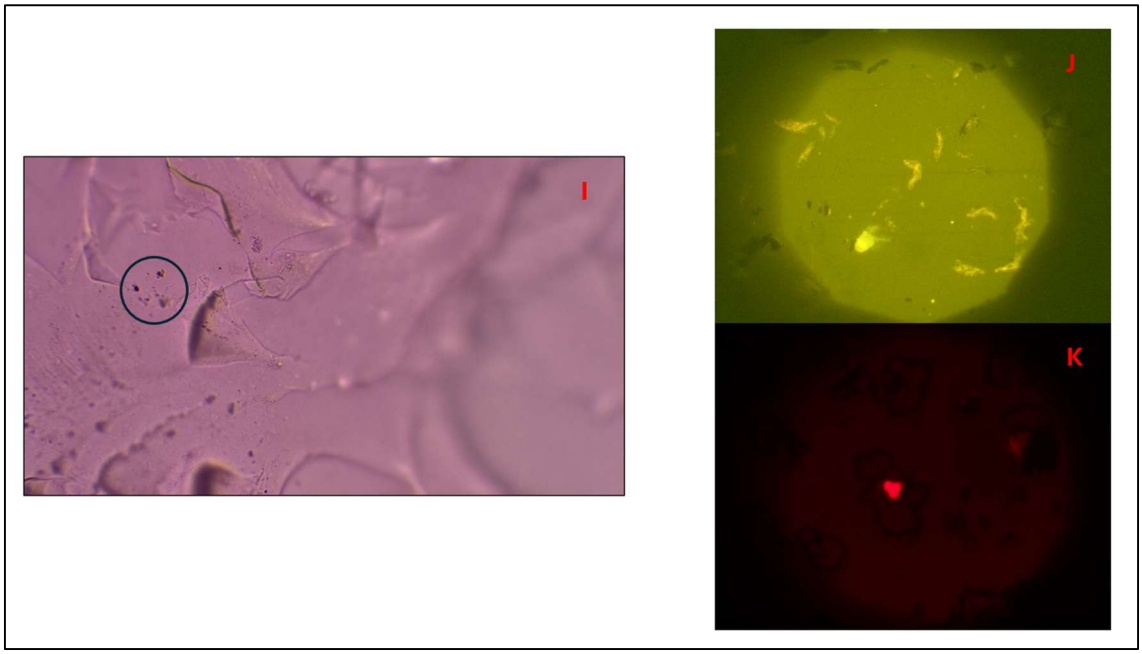

Figure 6.4: Images of (A) *Bacillus sp.*, (B) *Lysinibacillus sp.*, (C) *Pseudomonas sp., and* (D) *B. anthracis* under light microscope; (E) *Bacillus sp.*, (F) *Lysinibacillus sp.*, (G) *Pseudomonas sp.*, and (H) *B. anthracis* under inverted microscopy, (I) microorganisms in aerogel network, (J) living and (K) dead bacterial colony in aerogel network after AO/EB staining.

6.3.5. Crystallographic profiling: The crystallographic profiling of the prepared bacteria-doped aerogels was performed by XRD analysis. Fig. 6.5 shows the result of the comparative XRD analysis of the normal and bacteria-doped aerogel. From the figure, it can be stated that for both the aerogel samples, a peak at $2\Theta = 19.3^{o}$ was observed. Hema et al. (2009) reported that this peak is a characteristic peak of the PVA component. From the figure, a change in the XRD peak was also observed after adding bacteria into the aerogel network. In case of *Pseudomonas*-doped PVA-Si aerogel, two new peaks were observed at $2\Theta = 31.23^{o}$ and 41.01^{o} respectively, confirming the presence of silica inside the PVA network (Nguyen et al. 2022).

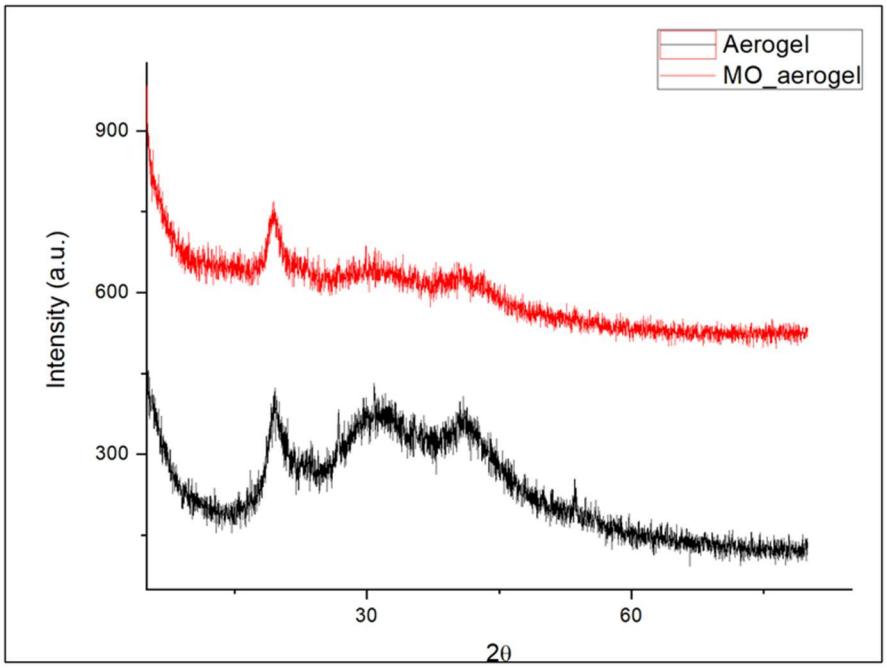

Figure 6.5: Comparative XRD analysis of aerogel before and after bacterial doping

6.3.6. Functional group analysis: Fig. 6.6 presents the ATR-FTIR analysis of bacteria-doped aerogels. From the figure, four major peaks were seen at 3226 cm^{-1}, 2940 cm^{-1}, 2910 cm^{-1}, 1645 cm^{-1}, 1411 cm^{-1}, and 1091 cm^{-1}, respectively. The presence of an aldehyde group in the aerogel was observed at 3373 cm^{-1} due to the usage of glutaraldehyde in the production process. Peaks at 2914 cm^{-1} and 1645 cm^{-1} are attributed to the C-H of alkyl groups and C=O groups, respectively (Mansur et al., 2004). The presence of C-O stretching of acetyl groups is represented by 1091 cm^{-1} (Nafee et al., 2017). As the PVA, biochar, and cellulose contain almost the same functional group compositions on their surface, no significant difference in the ATR-FTIR analysis was observed. However, in the case of PVA-Si aerogel, a distinct peak at 606 cm^{-1} was observed representing Si-O-Si vibration (Chuan-Chao et al., 2014).

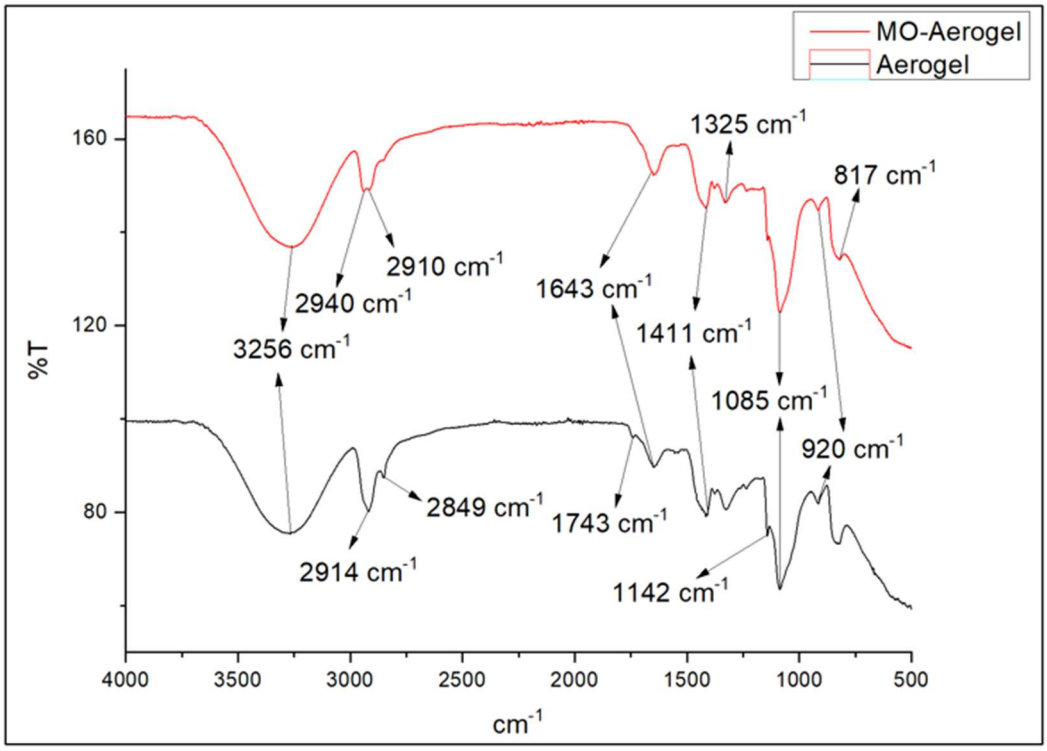

Figure 6.6: Comparative ATR-FTIR analysis of aerogel before and after bacterial doping

6.3.7. Scanning electron microscopy: The SEM images of normal and bacteria-doped aerogels are presented in Fig. 6.7 (A) and (B), respectively. In Fig. 6.7 (A), the surface of aerogel without bacterial doping is presented. Compared to that, the other picture of the aerogel surface shows a significant morphology change after bacterial doping. The presence of these cavities on the surface contributes to the high adsorption efficiency of the aerogels.

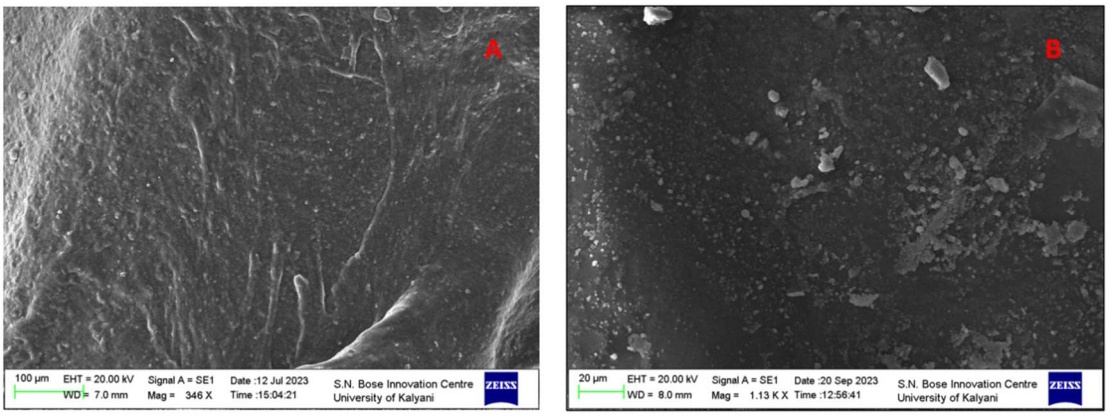

Figure 6.7: SEM images of aerogel (A) before and (B) after bacterial doping

6.3.8. Elemental analysis: The surface elemental composition of the aerogel before and after microbial doping was studied by EDAX analysis. The EDAX analysis was reported after bacterial doping inside the aerogel network was observed. Table 6.4 represents % of different materials present in the aerogel network. As represented in Table 6.2, from the study, it was found that normal aerogel contains 59.90% carbon and 40.10% oxygen. On the other hand, bacteria-doped aerogel contains 70.00% carbon along with 16.37% oxygen. Also, the presence of chlorine, sodium, and potassium was detected with 10.96%, 1.96% and 1.08% values. As represented in Figure 6.8. The presence of sodium, potassium, and chlorine was detected by treating aerogel with nutrient broth media.

Table 6.2: EDAX analysis of synthesised aerogels

Aerogels	Carbon atomic %	Oxygen atomic %	Chlorine atomic %	Sodium atomic %	Potassium atomic %
Normal aerogel	59.90	40.10			
Bacteria-doped aerogel	70.00	16.37	10.96	1.96	1.08

Figure 6.8: EDAX analysis of bacteria-doped aerogel

6.3.9. Thermal profiling: Fig. 6.9 (A) shows the comparative thermogravimetric analysis (TGA) of the prepared aerogel before and after bacterial doping. From this figure, a difference in the change in percentage of weight for temperature was observed. For aerogel before bacterial doping, the weight% decreased to 87.97% at the temperature 176ºC, and then it rapidly degraded to 0%. On the other hand, for bacteria-doped aerogel, the first stage of sample degradation was found in the range of 40ºC to 214.52ºC. The weight loss in this stage signifies the degradation of PVA. After that, the aerogel degraded rapidly. This stage is attributed to the degradation of the crosslinking of the PVA network. After that, for both aerogels, carbonation was observed till 327ºC (Yang, 2007). From the result of TGA analysis, it can be stated that after adding bacteria to the matrix, a slight change in the degradation was observed. The similar pattern of degradation indicates no significant change in the chemical structure of the gel, but the right shift shows the increase in biomass content after bacterial doping.

Fig. 6.9 (B) shows the differential thermal analysis (DTA) of the prepared aerogels. In the figure, the first step of the reaction, a downward peak was observed at 176.71ºC and 151.93ºC for aerogel before and after bacterial doping, respectively. These peaks represent an endothermic event during this analysis. In the second step of the reaction, a sudden exothermic shift was observed for both the aerogels. A third step was also observed for bacteria-doped aerogel, signifying an endothermic reaction from 588ºC until the end of the analysis.

Fig. 6.9 (C) shows the differential scanning calorimetry (DSC) analysis of the aerogels before and after bacterial doping. In that figure, a distinct endothermic peak for normal aerogel was observed at 176ºC supports the TGA data and rapid degradation. The gradual increase of heat flow for both samples suggests the continuous decomposition of the samples with increasing temperature. A divergence in the thermal curves was observed at a higher temperature, explaining their different thermal stability and behaviour.

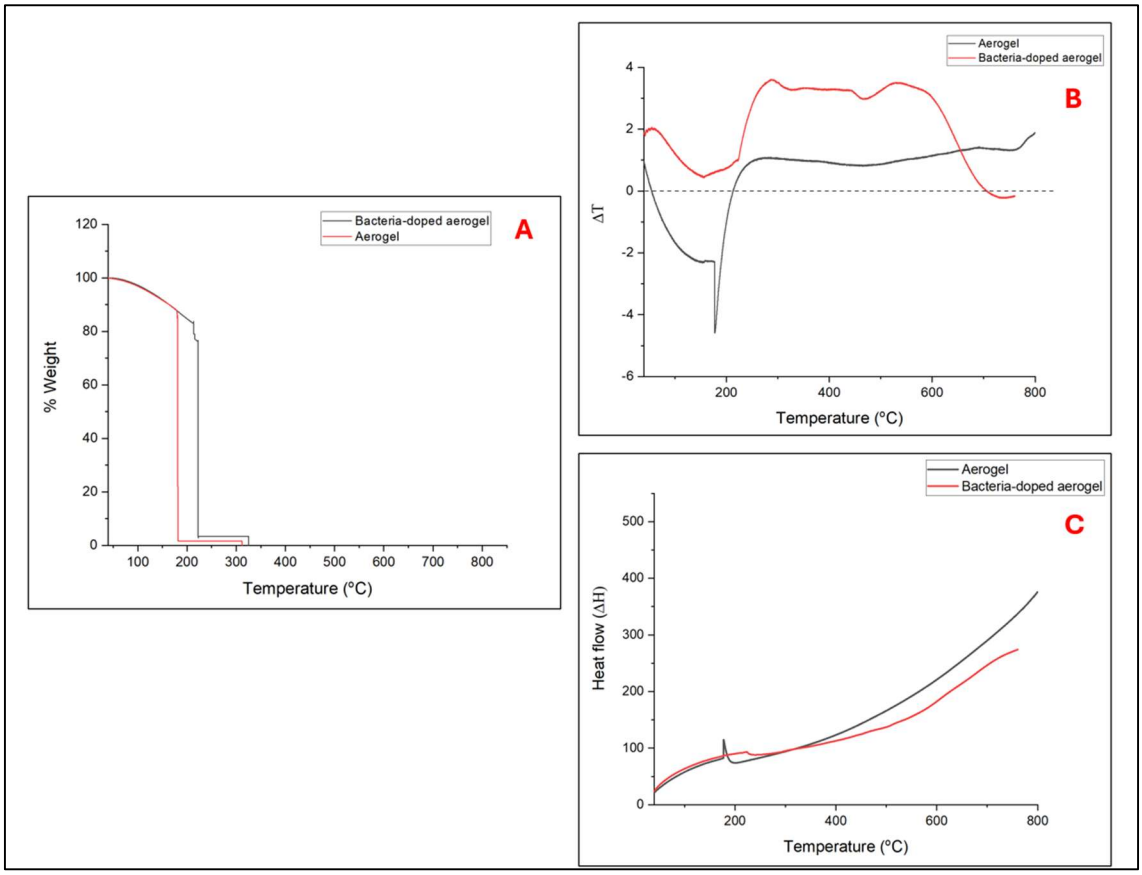

Figure 6.9: Comparative (A) TGA, (B) DTA, and (C) DSC analysis of aerogel before and after bacterial doping

6.3.10. Removal of naphthalene by bacteria: The bioremediation of naphthalene by all four selected bacteria, viz., *Bacillus sp., Lysinibacillus sp., Pseudomonas sp.,* and *B. anthracis,* was studied. Different parameters were varied to understand their effect on the removal.

6.3.10.1. Effect of treatment time: The effect of contact time on the bioremediation of naphthalene is shown in Fig. 6.10 (A). As represented in the figure, the removal of naphthalene increased with time, and the highest removal achieved in this study was 93.12% by *Pseudomonas sp.* after 5 days of treatment, while the other parameters were constant (pH 7, dose 1 mL/100 mL, concentration 5mg/L, and temperature at 303 K). For comparison, under the same conditions, *Bacillus sp., Lysinibacillus sp.,* and *B. anthracis* showed 86.68%, 83.14%, and 85.82% of removal, respectively. After 5 days of treatment, no significant change was observed in the concentration of the pollutant, indicating that the equilibrium was achieved. A previous study showed that pollutant removal by bacteria reached up to 94% (Mahapatra and Phale, 2021). This observation can be explained by considering the metabolism of bacteria and the interaction time of the bacteria with pollutant molecules (Abd El-Rahim et al., 2009). Before achieving the equilibrium, a

growth in bacterial culture was observed, which contributed to the significant removal of the contaminant.

6.3.10.2. Effect of microbial dose: The dosage of bacteria is a crucial parameter and affects the removal process significantly. This study considered four different dosages of bacteria, viz., 0.5 mL/100 mL, 1 mL/100 mL, 2 mL/100 mL, and 3 mL/100 mL, respectively. The effect of bacterial dose on the removal of pollutant is shown in Fig. 6.10 (B). As represented in the figure, with the increasing dose, the removal also increased till 2 mL/ 100mL, and after that, a decline was observed. Higher microbial dosage provides more microbial mass and metabolic activity, which results in higher removal (Santini et al., 2016); however, after a certain point, the increasing dose causes resource scarcity and an increase in concentration. Therefore, an opposite effect also occurred in the removal of the pollutant (Liu et al., 1993). In this study, the highest removal was achieved by *Bacillus sp.,* at 2 mL/ 100 mL dose, and the value was 99.52%.

6.3.10.3. Effect of pollutant concentration: Initial pollutant concentration is one of the key parameters to affect the adsorption process. The pollutant concentration has a significant role in the growth of the bacteria, interaction rate between contaminant molecules and bacterial intake sites (Sayara et al., 2010). The initial concentration of the solute acts as a driving force of the bioremediation process, favouring diffusion and mass transfer from the solution. In such water treatment systems, after the threshold limit, further increasing of substrate concentration may lead to saturation effects (Nocentini et al., 2000). In this study, five pollutant concentrations, viz., 1 mg/L, 3 mg/L, 5 mg/L, 7 mg/L, and 10 mg/L, respectively, were considered. As shown in Fig. 6.10 (C), the maximum removal of naphthalene was observed in the case of *Bacillus sp.*, at 10 mg/L concentration. The removal was 94.09%. It was also observed that with the increasing initial concentration, the removal decreased for all the bacteria but *Bacillus sp.*, showing different tolerance towards the pollutant. The least removal was observed in the case of *Lysinibacillus sp.,* at the concentration of 1 mg/L. The value of pollutant removal found in this study was 35.61%. At higher concentrations, the pollutants lead to toxicity and reduce the removal (Sharma and Indu, 2020).

6.3.10.4. Effect of temperature: Temperature is an important physiological parameter to influences the removal process of a pollutant, as this parameter has an important effect on microbial growth. In most cases, higher temperatures enhance the removal of

pollutants, but at extreme temperatures, the growth of microbes is reduced (Iqbal et al., 2007). It was observed that for every microbe, there is an optimum temperature, and at that temperature, the microbial activity is the maximum (Sanscartier et al., 2011). Topp et al. (1997) reported that most of the microbes show optimum temperature at a range of 298 K- 308 K. Fig. 6.10 (D) represents the effect of temperature on the removal of naphthalene by microorganisms. For this study, a total of three temperatures, viz., 298 K, 303 K, and 313 K were considered respectively. The highest removal was found in the case of *Pseudomonas sp.*, at 303 K temperature with the value of 93.137% removal. For the same bacteria, the removal at 298 K was 30.01%.

6.3.10.5. Effect of pH: pH is an important parameter of the bioremediation process. pH affects the process in various ways, viz., the chemistry of pollutants, the coexisting ions of the solution, and the ionic balance of microorganisms. pH also affects the adsorption mechanism and degree of ionisation. The effect of pH on the bioremediation of naphthalene is shown in Fig. 6.10 (E). For this study, six different pH values, viz., 2,4,6,7,8, and 10, were considered respectively. From the figure, it can be stated that for each bacterium, the maximum removal was observed at pH 7. The highest removal of naphthalene was found to be 93.11% in the case of *Pseudomonas sp.* This observation can be explained by the enzymatic activity of bacteria. At extreme pH, denaturation of bacterial enzymes can occur, significantly decreasing the removal efficiency (Megharaj et al., 2011).

6.3.10.6. Effect of salinity: The effect of salinity on the bacterial removal is presented in Fig. 6.10 (F). As observed from the figure, with the increasing salinity, the removal of the pollutant decreased significantly. The highest removal was found in the case of *Pseudomonas sp.,* with the value of 93.12%. Zhang et al. (2014) reported that with the increasing salinity, osmotic stress also increased, disrupting cells. Ion toxicity and metabolic disruption are also responsible for the inhibition of bacterial growth (Rath et al., 2018).

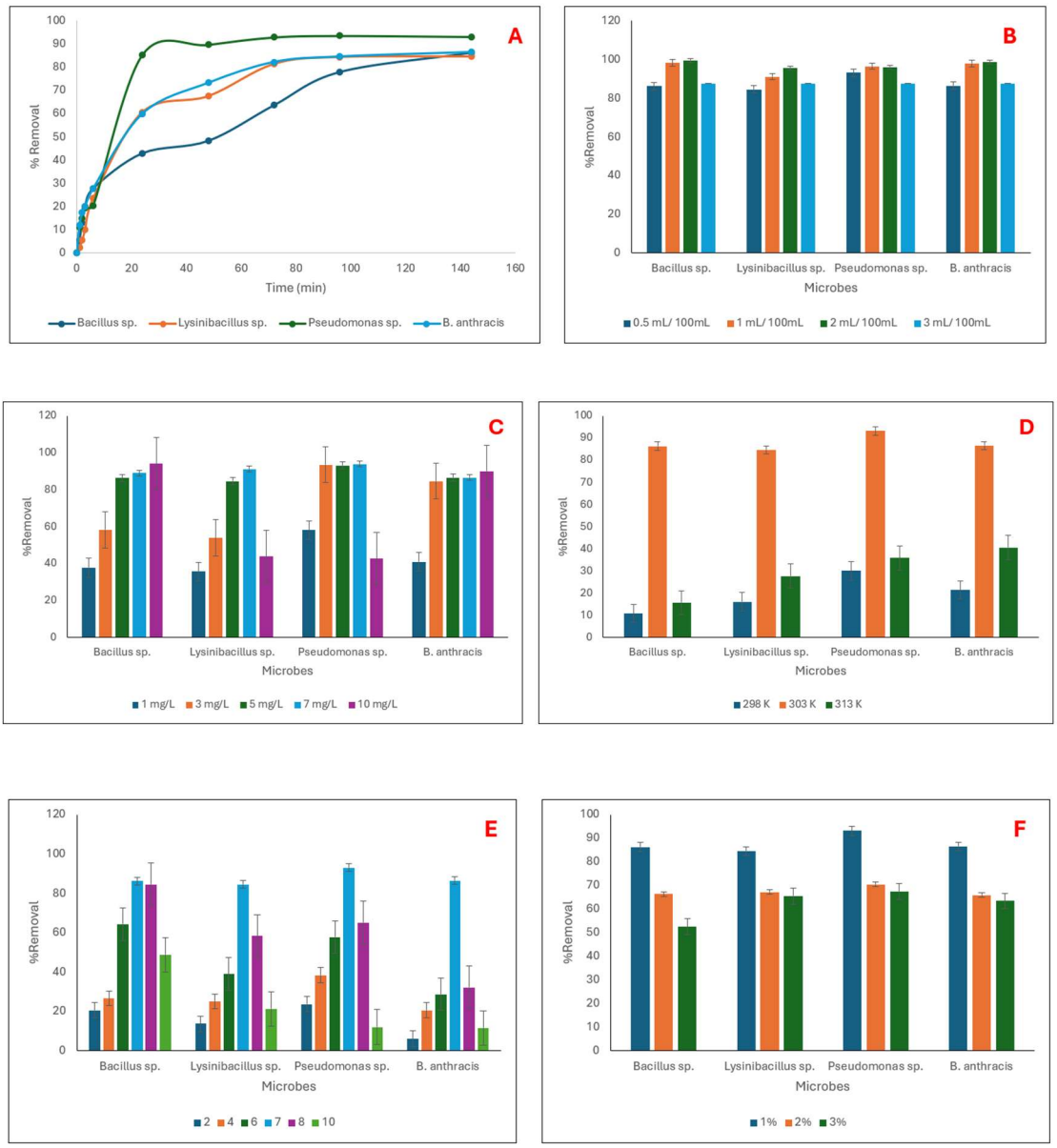

Figure 6.10: Effect of (A) treatment time, (B) microbial dose, (C) pollutant concentration, (D) temperature, (E) pH, and (F) salinity on bioremediation of naphthalene by bacteria

6.3.10.7. Analysis of naphthalene bioremediation by the Monod model: Table 6.3 shows the results of naphthalene bioremediation analysis by the Monod model. From the data, it was observed that *Pseudomonas sp.* has the best substrate affinity among all the aerogels, and *B. anthracis* shows the fastest growth rate in naphthalene solution. This result signifies that the application of *Pseudomonas sp.* is optimal at lower concentrations of naphthalene. Similar results were reported in previous studies (Oberoi et al., 2015; Mahapatra and Phale, 2021). Also, *B. anthracis* is found to excel in high-pollution scenarios.

Table 6.3: The Monod modelling of naphthalene removal by bacteria

Pollutant	Bacteria	μ_{max}	K_s
Naphthalene	*Bacillus sp.*	0.003371	5.28
	Lysinibacillus sp.	0.0034	3.73
	Pseudomonas sp.	0.002254	3.44
	B. anthracis	0.005129	6.11

6.3.11. Removal of phenol by bacteria: The bioremediation of phenol by all four selected bacteria, viz., *Bacillus sp., Lysinibacillus sp., Pseudomonas sp.,* and *B. anthracis,* was studied. Different parameters were varied to understand their effect on the removal.

6.3.11.1. Effect of treatment time: The effect of contact time on the bioremediation of phenol is shown in Fig. 6.11 (A). As represented in the figure, the removal of phenol increased with time, and the highest removal achieved in this study was 84.19% by *Pseudomonas sp.* after 5 days of treatment, while the other parameters were constant (pH 7, dose 1 mL/100 mL, concentration 5mg/L, and temperature at 303 K). For comparison, under the same conditions, *Bacillus sp., Lysinibacillus sp.,* and *B. anthracis* showed 83.68%, 83.14%, and 81.82% of removal, respectively. After 5 days of treatment, no significant change was observed in the concentration of the pollutant, indicating that the equilibrium was achieved. A previous study showed that pollutant removal by bacteria reached up to 94% (Mahapatra and Phale, 2021). This observation can be explained by considering the metabolism of bacteria and the interaction time of the bacteria with pollutant molecules (Abd El-Rahim et al., 2009). Before achieving the equilibrium, a growth in bacterial culture was observed, which contributed to the significant removal of the contaminant.

6.3.11.2. Effect of microbial dose: The dosage of bacteria is a crucial parameter and affects the removal process significantly. This study considered four different dosages of bacteria, viz., 0.5 mL/100 mL, 1 mL/100 mL, 2 mL/100 mL, and 3 mL/100 mL, respectively. The effect of bacterial dose on the removal of pollutant is shown in Fig. 6.11 (B). As represented in the figure, with the increasing dose, the removal also increased till 2 mL/ 100mL, and after that, a decline was observed. Higher microbial dosage provides more microbial mass and metabolic activity, which results in higher removal (Santini et

al., 2016); however, after a certain point, the increasing dose causes resource scarcity and an increase in concentration. Therefore, an opposite effect also occurred in the removal of the pollutant (Liu et al., 1993). In this study, the highest removal was achieved by *Pseudomonas sp.,* at 2 mL/ 100 mL dose, and the value was 96.12%.

6.3.11.3. Effect of pollutant concentration: Initial pollutant concentration is one of the key parameters to affect the adsorption process. The pollutant concentration has a significant role in the growth of the bacteria, interaction rate between contaminant molecules and bacterial intake sites (Sayara et al., 2010). The initial concentration of the solute acts as a driving force of the bioremediation process, favouring diffusion and mass transfer from the solution. In such water treatment systems, after the threshold limit, further increasing of substrate concentration may lead to saturation effects (Nocentini et al., 2000). In this study, five pollutant concentrations, viz., 1 mg/L, 3 mg/L 5 mg/L, 7 mg/L, and 10 mg/L, respectively, were considered. As shown in Fig. 6.11 (C), the maximum removal of phenol was observed in the case of *Bacillus sp.*, at 5 mg/L concentration. The removal was 85.09%. The least removal was observed in the case of *Lysinibacillus sp.,* at the concentration of 10 mg/L. The value of pollutant removal found in this study was 24.59%. At higher concentrations, the pollutants lead to toxicity and reduce the removal (Sharma and Indu, 2020).

6.3.11.4. Effect of temperature: Temperature is an important physiological parameter to influences the removal process of a pollutant, as this parameter has an important effect on microbial growth. In most cases, higher temperatures enhance the removal of pollutants, but at extreme temperatures, the growth of microbes is reduced (Iqbal et al., 2007). It was observed that for every microbe, there is an optimum temperature, and at that temperature, the microbial activity is the maximum (Sanscartier et al., 2011). Topp et al. (1997) reported that most of the microbes show optimum temperature at a range of 298 K- 313 K. Fig. 6.11 (D) represents the effect of temperature on the removal of phenol by microorganisms. For this study, a total of three temperatures, viz., 298 K, 303 K, and 313 K, were considered respectively. The highest removal was found in the case of *Bacillus sp.*, at 303 K temperature with the value of 85.86% removal. For the same bacteria, the removal at 298 K was 15.67%.

6.3.11.5. Effect of pH: pH is an important parameter of the bioremediation process. pH affects the process in various ways, viz., the chemistry of pollutants, the coexisting ions

of the solution, and the ionic balance of microorganisms. pH also affects the adsorption mechanism and degree of ionisation. The effect of pH on the bioremediation of phenol is shown in Fig. 6.11 (E). For this study, six different pH values, viz., 2,4,6,7,8, and 10, were considered respectively. From the figure, it can be stated that for each bacterium, the maximum removal was observed at pH 7. The highest removal of naphthalene was found to be 83.21% in the case of *Pseudomonas sp.* This observation can be explained by the enzymatic activity of bacteria. At extreme pH, denaturation of bacterial enzymes can occur, significantly decreasing the removal efficiency (Megharaj et al., 2011).

6.3.11.6. Effect of salinity: The effect of salinity on the bacterial removal is presented in Fig. 6.11 (F). As observed from the figure, with the increasing salinity, the removal of the pollutant decreased significantly. The highest removal was found in the case of *Bacillus sp.,* with the value of 85.28%. Zhang et al. (2014) reported that with the increasing salinity, osmotic stress also increased, disrupting cells. Ion toxicity and metabolic disruption are also responsible for the inhibition of bacterial growth (Rath et al., 2018).

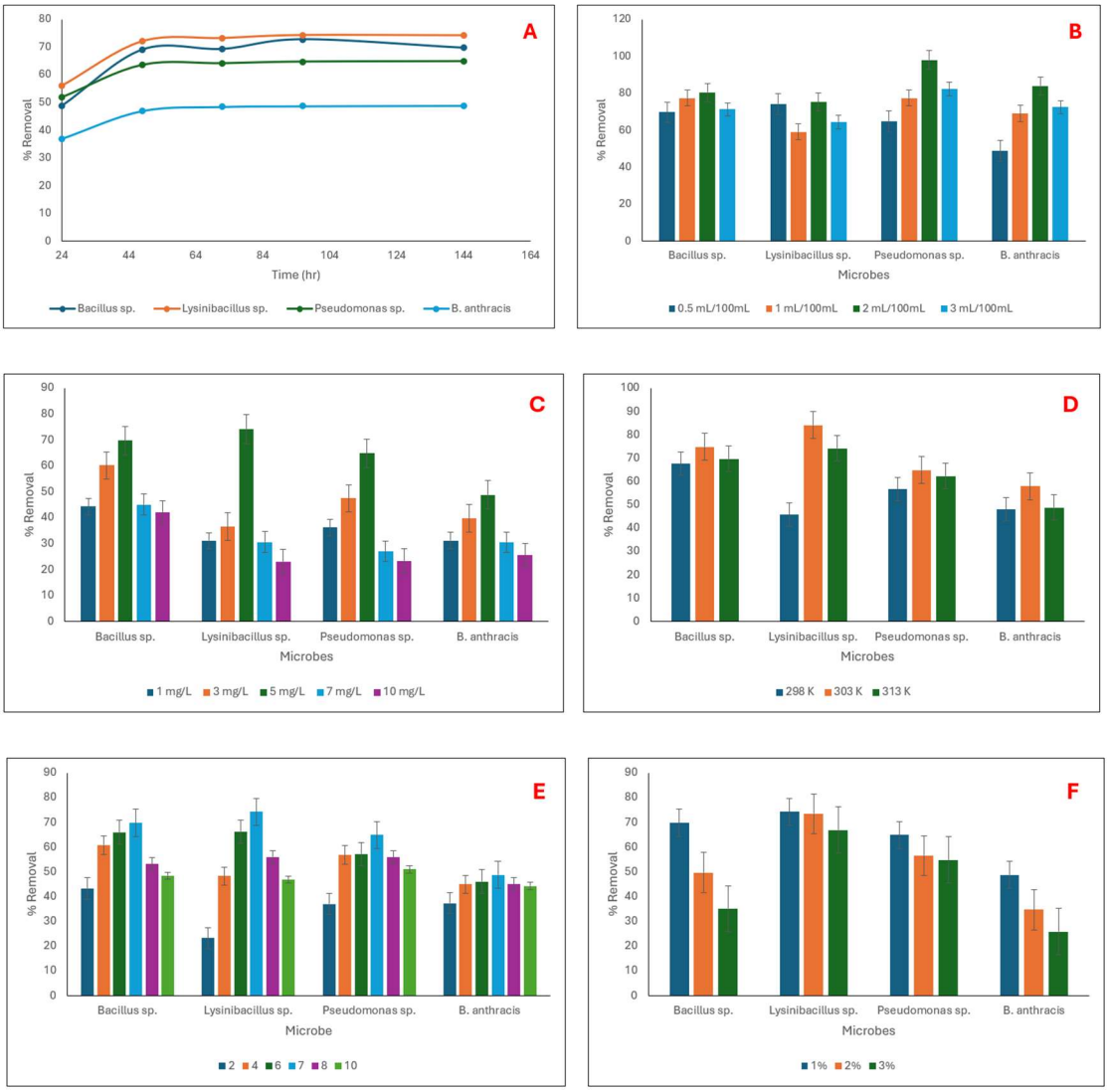

Figure 6.11: Effect of (A) treatment time, (B) microbial dose, (C) pollutant concentration, (D) temperature, (E) pH, and (F) salinity on bioremediation of phenol by bacteria

6.3.11.7. Analysis of phenol bioremediation by the Monod model: Table 6.4 shows the results of naphthalene bioremediation analysis by the Monod model. From the data, it was observed that *Pseudomonas sp.* has the best substrate affinity among all the aerogels, and *Lysinibacillus sp.* shows the fastest growth rate in naphthalene solution. This result signifies that the application of *Pseudomonas sp.* is optimal at lower concentrations of naphthalene. Similar results were reported in previous studies (Oberoi et al., 2015; Mahapatra and Phale, 2021). Also, *Lysinibacillus sp.* is found to excel in high-pollution scenarios.

Table 6.4: The Monod modelling of phenol removal by bacteria

Pollutant	**Bacteria**	**μ_{max}**	**K_s**

Phenol	*Bacillus sp.*	0.004261	5.28
	Lysinibacillus sp.	0.00573	6.27
	Pseudomonas sp.	0.003854	6.94
	B. anthracis	0.005117	4.27

6.3.12. Removal of acenaphthene by bacteria: The bioremediation of acenaphthene by all four selected bacteria, viz., *Bacillus sp., Lysinibacillus sp., Pseudomonas sp.,* and *B. anthracis,* was studied. Different parameters were varied to understand their effect on the removal.

6.3.12.1. Effect of treatment time: The effect of contact time on the bioremediation of acenaphthene is shown in Fig. 6.12 (A). As represented in the figure, the removal of acenaphthene increased with time, and the highest removal achieved in this study was 74.18% by *Lysinibacillus sp.* after 5 days of treatment, while the other parameters were constant (pH 7, dose 1 mL/100 mL, concentration 5mg/L, and temperature at 303 K). For comparison, under the same conditions, *Bacillus sp., Pseudomonas sp.,* and *B. anthracis* showed 64.68%, 74.14%, and 48.82% of removal, respectively. After 5 days of treatment, no significant change was observed in the concentration of the pollutant, indicating that the equilibrium was achieved. A previous study showed that pollutant removal by bacteria reached up to 94% (Mahapatra and Phale, 2021). This observation can be explained by considering the metabolism of bacteria and the interaction time of the bacteria with pollutant molecules (Abd El-Rahim et al., 2009). Before achieving the equilibrium, a growth in bacterial culture was observed, which contributed to the significant removal of the contaminant.

6.3.12.2. Effect of microbial dose: The dosage of bacteria is a crucial parameter and affects the removal process significantly. This study considered four different dosages of bacteria, viz., 0.5 mL/100 mL, 1 mL/100 mL, 2 mL/100 mL, and 3 mL/100 mL, respectively. The effect of bacterial dose on the removal of pollutant is shown in Fig. 6.12 (B). As represented in the figure, with the increasing dose, the removal also increased till 2 mL/ 100mL, and after that, a decline was observed. Higher microbial dosage provides more microbial mass and metabolic activity, which results in higher removal (Santini et al., 2016); however, after a certain point, the increasing dose causes resource scarcity and

an increase in concentration. Therefore, an opposite effect also occurred in the removal of the pollutant (Liu et al., 1993). In this study, the highest removal was achieved by *Pseudomonas sp.,* at 2 mL/ 100 mL dose, and the value was 98.06%.

6.3.12.3. Effect of pollutant concentration: Initial pollutant concentration is one of the key parameters to affect the adsorption process. The pollutant concentration has a significant role in the growth of the bacteria, interaction rate between contaminant molecules and bacterial intake sites (Sayara et al., 2010). The initial concentration of the solute acts as a driving force of the bioremediation process, favouring diffusion and mass transfer from the solution. In such water treatment systems, after the threshold limit, further increasing of substrate concentration may lead to saturation effects (Nocentini et al., 2000). In this study, five pollutant concentrations, viz., 1 mg/L, 3 mg/L, 5 mg/L, 7 mg/L, and 10 mg/L, respectively, were considered. As shown in Fig. 6.12 (C), the maximum removal of phenol was observed in the case of *Lysinibacillus sp.*, at a 5 mg/L concentration. The removal was 74.09%. The least removal was observed also in the case of *Lysinibacillus sp.,* at the concentration of 10 mg/L. The value of pollutant removal found in this study was 23.59%. At higher concentrations, the pollutants lead to toxicity and reduce the removal (Sharma and Indu, 2020).

6.3.12.4. Effect of temperature: Temperature is an important physiological parameter to influences the removal process of a pollutant, as this parameter has an important effect on microbial growth. In most cases, higher temperatures enhance the removal of pollutants, but at extreme temperatures, the growth of microbes is reduced (Iqbal et al., 2007). It was observed that for every microbe, there is an optimum temperature, and at that temperature, the microbial activity is the maximum (Sanscartier et al., 2011). Topp et al. (1997) reported that most of the microbes show optimum temperature at a range of 298 K- 313 K. Fig. 6.12 (D) represents the effect of temperature on the removal of acenaphthene by microorganisms. For this study, a total of three temperatures, viz., 298 K, 303 K, and 313 K were considered respectively. The highest removal was found in the case of *Lysinibacillus sp.*, at 303 K temperature with the value of 84.11% removal. For the same bacteria, the removal at 298 K was 45.65%.

6.3.12.5. Effect of pH: pH is an important parameter of the bioremediation process. pH affects the process in various ways, viz., the chemistry of pollutants, the coexisting ions of the solution, and the ionic balance of microorganisms. pH also affects the adsorption

mechanism and degree of ionisation. The effect of pH on the bioremediation of phenol is shown in Fig. 6.12 (E). For this study, six different pH values, viz., 2,4,6,7,8, and 10, were considered respectively. From the figure, it can be stated that for each bacterium, the maximum removal was observed at pH 7. The highest removal of naphthalene was found to be 69.21% in the case of *Bacillus sp.* This observation can be explained by the enzymatic activity of bacteria. At extreme pH, denaturation of bacterial enzymes can occur, significantly decreasing the removal efficiency (Megharaj et al., 2011).

6.3.12.6. Effect of salinity: The effect of salinity on the bacterial removal is presented in Fig. 6.12 (F). As observed from the figure, with the increasing salinity, the removal of the pollutant decreased significantly. The highest removal was found in the case of *Lysinibacillus sp.,* with the value of 74.18%. Zhang et al. (2014) reported that with the increasing salinity, osmotic stress also increased, disrupting cells. Ion toxicity and metabolic disruption are also responsible for the inhibition of bacterial growth (Rath et al., 2018).

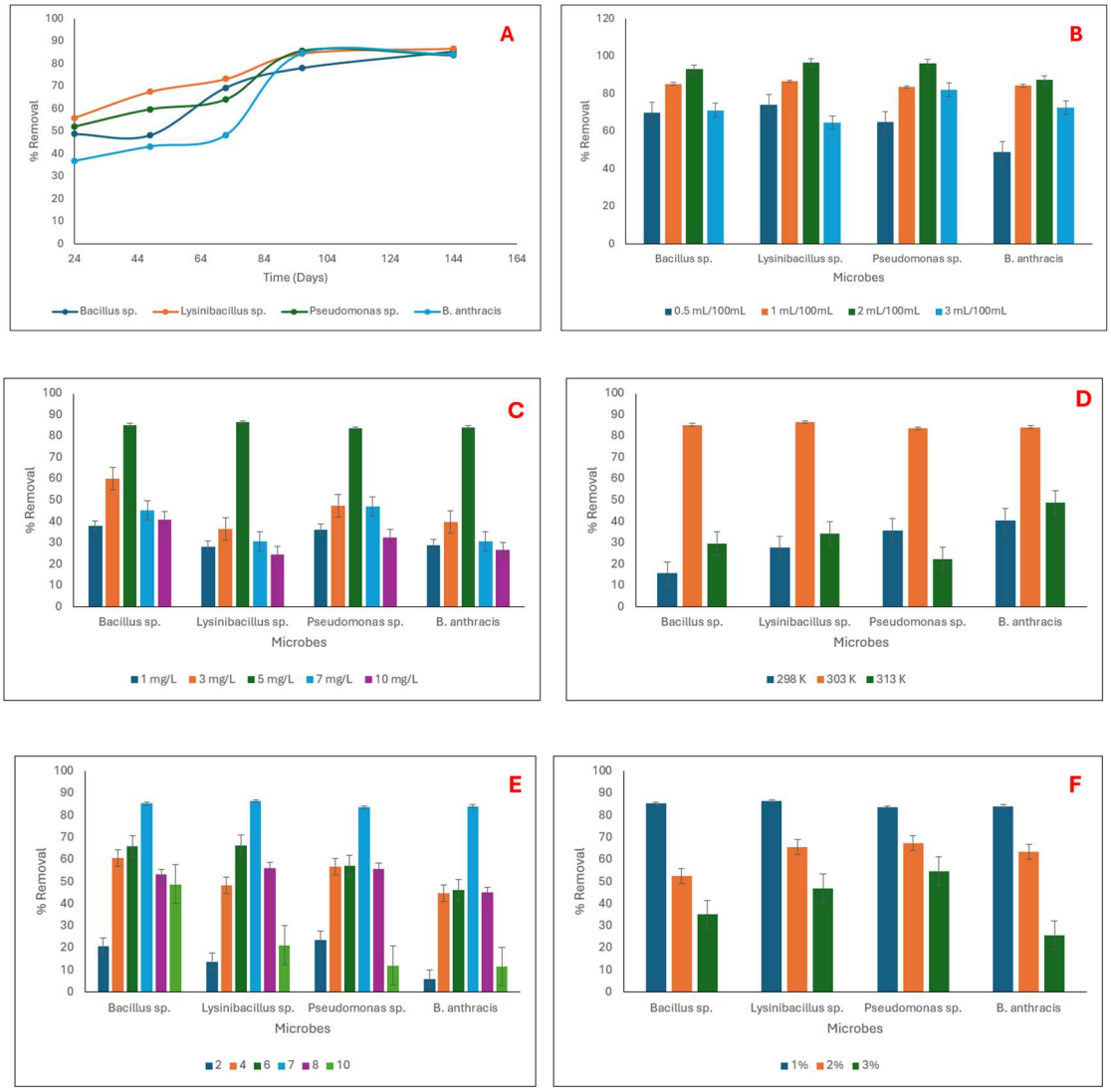

Figure 6.12: Effect of (A) treatment time, (B) microbial dose, (C) pollutant concentration, (D) temperature, (E) pH, and (F) salinity on bioremediation of acenaphthene by bacteria

6.3.12.7. Analysis of acenaphthene bioremediation by the Monod model: Table 6.5 shows the results of naphthalene bioremediation analysis by the Monod model. From the data, it was observed that *Lysinibacillus sp.* has the best substrate affinity among all the aerogels, and *B. anthracis* shows the fastest growth rate in naphthalene solution. This result signifies that the application of *Lysinibacillus sp.* is optimal at lower concentrations of naphthalene. Similar results were reported in previous studies (Oberoi et al., 2015; Mahapatra and Phale, 2021). Also, *B. anthracis* is found to excel in high-pollution scenarios.

Table 6.5: The Monod modelling of acenaphthene removal by bacteria

Pollutant	**Bacteria**	**μ_{max}**	**K_s**

Acenaphthene	*Bacillus sp.*	0.003251	3.28
	Lysinibacillus sp.	0.00274	6.53
	Pseudomonas sp.	0.003554	5.14
	B. anthracis	0.005219	6.25

6.3.13. Removal of pollutants by Bacteria-doped aerogel: From the previous bioremediation studies, three bacteria, viz., *Bacillus sp., Pseudomonas sp.,* and *B. anthracis,* were selected to be doped in the aerogel network. Using the bacteria-doped aerogel for pollutant removal results in two processes, viz., adsorption and bioremediation simultaneously. As shown in Fig. 6.13, in the initial stage of the removal, due to the high availability of surface area, a rapid uptake of pollutants occurs. this high concentration of pollutants stimulates the bacteria to grow and provide more nutrients. As the growth occurred, bioremediation took place to permanently degrade the pollutants, making this process sustainable and fast.

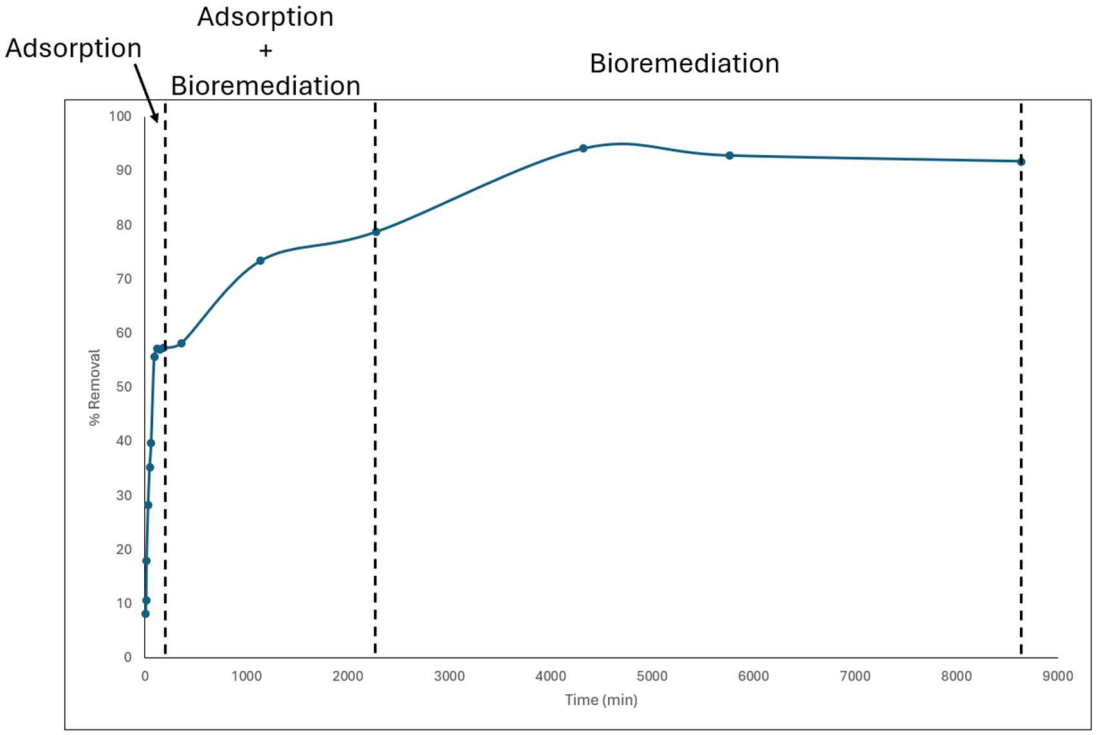

Figure 6.13: Mechanisms of pollutant removal by bacteria-doped aerogel

6.3.13.1. Removal of naphthalene: The removal of naphthalene by the bacteria-doped aerogel was investigated by a batch study; the parameters were varied to investigate their effect on the removal process.

6.3.13.1.1. Effect of treatment time: The effect of treatment time on pollutant removal is presented in Fig. 6.14. Fig. 6.14 (A), (B), (C), (D), (E), and (F) show the pollutant removal by bacteria doped PVA, PVA-RHBC, PVA-RHC, PVA-SDBC, PVA-SDC, and PVA-Si, respectively. From the result, it can be stated that PVA-Si-*Bacillus sp.* showed the highest removal with the value of 97.39% after five days of treatment. For the figure, it was observed that the equilibrium was achieved after 35 hr. of treatment. A previous study showed that for PVA-Si aerogel, the naphthalene removal reached up to 70.5% (Ghosh et al., 2024). This observation can be explained by considering the available surface area on the adsorbent surface and the interaction time of the adsorbent with adsorbate molecules. Before achieving the adsorption equilibrium, a large surface area and many pores on the adsorbent surface were available that contributed to the significant removal of the contaminant. But after a certain time, the active sites on the aerogel surface eventually got saturated, which ceased the rapid increase of the removal% (Gao et al., 2019). Another study showed that pollutant removal by bacteria reached up to 94% (Mahapatra and Phale, 2021). This observation can be explained by considering the metabolism of bacteria and the interaction time of the bacteria with pollutant molecules (Abd El-Rahim et al., 2009). Before achieving the equilibrium, a growth in bacterial culture was observed, which contributed to the significant removal of the contaminant.

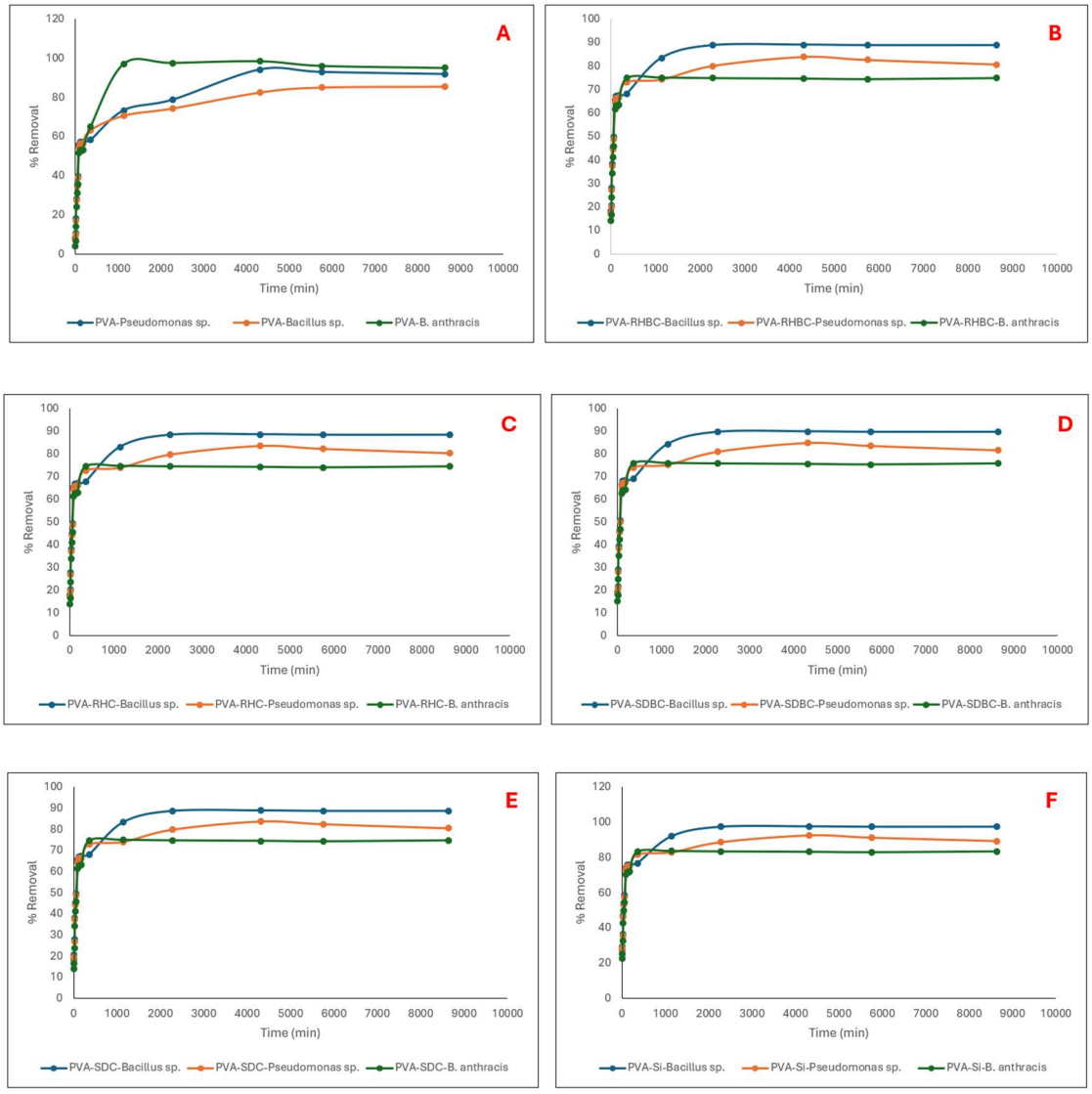

Figure 6.14: Effect of treatment time on naphthalene removal by bacteria doped (A) PVA, (B) PVA-RHBC, (C) PVA-RHC, (D) PVA-SDBC, (E) PVA-SDC, and (F) PVA-Si aerogel

6.3.13.1.2. Effect of adsorbent dose: As presented in Fig. 6.15, the adsorbent dose has a significant effect on the pollutant removal by bacteria-doped aerogel. Fig. 6.15 (A), (B), (C), (D), (E), and (F) show the pollutant removal by bacteria doped PVA, PVA-RHBC, PVA-RHC, PVA-SDBC, PVA-SDC, and PVA-Si, respectively. From the experimental data it was shown that PVA-Si-*Bacillus sp.* showed the highest removal with the value of 97.39% after five days of treatment with 1 g/L dosage. With the increase of dose, initially the the removal increased and then slightly decreased, signifying the dominance of bioremediation over adsorption phenomena in this process. This observation can be explained as the higher microbial dosage provides more microbial mass and metabolic activity, which results in higher removal (Santini et al., 2016); however, after a certain point, the increasing dose causes resource scarcity and an increase in concentration.

Therefore, an opposite effect also occurred in the removal of the pollutant (Liu et al., 1993).

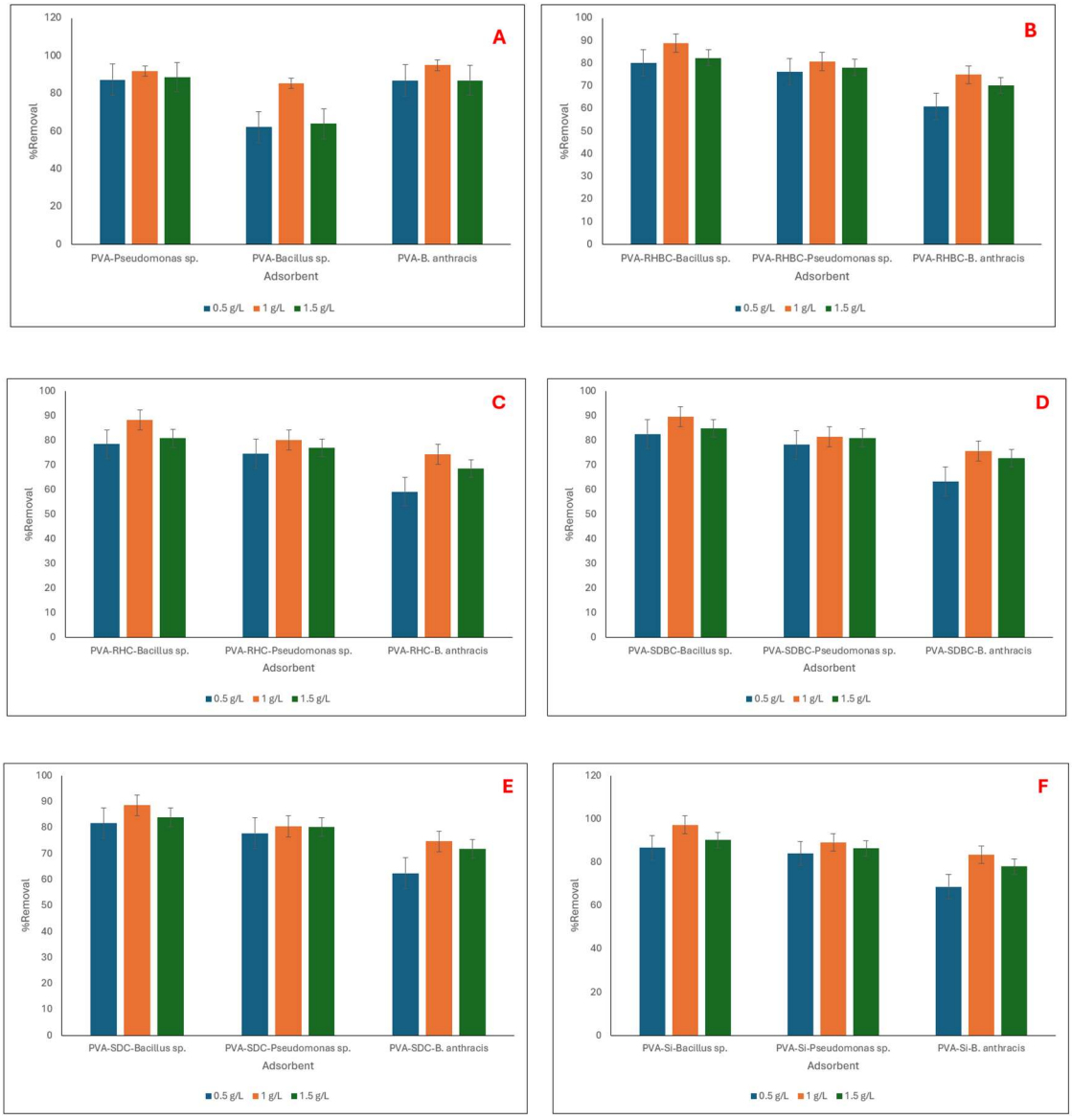

Figure 6.15: Effect of adsorbent dose on naphthalene removal by bacteria doped (A) PVA, (B) PVA-RHBC, (C) PVA-RHC, (D) PVA-SDBC, (E) PVA-SDC, and (F) PVA-Si aerogel

6.3.13.1.3. Effect of pollutant concentration: In Fig. 6.16, the effect of pollutant concentration on the pollutant removal is shown. Fig. 6.16 (A), (B), (C), (D), (E), and (F) show the pollutant removal by bacteria doped PVA, PVA-RHBC, PVA-RHC, PVA-SDBC, PVA-SDC, and PVA-Si, respectively. As shown in the figure, with the increase of pollutant concentration, the removal percentage also increased. The highest removal was observed in the case of PVA-*B. anthracis* aerogel at a 10 mg/L dosage. The removal was 96.55%. This observation can be explained by the saturation of adsorption sites on the adsorbent surface. At low pollutant concentration, the active site and contaminant

molecule's ratio is larger, allowing the molecules to rapidly interact with the active site and to be removed from the solution. As the concentration increased, the trend slowed down due to the increased competition (de Farias Silva and da Gama, 2020). However, unlike bioremediation, in this process, higher concentrations did not affect the process adversely. The probable cause of that can be explained as, though the aerogels increased the concentration of pollutants in some zones of the solution by adsorption, the microorganisms were not forced to consume all the pollutants due to the associated desorption process. This adsorption-desorption cycle maintained a balanced concentration and prevented the inhibition of microbial growth.

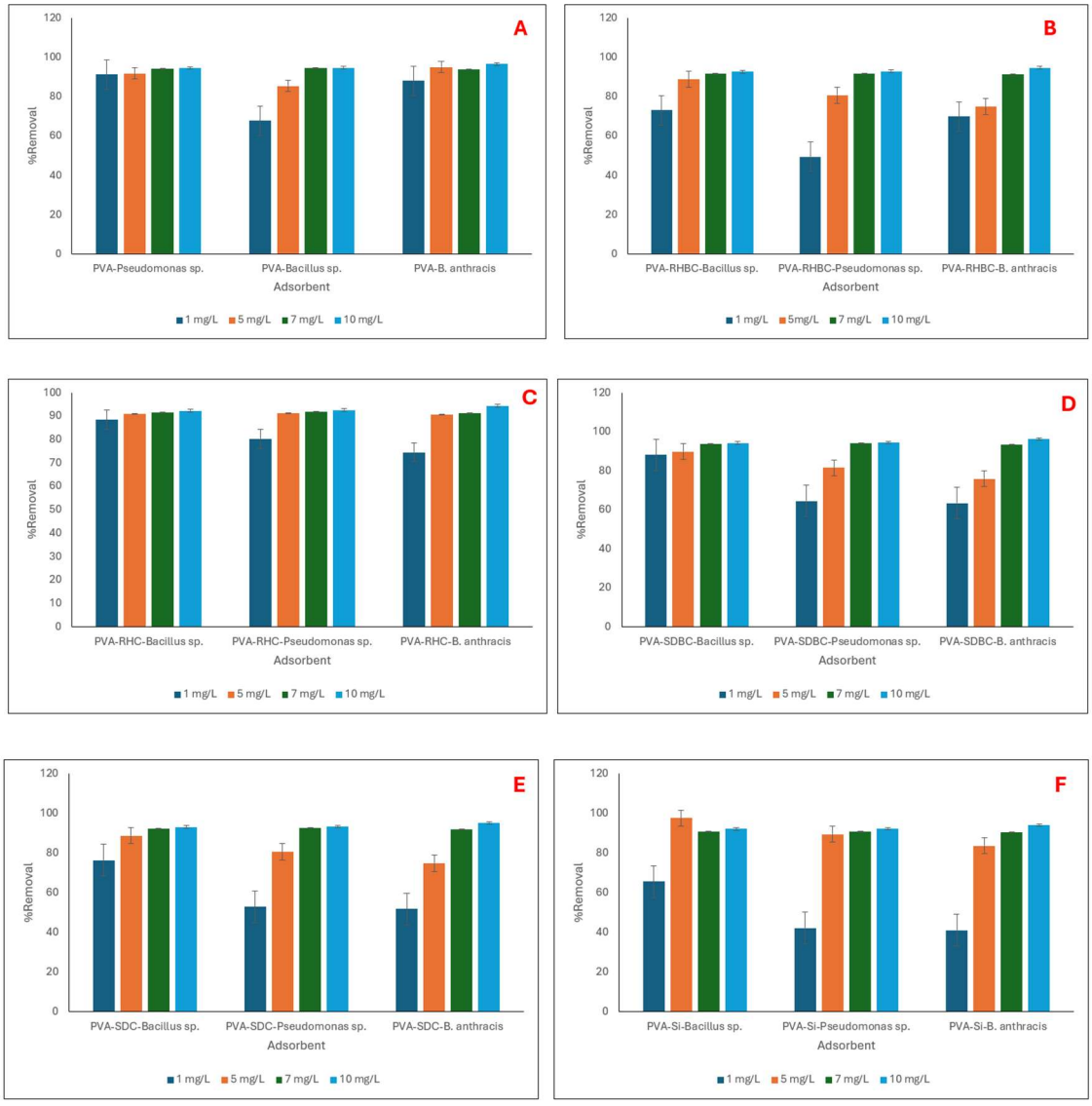

Figure 6.16: Effect of pollutant concentration on naphthalene removal by bacteria doped (A) PVA, (B) PVA-RHBC, (C) PVA-RHC, (D) PVA-SDBC, (E) PVA-SDC, and (F) PVA-Si aerogel

6.3.13.1.4. Effect of temperature: The effect of temperature on the pollutant removal by bacteria-doped aerogel is presented in Fig. 6.17. Fig. 6.17 (A), (B), (C), (D), (E), and (F)

show the pollutant removal by bacteria doped PVA, PVA-RHBC, PVA-RHC, PVA-SDBC, PVA-SDC, and PVA-Si, respectively. From the figure, it was shown that the optimal removal for all the adsorbents was found at 303 K temperature, signifying the dominance of microbial bioremediation over the adsorption process. In this experiment, the highest removal was found in the case of PVA-Si-*Bacillus sp.* aerogel at 303 K temperature with the value of 97.39%. This trend can be explained as temperature is an important factor in bioremediation. In most cases, higher temperatures enhance the removal of pollutants, but at extreme temperatures, the growth of microbes is reduced (Iqbal et al., 2007). It was observed that for every microbe, there is an optimum temperature, and at that temperature, the microbial activity is the maximum (Sanscartier et al., 2011). Topp et al. (1997) reported that most of the microbes show optimum temperature at a range of 298 K- 303 K.

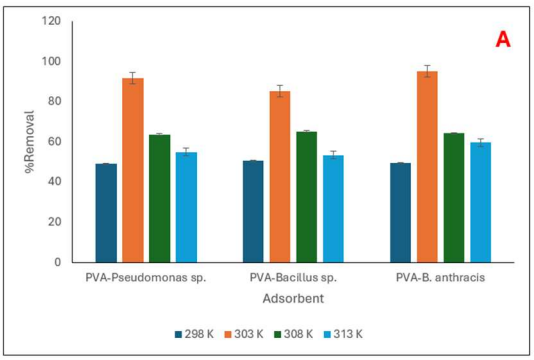

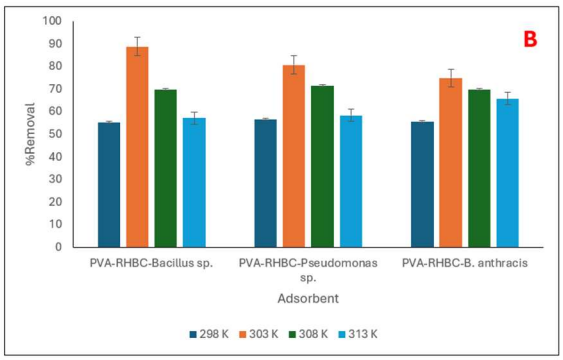

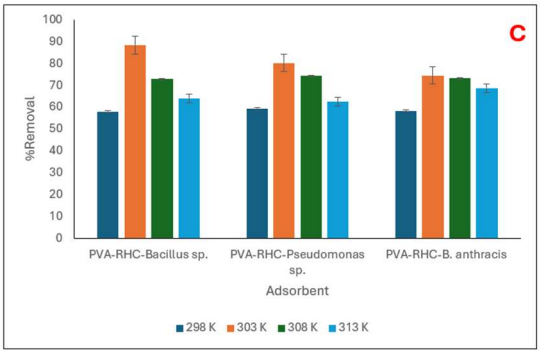

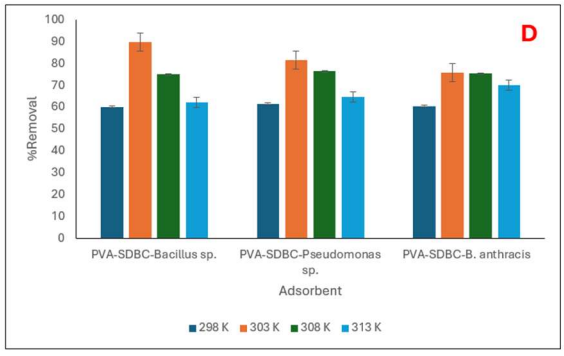

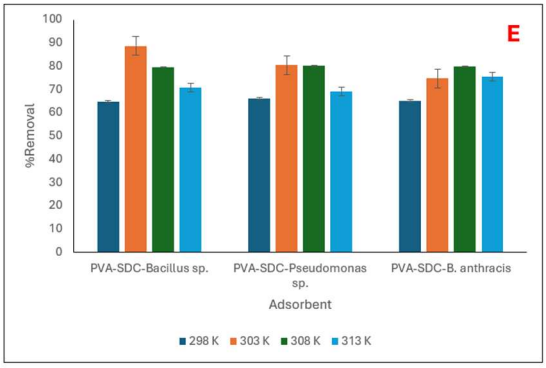

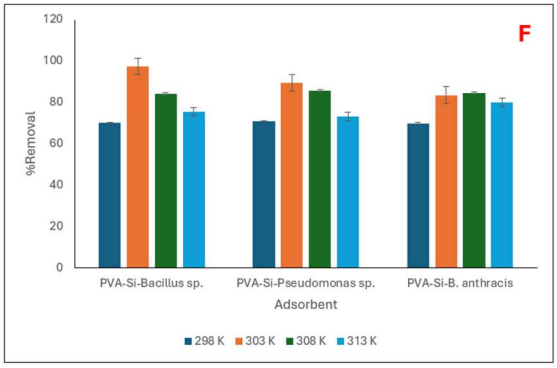

Figure 6.17: Effect of temperature on naphthalene removal by bacteria doped (A) PVA, (B) PVA-RHBC, (C) PVA-RHC, (D) PVA-SDBC, (E) PVA-SDC, and (F) PVA-Si aerogel

6.3.13.1.5. Effect of pH: The effect of pH on the removal process also shows a similar trend to bioremediation. Fig. 6.18 represents the effect of pH on the removal process. 6.18 (A), (B), (C), (D), (E), and (F) show the pollutant removal by bacteria doped PVA, PVA-RHBC, PVA-RHC, PVA-SDBC, PVA-SDC, and PVA-Si, respectively. PVA-Si-*Bacillus sp.* has shown the highest removal among all the adsorbents and pH, with the value of 97.85% at pH 7. This observation can be explained by considering the effect of pH on microbial cells. pH affects the process in various ways, viz., the chemistry of pollutants, the coexisting ions of the solution, and the ionic balance of microorganisms. pH also affects the adsorption mechanism and degree of ionisation.

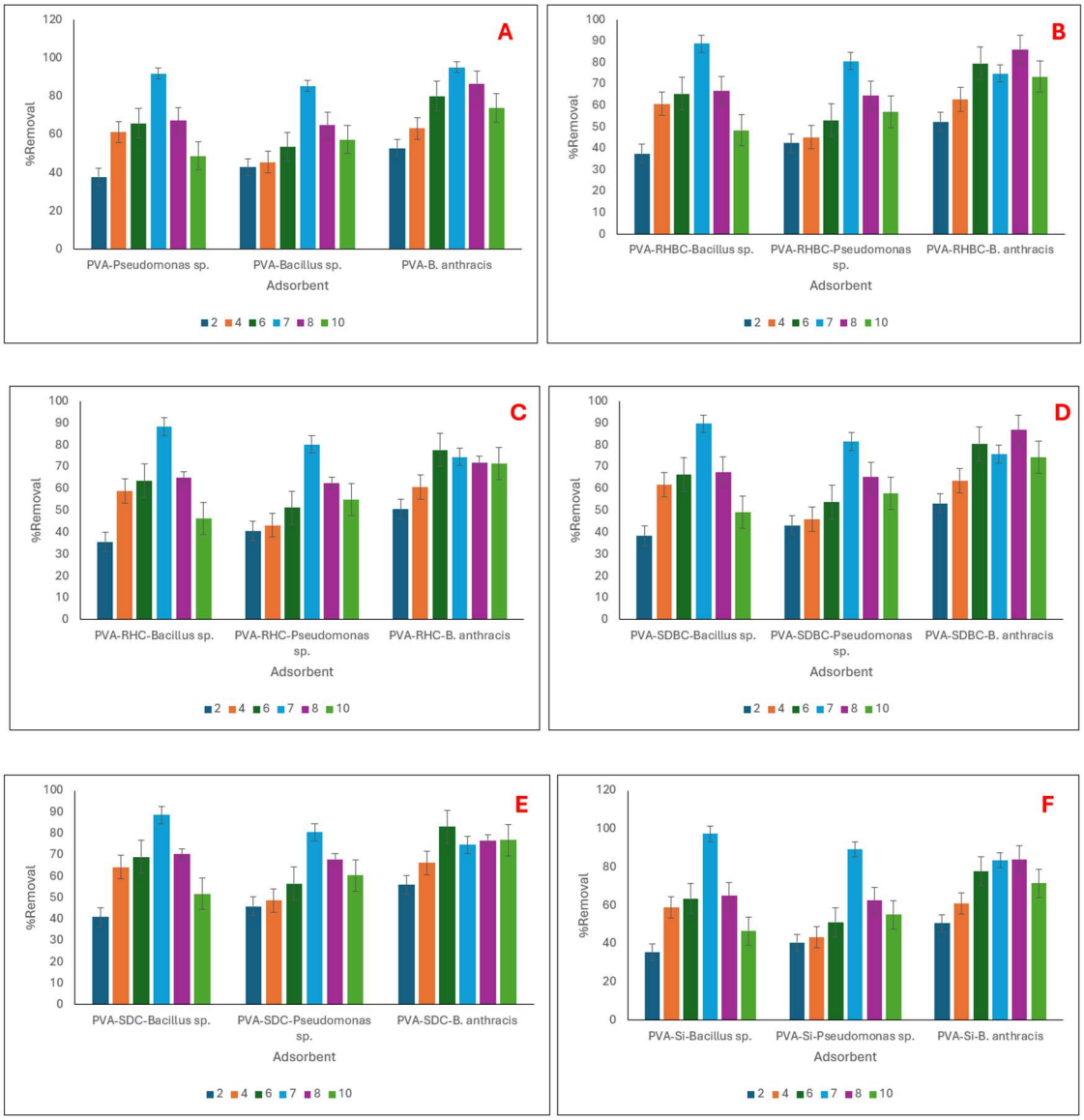

Figure 6.18: Effect of pH on naphthalene removal by bacteria doped (A) PVA, (B) PVA-RHBC, (C) PVA-RHC, (D) PVA-SDBC, (E) PVA-SDC, and (F) PVA-Si aerogel

6.3.13.1.6. Optimisation of removal: To optimise the naphthalene adsorption process, a Response Surface Methodology (RSM) study was performed (Aydar, 2018). A quadratic equation, presented as equation (6.3), was used to analyse and validate the experimental design. From the batch adsorption study, PVA-Si-*Bacillus sp.* was selected as the most suitable adsorbent for the process, and the RSM study was conducted with that adsorbent only.

$$R = 84.29 + 37.94 * A + 2.27 * B - 2.69 * C - 1.46 * AB + 1.43 * AC + 0.10 * BC - 24.69 * A^2 - 5.66 * B^2 - 3.37 * C^2 \quad \text{(6.3)}$$

Here, A, B, C, and R are reaction time (min), adsorbent dose (g/L), pollutant concentration (mg/L), and removal%, respectively.

6.3.13.1.6.1. Validation of the model: From the ANOVA analysis, it was observed that this model is significant with a P-value of 0.0001 (<0.05) and an F-value of 154.40 (>12). The correlation coefficient (R^2) value of the mentioned model was 0.99. The R^2 value also indicates that the predicted and observed data of this experiment are in reasonable agreement, indicating the significance of the model. Fig. 6.19 (A) shows the distribution of predicted and experimental values satisfying the validity of this model.

6.3.13.1.6.2. Response of time and adsorbent dosage: The response of time and adsorbent dosage is presented in Fig. 6.19 (B). The graph shows that the optimum removal% was observed at 1 g/ /L adsorbent dosage after 35 hr. of adsorption. The maximum pollutant removal under these conditions was found to be 97.42%.

6.3.13.1.6.3. Response of adsorbent dosage and pollutant concentration: In Fig. 6.19 (C), the response of adsorbent dosage and pollutant concentration is presented. From the figure, it can be stated that at the adsorbent dose of 1 g/L and 5 mg/L pollutant concentration, the optimum removal was achieved. The optimum removal in these conditions was 92.26%.

6.3.13.1.6.4. Response of pollutant concentration and time: The crosstalk between pollutant concentration and treatment time is represented in Fig. 6.19 (D). From the figure, it was observed that at a treatment time of 35 hr. and a 5 mg/L pollutant concentration, the highest removal was achieved. The optimum removal in this experiment was 98.2%.

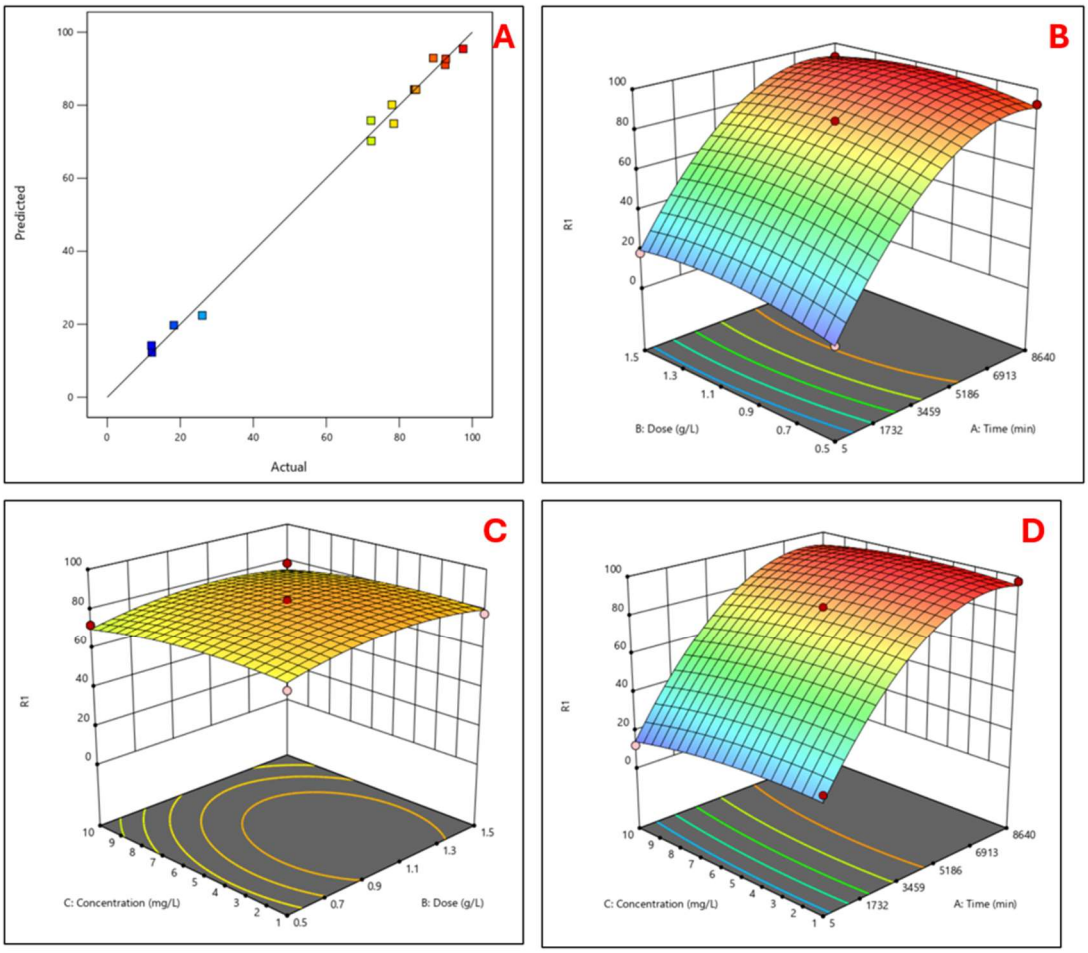

Figure 6.19: Optimisation of naphthalene removal by PVA-Si-*Bacillus sp.* aerogel using Response Surface Methodology, representing (A) comparison of actual and predicted results, (B) response of time and aerogel dose, (C) response of aerogel dose and pollutant concentration, (D) response of time and pollutant concentration.

6.3.13.1.7. GC-MS analysis of pollutant solution after treatment: Fig. 6.20 shows the result of GC-MS analysis of pollutant solution after treatment. Being the most effective adsorbent, PVA-Si-*Bacillus* was used to treat the solution for GC-MS analysis. As shown in the figure, major peaks at 4.37 min., 4.58 min., 6.07 min., 8.62 min., and 11.25 min. are detected respectively. The peaks were identified using the MS library and are presented in Table 6.6.

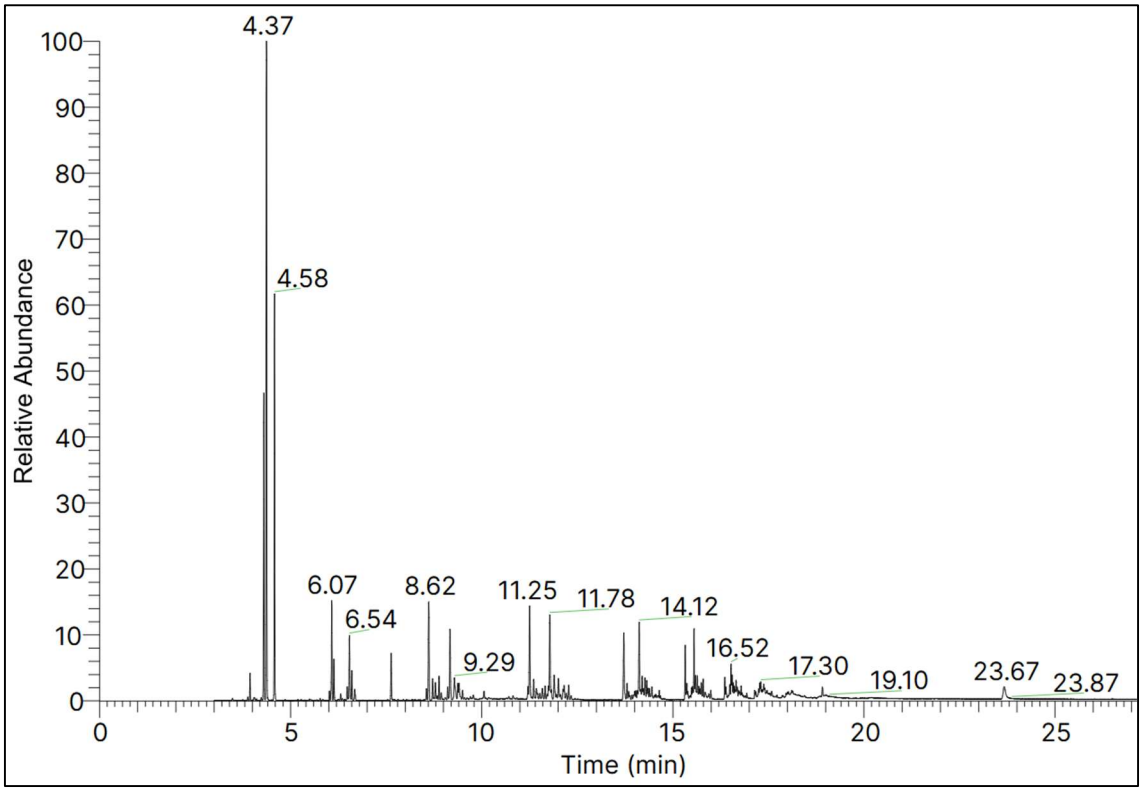

Figure 6.20: GC-MS analysis of naphthalene solution after treatment with PVA-Si-*Bacillus sp.* aerogel

Table 6.6: GC-MS analysis of naphthalene by PVA-Si-*Bacillus sp.* aerogel

Peak retention time (min.)	**Compound**
4.37	1,3-dimethyl benzene
4.58	O-Xylene
6.07	Dodecane
8.62	3,3-dimethyl-hexane
11.25	Decyl 2-ethylhexyl ester

6.3.13.2. Removal of phenol: The removal of phenol by the bacteria-doped aerogel was investigated by a batch study; the parameters were varied to investigate their effect on the removal process.

6.3.13.2.1. Effect of treatment time: The effect of treatment time on pollutant removal is presented in Fig. 6.21. Fig. 6.21 (A), (B), (C), (D), (E), and (F) show the pollutant removal by bacteria doped PVA, PVA-RHBC, PVA-RHC, PVA-SDBC, PVA-SDC, and PVA-Si, respectively. From the result, it can be stated that PVA-Si-*Bacillus sp.* showed the highest removal with the value of 97.29% after five days of treatment. For the figure,

it was observed that the equilibrium was achieved after 35 hr. of treatment. A previous study showed that for PVA-Si aerogel, the naphthalene removal reached up to 70.5% (Ghosh et al., 2024). This observation can be explained by considering the available surface area on the adsorbent surface and the interaction time of the adsorbent with adsorbate molecules. Before achieving the adsorption equilibrium, a large surface area and many pores on the adsorbent surface were available that contributed to the significant removal of the contaminant. But after a certain time, the active sites on the aerogel surface eventually got saturated, which ceased the rapid increase of the removal% (Gao et al., 2019). Another study showed that pollutant removal by bacteria reached up to 94% (Mahapatra and Phale, 2021). This observation can be explained by considering the metabolism of bacteria and the interaction time of the bacteria with pollutant molecules (Abd El-Rahim et al., 2009). Before achieving the equilibrium, a growth in bacterial culture was observed, which contributed to the significant removal of the contaminant.

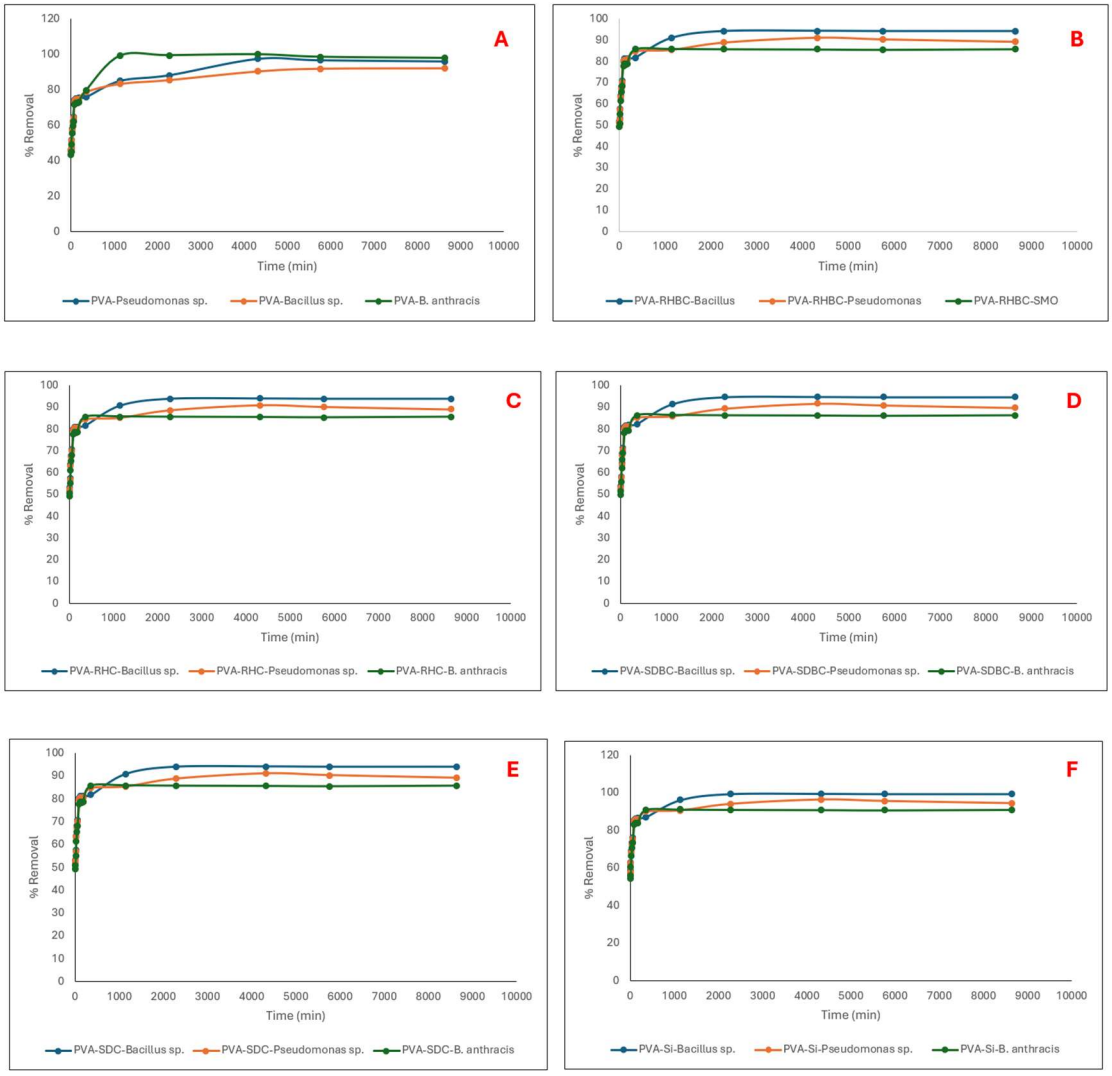

Figure 6.21: Effect of treatment time on phenol removal by bacteria doped (A) PVA, (B) PVA-RHBC, (C) PVA-RHC, (D) PVA-SDBC, (E) PVA-SDC, and (F) PVA-Si aerogel

6.3.13.2.2. Effect of adsorbent dose: As presented in Fig. 6.22, the adsorbent dose has a significant effect on the pollutant removal by bacteria-doped aerogel. Fig. 6.22 (A), (B), (C), (D), (E), and (F) show the pollutant removal by bacteria doped PVA, PVA-RHBC, PVA-RHC, PVA-SDBC, PVA-SDC, and PVA-Si, respectively. From the experimental data, it was shown that PVA-Si-*Bacillus sp.* showed the highest removal with the value of 96.39% after five days of treatment with a 1 g/L dosage. With the increase of dose, initially the removal increased and then slightly decreased, signifying the dominance of bioremediation over adsorption phenomena in this process. This observation can be explained as the higher microbial dosage provides more microbial mass and metabolic activity, which results in higher removal (Santini et al., 2016); however, after a certain point, the increasing dose causes resource scarcity and an increase in concentration. Therefore, an opposite effect also occurred in the removal of the pollutant (Liu et al., 1993).

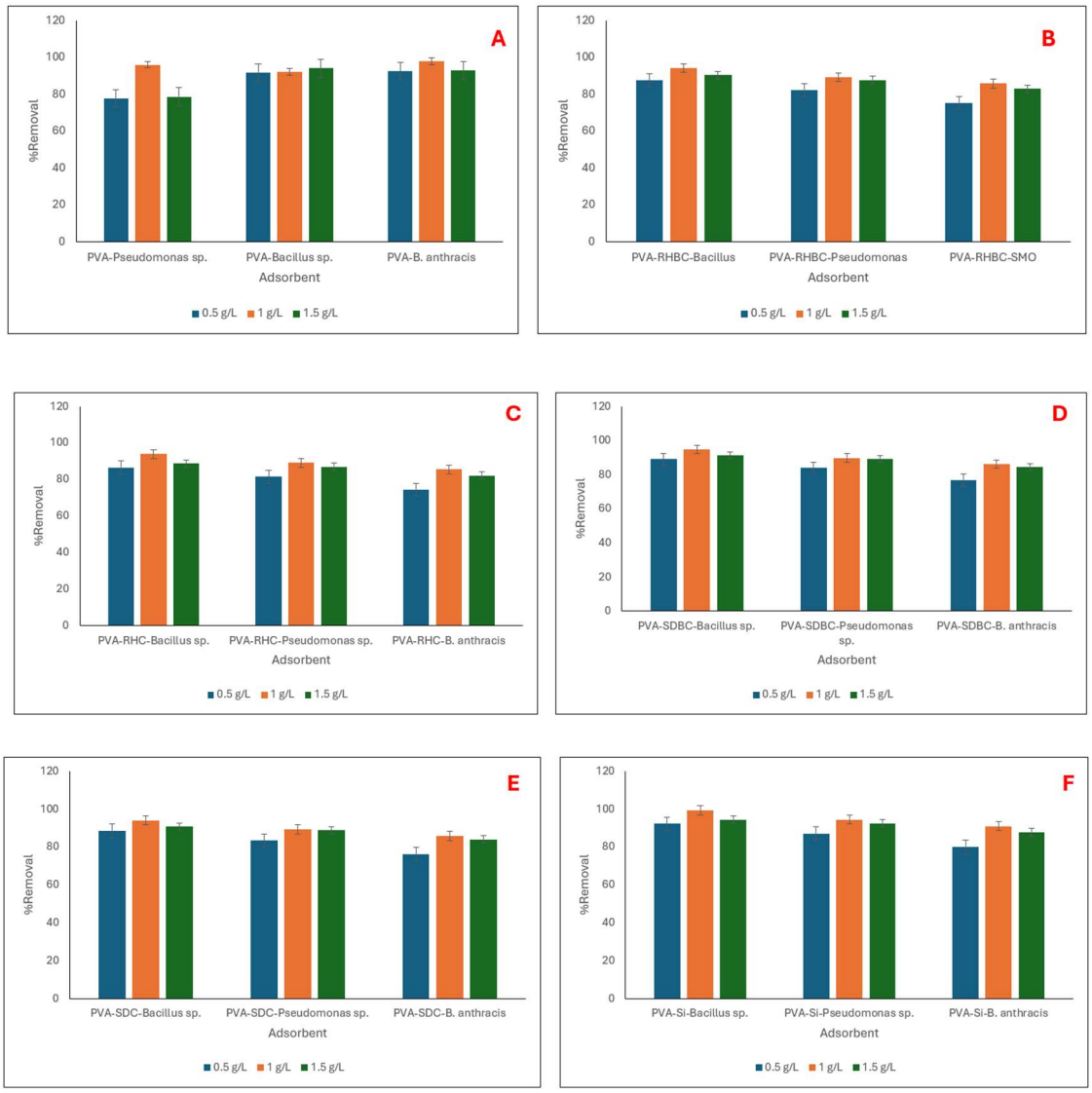

Figure 6.22: Effect of adsorbent dosage on phenol removal by bacteria doped (A) PVA, (B) PVA-RHBC, (C) PVA-RHC, (D) PVA-SDBC, (E) PVA-SDC, and (F) PVA-Si aerogel

6.3.13.2.3. Effect of pollutant concentration: In Fig. 6.23, the effect of pollutant concentration on the pollutant removal is shown. Fig. 6.23 (A), (B), (C), (D), (E), and (F) show the pollutant removal by bacteria doped PVA, PVA-RHBC, PVA-RHC, PVA-SDBC, PVA-SDC, and PVA-Si, respectively. As shown in the figure, with the increase of pollutant concentration, the removal percentage also increased. The highest removal was observed in the case of PVA-*B. anthracis* aerogel at a 10 mg/L dosage. The removal was 97.55%. This observation can be explained by the saturation of adsorption sites on the adsorbent surface. At low pollutant concentration, the active site and contaminant molecule's ratio is larger, allowing the molecules to rapidly interact with the active site and to be removed from the solution. As the concentration increased, the trend slowed down due to the increased competition (de Farias Silva and da Gama, 2020). However,

unlike bioremediation, in this process, higher concentrations did not affect the process adversely. The probable cause of that can be explained as, though the aerogels increased the concentration of pollutants in some zones of the solution by adsorption, the microorganisms were not forced to consume all the pollutants due to the associated desorption process. This adsorption-desorption cycle maintained a balanced concentration and prevented the inhibition of microbial growth.

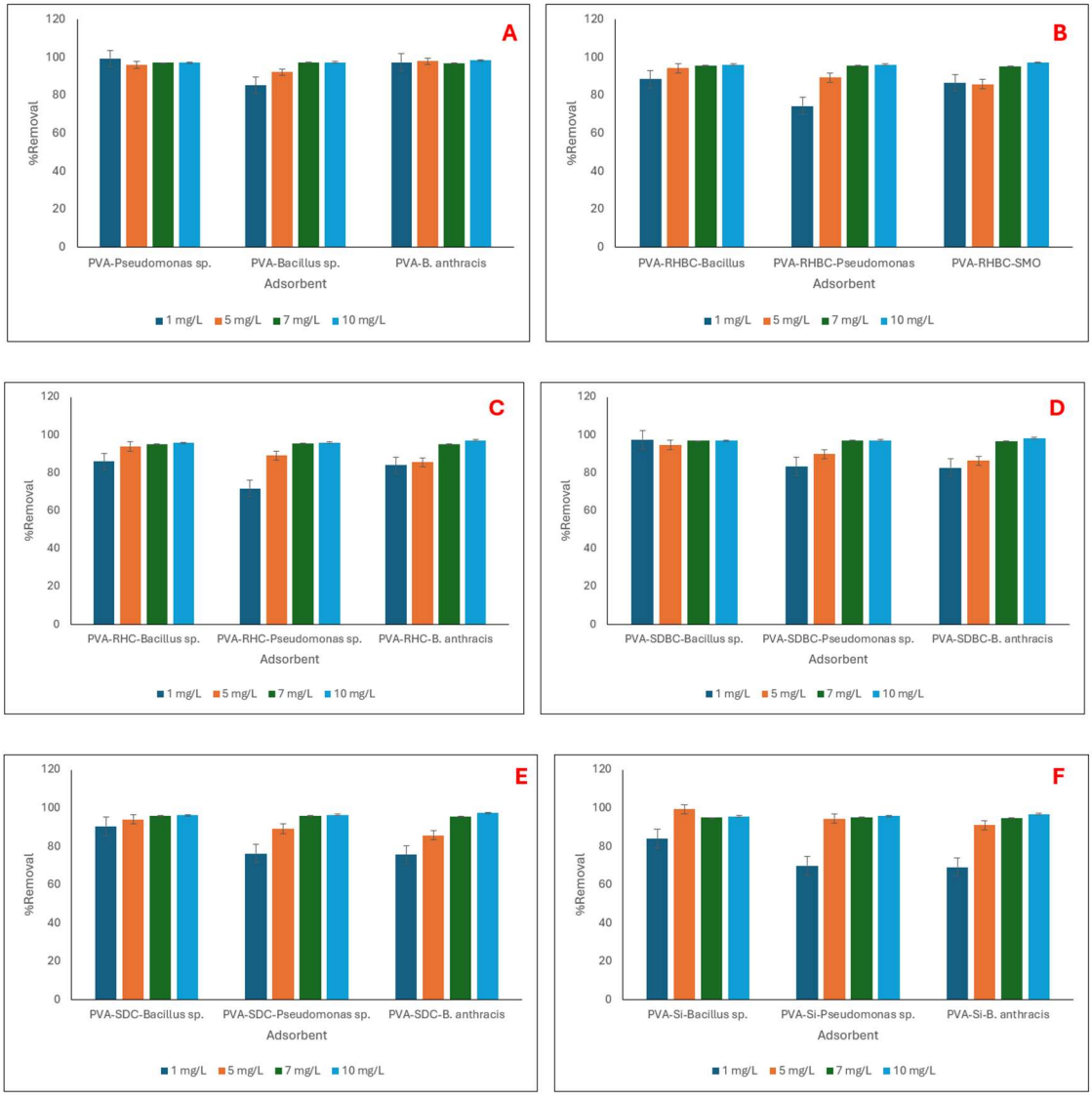

Figure 6.23: Effect of pollutant concentration on phenol removal by bacteria doped (A) PVA, (B) PVA-RHBC, (C) PVA-RHC, (D) PVA-SDBC, (E) PVA-SDC, and (F) PVA-Si aerogel

6.3.13.2.4. Effect of temperature: The effect of temperature on the pollutant removal by bacteria-doped aerogel is presented in Fig. 6.24. Fig. 6.24 (A), (B), (C), (D), (E), and (F) show the pollutant removal by bacteria doped PVA, PVA-RHBC, PVA-RHC, PVA-SDBC, PVA-SDC, and PVA-Si, respectively. From the figure, it was shown that the optimal removal for all the adsorbents was found at 303 K temperature, signifying the

dominance of microbial bioremediation over the adsorption process. In this experiment, the highest removal was found in the case of PVA-Si-*Bacillus sp.* aerogel at 303 K temperature with the value of 97.39%. This trend can be explained as temperature is an important factor in bioremediation. In most cases, higher temperatures enhance the removal of pollutants, but at extreme temperatures, the growth of microbes is reduced (Iqbal et al., 2007). It was observed that for every microbe, there is an optimum temperature, and at that temperature, the microbial activity is the maximum (Sanscartier et al., 2011). Topp et al. (1997) reported that most of the microbes show optimum temperature at a range of 298 K- 313 K.

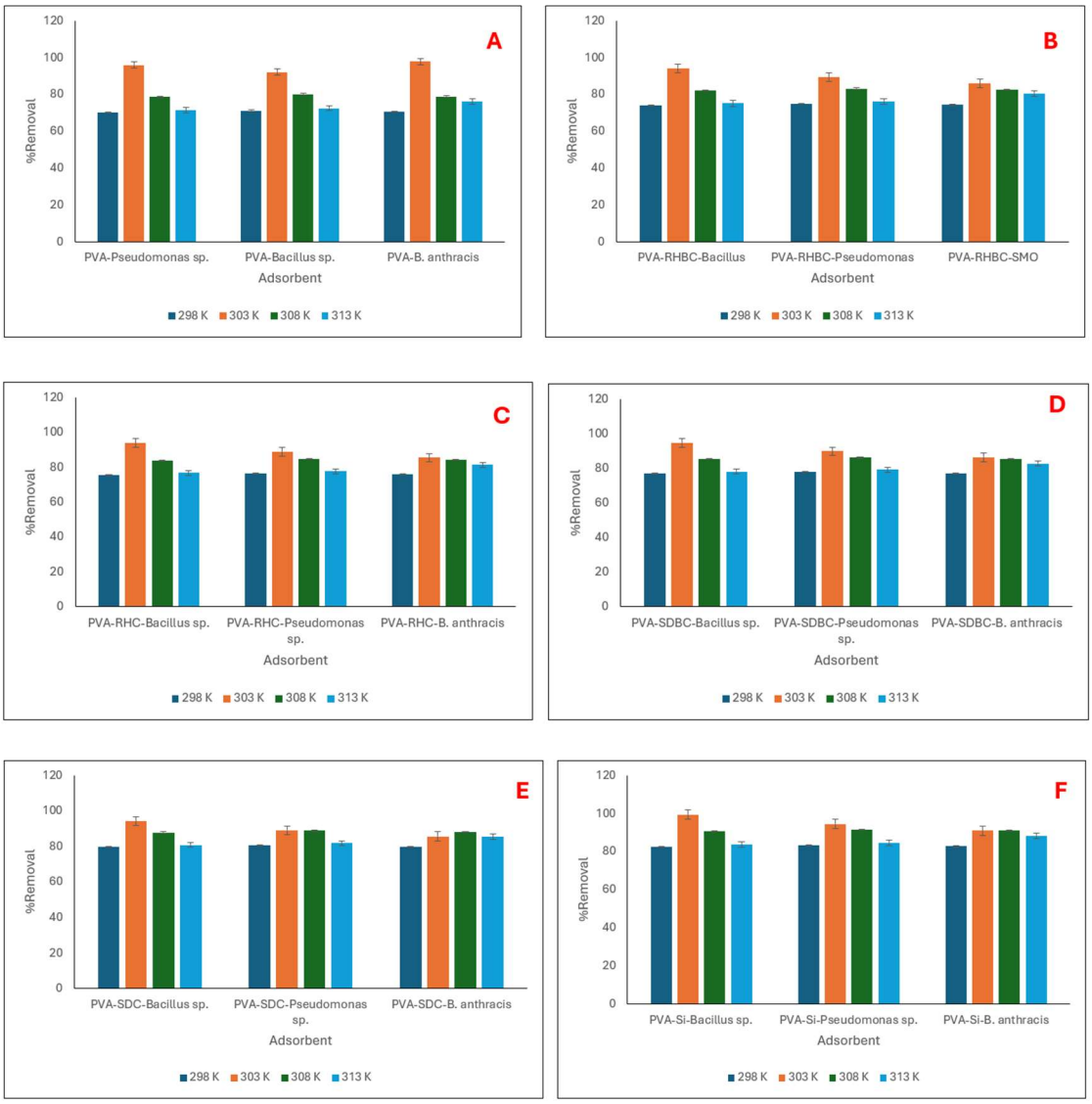

Figure 6.24: Effect of temperature on phenol removal by bacteria doped (A) PVA, (B) PVA-RHBC, (C) PVA-RHC, (D) PVA-SDBC, (E) PVA-SDC, and (F) PVA-Si aerogel

6.3.13.2.5. Effect of pH: The effect of pH on the removal process also shows a similar trend to bioremediation. Fig. 6.25 represents the effect of pH on the removal process. 6.25 (A), (B), (C), (D), (E), and (F) show the pollutant removal by bacteria doped PVA, PVA-RHBC, PVA-RHC, PVA-SDBC, PVA-SDC, and PVA-Si, respectively. PVA-Si-*Bacillus sp.* has shown the highest removal among all the adsorbents and pH, with the value of 97.85% at pH 7. This observation can be explained by considering the effect of pH on microbial cells. pH affects the process in various ways, viz., the chemistry of pollutants, the coexisting ions of the solution, and the ionic balance of microorganisms. pH also affects the adsorption mechanism and degree of ionisation.

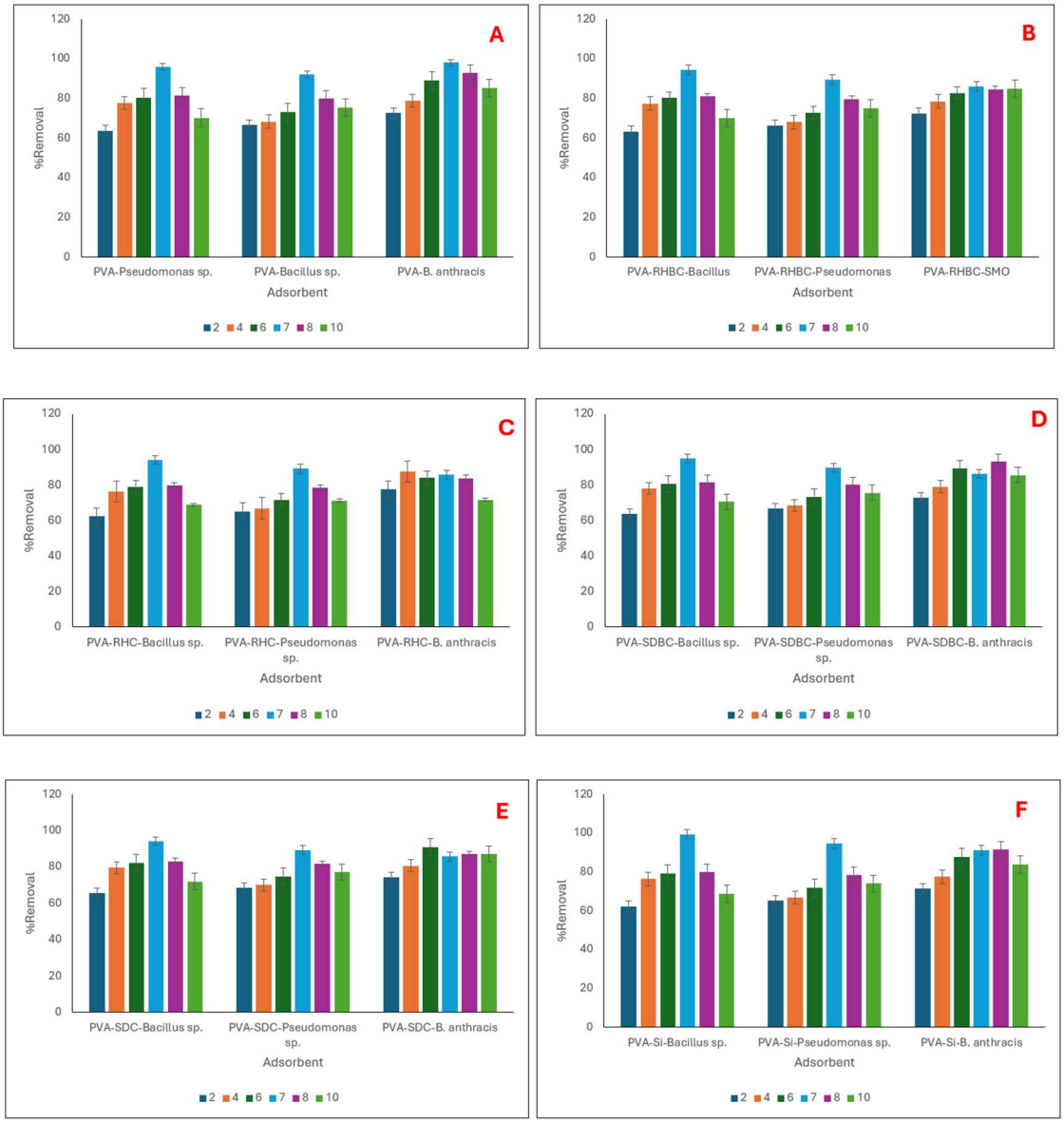

Figure 6.25: Effect of pH on phenol removal by bacteria doped (A) PVA, (B) PVA-RHBC, (C) PVA-RHC, (D) PVA-SDBC, (E) PVA-SDC, and (F) PVA-Si aerogel

6.3.13.2.6. Optimisation of removal: To optimise the phenol adsorption process, a Response Surface Methodology (RSM) study was performed (Aydar, 2018). A quadratic equation, presented as equation (6.4), was used to analyse and validate the experimental design. From the batch adsorption study, PVA-Si-*Bacillus sp.* was selected as the most suitable adsorbent for the process, and the RSM study was conducted with that adsorbent only.

$$R = 74.29 + 41.32 * A + 0.93 * B - 3.81 * C - 2.39 * AB - 2.99 * AC - 2.90 * BC - 28.18 * A^2 + 6.50 * B^2 + 3.32 * C^2 \quad \text{(6.4)}$$

Here, A, B, C, and R are reaction time (min), adsorbent dose (g/L), pollutant concentration (mg/L), and removal%, respectively.

6.3.13.2.6.1. Validation of the model: From the ANOVA analysis, it was observed that this model is significant with a P-value of 0.001 (<0.05) and an F-value of 25.95 (>12). The correlation coefficient (R^2) value of the mentioned model was 0.97. The R^2 value also indicates that the predicted and observed data of this experiment are in reasonable agreement, indicating the significance of the model. Fig. 6.26 (A) shows the distribution of predicted and experimental values satisfying the validity of this model.

6.3.13.2.6.2. Response of time and adsorbent dosage: The response of time and adsorbent dosage is presented in Fig. 6.26 (B). The graph shows that the optimum removal% was observed at 1 g/ /L adsorbent dosage after 35 hr. of adsorption. The maximum pollutant removal under these conditions was found to be 96.42%.

6.3.13.2.6.3. Response of adsorbent dosage and pollutant concentration: In Fig. 6.26 (C), the response of adsorbent dosage and pollutant concentration is presented. From the figure, it can be stated that at the adsorbent dose of 1 g/L and 5 mg/L pollutant concentration, the optimum removal was achieved. The optimum removal in these conditions was 95.26%.

6.3.13.2.6.4. Response of pollutant concentration and time: The crosstalk between pollutant concentration and treatment time is represented in Fig. 6.26 (D). From the figure, it was observed that at a treatment time of 35 hr. and a 5 mg/L pollutant concentration, the highest removal was achieved. The optimum removal in this experiment was 97.82%.

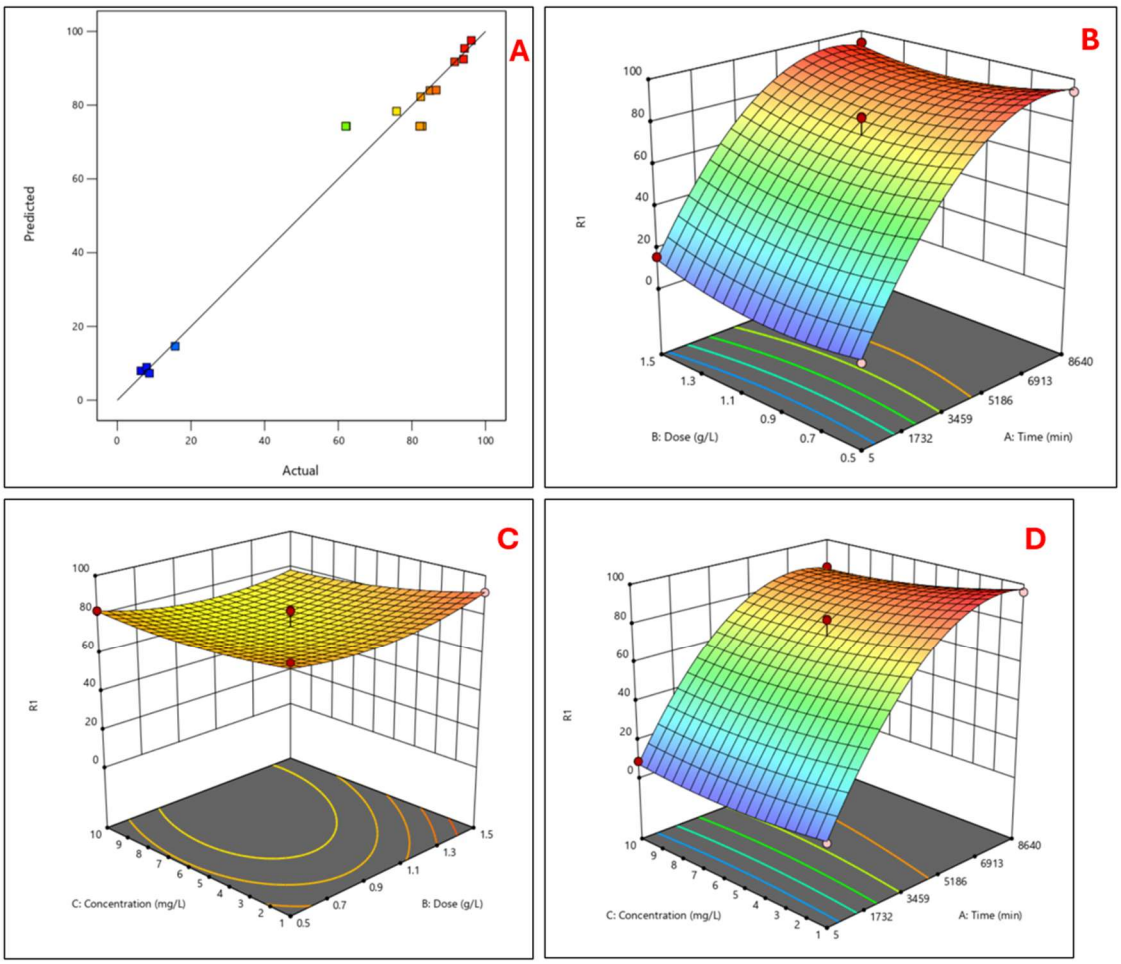

Figure 6.26: Optimisation of phenol removal by PVA-Si-*Bacillus sp.* aerogel using Response Surface Methodology, representing (A) comparison of actual and predicted results, (B) response of time and aerogel dose, (C) response of aerogel dose and pollutant concentration, (D) response of time and pollutant concentration.

6.3.13.2.7. GC-MS analysis of pollutant solution after treatment: Fig. 6.27 shows the result of GC-MS analysis of pollutant solution after treatment. Being the most effective adsorbent, PVA-Si-*Bacillus* was used to treat the solution for GC-MS analysis. As shown in the figure, major peaks at 4.41 min., 4.60 min., 6.09 min., 11.26 min., and 14.12 min. are detected respectively. The peaks were identified using the MS library and are presented in Table 6.7.

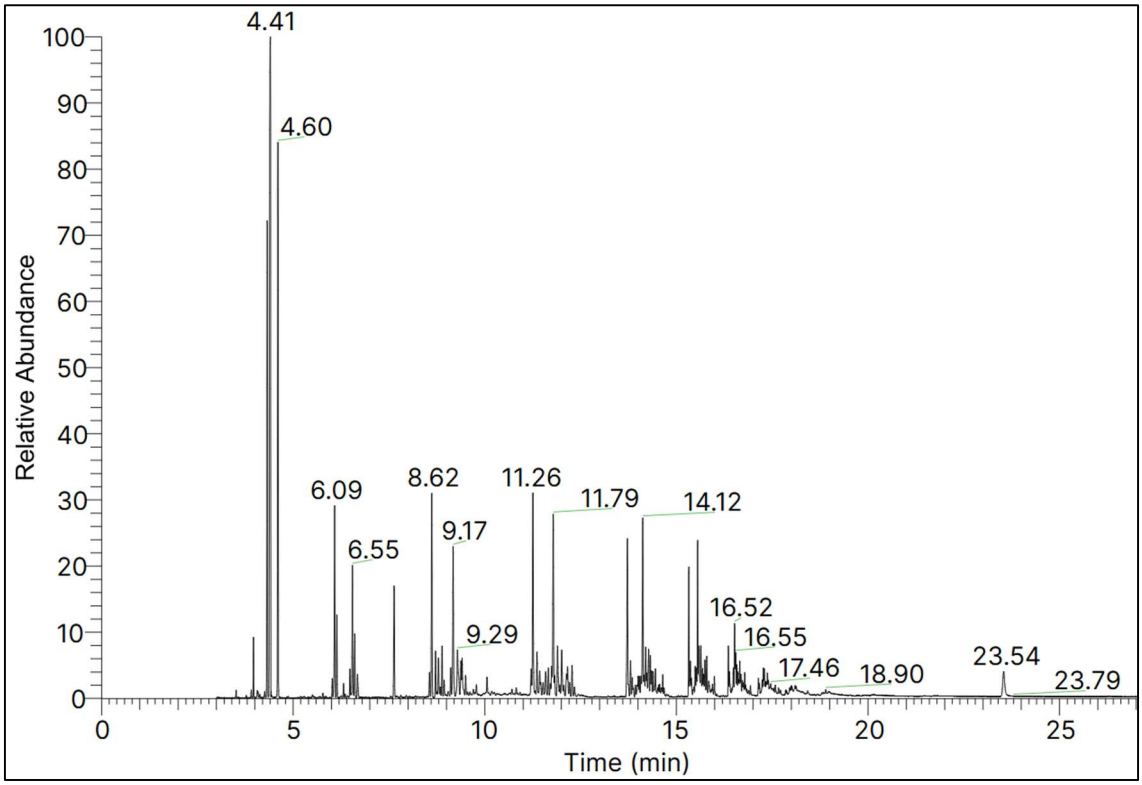

Figure 6.27: GC-MS analysis of phenol solution after treatment with PVA-Si-*Bacillus sp.* aerogel

Table 6.7: GC-MS analysis of phenol by PVA-Si-*Bacillus sp.* aerogel

Peak retention time (min.)	**Compound**
4.41	Ethylbenzene
4.60	2,4-Octadiyne
6.09	3,3-dimethylhexane
11.26	1-iodo-tridecane
14.12	2-methyl-eicosane

6.3.13.3. Removal of acenaphthene: The removal of acenaphthene by the bacteria-doped aerogel was investigated by a batch study; the parameters were varied to investigate their effect on the removal process.

6.3.13.3.1. Effect of treatment time: The effect of treatment time on pollutant removal is presented in Fig. 6.28. Fig. 6.28 (A), (B), (C), (D), (E), and (F) show the pollutant removal by bacteria doped PVA, PVA-RHBC, PVA-RHC, PVA-SDBC, PVA-SDC, and PVA-Si, respectively. From the result, it can be stated that PVA-Si-*Bacillus sp.* showed the highest removal with the value of 93.95% after five days of treatment. From the

figure, it was observed that the equilibrium was achieved after 35 hr. of treatment. A previous study showed that for PVA-Si aerogel, the pollutant removal reached up to 70.5% (Ghosh et al., 2024). This observation can be explained by considering the available surface area on the adsorbent surface and the interaction time of the adsorbent with adsorbate molecules. Before achieving the adsorption equilibrium, a large surface area and many pores on the adsorbent surface were available that contributed to the significant removal of the contaminant. But after a certain time, the active sites on the aerogel surface eventually got saturated, which ceased the rapid increase of the removal% (Gao et al., 2019). Another study showed that pollutant removal by bacteria reached up to 94% (Mahapatra and Phale, 2021). This observation can be explained by considering the metabolism of bacteria and the interaction time of the bacteria with pollutant molecules (Abd El-Rahim et al., 2009). Before achieving the equilibrium, a growth in bacterial culture was observed, which contributed to the significant removal of the contaminant.

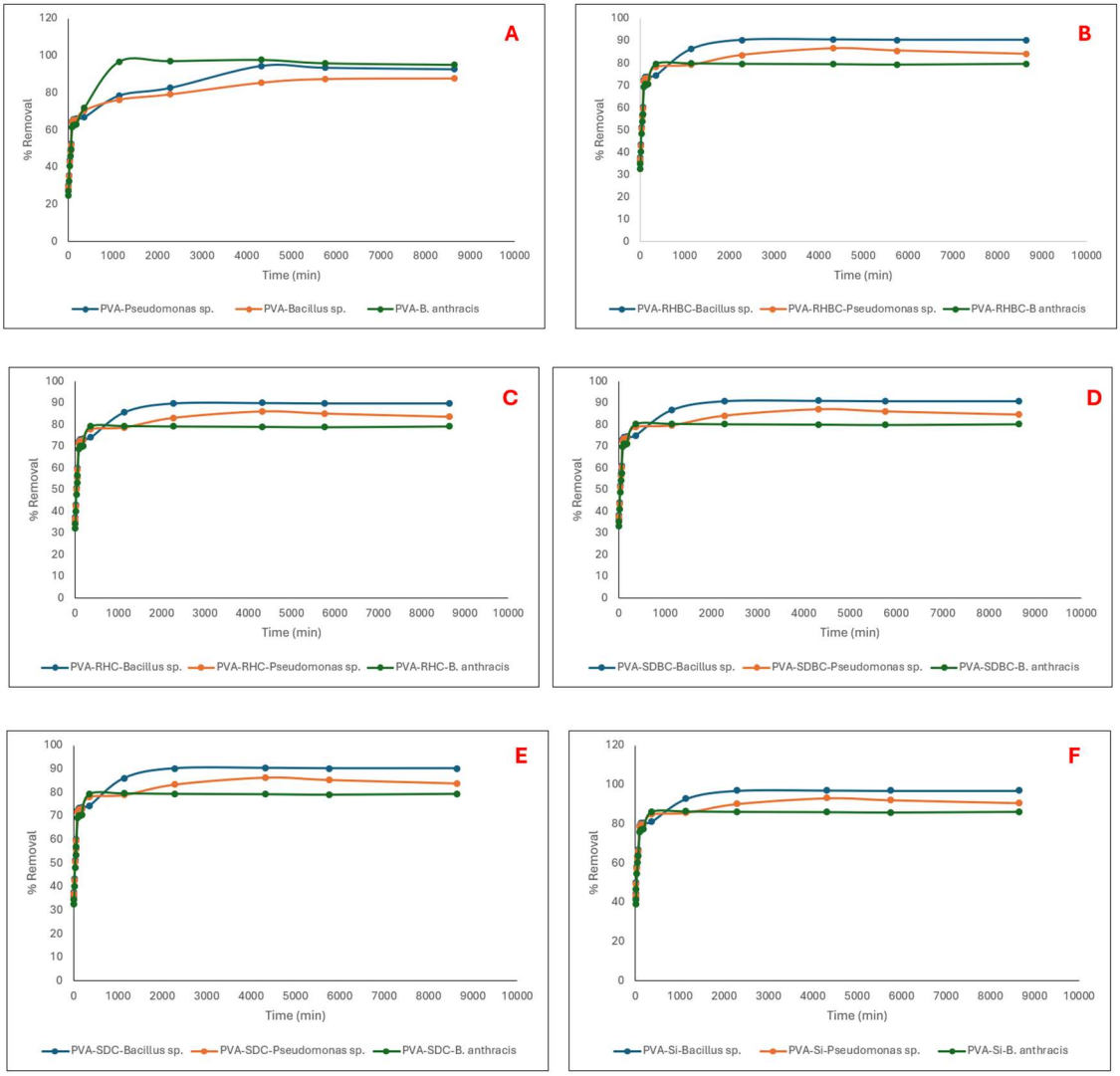

Figure 6.28: Effect of treatment time on acenaphthene removal by bacteria doped (A) PVA, (B) PVA-RHBC, (C) PVA-RHC, (D) PVA-SDBC, (E) PVA-SDC, and (F) PVA-Si aerogel

6.3.13.3.2. Effect of adsorbent dose: As presented in Fig. 6.29, the adsorbent dose has a significant effect on the pollutant removal by bacteria-doped aerogel. Fig. 6.29 (A), (B), (C), (D), (E), and (F) show the pollutant removal by bacteria doped PVA, PVA-RHBC, PVA-RHC, PVA-SDBC, PVA-SDC, and PVA-Si, respectively. From the experimental data, it was shown that PVA-Si-*Bacillus sp.* showed the highest removal with the value of 97.02% after five days of treatment with a 1 g/L dosage. With the increase of dose, initially the removal increased and then slightly decreased, signifying the dominance of bioremediation over adsorption phenomena in this process. This observation can be explained as the higher microbial dosage provides more microbial mass and metabolic activity, which results in higher removal (Santini et al., 2016); however, after a certain point, the increasing dose causes resource scarcity and an increase in concentration.

Therefore, an opposite effect also occurred in the removal of the pollutant (Liu et al., 1993).

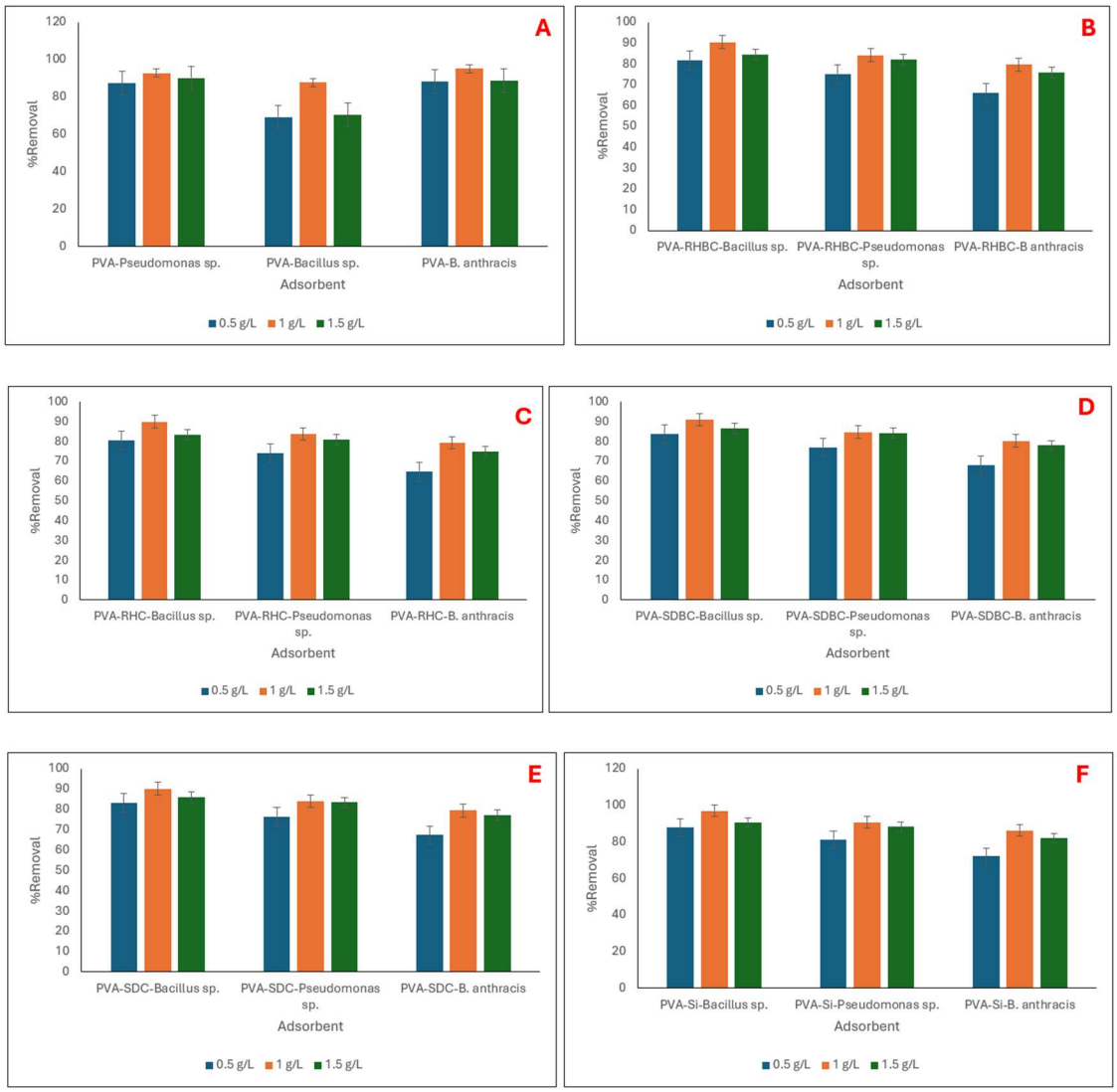

Figure 6.29: Effect of adsorbent dose on acenaphthene removal by bacteria doped (A) PVA, (B) PVA-RHBC, (C) PVA-RHC, (D) PVA-SDBC, (E) PVA-SDC, and (F) PVA-Si aerogel

6.3.13.3.3. Effect of pollutant concentration: In Fig. 6.30, the effect of pollutant concentration on the pollutant removal is shown. Fig. 6.30 (A), (B), (C), (D), (E), and (F) show the pollutant removal by bacteria doped PVA, PVA-RHBC, PVA-RHC, PVA-SDBC, PVA-SDC, and PVA-Si, respectively. As shown in the figure, with the increase of pollutant concentration, the removal percentage also increased. The highest removal was observed in the case of PVA-*B. anthracis* aerogel at a 10 mg/L dosage. The removal was 96.55%. This observation can be explained by the saturation of adsorption sites on the adsorbent surface. At low pollutant concentration, the active site and contaminant molecule's ratio is larger, allowing the molecules to rapidly interact with the active site

and to be removed from the solution. As the concentration increased, the trend slowed down due to the increased competition (de Farias Silva and da Gama, 2020). However, unlike bioremediation, in this process, higher concentrations did not affect the process adversely. The probable cause of that can be explained as, though the aerogels increased the concentration of pollutants in some zones of the solution by adsorption, the microorganisms were not forced to consume all the pollutants due to the associated desorption process. This adsorption-desorption cycle maintained a balanced concentration and prevented the inhibition of microbial growth.

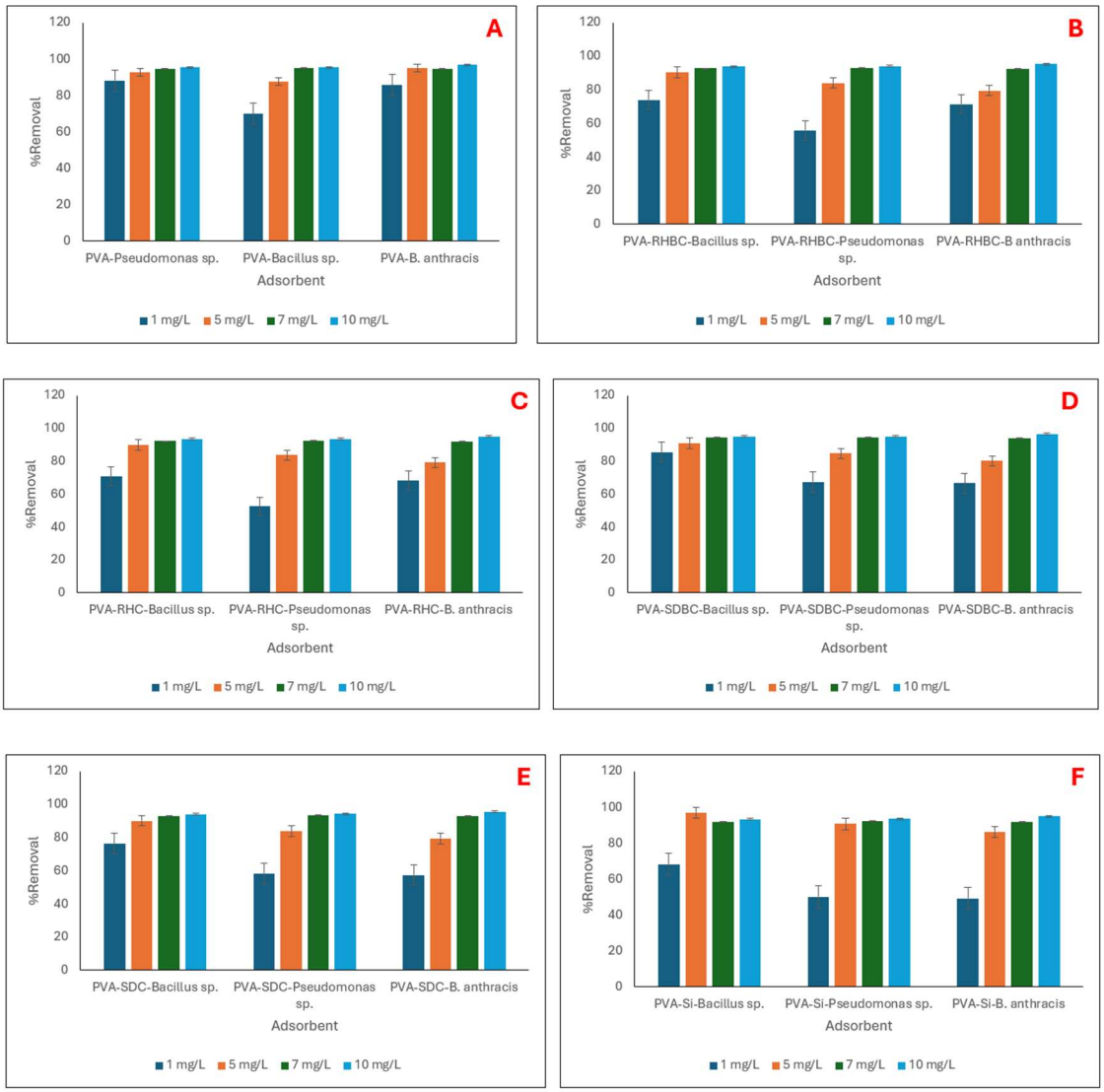

Figure 6.30: Effect of pollutant concentration on acenaphthene removal by bacteria doped (A) PVA, (B) PVA-RHBC, (C) PVA-RHC, (D) PVA-SDBC, (E) PVA-SDC, and (F) PVA-Si aerogel

6.3.13.3.4. Effect of temperature: The effect of temperature on the pollutant removal by bacteria-doped aerogel is presented in Fig. 6.31. Fig. 6.31 (A), (B), (C), (D), (E), and (F) show the pollutant removal by bacteria doped PVA, PVA-RHBC, PVA-RHC, PVA-

SDBC, PVA-SDC, and PVA-Si, respectively. From the figure, it was shown that the optimal removal for all the adsorbents was found at 303 K temperature, signifying the dominance of microbial bioremediation over the adsorption process. In this experiment, the highest removal was found in the case of PVA-Si-*Bacillus sp.* aerogel at 303 K temperature with the value of 98.29%. This trend can be explained as temperature is an important factor in bioremediation. In most cases, higher temperatures enhance the removal of pollutants, but at extreme temperatures, the growth of microbes is reduced (Iqbal et al., 2007). It was observed that for every microbe, there is an optimum temperature, and at that temperature, the microbial activity is the maximum (Sanscartier et al., 2011). Topp et al. (1997) reported that most of the microbes show optimum temperature at a range of 298 K- 303 K.

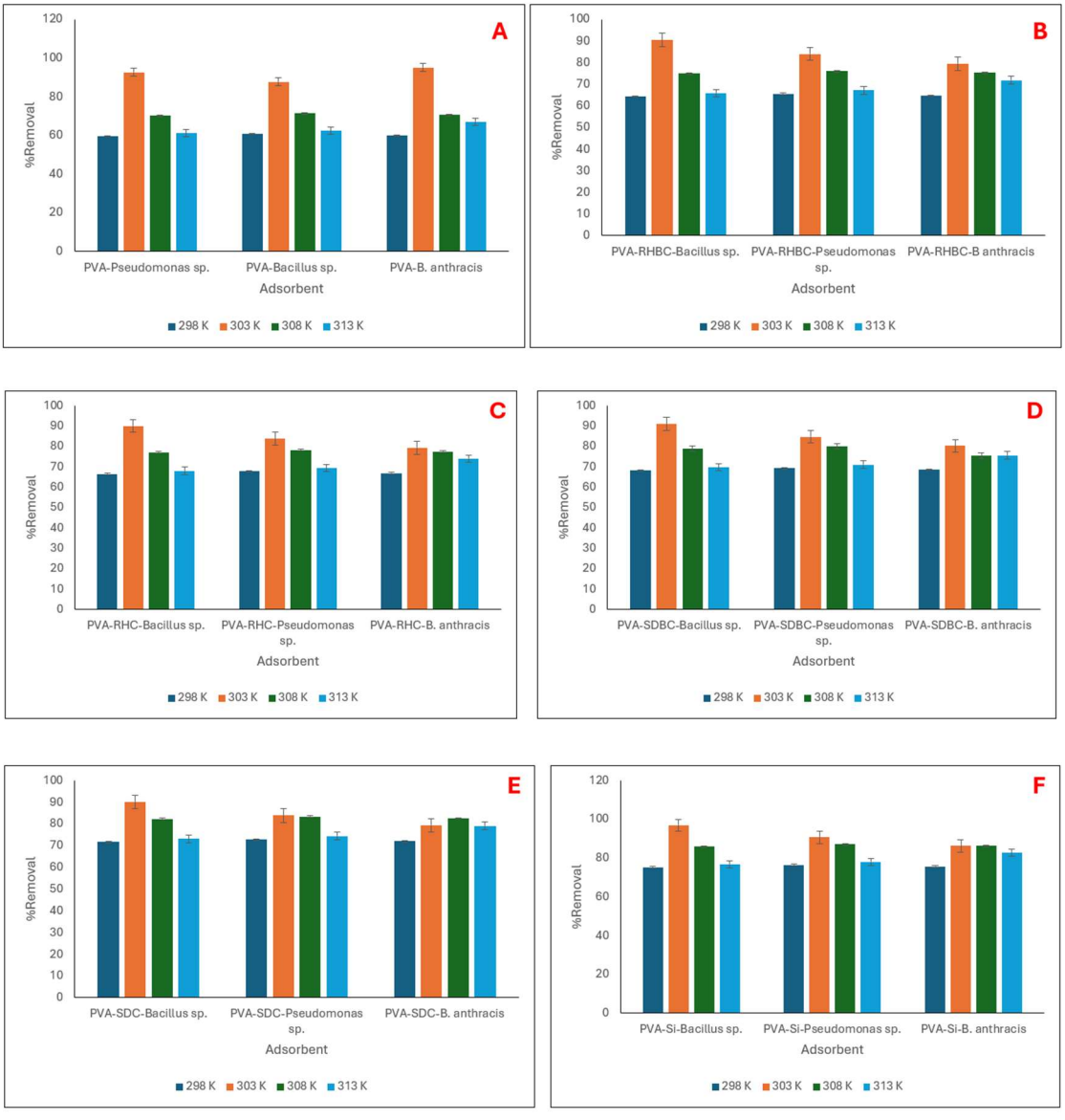

Figure 6.31: Effect of temperature on acenaphthene removal by bacteria doped (A) PVA, (B) PVA-RHBC, (C) PVA-RHC, (D) PVA-SDBC, (E) PVA-SDC, and (F) PVA-Si aerogel

6.3.13.3.5. Effect of pH: The effect of pH on the removal process also shows a similar trend to bioremediation. Fig. 6.32 represents the effect of pH on the removal process. 6.32 (A), (B), (C), (D), (E), and (F) show the pollutant removal by bacteria doped PVA, PVA-RHBC, PVA-RHC, PVA-SDBC, PVA-SDC, and PVA-Si, respectively. PVA-Si-*Bacillus sp.* has shown the highest removal among all the adsorbents and pH, with the value of 97.85% at pH 7. This observation can be explained by considering the effect of pH on microbial cells. pH affects the process in various ways, viz., the chemistry of pollutants, the coexisting ions of the solution, and the ionic balance of microorganisms. pH also affects the adsorption mechanism and degree of ionisation.

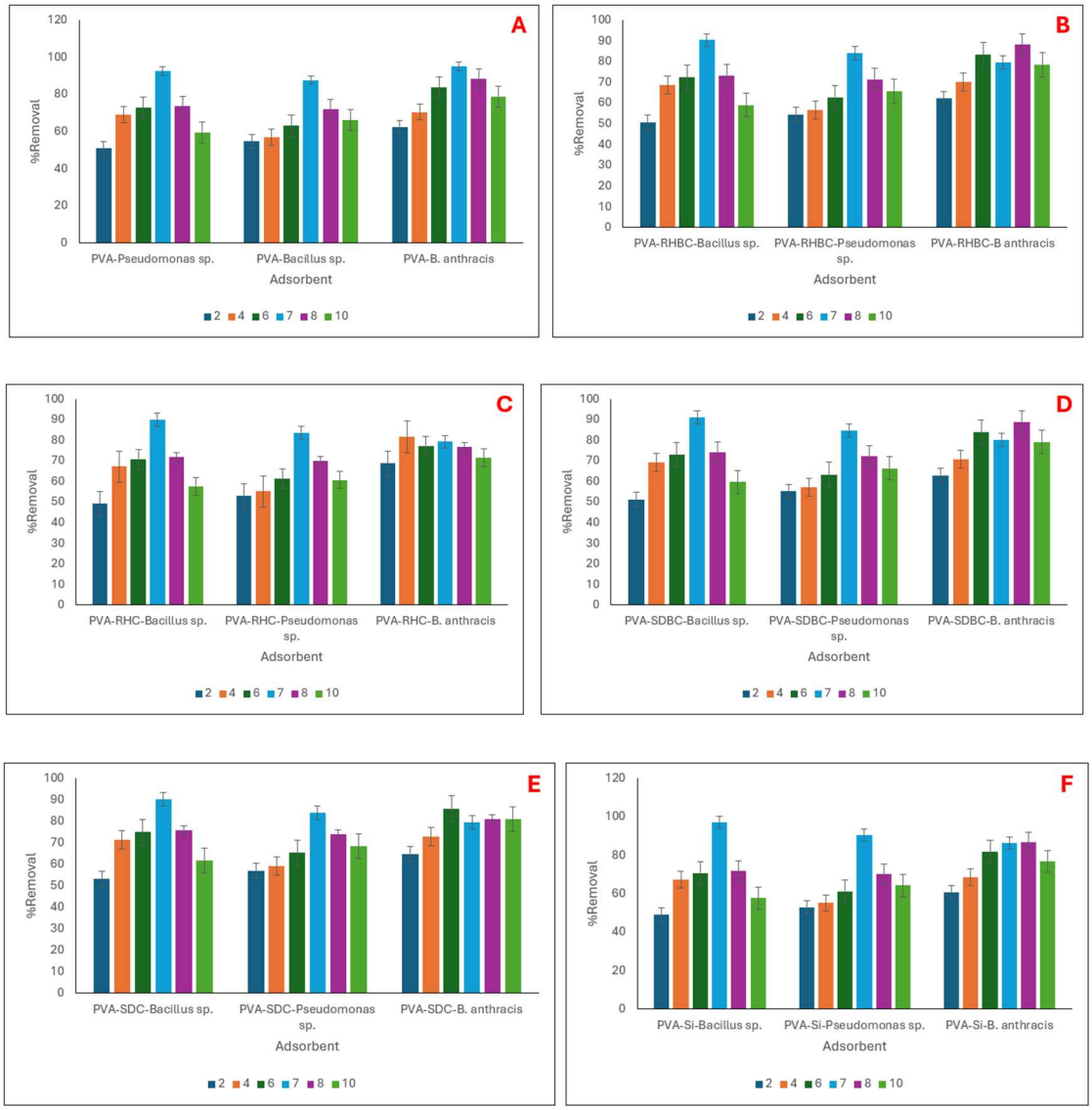

Figure 6.32: Effect of pH on acenaphthene removal by bacteria doped (A) PVA, (B) PVA-RHBC, (C) PVA-RHC, (D) PVA-SDBC, (E) PVA-SDC, and (F) PVA-Si aerogel

6.3.13.3.6. Optimisation of removal: To optimise the naphthalene adsorption process, a Response Surface Methodology (RSM) study was performed (Aydar, 2018). A quadratic equation, presented as equation (6.5), was used to analyse and validate the experimental design. From the batch adsorption study, PVA-Si-*Bacillus sp.* was selected as the most suitable adsorbent for the process, and the RSM study was conducted with that adsorbent only.

$$R = 84.52 + 38.55 * A + 1.62 * B - 3.43 * C - 4.14 * AB + 1.22 * AC + 1.48 * BC - 32.09 * A^2 - 4.15 * B^2 - 3.86 * C^2 \quad \text{(6.5)}$$

Here, A, B, C, and R are reaction time (min), adsorbent dose (g/L), pollutant concentration (mg/L), and removal%, respectively.

6.3.13.3.6.1. Validation of the model: From the ANOVA analysis, it was observed that this model is significant with a P-value of 0.0001 (<0.05) and an F-value of 326.61 (>12). The correlation coefficient (R^2) value of the mentioned model was 0.99. The R^2 value also indicates that the predicted and observed data of this experiment are in reasonable agreement, indicating the significance of the model. Fig. 6.33 (A) shows the distribution of predicted and experimental values satisfying the validity of this model.

6.3.13.3.6.2. Response of time and adsorbent dosage: The response of time and adsorbent dosage is presented in Fig. 6.33 (B). The graph shows that the optimum removal% was observed at 1 g/ /L adsorbent dosage after 35 hr. of adsorption. The maximum pollutant removal under these conditions was found to be 97.42%.

6.3.13.3.6.3. Response of adsorbent dosage and pollutant concentration: In Fig. 6.33 (C), the response of adsorbent dosage and pollutant concentration is presented. From the figure, it can be stated that at the adsorbent dose of 1 g/L and 5 mg/L pollutant concentration, the optimum removal was achieved. The optimum removal in these conditions was 92.26%.

6.3.13.3.6.4. Response of pollutant concentration and time: The crosstalk between pollutant concentration and treatment time is represented in Fig. 6.33 (D). From the figure, it was observed that at a treatment time of 35 hr. and a 5 mg/L pollutant concentration, the highest removal was achieved. The optimum removal in this experiment was 98.2%.

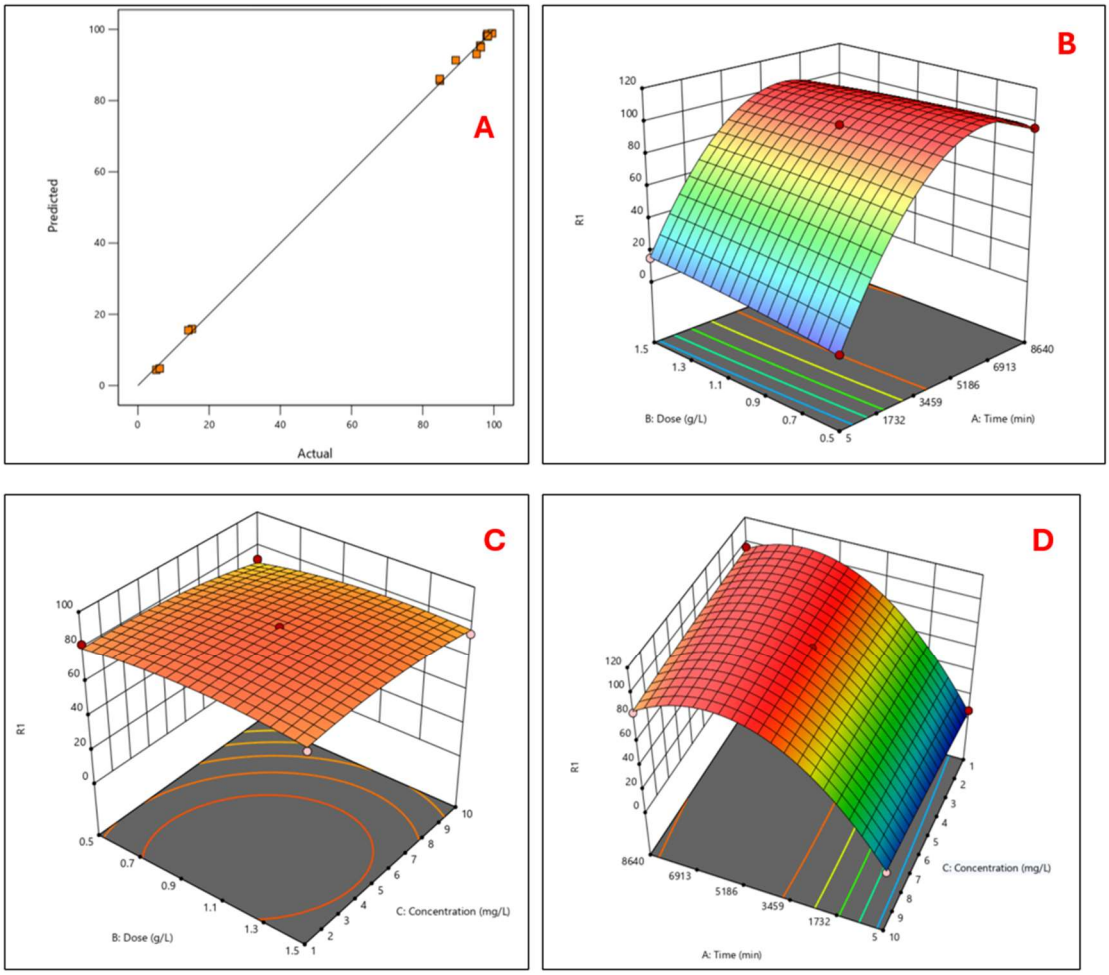

Figure 6.33: Optimisation of acenaphthene removal by PVA-Si-*Bacillus sp.* aerogel using Response Surface Methodology, representing (A) comparison of actual and predicted results, (B) response of time and aerogel dose, (C) response of aerogel dose and pollutant concentration, (D) response of time and pollutant concentration.

6.3.13.3.7. GC-MS analysis of pollutant solution after treatment: Fig. 6.34 shows the result of GC-MS analysis of pollutant solution after treatment. Being the most effective adsorbent, PVA-Si-*Bacillus* was used to treat the solution for GC-MS analysis. As shown in the figure, major peaks at 4.35 min., 4.57 min., 6.07 min., 8.61 min., and 11.77 min. are detected respectively. The peaks were identified using the MS library and are presented in Table 6.8.

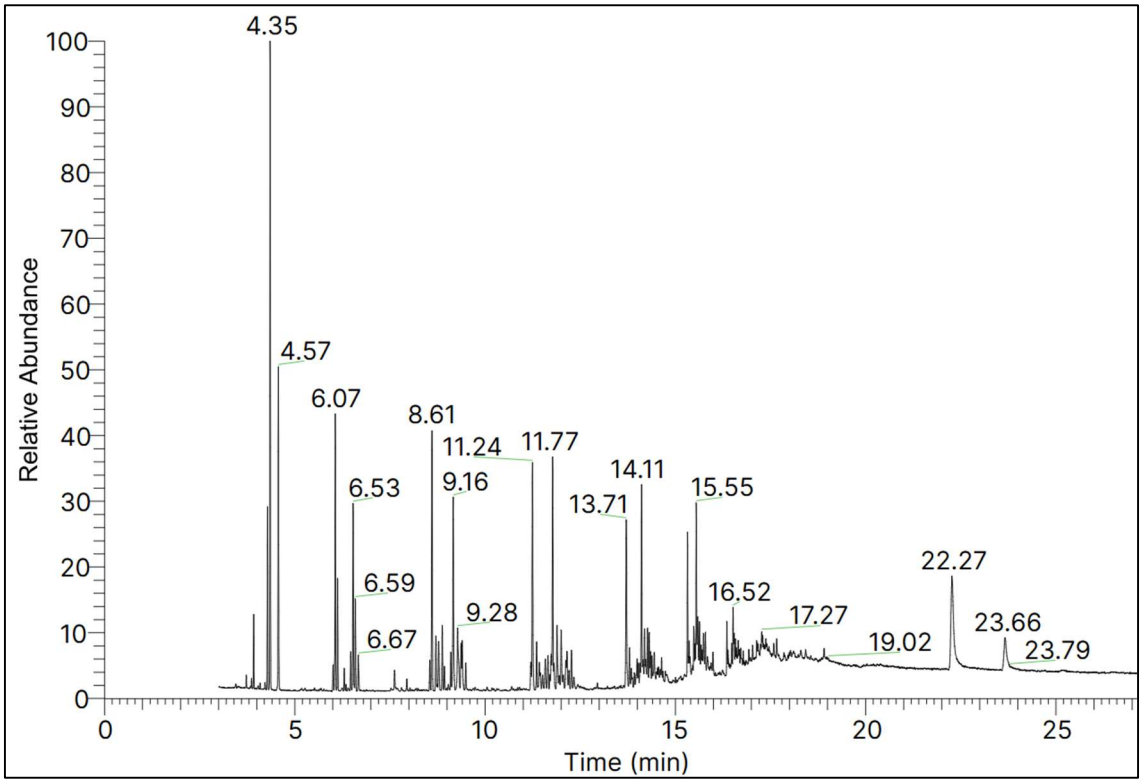

Figure 6.34: GC-MS analysis of acenaphthene solution after treatment with PVA-Si-*Bacillus sp.* aerogel

Table 6.8: GC-MS analysis of acenaphthene by PVA-Si-*Bacillus sp.* aerogel

Peak retention time (min.)	**Compound**
4.35	Ethylbenzene
4.57	O-Xylene
6.07	3,3-dimethyl-hexane
8.61	2,6,11-trimethyl-dodecane
11.77	3-ethyl-3-methyl-decane

6.4. Conclusion:

This chapter of the study focused on both the drawbacks of adsorption and bioremediation and combined the processes to achieve a more effective removal technique. The development of bacteria-doped aerogels and their application in wastewater treatment, on one hand, solves the problem associated with the disposal of used adsorbent and other hand, addresses the time-consuming nature of bioremediation. From the result of the batch study, it is visible that the combination of these two processes left-shifted the equilibrium point of the removal process, as well as the simultaneous bioremediation

increased the effectiveness of the adsorption. From the MIC analysis and the Monod model, it can be concluded that the selected bacteria have a high affinity to mitigate the pollution associated with naphthalene, phenol, and acenaphthene. Also, from the RSM study, it validity of the removal process by bacteria-doped aerogel was confirmed. Furthermore, the AO/EB staining method confirms the successful doping of the bacteria in the aerogel matrix. From the GC-MS analysis, the produced products of the bioremediation of pollutants were investigated. This analysis confirms the breakdown of pollutants and their entry into the Krebs' cycle of bacterial metabolism pathway. However, another important consideration of bioremediation is the toxicity of by-products. In some cases, the produced products are more harmful to the environment compared to the mother compound. The next chapter of this thesis will investigate the phytotoxic effect of treated solutions.

Chapter: 7

PHYTOTOXICITY STUDY OF POLLUTANT SOLUTION AFTER TREATMENT

7.1. Introduction:

Toxicity is a critical parameter to ensure the safety and efficacy of adsorbents for various applications, including and not limited to environmental remediation, water treatments, and industrial processes (Burgess et al., 2013). Toxicity analysis of any remediation process is important, as in some cases, the by-products produced show more adverse effects on the environment compared to the mother compound. Also, for adsorption, a toxicity study is required. Adsorbents are substances capable to attract and bind other molecules onto their surface (Ruthven et al., 1984). The introduction of new adsorbents into applications requires thorough evaluation to determine their potential impact on the environment, human health, and non-target organisms (Neagu et al., 2023; Kong et al., 2022). In the previous chapter of this thesis, the treatment of different pollutant solutions with prepared adsorbents was discussed in detail. The adsorbents performed adsorption and bioremediation simultaneously. In this chapter, the toxicity analysis of the treated solutions will be explored on the moong bean (*Vigna radiata*). A total of three treated solutions for each pollutant will be considered for this study, considering the inclusion of all used bacteria with the highest removal efficiency. Different phytotoxicity indices will be analysed along with carbohydrate and protein profiling of the model organism.

7.2. Materials and Methods:

7.2.1. Materials: The moong beans (*Vigna radiata*) were purchased from a local grocery shop at Jadavpur, Kolkata. Hydrogen peroxide (H_2O_2), anthrone reagent, sulphuric acid (H_2SO_4), sodium hydroxide (NaOH), sodium carbonate (Na_2CO_3), copper sulphate ($CuSO_4$), and sodium potassium tartrate ($KNaC_4H_4O_6$) were purchased from Marck (Germany). Folin-Ciocalteau reagent, sodium chloride (NaCl), potassium chloride (KCl), disodium hydrogen phosphate (Na_2HPO_4), ethanol and potassium dihydrogen phosphate (KH_2PO_4) were purchased from Loba Chemie (India).

In the previous chapter, it was observed that PVA-*Bacillus sp.,* PVA—*B. anthracis,* and PVA-Si-*Pseudomonas sp.* showed the most effective removal for all the pollutants.

Hence, solutions treated with the mentioned adsorbents were considered for the phytotoxicity study.

7.2.2. Sterilisation of moong beans: To prevent any fungal growth or contamination during the experiment, the experiment, the moong beans were washed with 3% H_2O_2 solution. To prepare the solution, 3 mL of H_2O_2 was mixed with DI water in an Erlenmeyer flask, and the total volume was 100 mL. The solution was stirred on a magnetic stirrer for 10 min. On the other hand, the moong beans were cleaned with DI water and submerged in the H_2O_2 solution for 30 min. Following that, the beans were collected and washed with 70% ethanol. After washing the beans with ethanol, they were again washed with DI water several times to clean out any excess ethanol or H_2O_2.

7.2.3. Preparation of phosphate buffer (PBS) solution: The PBS was prepared as described in section 6.2.8.10.1.

7.2.4. Treatment of moong beans: For phytotoxicity indexing, in a Petri plate, a circular filter paper (Whatman 10) was placed and sterilised under UV light for 10 min. After that, 10 moong beans were placed on the filter paper, and 5 mL of the pollutant solution was poured with a micropipette. The plates were sealed and incubated inside a BOD shaker incubator (Remi) for 5 days at 303 K. After incubation, the seeds were collected, and the root and shoot lengths were measured along with the number of germinated seeds. From the root-shoot length and the germinated sheet number, phytotoxicity indices were calculated.

For the biochemical assay, in a Falcon tube, 30 mL of pollutant solution was taken. The sterilised moong beans were submerged in the solution and incubated inside a BOD shaker incubator for 72 hr. at 303 K. After treatment, the seeds were collected and crushed with a mortar pestle, while mixing the seed with 10 mL of phosphate buffer. This sample was preserved at 278 K for carbohydrate analysis. On the other hand, the crushed seeds were mixed with the buffer solution and centrifuged at 10000 rpm for 5 min. while maintaining the temperature at 278 K. The supernatant was collected and stored at 278 K for protein analysis.

A control and a wild-type set was also considered in this experiment. The controlled set was the pollutant solutions without any treatment and the “wild-type” was a set of beans the was grown without any environmental stress.

7.2.5. Phytotoxicity indices study: Phytotoxicity indices are the measurement of the toxic effect of any substance on plants. In this research, germination rate, germination energy, inhibition rate, and germination index were analysed respectively.

7.2.5.1. Germination index (GI): GI is a widely used metric in seed science to evaluate both the percentage and speed of seed germination. A high GI indicates a seed with both a high germination percentage and germination speed; on the other hand, a low GI indicates poor growth of the seed. The GI is calculated according to equation (7.1).

$$GI = \sum_{1}^{t} \frac{G_t}{D_t} \ldots\ldots\ldots\ldots\ldots\ldots \quad (7.1)$$

Here, G_t is the number of seeds germinated during t time, and D_t is the number of days.

7.2.5.2. Germination rate: Germination rate is the percentage of seeds in a given batch that successfully germinated in a given period. A good germination rate indicates a good quality of the seeds. The germination rate was calculated using equation (7.2).

$$Germination\ rate\ (\%) = \frac{Total\ number\ of\ germinated\ seed}{Total\ number\ of\ seed} x100 \ldots\ldots\ldots\ldots\ldots\ldots \quad (7.2)$$

7.2.5.3. Germination energy (GE): Germination energy refers to the percentage of seeds in a sample that germinate within a specific, early period. This parameter differs from germination rate, as the germination rate observes the germination over the total time of the experiment, and GE only considers the early period. In this experiment, germination energy was calculated using equation (7.3).

$$GE = \frac{Seed\ germinated\ withi\ \ 3\ days}{Total\ number\ of\ seeeds} x100 \ldots\ldots\ldots\ldots\ldots\ldots\ldots\ldots \quad (7.3)$$

7.2.5.4. Inhibition rate: Inhibition rate refers to the degree to which a certain factor (environmental or chemical stress) reduces the germination of seeds compared to an untreated control group. The inhibition rate was calculated using equation (7.4).

$$Inhibition\ rate\ (\%) = \frac{Germination\ in\ control - Germ\ \ \ \ \ \ \ \ in\ treatment}{Germination\ in\ control} x100 \ldots\ldots\ldots (7.4)$$

7.2.6: Carbohydrate content analysis: The carbohydrate content analysis of seeds was conducted by anthrone test as described in section 4.2.4.

7.2.7. Protein content analysis: The protein content analysis was performed by the Folin-Lowry method. The principle behind this method is the reaction of peptide nitrogen

present in the protein molecule with the copper (II) ions under alkaline conditions. In this reaction, the conversion of copper ions (Cu^{+2}) to cuprous ions (Cu^{+}) occurs, and the cuprous ions reduce the Folin-Ciocalteu (F-C) reagent, resulting in the formation of a blue-coloured complex, known as heteropolymolybdenum blue.

7.2.7.1. Preparation of reagents: A total of five reagent solutions were required for protein estimation by this process and were prepared as mentioned below.

7.2.7.1.1. Preparation of sodium carbonate solution: 2 g of NaOH was measured using a weighing machine (Sartorius, Germany) and taken in an Erlenmeyer flask. 900 mL of DI water was poured into the flask and stirred on a magnetic stirrer. After the solution was prepared, the final volume was made up to 1 L. Sodium carbonate was measured using a weighing machine (Sartorius, Germany) and added to the NaOH solution in a 2% (w/v) ratio. The solution was again stirred on a magnetic stirrer and stored for future use.

7.2.7.1.2. Preparation of copper sulphate solution: 1 g of copper sulphate was measured using a weighing machine (Sartorius, Germany) and mixed with 100 mL of DI water in an Erlenmeyer flask on a magnetic stirrer. After the solution was prepared, it was stored for future use.

7.2.7.1.3. Preparation of sodium-potassium tartrate solution: 2 g of sodium-potassium tartrate was measured using a weighing machine (Sartorius, Germany) and mixed with 100 mL of DI water in an Erlenmeyer flask on a magnetic stirrer. After the solution was prepared, it was stored for future use.

7.2.7.1.4. Preparation of copper reagent: The previously prepared sodium carbonate solution, copper sulphate solution, and sodium-potassium tartrate solution were mixed in a 1:1:10 volumetric ratio.

7.2.7.2. Experimental procedure: The reaction mixture was prepared by mixing 1 mL of sample solution (section 7.2.4) with 0.5 mL of F-C reagent and 5 mL of copper reagent. The mixture was stood for 30 min., and the absorbance was measured using a UV-Vis spectrophotometer (PerkinElmer, USA) at 750 nm.

7.3. Result:

7.3.1. Germination rate: The impact of phenol, acenaphthene, and naphthalene solutions after treatment on the germination rate of moong beans is presented in Fig. 7.1 (A). The

figure showed that the highest germination rate was found in the wild-type samples, reflecting the high germination rate of the model organisms without any influence. In the control group, the moong beans samples were exposed to the pollutants without any bacterial treatment. They showed significantly reduced germination rate, confirming the phytotoxic effects of naphthalene, phenol, and acenaphthene. In the case of PVA-*Bacillus sp.* treatment, germination rates were 72%, 80%, and 70% for naphthalene, phenol, and acenaphthene, respectively. This result indicated an effective remediation of the pollutants. Similar to this result, PVA-Si-*Pseudomonas sp.* also showed an effective increase in germination rate with 70%, 72%, and 62% for naphthalene, acenaphthene, and phenol, respectively. On the other hand, though the germination rate improved, the efficacy was slightly lower in the case of PVA-*B. anthracis* aerogel. Mihelcic and Luthy (1988) reported the degradation of acenaphthene by microorganisms, and observed an improvement in the phytotoxicity index also supports the observation of this study.

7.3.2. Germination energy: The impact of phenol, acenaphthene, and naphthalene solutions after treatment on the germination energy of moong beans is presented in Fig. 7.1 (B). The wild-type moong beans culture showed the highest germination energy. On the other hand, the lowest value was observed in the case of the control culture at approximately 10%. This observation indicated that the pollutants can significantly affect the germination energy of the species. After treating with the prepared adsorbents, a significant improvement in the germination energy was observed. In the case of PVA-*Bacillus sp.,* the germination energy was 40% for naphthalene and acenaphthene, but in the case of phenol, it dropped to 30%. Similarly, for PVA-*B. anthracis,* the germination energy was close to 40% in the case of naphthalene and acenaphthene, and 30% for phenol. A similar result was reported in a previously conducted study, which showed that degradation of organic pollutants can effectively reduce their toxic effects (Dutta et al., 2018).

7.3.3. Germination index: The impact of phenol, acenaphthene, and naphthalene solutions after treatment on the germination index of moong beans is presented in Fig. 7.1 (C). In the figure, it was shown that in the control culture, the index is lowest. In the case of naphthalene, the index was about 0.66. On the other hand, in the wild-type sample, the value was 3. After treatment of the samples, the index significantly improved. For each treatment, the highest value was 2.6. This result indicated that the pollutants delayed the growth of the moong beans. Also, as observed in germination rate analysis, the

germination rate was also decreased. From this observation, the statement could be made that the adverse effects of pollutants can be remediated by the prepared adsorbents.

7.3.4. Inhibition rate: The impact of phenol, acenaphthene, and naphthalene solutions after treatment on the inhibition rate of moong beans is presented in Fig. 7.1 (D). The inhibition rate in the case of the wild-type sample was found to be 0%, indicating high germination capability of the species. Though germination rate, germination energy, and germination index significantly increased after treatment of the solution, the inhibition rate did not show effective development. For all the adsorbents, the inhibition rate was found to range between 60%-80%. The data suggested that this enhancement could be attributed to the interaction between the bacteria and the compounds, leading to a synergistic effect.

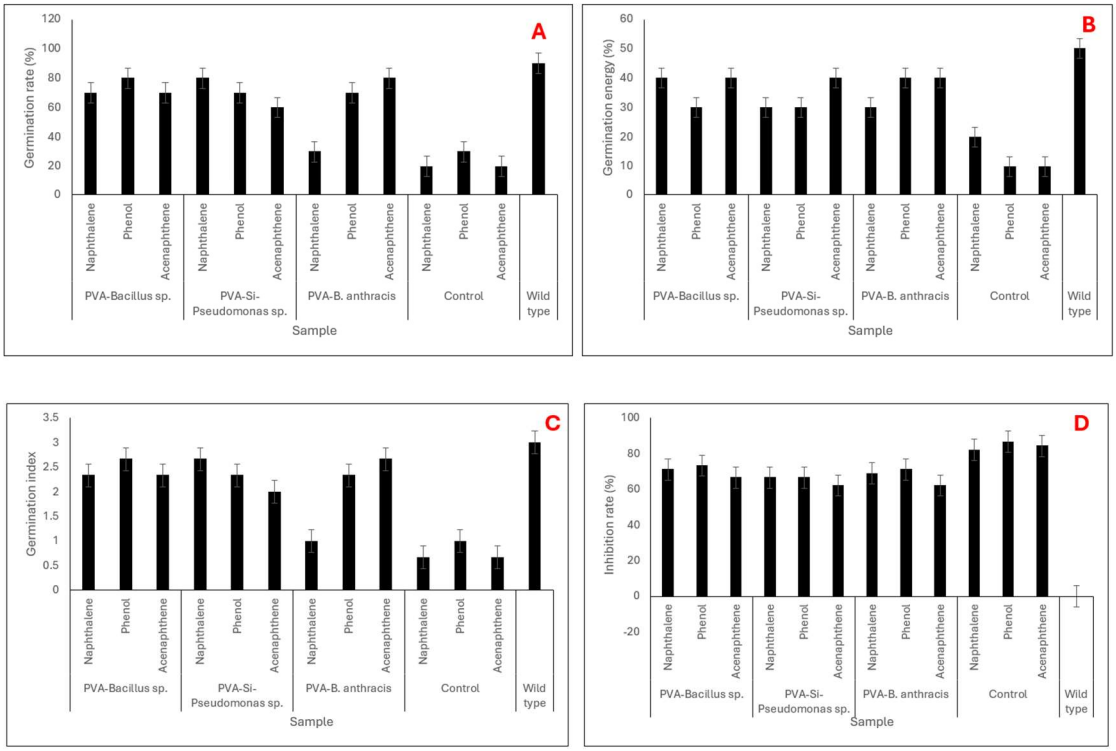

Figure 7.1: Toxicity indices of *Vigna radiata* representing (A) germination rate, (B) germination energy, (C) germination index, and (D) inhibition index.

7.3.5. Carbohydrate content analysis: The impact of phenol, acenaphthene, and naphthalene solutions after treatment on the carbohydrate content of moong beans is presented in Fig. 7.2 (A). As presented in the figure, the carbohydrate content of the species significantly decreased while treated with the pollutants. This observation indicated that the organic pollutants could interfere with the metabolic pathway of moong beans affecting the nutrient value of the samples. However, significant improvement in

the carbohydrate content was observed after treating them with the prepared adsorbents. The highest value was found in the case of acenaphthene after treating it with PVA-Si-*Pseudomonas sp.* This sample showed a carbohydrate content of 338.8 mg/g, comparable with the wild-type sample, that showed the carbohydrate content of 412.38 mg/g.

7.3.6. Protein content analysis: The impact of phenol, acenaphthene, and naphthalene solutions after treatment on the protein content of moong beans is presented in Fig. 7.2 (B). Similar to carbohydrate analysis, in this case, a decreased amount of protein was found while treating the moong beans with pollutant solutions. The lowest protein content was observed in the case of acenaphthene treated beans, with the value of 40.19 mg/g. On the other hand, in the case of wild-type samples, the protein content was found to be 258.01 mg/g. After treating the pollutant solutions with prepared adsorbents, the protein content increased. The highest protein content was found in the case of phenol solution treated with PVA-*Bacillus sp.* with the value of 208.35 mg/g.

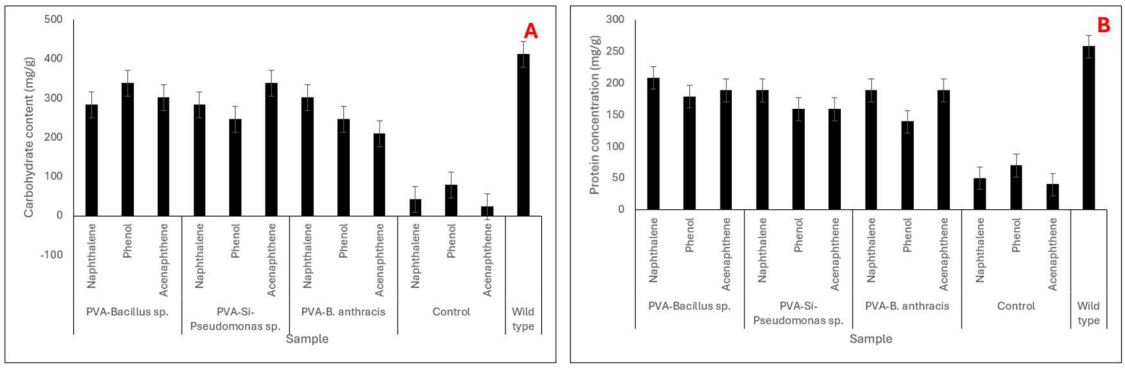

Figure 7.2: Biochemical assay of *Vigna radiata* representing (A) carbohydrate content and (B) protein content

7.4. Conclusion:

This chapter of the thesis focused on the phytotoxicity profiling of naphthalene, acenaphthene, and phenol before and after adsorbent treatment. From the experiment it was found, that before treatment the pollutant solutions exhibit adverse effects on the phytotoxicity index and biochemical profile of *Vigna radiata*. This phenomenon can occur due to various reasons, viz., cell necrosis, cell wall damage, and inhibition in nutrient uptake. However, the most probable reason can be, being organic in nature, these pollutants interfere with the metabolic pathways and enzymatic activities of the species. From this study it was also observed that after treating the solutions with prepared adsorbents, the adverse effects significantly reduced. This observation indicates that the prepared by-products of this process are less harmful compared to the mother compound

and can be discharged in the environment safely. This result also enhances the acceptance of the prepared adsorbents as a sustainable method of wastewater treatment.

CONCLUSION AND FUTURE PERSPECTIVE

Solid biotic waste generation and disposal problems are increasing every day. Waste materials like sawdust and rice husk and sawdust is very common in developing countries like India as a form of agricultural by-products and industrial waste, respectively. These components, also known as lignocellulosic materials, can act as the precursor of different value-added products in they are treated with chemical or biological methods.

In this process, the chemical agents or biological enzymes break down the biochemical structures of lignocellulosic biomass and separate all the building block chemicals. In this study, a sonochemical method was used to treat the rice husk and sawdust and extract cellulose, lignin, and hemicellulose from it. It was found that after applying sonication along with chemical agents, the cellulose yield significantly improved. The highest concentration of cellulose achieved in this study was 958.88 mg/g of biomass, after treating sawdust with a 4% NaOH solution and sonication. It was also observed that sonication did not directly affect the total reducing sugar (TRS) yield but rather followed the trend of cellulose yield. Moreover, it was also found that by adjusting different physical parameters and experimental conditions, the yield can increase significantly. It was observed that in all the cases, the highest ethanol yield was achieved after treating the samples for five days, at pH 7, biomass concentration of 3 g/L, microbial concentration of 1 mL/100 mL, and temperature at 303 K. The highest concentration of ethanol found in this study was 5.84 mg/g from rice husk, after treating it with a 6% NaOH solution. Hemicellulose and lignin were also extracted during this process, and furfural was produced from the extracted cellulose.

Moreover, biochar was prepared from the raw materials as well, and silica was extracted. The extracted silica, cellulose, and prepared biochar were used as filler materials for PVA aerogel synthesis. It was found that the prepared aerogels have a high affinity for pollutants like dye and organic pollutants. From this study, it was also observed that the aerogels can adsorb 98.23% phenanthrene from aqueous solution. Also, the removal of 97.34% of naphthalene, 94.87% of phenol, 88.36% of acenaphthene, 94.21% of congo red, and 95.62% of methylene blue was found by using the prepared aerogels. From different characterisation studies of the aerogels, a clearer picture of the adsorbents was generated. From the microscopy and SEM analysis, the uneven surface of aerogels was observed, which played a significant role in the adsorption behaviour. From the ATR-

FTIR analysis, it was concluded that the presence of functional groups, like C-H, C=O, C-O, and Si-O-Si, made them significant adsorbents for industrial scale usage. It was also observed that the aerogels were thermally stable, highly porous and lightweight materials, satisfying all the criteria of aerogels previously created by the supercritical drying method.

From the modelling of the adsorption processes, it was found that the processes were endothermic and spontaneous. They were observed to follow the pseudo-2nd-order kinetic model. The isotherm model, though, was found to depend on the adsorbent type. In general, the aerogels containing sawdust materials as filler followed the Langmuir isotherm model; on the other hand, the rest of the aerogels were found to better fit the Freundlich isotherm model, allowing multilayer adsorption.

To enhance the removal capacity of the prepared aerogels, bacteria, viz., *Bacillus sp., Pseudomonas sp.,* and *B. anthracis,* were doped inside the PVA matrix. In this study, the bacteria were found to be resistant to the pollutants of interest with a minimal MIC value. In all the scenarios, PVA-Si aerogel was found to be the best matrix for bacterial doping and enhancing its capability. After doping the bacteria inside the aerogel network, the adsorption equilibrium was found after 2 days of treatment, compared to almost five days of treatment in the case of normal bioremediation. It was also found that the adsorption efficiency of the aerogels increased significantly after bacterial doping. Where the highest removal of naphthalene was found to be 92% in the case of PVA-Si aerogel, which increased up to 98% after doping with *Bacillus sp.*

From the phytotoxicity analysis, it was found that after treating the pollutant solutions with bacteria-doped aerogels, the phytotoxicity decreased significantly. The study was conducted on *Vigna radiata* as the model organism, and it was found that for each phytotoxicity index, the value increased significantly after treating them with the prepared adsorbents.

This study was conducted with multiple approaches associated with energy and the environment. From this study, it was found that rice husk and sawdust can be used as the raw material for valorisation and produce different products, like, cellulose, lignin, hemicellulose, bioethanol, and furfural. Also, the extracted silica and cellulose, along with the produced biochar, were used to synthesise aerogels for wastewater treatment. Though the aerogels were found to be efficient adsorbents for organic pollutants and dye

removal, doping of microorganisms in the PVA matrix significantly improved the output. Also, the remediation of the toxic effects of the pollutants was found after treating them with the prepared bacteria-doped aerogels.

Though this study focuses on multiple perspectives and addresses various problems, there are a few areas where scopes were identified to conduct further research.

1. The chemical and biological pretreatment methods for lignocellulosic biomass can be combined to investigate the effects.

2. In this study, *Saccharomyces cerevisiae* was used to ferment the extracted cellulose. However, other microbes, like *Zymomonas mobilis,* can be used to observe if there is any improvement.

3. New processes of hemicellulose and lignin extraction can be investigated to minimise the cost of the extraction process, as these extractions require absolute ethanol, affecting the cost-benefit analysis on an industrial scale.

4. Produced biochar can further be modified to nanotubes, nanosheets, and metal-organic frameworks to synthesize more new types of aerogels with more diverse applications.

5. The metabolic pathways of bacteria can be studied and engineered to enhance the bioremediation efficiency.

6. Column studies and rotary packed bed studies can be performed to further optimise the removal process.

7. Simulation of the experiments using different software (ProsimDAC, Protox-II) can be done to understand the processes in more details for large scale applications.

REFERENCE

Abarca-Rivas, C., Martín-Garcia, A., Riu-Aumatell, M., Bidon-Chanal, A., & López-Tamames, E. (2023). Effect of fermentation temperature on oenological parameters and volatile compounds in wine. *BIO Web of Conferences*, *56*, 02034.

Abd El-Rahim, W. M., El-Ardy, O. A. M., & Mohammad, F. H. A. (2009). The effect of pH on bioremediation potential for the removal of direct violet textile dye by Aspergillus niger. *Desalination*, *249*(3), 1206–1211.

Abebe, B., Murthy, H. C. A., & Amare, E. (2018). Summary on adsorption and photocatalysis for pollutant remediation: mini review. *Journal of Encapsulation and Adsorption Sciences*, *8*(4), 225–255.

Adamu, G. D., Shuaibu, H. Y., Maharaz, M. N., Chifu, E. N., Silikwa, N. W., Lariski, F. M., Zarma, S. S., Dankawu, U. M., & Benedict, J. N. (2020). Elemental analysis of rice husk using X-ray fluorescence techniques–a case study of Jigawa State, Nigeria. *Dutse Journal of Pure and Applied Sciences*, *7*(4b).

Adegoke, C. O., & Mohammed, T. I. (2002). Investigation of sawdust briquette as high grade fuel. *West Ind. J. Engin*, *25*(1), 1–8.

Adegoke, K. A., & Bello, O. S. (2015). Dye sequestration using agricultural wastes as adsorbents. *Water Resources and Industry*, *12*, 8–24.

Adewuyi, Y. G. (2005). Sonochemistry in environmental remediation. 1. Combinative and hybrid sonophotochemical oxidation processes for the treatment of pollutants in water. *Environmental Science & Technology*, *39*(10), 3409–3420.

Aftab, A., Ismail, A. R., Ibupoto, Z. H., Akeiber, H., & Malghani, M. G. K. (2017). Nanoparticles based drilling muds a solution to drill elevated temperature wells: A review. *Renewable and Sustainable Energy Reviews*, *76*, 1301–1313.

Agabo-García, C., Romero-García, L. I., Álvarez-Gallego, C. J., & Blandino, A. (2023). Valorisation of the invasive alga Rugulopteryx okamurae through the production of monomeric sugars. *Applied Microbiology and Biotechnology*, *107*(5), 1971–1982.

Agbor, V. B., Cicek, N., Sparling, R., Berlin, A., & Levin, D. B. (2011). Biomass pretreatment: fundamentals toward application. *Biotechnology Advances*, *29*(6), 675–685.

Ahn, G. C., Jang, S. S., Kwak, H. J., Lee, S. R., Oh, Y. K., & Park, K. K. (2016). Characteristics of rice hulls, sawdust, wood shavings and mixture of sawdust and wood shavings, and their usefulness according to the pen location for Hanwoo cattle. *Asian-Australasian Journal of Animal Sciences*, *29*(4), 599.

Altmann, J., Sperlich, A., & Jekel, M. (2015). Integrating organic micropollutant removal into tertiary filtration: Combining PAC adsorption with advanced phosphorus removal. *Water Research*, *84*, 58–65.

Amaefule, D., Nwakaire, J., Ogbuagu, N., Anyadike, C., Ogenyi, C., Ohagwu, C., & Egbuhuzor, O. (2023). Effect of production factors on the bioethanol yield of tropical sawdust. *International Journal of Energy Research*, *2023*(1), 9983840.

Amaly, N., EL-Moghazy, A. Y., Nitin, N., Sun, G., & Pandey, P. K. (2022). Synergistic adsorption-photocatalytic degradation of tetracycline by microcrystalline cellulose composite aerogel dopped with montmorillonite hosted methylene blue. *Chemical Engineering Journal*, *430*, 133077.

Amer, H., Nypelö, T., Sulaeva, I., Bacher, M., Henniges, U., Potthast, A., & Rosenau, T. (2016). Synthesis and characterization of periodate-oxidized polysaccharides: dialdehyde xylan (DAX). *Biomacromolecules*, *17*(9), 2972–2980.

Andrew, N. E., & Gbabo, A. (2015). *The physical, proximate and ultimate analysis of rice husk briquettes produced from a vibratory block mould briquetting machine*.

Arboleda, J. C., Hughes, M., Lucia, L. A., Laine, J., Ekman, K., & Rojas, O. J. (2013). Soy protein–nanocellulose composite aerogels. *Cellulose*, *20*, 2417–2426.

Aydar, A. Y. (2018). Utilization of response surface methodology in optimization of extraction of plant materials. *Statistical Approaches with Emphasis on Design of Experiments Applied to Chemical Processes*, *73690*, 157–169.

Azhar, S. H. M., Abdulla, R., Jambo, S. A., Marbawi, H., Gansau, J. A., Faik, A. A. M., & Rodrigues, K. F. (2017). Yeasts in sustainable bioethanol production: A review. *Biochemistry and Biophysics Reports*, *10*, 52–61.

Baby, R., Saifullah, B., & Hussein, M. Z. (2019). Palm Kernel Shell as an effective adsorbent for the treatment of heavy metal contaminated water. *Scientific Reports*, *9*(1), 18955.

Badawy, A. A., Ibrahim, S. M., & Essawy, H. A. (2020). Enhancing the textile dye removal from aqueous solution using cobalt ferrite nanoparticles prepared in presence of fulvic acid. *Journal of Inorganic and Organometallic Polymers and Materials*, *30*(5), 1798–1813.

Bajpai, P., & Margaritis, A. (1987). The effect of temperature and pH on ethanol production by free and immobilized cells of Kluyveromyces marxianus grown on Jerusalem artichoke extract. *Biotechnology and Bioengineering*, *30*(2), 306–313.

Bani-Atta, S. A. (2022). Potassium permanganate dye removal from synthetic wastewater using a novel, low-cost adsorbent, modified from the powder of Foeniculum vulgare seeds. *Scientific Reports*, *12*(1), 4547.

Banta, M. T. A., & De Leon, R. L. (2018). Parametric study of rice husk torrefaction for the development of sustainable solid fuel. *Int. J. Smart Grid Clean Energy*, *7*, 207–217.

Baumann, T. F., Gash, A. E., Chinn, S. C., Sawvel, A. M., Maxwell, R. S., & Satcher, J. H. (2005). Synthesis of high-surface-area alumina aerogels without the use of alkoxide precursors. *Chemistry of Materials*, *17*(2), 395–401.

Bellahsen, N., Varga, G., Halyag, N., Kertész, S., Tombácz, E., & Hodúr, C. (2021). Pomegranate peel as a new low-cost adsorbent for ammonium removal. *International Journal of Environmental Science and Technology*, *18*, 711–722.

Bennion, D. B., Thomas, F. B., Jamaluddin, A. M. M., & Ma, T. (2000). Using underbalanced drilling to reduce invasive formation damage and improve well productivity-an update. *Journal of Canadian Petroleum Technology*, *39*(07).

Bhattacharyya, S., Bhattacharjee, C., & Datta, S. (2011). Increasing the extraction of total reducing sugar (TRS) from wheat straw through sonication treatment after dilute acid hydrolysis. *Cellulose*, *32*, 0–5.

Bhattacharyya, S., Chakraborty, S., Datta, S., Drioli, E., & Bhattacharjee, C. (2013). Production of total reducing sugar (TRS) from acid hydrolysed potato peels by sonication and its optimization. *Environmental Technology*, *34*(9), 1077–1084.

Bhattacharyya, S., Dutta, S., Datta, S., & Bhattacharjee, C. (2012). Improve the Recovery of Fermentable Sugar from Rice Straw by Sonication and Its Mathematical Modeling. *Journal of The Institution of Engineers (India): Series E*, *93*, 37–43.

Bhuvaneshwari, S., Hettiarachchi, H., & Meegoda, J. N. (2019). Crop residue burning in India: policy challenges and potential solutions. *International Journal of Environmental Research and Public Health*, *16*(5), 832.

Bi, H., Yin, Z., Cao, X., Xie, X., Tan, C., Huang, X., Chen, B., Chen, F., Yang, Q., & Bu, X. (2013). Carbon fiber aerogel made from raw cotton: a novel, efficient and recyclable sorbent for oils and organic solvents. *Advanced Materials*, *25*(41), 5916–5921.

Biesmans, G., Randall, D., Francais, E., & Perrut, M. (1998). Polyurethane-based organic aerogels' thermal performance. *Journal of Non-Crystalline Solids*, *225*, 36–40.

Bigall, N. C., Herrmann, A.-K., Vogel, M., Rose, M., Simon, P., Carrillo-Cabrera, W., Dorfs, D., Kaskel, S., Gaponik, N., & Eychmüller, A. (2009). Hydrogels and aerogels from noble metal nanoparticles. *Angew. Chem., Int. Ed*, *48*(51), 9731–9734.

Binder, J. B., Blank, J. J., Cefali, A. V, & Raines, R. T. (2010). Synthesis of furfural from xylose and xylan. *ChemSusChem*, *3*(11), 1268.

Briscoe, J. (2005). *India's water economy, bracing for a turbulent future*.

Brodin, I., Sjöholm, E., & Gellerstedt, G. (2009). *Kraft lignin as feedstock for chemical products: The effects of membrane filtration*.

Burachevskaya, M., Minkina, T., Bauer, T., Lobzenko, I., Fedorenko, A., Mazarji, M., Sushkova, S., Mandzhieva, S., Nazarenko, A., & Butova, V. (2023). Fabrication of biochar derived from different types of feedstocks as an efficient adsorbent for soil heavy metal removal. *Scientific Reports*, *13*(1), 2020.

Burgess, R. M., Ho, K. T., Brack, W., & Lamoree, M. (2013). Effects-directed analysis (EDA) and toxicity identification evaluation (TIE): Complementary but different

approaches for diagnosing causes of environmental toxicity. *Environmental Toxicology and Chemistry*, *32*(9), 1935–1945.

Bussemaker, M. J., Xu, F., & Zhang, D. (2013). Manipulation of ultrasonic effects on lignocellulose by varying the frequency, particle size, loading and stirring. *Bioresource Technology*, *148*, 15–23.

Bussemaker, M. J., & Zhang, D. (2013). Effect of ultrasound on lignocellulosic biomass as a pretreatment for biorefinery and biofuel applications. *Industrial & Engineering Chemistry Research*, *52*(10), 3563–3580.

Butt, W. A., Gupta, K., & Jha, J. N. (2016). Strength behavior of clayey soil stabilized with saw dust ash. *International Journal of Geo-Engineering*, *7*, 1–9.

Caenn, R., & Chillingar, G. V. (1996). Drilling fluids: State of the art. *Journal of Petroleum Science and Engineering*, *14*(3–4), 221–230.

Cao, Y., & Tan, H. (2004). Structural characterization of cellulose with enzymatic treatment. *Journal of Molecular Structure*, *705*(1–3), 189–193.

Casas, A., Alonso, M. V., Oliet, M., Rojo, E., & Rodríguez, F. (2012). FTIR analysis of lignin regenerated from Pinus radiata and Eucalyptus globulus woods dissolved in imidazolium-based ionic liquids. *Journal of Chemical Technology & Biotechnology*, *87*(4), 472–480.

Chandrasekhar, S., Pramada, P. N., & Majeed, J. (2006). Effect of calcination temperature and heating rate on the optical properties and reactivity of rice husk ash. *Journal of Materials Science*, *41*, 7926–7933.

Chaturvedi, T., Hulkko, L. S. S., Fredsgaard, M., & Thomsen, M. H. (2022). Extraction, isolation, and purification of value-added chemicals from lignocellulosic biomass. *Processes*, *10*(9), 1752.

Chen, H., Ferrari, C., Angiuli, M., Yao, J., Raspi, C., & Bramanti, E. (2010). Qualitative and quantitative analysis of wood samples by Fourier transform infrared spectroscopy and multivariate analysis. *Carbohydrate Polymers*, *82*(3), 772–778.

Chen, H., & Yokochi, A. (2000). X-ray diffractometric study of microcrystallite size of naturally colored cottons. *Journal of Applied Polymer Science*, *76*(9), 1466–1471.

Chen, L., Lu, H., Jiang, X., Qu, N., Hasi, Q., Zhang, Y., Zhang, B., & Jiang, S. (2024). Microorganisms immobilized hydroxyethyl cellulose/luffa composite sponge for selective adsorption and biodegradation of oils in wastewater. *International Journal of Biological Macromolecules*, *277*, 133477.

Chen, W., Yu, H., Li, Q., Liu, Y., & Li, J. (2011). Ultralight and highly flexible aerogels with long cellulose I nanofibers. *Soft Matter*, *7*(21), 10360–10368.

Chikri, R., Elhadiri, N., Benchanaa, Mjj., & El Maguana, Y. (2020). Efficiency of sawdust as low-cost adsorbent for dyes removal. *Journal of Chemistry*, *2020*(1), 8813420.

Choudhary, A. (2017). Removal of oil from seawater using charcoal and rice hull. *IOP Conference Series: Materials Science and Engineering*, *263*(3), 032007.

Chowdhury, S., Mishra, R., Saha, P., & Kushwaha, P. (2011). Adsorption thermodynamics, kinetics and isosteric heat of adsorption of malachite green onto chemically modified rice husk. *Desalination*, *265*(1–3), 159–168.

Costa-Júnior, E. S., Barbosa-Stancioli, E. F., Mansur, A. A. P., Vasconcelos, W. L., & Mansur, H. S. (2009). Preparation and characterization of chitosan/poly (vinyl alcohol) chemically crosslinked blends for biomedical applications. *Carbohydrate Polymers*, *76*(3), 472–481.

Crestini, C., Lange, H., Sette, M., & Argyropoulos, D. S. (2017). On the structure of softwood kraft lignin. *Green Chemistry*, *19*(17), 4104–4121.

Crini, G. (2006). Non-conventional low-cost adsorbents for dye removal: a review. *Bioresource Technology*, *97*(9), 1061–1085.

Crini, G., & Lichtfouse, E. (2019). Advantages and disadvantages of techniques used for wastewater treatment. *Environmental Chemistry Letters*, *17*, 145–155.

da Rocha, H. D., Reis, E. S., Ratkovski, G. P., da Silva, R. J., Gorza, F. D. S., Pedro, G. C., & de Melo, C. P. (2020). Use of PMMA/(rice husk ash)/polypyrrole membranes for the removal of dyes and heavy metal ions. *Journal of the Taiwan Institute of Chemical Engineers*, *110*, 8–20.

da Silva Lacerda, V., López-Sotelo, J. B., Correa-Guimarães, A., Hernández-Navarro, S., Sánchez-Bascones, M., Navas-Gracia, L. M., Martín-Ramos, P., Pérez-Lebeña, E., & Martín-Gil, J. (2015). A kinetic study on microwave-assisted conversion of

cellulose and lignocellulosic waste into hydroxymethylfurfural/furfural. *Bioresource Technology*, *180*, 88–96.

Daffalla, S. B., Mukhtar, H., & Shaharun, M. S. (2020). Preparation and characterization of rice husk adsorbents for phenol removal from aqueous systems. *PloS One*, *15*(12), e0243540.

Dalkhsuren, D., Iwabuchi, K., Itoh, T., Narita, T., Piash, M. I., Nachin, B., & Sukhbaatar, G. (2023). Effects of ash composition and combustion temperature on reduced particulate matter emission by biomass carbonization. *BioEnergy Research*, *16*(3), 1629–1638.

Das, K., Ray, D., Bandyopadhyay, N. R., & Sengupta, S. (2010). Study of the properties of microcrystalline cellulose particles from different renewable resources by XRD, FTIR, nanoindentation, TGA and SEM. *Journal of Polymers and the Environment*, *18*, 355–363.

Das, L., Sengupta, S., Das, P., Bhowal, A., & Bhattacharjee, C. (2021). Experimental and Numerical modeling on dye adsorption using pyrolyzed mesoporous biochar in Batch and fixed-bed column reactor: Isotherm, Thermodynamics, Mass transfer, Kinetic analysis. *Surfaces and Interfaces*, *23*, 100985.

de Farias Silva, C. E., da Gama, B. M. V., da Silva Gonçalves, A. H., Medeiros, J. A., & de Souza Abud, A. K. (2020). Basic-dye adsorption in albedo residue: Effect of pH, contact time, temperature, dye concentration, biomass dosage, rotation and ionic strength. *Journal of King Saud University-Engineering Sciences*, *32*(6), 351–359.

De Fraiture, C., Giordano, M., & Liao, Y. (2008). Biofuels and implications for agricultural water use: blue impacts of green energy. *Water Policy*, *10*(S1), 67–81.

Delhomme, C., Weuster-Botz, D., & Kühn, F. E. (2009). Succinic acid from renewable resources as a C 4 building-block chemical—a review of the catalytic possibilities in aqueous media. *Green Chemistry*, *11*(1), 13–26.

Dimos, K., Paschos, T., Louloudi, A., Kalogiannis, K. G., Lappas, A. A., Papayannakos, N., Kekos, D., & Mamma, D. (2019). Effect of various pretreatment methods on bioethanol production from cotton stalks. *Fermentation*, *5*(1), 5.

Du, A., Zhou, B., Zhang, Z., & Shen, J. (2013). A special material or a new state of matter: a review and reconsideration of the aerogel. *Materials*, *6*(3), 941–968.

Ebringerová, A., Hromádková, Z., & Heinze, T. (2005). Hemicellulose. *Polysaccharides I: Structure, Characterization and Use*, 1–67.

Edokpayi, J. N., Odiyo, J. O., & Durowoju, O. S. (2017). Impact of wastewater on surface water quality in developing countries: a case study of South Africa. *Water Quality*, *10*(66561), 10–5772.

El-Mekkawi, S. A., Abdo, S. M., Samhan, F. A., & Ali, G. H. (2019). Optimization of some fermentation conditions for bioethanol production from microalgae using response surface method. *Bulletin of the National Research Centre*, *43*, 1–8.

Evate, N., Ngwasiri, P. N., Ambindei, W. A., Ngwabie, N. M., & Ngassoum, M. B. (2023). Effect of Lignocellulose Waste-Biomass Pretreatment of the Peels of Musa acuminata (Banana) and Ananas comosus (Pineapple) on the Production of Bioethanol via Solid-State Fermentation. *Open Access Library Journal*, *10*(8), 1–28.

Feng, L., Cao, M., Ma, X., Zhu, Y., & Hu, C. (2012). Superparamagnetic high-surface-area Fe3O4 nanoparticles as adsorbents for arsenic removal. *Journal of Hazardous Materials*, *217*, 439–446.

Ferrero, F. (2007). Dye removal by low cost adsorbents: hazelnut shells in comparison with wood sawdust. *Journal of Hazardous Materials*, *142*(1–2), 144–152.

Foner, H. A., & Adan, N. (1983). The characterization of papers by X-ray diffraction (XRD): measurement of cellulose crystallinity and determination of mineral composition. *Journal of the Forensic Science Society*, *23*(4), 313–321.

Frank, R. G., Conti, R. M., & Goldman, H. H. (2005). Mental health policy and psychotropic drugs. *The Milbank Quarterly*, *83*(2), 271–298.

Fricke, J., & Emmerling, A. (2005). Aerogels—Preparation, properties, applications. *Chemistry, Spectroscopy and Applications of Sol-Gel Glasses*, 37–87.

Gao, M., Wang, Z., Yang, C., Ning, J., Zhou, Z., & Li, G. (2019). Novel magnetic graphene oxide decorated with persimmon tannins for efficient adsorption of

malachite green from aqueous solutions. *Colloids and Surfaces A: Physicochemical and Engineering Aspects*, *566*, 48–57.

Garside, P., & Wyeth, P. (2003). Identification of cellulosic fibres by FTIR spectroscopy-thread and single fibre analysis by attenuated total reflectance. *Studies in Conservation*, *48*(4), 269–275.

Gheorghe, I. F., & Ion, B. (2011). The effects of air pollutants on vegetation and the role of vegetation in reducing atmospheric pollution. *The Impact of Air Pollution on Health, Economy, Environment and Agricultural Sources*, *29*, 241–280.

Ghoreishi, S. M., & Haghighi, R. (2003). Chemical catalytic reaction and biological oxidation for treatment of non-biodegradable textile effluent. *Chemical Engineering Journal*, *95*(1–3), 163–169.

Ghosh, S., Chakraborty, P., Bhowal, A., Manna, S., & Das, P. (2024). Synthesis of polymeric aerogels with different fillers and their application for the removal of emerging pollutants: a comparative study. *Biomass Conversion and Biorefinery*, 1–14.

Ghosh, S., Roy, S., & Das, P. (2025). Beyond waste: waste rice husk to value-added products using sonic waves and chemical treatment and principal component analysis of extraction. *Biomass Conversion and Biorefinery*, *15*(7), 11217–11229.

Ghosh, S., Sarkar, S., Mukherjee, S., Ganguly, S., & Das, P. (2024). Silica-coated cellulose using Shorea robusta sawdust biomass and its application for methylene blue dye removal from aqueous solution. *Biomass Conversion and Biorefinery*, 1–13.

Gilliom, R. J. (2007). *Pesticides in US streams and groundwater*. ACS Publications.

Gondim, R. S., Muniz, C. R., Lima, C. E. P., & SANTOS, C. L. A. D. O. S. (2018). Explaining the water-holding capacity of biochar by scanning electron microscope images. *Revista Caatinga*, *31*, 972–979.

Goudarzi, A., Lin, L.-T., & Ko, F. K. (2014). X-ray diffraction analysis of kraft lignins and lignin-derived carbon nanofibers. *Journal of Nanotechnology in Engineering and Medicine*, *5*(2), 021006.

Gray, K. A., Zhao, L., & Emptage, M. (2006). Bioethanol. *Current Opinion in Chemical Biology*, *10*(2), 141–146.

Gui, X., Wei, J., Wang, K., Cao, A., Zhu, H., Jia, Y., Shu, Q., & Wu, D. (2010). Carbon nanotube sponges. *Advanced Materials*, *22*(5), 617–621.

Gul, O., Saricaoglu, F. T., Atalar, I., Gul, L. B., Tornuk, F., & Simsek, S. (2023). Structural characterization, technofunctional and rheological properties of sesame proteins treated by high-intensity ultrasound. *Foods*, *12*(9), 1791.

Gupta, A. K., Mohanty, S., & Nayak, S. K. (2015). Preparation and characterization of lignin nanofibre by electrospinnig technique. *Int. J. Sci. Eng. Appl. Sci*, *1*(3), 184–190.

Gupta, R. (2012). *Causes of emissions from agricultural residue burning in north-west India: evaluation of a technology policy response*. The Institute of Development Studies and Partner Organisations.

Gupta, V. Ks. (2009). Application of low-cost adsorbents for dye removal–a review. *Journal of Environmental Management*, *90*(8), 2313–2342.

Hackmann, T. J., & Firkins, J. L. (2015). Maximizing efficiency of rumen microbial protein production. *Frontiers in Microbiology*, *6*, 465.

Haimer, E., Wendland, M., Potthast, A., Henniges, U., Rosenau, T., & Liebner, F. (2010). Controlled precipitation and purification of hemicellulose from DMSO and DMSO/water mixtures by carbon dioxide as anti-solvent. *The Journal of Supercritical Fluids*, *53*(1–3), 121–130.

Hammouda, L. Ben, Mejri, I., Younes, M. K., & Ghorbel, A. (2011). ZrO 2 aerogels. *Aerogels Handbook*, 127–143.

Hamza, W., Dammak, N., Hadjltaief, H. B., Eloussaief, M., & Benzina, M. (2018). Sono-assisted adsorption of Cristal Violet dye onto Tunisian Smectite Clay: Characterization, kinetics and adsorption isotherms. *Ecotoxicology and Environmental Safety*, *163*, 365–371.

Han, C., Wang, M., Ren, Y., Zhang, L., Ji, Y., Zhu, W., Song, Y., & He, J. (2021). Characterization of pruned tea branch biochar and the mechanisms underlying its adsorption for cadmium in aqueous solution. *RSC Advances*, *11*(43), 26832–26843.

He, S., Huang, Y., Chen, G., Feng, M., Dai, H., Yuan, B., & Chen, X. (2019). Effect of heat treatment on hydrophobic silica aerogel. *Journal of Hazardous Materials*, *362*, 294–302.

Heinze, T., & Liebert, T. (2012). Celluloses and polyoses/hemicelluloses. *Polymer Science: A Comprehensive Reference*, 83–152.

Hema, M., Selvasekarapandian, S., Arunkumar, D., Sakunthala, A., & Nithya, H. (2009). FTIR, XRD and ac impedance spectroscopic study on PVA based polymer electrolyte doped with NH4X (X= Cl, Br, I). *Journal of Non-Crystalline Solids*, *355*(2), 84–90.

Hirashima, H. (2011). Preparation of TiO 2 aerogels-like materials under ambient pressure. *Aerogels Handbook*, 145–153.

Hossen, M. R., Talbot, M. W., Kennard, R., Bousfield, D. W., & Mason, M. D. (2020). A comparative study of methods for porosity determination of cellulose based porous materials. *Cellulose*, *27*, 6849–6860.

Hube, S., Eskafi, M., Hrafnkelsdóttir, K. F., Bjarnadóttir, B., Bjarnadóttir, M. Á., Axelsdóttir, S., & Wu, B. (2020). Direct membrane filtration for wastewater treatment and resource recovery: A review. *Science of the Total Environment*, *710*, 136375.

Hurley, J. R. (1959). *Cement compositions and process of cementing wells*. Google Patents.

Ibrahim, M. M., Agblevor, F. A., & El-Zawawy, W. K. (2010). Isolation and characterization of cellulose and lignin from steam-exploded lignocellulosic biomass. *BioResources*, *5*(1).

Ingale, S. V, Wagh, P. B., Tripathi, A. K., Kamble, V. S., Kumar, R., & Gupta, S. C. (2011). Physico-chemical properties of silica aerogels prepared from TMOS/MTMS mixtures. *Journal of Porous Materials*, *18*, 567–572.

Iqbal, J., Metosh-Dickey, C., & Portier, R. J. (2007). Temperature effects on bioremediation of PAHs and PCP contaminated south Louisiana soils: a laboratory mesocosm study. *Journal of Soils and Sediments*, *7*, 153–158.

Javadi, A., Zheng, Q., Payen, F., Javadi, A., Altin, Y., Cai, Z., Sabo, R., & Gong, S. (2013). Polyvinyl alcohol-cellulose nanofibrils-graphene oxide hybrid organic aerogels. *ACS Applied Materials & Interfaces*, *5*(13), 5969–5975.

Jaward, F. M., Alegria, H. A., Galindo Reyes, J. G., & Hoare, A. (2012). Levels of PAHs in the waters, sediments, and shrimps of Estero de Urias, an estuary in Mexico, and their toxicological effects. *The Scientific World Journal*, *2012*(1), 687034.

Jewell, J. (2011). Ready for nuclear energy?: An assessment of capacities and motivations for launching new national nuclear power programs. *Energy Policy*, *39*(3), 1041–1055.

Jia, Y., Li, Z., Wang, Y., Wang, X., Lou, C., Xiao, B., & Lim, M. (2021). Visualization of combustion phases of biomass particles: Effects of fuel properties. *ACS Omega*, *6*(42), 27702–27710.

Jiang, Z., Hu, D., Zhao, Z., Yi, Z., Chen, Z., & Yan, K. (2021). Mini-review on the synthesis of furfural and levulinic acid from lignocellulosic biomass. *Processes*, *9*(7), 1234.

Kačuráková, M., Smith, A. C., Gidley, M. J., & Wilson, R. H. (2002). Molecular interactions in bacterial cellulose composites studied by 1D FT-IR and dynamic 2D FT-IR spectroscopy. *Carbohydrate Research*, *337*(12), 1145–1153.

Kai, D., Tan, M. J., Chee, P. L., Chua, Y. K., Yap, Y. L., & Loh, X. J. (2016). Towards lignin-based functional materials in a sustainable world. *Green Chemistry*, *18*(5), 1175–1200.

Kalami, S., Chen, N., Borazjani, H., & Nejad, M. (2018). Comparative analysis of different lignins as phenol replacement in phenolic adhesive formulations. *Industrial Crops and Products*, *125*, 520–528.

Kamal, S., Rehman, S., Rehman, K., Ghaffar, A., Bibi, I., Ahmed, T., Maqsood, S., Nazish, N., & Iqbal, H. M. N. (2022). Sustainable and optimized bioethanol production using mix microbial consortium of Saccharomyces cerevisiae and Candida cantarelli. *Fuel*, *314*, 122763.

Kant, Y., Chauhan, P., Natwariya, A., Kannaujiya, S., & Mitra, D. (2022). Long term influence of groundwater preservation policy on stubble burning and air pollution over North-West India. *Scientific Reports*, *12*(1), 2090.

Karthäuser, J., Biziks, V., Mai, C., & Militz, H. (2021). Lignin and lignin-derived compounds for wood applications—A review. *Molecules*, *26*(9), 2533.

Katheresan, V., Kansedo, J., & Lau, S. Y. (2018). Efficiency of various recent wastewater dye removal methods: A review. *Journal of Environmental Chemical Engineering*, *6*(4), 4676–4697.

Khasri, A., Jamir, M. R. M., Ahmad, A. A., & Ahmad, M. A. (2021). Adsorption of Remazol Brilliant Violet 5R dye from aqueous solution onto melunak and rubberwood sawdust based activated carbon: interaction mechanism, isotherm, kinetic and thermodynamic properties. *Desalination and Water Treatment*, *216*, 401–411.

Kim, C.-Y., Lee, J.-K., & Kim, B.-I. (2008). Synthesis and pore analysis of aerogel–glass fiber composites by ambient drying method. *Colloids and Surfaces A: Physicochemical and Engineering Aspects*, *313*, 179–182.

Kim, S. H., Lee, C. M., & Kafle, K. (2013). Characterization of crystalline cellulose in biomass: Basic principles, applications, and limitations of XRD, NMR, IR, Raman, and SFG. *Korean Journal of Chemical Engineering*, *30*, 2127–2141.

Kistler, S. S. (1931). Coherent expanded aerogels and jellies. *Nature*, *127*(3211), 741.

Kondo, T. (2005). Hydrogen bonds in cellulose and cellulose derivatives. *Polysaccharides: Structural Diversity and Functional Versatility*, 69–98.

Kong, H., Chen, Y., Yang, G., Liu, B., Guo, L., Wang, Y., Zhou, X., & Wei, G. (2022). Two-dimensional material-based functional aerogels for treating hazards in the environment: synthesis, functional tailoring, applications, and sustainability analysis. *Nanoscale Horizons*, *7*(2), 112–140.

Kopsahelis, N., Agouridis, N., Bekatorou, A., & Kanellaki, M. (2007). Comparative study of spent grains and delignified spent grains as yeast supports for alcohol production from molasses. *Bioresource Technology*, *98*(7), 1440–1447.

Korhonen, J. T., Kettunen, M., Ras, R. H. A., & Ikkala, O. (2011). Hydrophobic nanocellulose aerogels as floating, sustainable, reusable, and recyclable oil absorbents. *ACS Applied Materials & Interfaces*, *3*(6), 1813–1816.

Kostryukov, S. G., Matyakubov, H. B., Masterova, Y. Y., Kozlov, A. S., Pryanichnikova, M. K., Pynenkov, A. A., & Khluchina, N. A. (2023). Determination of lignin, cellulose, and hemicellulose in plant materials by FTIR spectroscopy. *Journal of Analytical Chemistry*, *78*(6), 718–727.

Koti, S., Govumoni, S. P., Gentela, J., & Venkateswar Rao, L. (2016). Enhanced bioethanol production from wheat straw hemicellulose by mutant strains of pentose fermenting organisms Pichia stipitis and Candida shehatae. *Springerplus*, *5*, 1–9.

Krishnamachari, P., Hashaikeh, R., & Tiner, M. (2011). Modified cellulose morphologies and its composites; SEM and TEM analysis. *Micron*, *42*(8), 751–761.

Krivoshein, P. K., Volkov, D. S., Rogova, O. B., & Proskurnin, M. A. (2022). FTIR photoacoustic and ATR spectroscopies of soils with aggregate size fractionation by dry sieving. *ACS Omega*, *7*(2), 2177–2197.

Kumar, P., Kumar, S., & Joshi, L. (2015). *Socioeconomic and environmental implications of agricultural residue burning: A case study of Punjab, India*. Springer Nature.

Lankin, A. V, Kreslavski, V. D., Khudyakova, A. Y., Zharmukhamedov, S. K., & Allakhverdiev, S. I. (2014). Effect of naphthalene on photosystem 2 photochemical activity of pea plants. *Biochemistry (Moscow)*, *79*, 1216–1225.

Lavoine, N., Desloges, I., Dufresne, A., & Bras, J. (2012). Microfibrillated cellulose–Its barrier properties and applications in cellulosic materials: A review. *Carbohydrate Polymers*, *90*(2), 735–764.

Lee, H.-J., Song, J.-H., & Kim, J.-H. (1998). Synthesis of resorcinol/formaldehyde gel particles by the sol-emulsion–gel technique. *Materials Letters*, *37*(4–5), 197–200.

Li, W., Gao, S., Wu, L., Qiu, S., Guo, Y., Geng, X., Chen, M., Liao, S., Zhu, C., & Gong, Y. (2013). High-density three-dimension graphene macroscopic objects for high-capacity removal of heavy metal ions. *Scientific Reports*, *3*(1), 2125.

Li, Y.-Q., Samad, Y. A., Polychronopoulou, K., Alhassan, S. M., & Liao, K. (2014). Carbon aerogel from winter melon for highly efficient and recyclable oils and

organic solvents absorption. *ACS Sustainable Chemistry & Engineering*, *2*(6), 1492–1497.

Liang, C. Y., & Marchessault, R. H. (1959). Infrared spectra of crystalline polysaccharides. II. Native celluloses in the region from 640 to 1700 cm.− 1. *Journal of Polymer Science*, *39*(135), 269–278.

Liang, T., & Wang, L. (2017). Thermal treatment of poplar hemicelluloses at 180 to 220 C under nitrogen atmosphere. *BioResources*, *12*(1), 1128–1135.

Lin, C., Nguyen, K. A., Vu, C. T., Senoro, D., & Villanueva, M. C. (2017). Contamination levels and potential sources of organic pollution in an Asian river. *Water Science and Technology*, *76*(9), 2434–2444.

Lin, Y., Sun, W., Wang, G., Chen, H., Pei, X., Jin, Y., Yang, S.-T., & Wang, M. (2022). Production of Butyric Acid from Hydrolysate of Rice Husk Treated by Alkali and Enzymes in Immobilized Fermentation by Clostridium tyrobutyricum CtΔ pta. *Fermentation*, *8*(10), 531.

Linhares, T., de Amorim, M. T. P., & Durães, L. (2019). Silica aerogel composites with embedded fibres: a review on their preparation, properties and applications. *Journal of Materials Chemistry A*, *7*(40), 22768–22802.

Liu, H., Sha, W., Cooper, A. T., & Fan, M. (2009). Preparation and characterization of a novel silica aerogel as adsorbent for toxic organic compounds. *Colloids and Surfaces A: Physicochemical and Engineering Aspects*, *347*(1–3), 38–44.

Liu, S., & Suflita, J. M. (1993). Ecology and evolution of microbial populations for bioremediation. *Trends in Biotechnology*, *11*(8), 344–352.

Liu, X., Shan, Y., Zhang, S., Kong, Q., & Pang, H. (2023). Application of metal organic framework in wastewater treatment. *Green Energy & Environment*, *8*(3), 698–721.

Liu, Y., He, Z., & Uchimiya, M. (2015). Comparison of biochar formation from various agricultural by-products using FTIR spectroscopy. *Modern Applied Science*, *9*(4), 246.

Livage, J., Henry, M., & Sanchez, C. (1988). Sol-gel chemistry of transition metal oxides. *Progress in Solid State Chemistry*, *18*(4), 259–341.

Louis, A. C. F., & Venkatachalam, S. (2020). Energy efficient process for valorization of corn cob as a source for nanocrystalline cellulose and hemicellulose production. *International Journal of Biological Macromolecules*, *163*, 260–269.

Luyten, J., Mullens, S., & Thijs, I. (2010). Designing with pores-synthesis and applications. *KONA Powder and Particle Journal*, *28*, 131–142.

Ma, C. M., Hong, G. B., & Wang, Y. K. (2020). Performance evaluation and optimization of dyes removal using rice bran-based magnetic composite adsorbent. *Materials*, *13*(12), 2764.

Ma, Z., Sun, Q., Ye, J., Yao, Q., & Zhao, C. (2016). Study on the thermal degradation behaviors and kinetics of alkali lignin for production of phenolic-rich bio-oil using TGA–FTIR and Py–GC/MS. *Journal of Analytical and Applied Pyrolysis*, *117*, 116–124.

Mahmoud, H. R., Ibrahim, S. M., & El-Molla, S. A. (2016). Textile dye removal from aqueous solutions using cheap MgO nanomaterials: adsorption kinetics, isotherm studies and thermodynamics. *Advanced Powder Technology*, *27*(1), 223–231.

Maleki, H. (2016). Recent advances in aerogels for environmental remediation applications: A review. *Chemical Engineering Journal*, *300*, 98–118.

Malfait, W. J., Zhao, S., Verel, R., Iswar, S., Rentsch, D., Fener, R., Zhang, Y., Milow, B., & Koebel, M. M. (2015). Surface chemistry of hydrophobic silica aerogels. *Chemistry of Materials*, *27*(19), 6737–6745.

Mallick, S. (2019). Biodegradation of acenaphthene by Sphingobacterium sp. strain RTSB involving trans-3-carboxy-2-hydroxybenzylidenepyruvic acid as a metabolite. *Chemosphere*, *219*, 748–755.

Mannaa, M., & Kim, K. D. (2018). Effect of temperature and relative humidity on growth of Aspergillus and Penicillium spp. and biocontrol activity of Pseudomonas protegens AS15 against aflatoxigenic Aspergillus flavus in stored rice grains. *Mycobiology*, *46*(3), 287–295.

Mansur, H. S., Oréfice, R. L., & Mansur, A. A. P. (2004). Characterization of poly (vinyl alcohol)/poly (ethylene glycol) hydrogels and PVA-derived hybrids by small-angle X-ray scattering and FTIR spectroscopy. *Polymer*, *45*(21), 7193–7202.

Martini, S., Afroze, S., & Roni, K. A. (2020). Modified eucalyptus bark as a sorbent for simultaneous removal of COD, oil, and Cr (III) from industrial wastewater. *Alexandria Engineering Journal*, *59*(3), 1637–1648.

Mason, T. J. (2002). Uses of power ultrasound in chemistry and processing. *Applied Sonochemistry*.

Mathurasa, L., & Damrongsiri, S. (2018). Low cost andÂ easy rice husk modifcation toÂ efciently enhance ammonium andÂ nitrate adsorption. *International Journal of Recycling of Organic Waste in Agriculture*, *7*(2).

Menzel, N., Ortel, E., Kraehnert, R., & Strasser, P. (2012). Electrocatalysis using porous nanostructured materials. *ChemPhysChem*, *13*(6), 1385–1394.

Mihelcic, J. R., & Luthy, R. G. (1988). Microbial degradation of acenaphthene and naphthalene under denitrification conditions in soil-water systems. *Applied and Environmental Microbiology*, *54*(5), 1188–1198.

Mishra, U. C. (2004). Environmental impact of coal industry and thermal power plants in India. *Journal of Environmental Radioactivity*, *72*(1–2), 35–40.

Mo, J., Yang, Q., Zhang, N., Zhang, W., Zheng, Y., & Zhang, Z. (2018). A review on agro-industrial waste (AIW) derived adsorbents for water and wastewater treatment. *Journal of Environmental Management*, *227*, 395–405.

Moayedi, H., Aghel, B., Abdullahi, M. M., Nguyen, H., & Rashid, A. S. A. (2019). Applications of rice husk ash as green and sustainable biomass. *Journal of Cleaner Production*, *237*, 117851.

Mohapatra, B., & Phale, P. S. (2021). Microbial degradation of naphthalene and substituted naphthalenes: metabolic diversity and genomic insight for bioremediation. *Frontiers in Bioengineering and Biotechnology*, *9*, 602445.

Mohapatra, S., Padhy, S., Mohapatra, P. K. Das, & Thatoi, H. N. (2018). Enhanced reducing sugar production by saccharification of lignocellulosic biomass, Pennisetum species through cellulase from a newly isolated Aspergillus fumigatus. *Bioresource Technology*, *253*, 262–272.

Montoya-Escobar, N., Ospina-Acero, D., Velásquez-Cock, J. A., Gómez-Hoyos, C., Serpa Guerra, A., Gañan Rojo, P. F., Vélez Acosta, L. M., Escobar, J. P., Correa-

Hincapié, N., & Triana-Chávez, O. (2022). Use of fourier series in X-ray diffraction (XRD) analysis and fourier-transform infrared spectroscopy (FTIR) for estimation of crystallinity in cellulose from different sources. *Polymers*, *14*(23), 5199.

Moon, R. J., Martini, A., Nairn, J., Simonsen, J., & Youngblood, J. (2011). Cellulose nanomaterials review: structure, properties and nanocomposites. *Chemical Society Reviews*, *40*(7), 3941–3994.

Mtibe, A., Linganiso, L. Z., Mathew, A. P., Oksman, K., John, M. J., & Anandjiwala, R. D. (2015). A comparative study on properties of micro and nanopapers produced from cellulose and cellulose nanofibres. *Carbohydrate Polymers*, *118*, 1–8.

Mulik, S., & Sotiriou-Leventis, C. (2011). Resorcinol–formaldehyde aerogels. *Aerogels Handbook*, 215–234.

Mutuku, K. (2019). Characterization of Physical Properties of Biomass Waste Materials in Kenya for Gasification: Rice Husks and Coffee Husks. *Int. J. Eng. Res. Gen. Sci*, *7*(2), 20–25.

Nafee, S. S., Hamdalla, T. A., & Shaheen, S. A. (2017). FTIR and optical properties for irradiated PVA–GdCl3 and its possible use in dosimetry. *Phase Transitions*, *90*(5), 439–448.

Nair, S. S., Zhu, J. Y., Deng, Y., & Ragauskas, A. J. (2014). High performance green barriers based on nanocellulose. *Sustainable Chemical Processes*, *2*, 1–7.

Nandiyanto, A. B. D., Oktiani, R., & Ragadhita, R. (2019). How to read and interpret FTIR spectroscope of organic material. *Indonesian Journal of Science and Technology*, *4*(1), 97–118.

Nashiruddin, N. I., Abd Rahman, N. H., A. Rahman, R., Md. Illias, R., Ghazali, N. F., Abomoelak, B., & El Enshasy, H. A. (2022). Improved sugar recovery of alkaline pre-treated pineapple leaf fibres via enzymatic hydrolysis and its enzymatic kinetics. *Fermentation*, *8*(11), 640.

Nayak, S. K., & Mishra, P. C. (2016). Emissions from sawdust biomass and diesel blends fuels. *Energy Sources, Part A: Recovery, Utilization, and Environmental Effects*, *38*(14), 2050–2057.

Neagu, M., Grisi, F., Pulvirenti, A., Simón-Vázquez, R., García-González, C. A., & Boccia, A. C. (2023). Updated Aspects of Safety Regulations for Biomedical Applications of Aerogel Compounds—Compendia-Like Evaluation. *Safety*, *9*(4), 80.

Nguyen, M. T. (2006). The effect of temperature on the growth of the bacteria Escherichia coli DH5α. *Saint Martin's University Biology Journal*, *1*(5), 87–94.

Nguyen, N. T., Tran, N. T., Phan, T. P., Nguyen, A. T., Nguyen, M. X. T., Nguyen, N. N., Ko, Y. H., Nguyen, D. H., Van, T. T. T., & Hoang, D. (2022). The extraction of lignocelluloses and silica from rice husk using a single biorefinery process and their characteristics. *Journal of Industrial and Engineering Chemistry*, *108*, 150–158.

Nitayavardhana, S., Rakshit, S. K., Grewell, D., Van Leeuwen, J., & Khanal, S. K. (2008). Ultrasound pretreatment of cassava chip slurry to enhance sugar release for subsequent ethanol production. *Biotechnology and Bioengineering*, *101*(3), 487–496.

Nocentini, M., Pinelli, D., & Fava, F. (2000). Bioremediation of a soil contaminated by hydrocarbon mixtures: the residual concentration problem. *Chemosphere*, *41*(8), 1115–1123.

Oberoi, A. S., Philip, L., & Bhallamudi, S. M. (2015). Biodegradation of various aromatic compounds by enriched bacterial cultures: part a–monocyclic and polycyclic aromatic hydrocarbons. *Applied Biochemistry and Biotechnology*, *176*, 1870–1888.

Ong, H. K., & Sashikala, M. (2007). Identification of furfural synthesized from pentosan in rice husk. *J Trop Agric Food Sci*, *35*, 305–312.

Otero, M., & Coimbra, R. N. (2025). Polymeric Materials for Wastewater Treatment Applications. In *Polymers* (Vol. 17, Issue 4, p. 552). MDPI.

Ozaki, N., Yamauchi, T., Kindaichi, T., & Ohashi, A. (2019). Stormwater inflow loading of polycyclic aromatic hydrocarbons into urban domestic wastewater treatment plant for separate sewer system. *Water Science and Technology*, *79*(7), 1426–1436.

Pamuk, V., Yılmaz, M., & Alıcılar, A. (2001). The preparation of d-glucaric acid by oxidation of molasses in packed beds. *Journal of Chemical Technology &*

Biotechnology: International Research in Process, Environmental & Clean Technology, *76*(2), 186–190.

Pandey, J. K., Reddy, K. R., Mohanty, A. K., & Misra, M. (2014). *Handbook of Polymernanocomposites: Processing, Performance and Application* (Vol. 100). Springer.

Pandey, K. K., & Pitman, A. J. (2003). FTIR studies of the changes in wood chemistry following decay by brown-rot and white-rot fungi. *International Biodeterioration & Biodegradation*, *52*(3), 151–160.

Pandit, M. K., & Grumbine, R. E. (2012). Potential effects of ongoing and proposed hydropower development on terrestrial biological diversity in the Indian Himalaya. *Conservation Biology*, *26*(6), 1061–1071.

Paredes, L., Alfonsin, C., Allegue, T., Omil, F., & Carballa, M. (2018). Integrating granular activated carbon in the post-treatment of membrane and settler effluents to improve organic micropollutants removal. *Chemical Engineering Journal*, *345*, 79–86.

Pathak, H., Kumar, M., Molla, K. A., & Chakraborty, K. (2021). *Abiotic stresses in rice production: impacts and management.*

Pathak, S., Pant, K. K., & Kaushal, P. (2024). Analysis of naphthalene adsorption from wastewater using activated and non-activated biochar produced from bagasse. *Biomass Conversion and Biorefinery*, *14*(16), 19661–19674.

Pauly, M., & Keegstra, K. (2016). Biosynthesis of the plant cell wall matrix polysaccharide xyloglucan. *Annual Review of Plant Biology*, *67*(1), 235–259.

Peng, B. L., Dhar, N., Liu, H. L., & Tam, K. C. (2011). Chemistry and applications of nanocrystalline cellulose and its derivatives: a nanotechnology perspective. *The Canadian Journal of Chemical Engineering*, *89*(5), 1191–1206.

Peng, B., Yao, Z., Wang, X., Crombeen, M., Sweeney, D. G., & Tam, K. C. (2020). Cellulose-based materials in wastewater treatment of petroleum industry. *Green Energy & Environment*, *5*(1), 37–49.

Peng, H., Wang, N., Hu, Z., Yu, Z., Liu, Y., Zhang, J., & Ruan, R. (2012). Physicochemical characterization of hemicelluloses from bamboo (Phyllostachys pubescens Mazel) stem. *Industrial Crops and Products*, *37*(1), 41–50.

Pernyeszi, T., Farkas, R., & Kovács, J. (2019). Methylene blue adsorption study on microcline particles in the function of particle size range and temperature. *Minerals*, *9*(9), 555.

Phan, P. T., Nguyen, T. T., Nguyen, N. H., & Padungthon, S. (2019). Triamine-bearing activated rice husk ash as an advanced functional material for nitrate removal from aqueous solution. *Water Science and Technology*, *79*(5), 850–856.

Pierre, A. C., & Pajonk, G. M. (2002). Chemistry of aerogels and their applications. *Chemical Reviews*, *102*(11), 4243–4266.

Pierre, A. C., & Rigacci, A. (2011). SiO 2 aerogels. *Aerogels Handbook*, 21–45.

Prasetyo, J., Sumita, S., Okuda, N., & Park, E. Y. (2010). Response of cellulase activity in pH-controlled cultures of the filamentous fungus Acremonium cellulolyticus. *Applied Biochemistry and Biotechnology*, *162*, 52–61.

Puri, L., Hu, Y., & Naterer, G. (2024). Critical review of the role of ash content and composition in biomass pyrolysis. *Frontiers in Fuels*, *2*, 1378361.

Qaseem, M. F., Shaheen, H., & Wu, A.-M. (2021). Cell wall hemicellulose for sustainable industrial utilization. *Renewable and Sustainable Energy Reviews*, *144*, 110996.

Qi, G., Xiong, L., Li, H., Huang, Q., Luo, M., Tian, L., Chen, X., Huang, C., & Chen, X. (2019). Hydrotropic pretreatment on wheat straw for efficient biobutanol production. *Biomass and Bioenergy*, *122*, 76–83.

Rajbir Singh, R. S., Gulshan Mahajan, G. M., Simerjeet Kaur, S. K., & Chauhan, B. S. (2018). *Issues and strategies for rice residue management to unravel winter smog in North India.*

Rápó, E., Aradi, L. E., Szabó, Á., Posta, K., Szép, R., & Tonk, S. (2020). Adsorption of remazol brilliant violet-5R textile dye from aqueous solutions by using eggshell waste biosorbent. *Scientific Reports*, *10*(1), 8385.

Rápó, E., Posta, K., Suciu, M., Szép, R., & Tonk, S. (2019). Adsorptive Removal of Remazol Brilliant Violet-5R Dye from Aqueous Solutions using Calcined Eggshell as Biosorbent. *Acta Chimica Slovenica*, *66*(3).

Rashad, E., Saleh, H. N., Eltaweil, A. S., Saleh, M. E., Sillanpaa, M., & Mostafa, A. R. (2023). Pinewood sawdust biochar as an effective biosorbent for PAHs removal from wastewater. *Biomass Conversion and Biorefinery*, *13*(15), 13443–13459.

Rashid, R., Shafiq, I., Akhter, P., Iqbal, M. J., & Hussain, M. (2021). A state-of-the-art review on wastewater treatment techniques: the effectiveness of adsorption method. *Environmental Science and Pollution Research*, *28*, 9050–9066.

Rath, K. M., Fierer, N., Murphy, D. V, & Rousk, J. (2019). Linking bacterial community composition to soil salinity along environmental gradients. *The ISME Journal*, *13*(3), 836–846.

Rathi, B. S., & Kumar, P. S. (2021). Application of adsorption process for effective removal of emerging contaminants from water and wastewater. *Environmental Pollution*, *280*, 116995.

Ratnakumar, A., Samarasekara, A., Amarasinghe, D. A. S., & Karunanayake, L. (2022). The influence of particle size on the extraction of cellulose nanofibers using chemical-ultrasonic process. *Materials Today: Proceedings*, *64*, 274–278.

Ray, A., Banerjee, A., & Dubey, A. (2020). Characterization of biochars from various agricultural by-products using FTIR spectroscopy, SEM focused with image processing. *International Journal of Agriculture, Environment and Biotechnology*, *13*(4), 423–430.

Razaq, A., Nyholm, L., Sjödin, M., Strømme, M., & Mihranyan, A. (2012). Paper-based energy-storage devices comprising carbon fiber-reinforced polypyrrole-cladophora nanocellulose composite electrodes. *Advanced Energy Materials*, *2*(4), 445–454.

Rennie, E. A., & Scheller, H. V. (2014). Xylan biosynthesis. *Current Opinion in Biotechnology*, *26*, 100–107.

Reyes-Rivera, J., & Terrazas, T. (2017). Lignin Analysis by HPLC and FTIR. *Xylem: Methods and Protocols*, 193–211.

Rezania, S., Alizadeh, H., Park, J., Din, M. F. M., Darajeh, N., Ebrahimi, S. S., Saha, B. B., & Kamyab, H. (2019). *Effect of various pretreatment methods on sugar and ethanol production from cellulosic water hyacinth*.

Rigacci, A., & Achard, P. (2011). Cellulosic and polyurethane aerogels. *Aerogels Handbook*, 191–214.

Rinaldi, R., Jastrzebski, R., Clough, M. T., Ralph, J., Kennema, M., Bruijnincx, P. C. A., & Weckhuysen, B. M. (2016). Paving the way for lignin valorisation: recent advances in bioengineering, biorefining and catalysis. *Angewandte Chemie International Edition*, *55*(29), 8164–8215.

Roberto, I. C., Sato, S., & De Mancilha, I. M. (1996). Effect of inoculum level on xylitol production from rice straw hemicellulose hydrolysate by Candida guilliermondii. *Journal of Industrial Microbiology and Biotechnology*, *16*(6), 348–350.

Rominiyi, O. L., Adaramola, B. A., Ikumapayi, O. M., Oginni, O. T., & Akinola, S. A. (2017). Potential utilization of sawdust in energy, manufacturing and agricultural industry; waste to wealth. *World Journal of Engineering and Technology*, *5*(3), 526–539.

Roshan, A., & Kumar, M. (2020). Water end-use estimation can support the urban water crisis management: A critical review. *Journal of Environmental Management*, *268*, 110663.

Rosli, N. A., Ahmad, I., & Abdullah, I. (2013). Isolation and Characterization of Cellulose Nanocrystals from Agave angustifolia Fibre. *BioResources*, *8*(2).

Rubaay, H. Al, & Ali, S. (2022). Production of bioethanol from wood sawdust using Saccharomyces cervisae. *AIP Conference Proceedings*, *2386*(1).

Ruthven, D. M. (1984). *Principles of adsorption and adsorption processes*. John Wiley & Sons.

Saeed, A. A. H., Yub Harun, N., Bilad, M. R., Afzal, M. T., Parvez, A. M., Roslan, F. A. S., Abdul Rahim, S., Vinayagam, V. D., & Afolabi, H. K. (2021). Moisture content impact on properties of briquette produced from rice husk waste. *Sustainability*, *13*(6), 3069.

Saeed, M. U., Hussain, N., Sumrin, A., Shahbaz, A., Noor, S., Bilal, M., Aleya, L., & Iqbal, H. M. N. (2022). Microbial bioremediation strategies with wastewater treatment potentialities–A review. *Science of the Total Environment*, *818*, 151754.

Sahai, S., Sharma, C., Singh, S. K., & Gupta, P. K. (2011). Assessment of trace gases, carbon and nitrogen emissions from field burning of agricultural residues in India. *Nutrient Cycling in Agroecosystems*, *89*, 143–157.

Sampath, U. G. T. M., Ching, Y. C., Chuah, C. H., Singh, R., & Lin, P.-C. (2017). Preparation and characterization of nanocellulose reinforced semi-interpenetrating polymer network of chitosan hydrogel. *Cellulose*, *24*, 2215–2228.

Sánchez-Clemente, R., Igeño, M. I., Población, A. G., Guijo, M. I., Merchán, F., & Blasco, R. (2018). Study of pH changes in media during bacterial growth of several environmental strains. *Proceedings*, *2*(20), 1297.

Sanscartier, D., Reimer, K., Zeeb, B., & Koch, I. (2011). The effect of temperature and aeration rate on bioremediation of diesel-contaminated soil in solid-phase bench-scale bioreactors. *Soil and Sediment Contamination*, *20*(4), 353–369.

Santhosh, C., Daneshvar, E., Tripathi, K. M., Baltrėnas, P., Kim, T., Baltrėnaitė, E., & Bhatnagar, A. (2020). Synthesis and characterization of magnetic biochar adsorbents for the removal of Cr (VI) and Acid orange 7 dye from aqueous solution. *Environmental Science and Pollution Research*, *27*, 32874–32887.

Santos, D., Silva, U. F., Duarte, F. A., Bizzi, C. A., Flores, E. M. M., & Mello, P. A. (2018). Ultrasound-assisted acid hydrolysis of cellulose to chemical building blocks: Application to furfural synthesis. *Ultrasonics Sonochemistry*, *40*, 81–88.

Sayara, T., Sarrà, M., & Sánchez, A. (2010). Effects of compost stability and contaminant concentration on the bioremediation of PAHs-contaminated soil through composting. *Journal of Hazardous Materials*, *179*(1–3), 999–1006.

Selmer, I., Kleemann, C., Kulozik, U., Heinrich, S., & Smirnova, I. (2015). Development of egg white protein aerogels as new matrix material for microencapsulation in food. *The Journal of Supercritical Fluids*, *106*, 42–49.

Şentürk, İ., & Alzein, M. (2020). Adsorption of acid violet 17 onto acid-activated pistachio shell: isotherm, kinetic and thermodynamic studies. *Acta Chimica Slovenica*, *67*(1), 55–69.

Sharma, R. K., Wooten, J. B., Baliga, V. L., Lin, X., Chan, W. G., & Hajaligol, M. R. (2004). Characterization of chars from pyrolysis of lignin. *Fuel*, *83*(11–12), 1469–1482.

Shen, D. K., Gu, S., & Bridgwater, A. V. (2010). Study on the pyrolytic behaviour of xylan-based hemicellulose using TG–FTIR and Py–GC–FTIR. *Journal of Analytical and Applied Pyrolysis*, *87*(2), 199–206.

Shen, Y. (2017). Rice husk silica derived nanomaterials for sustainable applications. *Renewable and Sustainable Energy Reviews*, *80*, 453–466.

Shi, J., Fan, X., Tsang, D. C. W., Wang, F., Shen, Z., Hou, D., & Alessi, D. S. (2019). Removal of lead by rice husk biochars produced at different temperatures and implications for their environmental utilizations. *Chemosphere*, *235*, 825–831.

Shigehisa, T., Nakagawa, T., & Yamamoto, S. (2014). Briquetting of UBC by a double roll press: Part II: Improvement of the Johanson model. *Powder Technology*, *264*, 614–619.

Shukla, A., Kumar, D., Girdhar, M., Kumar, A., Goyal, A., Malik, T., & Mohan, A. (2023). Strategies of pretreatment of feedstocks for optimized bioethanol production: distinct and integrated approaches. *Biotechnology for Biofuels and Bioproducts*, *16*(1), 44.

Si, J., Cui, Z., Wang, Q., Liu, Q., & Liu, C. (2016). Biomimetic composite scaffolds based on mineralization of hydroxyapatite on electrospun poly (ε-caprolactone)/nanocellulose fibers. *Carbohydrate Polymers*, *143*, 270–278.

Siddique, R., Singh, M., Mehta, S., & Belarbi, R. (2020). Utilization of treated saw dust in concrete as partial replacement of natural sand. *Journal of Cleaner Production*, *261*, 121226.

Silva, E. N., Cantillo-Castrillon, M., Dantas, T. M., Mesquita, Y. M., Maia, D. A. S., Bastos-Neto, M., Barcellos, W. M., & Azevedo, D. C. S. (2021). Siloxane adsorption

by porous silica synthesized from residual sand of wastewater treatment. *Journal of Environmental Chemical Engineering*, *9*(2), 104805.

Singh, R. (2018). Energy sufficiency aspirations of India and the role of renewable resources: Scenarios for future. *Renewable and Sustainable Energy Reviews*, *81*, 2783–2795.

Sukmana, H., Bellahsen, N., Pantoja, F., & Hodur, C. (2021). Adsorption and coagulation in wastewater treatment–Review. *Progress in Agricultural Engineering Sciences*, *17*(1), 49–68.

Suleiman, B., Abdulkareem, S. A., Afolabi, E. A., Musa, U., Mohammed, I. A., & Eyikanmi, T. A. (2016). Optimization of bioethanol production from nigerian sugarcane juice using factorial design. *Advances in Energy Research*, *4*(1), 069.

Sun, Y., & Cheng, J. (2002). Hydrolysis of lignocellulosic materials for ethanol production: a review. *Bioresource Technology*, *83*(1), 1–11.

Swanckaert, B., Geltmeyer, J., Rabaey, K., De Buysser, K., Bonin, L., & De Clerck, K. (2022). A review on ion-exchange nanofiber membranes: properties, structure and application in electrochemical (waste) water treatment. *Separation and Purification Technology*, *287*, 120529.

Tamon, H., Ishizaka, H., Yamamoto, T., & Suzuki, T. (1999). Preparation of mesoporous carbon by freeze drying. *Carbon*, *37*(12), 2049–2055.

Tan, K. L., & Hameed, B. H. (2017). Insight into the adsorption kinetics models for the removal of contaminants from aqueous solutions. *Journal of the Taiwan Institute of Chemical Engineers*, *74*, 25–48.

Tao, Y., Endo, M., & Kaneko, K. (2008). A review of synthesis and nanopore structures of organic polymer aerogels and carbon aerogels. *Recent Patents on Chemical Engineering*, *1*(3), 192–200.

Tchounwou, P. B., Yedjou, C. G., Patlolla, A. K., & Sutton, D. J. (2012). Heavy metal toxicity and the environment. *Molecular, Clinical and Environmental Toxicology: Volume 3: Environmental Toxicology*, 133–164.

Terangpi, P., & Chakraborty, S. (2017). Adsorption kinetics and equilibrium studies for removal of acid azo dyes by aniline formaldehyde condensate. *Applied Water Science*, *7*, 3661–3671.

Thoorens, G., Krier, F., Rozet, E., Carlin, B., & Evrard, B. (2015). Understanding the impact of microcrystalline cellulose physicochemical properties on tabletability. *International Journal of Pharmaceutics*, *490*(1–2), 47–54.

Timung, R., Naik Deshavath, N., Goud, V. V, & Dasu, V. V. (2016). Effect of subsequent dilute acid and enzymatic hydrolysis on reducing sugar production from sugarcane bagasse and spent citronella biomass. *Journal of Energy*, *2016*(1), 8506214.

Topp, E., Vallaeys, T., & Soulas, G. (1997). *Pesticides: microbial degradation and effects on microorganisms.*

Torresi, E., Tang, K., Deng, J., Sund, C., Smets, B. F., Christensson, M., & Andersen, H. R. (2019). Removal of micropollutants during biological phosphorus removal: Impact of redox conditions in MBBR. *Science of the Total Environment*, *663*, 496–506.

Tremblay, L. A., Gielen, G., & Northcott, G. L. (2016). Organic Materials Guidelines–Organic Contaminants Review. *Centre for Integrated Biowaste Research: Hamilton, New Zealand*, *23*.

Tripathy, J., Mishra, A., Pandey, M., Thakur, R. R., Chand, S., Rout, P. R., & Shahid, M. K. (2024). Advances in nanoparticles and nanocomposites for water and wastewater treatment: a review. *Water*, *16*(11), 1481.

Vârban, R., Crișan, I., Vârban, D., Ona, A., Olar, L., Stoie, A., & Ștefan, R. (2021). Comparative FT-IR prospecting for cellulose in stems of some fiber plants: Flax, velvet leaf, hemp and jute. *Applied Sciences*, *11*(18), 8570.

Wan, Y., Liu, Z.-Y., Song, P., Zhang, X.-Q., Song, J.-C., Fu, Y.-J., Yao, X.-H., Wang, J., Chen, T., & Zhang, D.-Y. (2019). Ionic liquid groups modified 3D porous cellulose microspheres for selective adsorption of AO7 dye. *Journal of Cleaner Production*, *240*, 118201.

Wang, D., Silbaugh, T., Pfeffer, R., & Lin, Y. S. (2010). Removal of emulsified oil from water by inverse fluidization of hydrophobic aerogels. *Powder Technology*, *203*(2), 298–309.

Wang, H., Xie, H., Du, H., Wang, X., Liu, W., Duan, Y., Zhang, X., Sun, L., Zhang, X., & Si, C. (2020). Highly efficient preparation of functional and thermostable cellulose nanocrystals via H2SO4 intensified acetic acid hydrolysis. *Carbohydrate Polymers*, *239*, 116233.

Wang, N., Chen, J., Wang, J., Feng, J., & Yan, W. (2019). Removal of methylene blue by Polyaniline/TiO2 hydrate: Adsorption kinetic, isotherm and mechanism studies. *Powder Technology*, *347*, 93–102.

Wang, S., Tian, R., Liu, B., Wang, H., Liu, J., Li, C., Li, M., Evivie, S. E., & Li, B. (2021). Effects of carbon concentration, oxygen, and controlled pH on the engineering strain Lactiplantibacillus casei E1 in the production of bioethanol from sugarcane molasses. *AMB Express*, *11*, 1–13.

Wang, S., Zhang, Q., Wang, Z., & Pu, J. (2020). Facile fabrication of an effective nanocellulose-based aerogel and removal of methylene blue from aqueous system. *Journal of Water Process Engineering*, *37*, 101511.

Wang, X., Guo, Z., Hu, Z., & Zhang, J. (2020). Recent advances in biochar application for water and wastewater treatment: a review. *PeerJ*, *8*, e9164.

Wang, Y., Wang, Q., He, J., & Zhang, Y. (2017). Highly effective C–C bond cleavage of lignin model compounds. *Green Chemistry*, *19*(13), 3135–3141.

Wen, Y., Schoups, G., & Van De Giesen, N. (2017). Organic pollution of rivers: Combined threats of urbanization, livestock farming and global climate change. *Scientific Reports*, *7*(1), 43289.

Worsley, M. A., Satcher Jr, J. H., & Baumann, T. F. (2008). Synthesis and characterization of monolithic carbon aerogel nanocomposites containing double-walled carbon nanotubes. *Langmuir*, *24*(17), 9763–9766.

Xin, S., Yang, H., Chen, Y., Yang, M., Chen, L., Wang, X., & Chen, H. (2015). Chemical structure evolution of char during the pyrolysis of cellulose. *Journal of Analytical and Applied Pyrolysis*, *116*, 263–271.

Xu, F., Sun, J.-X., Sun, R., Fowler, P., & Baird, M. S. (2006). Comparative study of organosolv lignins from wheat straw. *Industrial Crops and Products*, *23*(2), 180–193.

Xu, J., Song, W., Wu, N., Tong, J., & Ren, L. (2021). Preparation and characterization of chitosan/polyvinyl porous alcohol aerogel microspheres with stable physicochemical properties. *International Journal of Biological Macromolecules*, *187*, 614–623.

Yam, R. C. M., & Mak, D. M. T. (2014). A cleaner production of rice husk-blended polypropylene eco-composite by gas-assisted injection moulding. *Journal of Cleaner Production*, *67*, 277–284.

Yang, C.-C. (2007). Synthesis and characterization of the cross-linked PVA/TiO2 composite polymer membrane for alkaline DMFC. *Journal of Membrane Science*, *288*(1–2), 51–60.

Yang, H., Yan, R., Chen, H., Lee, D. H., & Zheng, C. (2007). Characteristics of hemicellulose, cellulose and lignin pyrolysis. *Fuel*, *86*(12–13), 1781–1788.

Yang, X., Xie, H., Du, H., Zhang, X., Zou, Z., Zou, Y., Liu, W., Lan, H., Zhang, X., & Si, C. (2019). Facile extraction of thermally stable and dispersible cellulose nanocrystals with high yield via a green and recyclable FeCl3-catalyzed deep eutectic solvent system. *ACS Sustainable Chemistry & Engineering*, *7*(7), 7200–7208.

Ye, Y.-F., Ma, F.-Y., Wu, M., Wei, X.-Y., & Liu, J.-M. (2016). Increase of acenaphthene content in creosote oil by hydrodynamic cavitation. *Chemical Engineering and Processing: Process Intensification*, *104*, 66–74.

Yeow, P. K., Wong, S. W., & Hadibarata, T. (2021). Removal of azo and anthraquinone dye by plant biomass as adsorbent–a review. *Biointerface Res. Appl. Chem*, *11*(1), 8218–8232.

Ying, W., Shi, Z., Yang, H., Xu, G., Zheng, Z., & Yang, J. (2018). Effect of alkaline lignin modification on cellulase–lignin interactions and enzymatic saccharification yield. *Biotechnology for Biofuels*, *11*, 1–13.

Yokogawa, H., & Yokoyama, M. (1995). Hydrophobic silica aerogels. *Journal of Non-Crystalline Solids*, *186*, 23–29.

Zhang, C.-C., Zhang, L.-J., Liao, W., Yan, Z.-H., Chen, J., Jiang, Y.-L., Wang, H.-J., Luan, X.-Y., Ye, Y.-Y., & Zheng, W.-G. (2015). ATR-FTIR spectroscopic studies on density changes of fused silica induced by localized CO2 laser treatment. *Chinese Physics B*, *24*(2), 024220.

Zhang, H., Li, L., Dai, F., Zhang, H., Ni, B., Zhou, W., Yang, X., & Wu, Y. (2012). Preparation and characterization of silk fibroin as a biomaterial with potential for drug delivery. *Journal of Translational Medicine*, *10*, 1–9.

Zhang, L., Gao, G., Tang, X., & Shao, K. (2014). Impacts of different salinities on bacterial biofilm communities in fresh water. *Canadian Journal of Microbiology*, *60*(5), 319–326.

Zhang, L., Yan, L., Wang, Z., Laskar, D. D., Swita, M. S., Cort, J. R., & Yang, B. (2015). Characterization of lignin derived from water-only and dilute acid flowthrough pretreatment of poplar wood at elevated temperatures. *Biotechnology for Biofuels*, *8*, 1–14.

Zhang, S. Q., Wang, J., Shen, J., Deng, Z. S., Lai, Z. Q., Zhou, B., Attia, S. M., & Chen, L. Y. (1999). The investigation of the adsorption character of carbon aerogels. *Nanostructured Materials*, *11*(3), 375–381.

Zhang, X., Xu, S., Li, Q., Zhou, G., & Xia, H. (2021). Recent advances in the conversion of furfural into bio-chemicals through chemo-and bio-catalysis. *RSC Advances*, *11*(43), 27042–27058.

Zhao, C., Zhou, J., Yan, Y., Yang, L., Xing, G., Li, H., Wu, P., Wang, M., & Zheng, H. (2021). Application of coagulation/flocculation in oily wastewater treatment: A review. *Science of The Total Environment*, *765*, 142795.

Zhao, H., Kwak, J. H., Zhang, Z. C., Brown, H. M., Arey, B. W., & Holladay, J. E. (2007). Studying cellulose fiber structure by SEM, XRD, NMR and acid hydrolysis. *Carbohydrate Polymers*, *68*(2), 235–241.

Ziaei-Rad, Z., Pazouki, M., Fooladi, J., Azin, M., Gummadi, S. N., & Allahverdi, A. (2023). Investigation of a robust pretreatment technique based on ultrasound-

assisted, cost-effective ionic liquid for enhancing saccharification and bioethanol production from wheat straw. *Scientific Reports*, *13*(1), 446.

Zulkania, A., Iqbal, M., & Syamsumarlin, S. (2020). Characterization of adsorbents derived from palm fiber waste and its potential on methylene blue adsorption. *Key Engineering Materials*, *841*, 273–277.

Biomass Conversion and Biorefinery
https://doi.org/10.1007/s13399-024-05715-x

ORIGINAL ARTICLE

Synthesis of polymeric aerogels with different fillers and their application for the removal of emerging pollutants: a comparative study

Subhasis Ghosh[1,2] · Poushali Chakraborty[1,2] · Avijit Bhowal[1,2] · Suvendu Manna[3] · Papita Das[1,2]

Received: 13 March 2024 / Revised: 23 April 2024 / Accepted: 29 April 2024

Abstract

In this study, two main steps of traditional aerogel preparation method, viz., solvent substitution and supercritical drying, are substituted with cooling the hydrogel at 277 K and freeze-drying. Different modification agents or fillers were used in the preparation process to study their effects on their physical and chemical properties. Different parameters, viz., pH, salinity, moisture content, and temperature, were considered to investigate their effects on the aerogels. A significant difference in the physical properties was observed as the effect of different fillers present in the polyvinyl alcohol (PVA) matrix. The PVA-rice husk biochar (PVA-RHBC) aerogel showed the highest density at 0.26 g/cm^3. The highest porosity was observed in the case of PVA-silica (PVA-Si) aerogel at 97.05% along with the highest swelling tendency that to be 187.24%. The prepared aerogels showed the least degradation at pH 6 proving this pH as the optimum pH condition. Also, the adsorption property of the prepared aerogels was investigated with respect to six different pollutants that include organic pollutants, metal ion, and dye. The highest removal was shown by PVA-Si aerogel in each case. The highest removal was found in the case of methylene blue at 89.71%. The lowest removal was 21.39%, achieved by PVA aerogel in the case of Cr (VI). In the case of PAHs, the highest removal was found to be 70.5% for naphthalene.

Keywords Aerogels · Removal · Emerging pollutants · Hydrogel

1 Introduction

Recent decades have evidence of the development of new materials like aerogels for wide applications in science and technology. Aerogels are solid substances with exclusive properties such as high specific surface area (approximately 500–1200 m^2 g^{-1}), high thermal insulation, low dielectric constant, low density (approximately 0.003–0.5 g cm^{-3}), high porosity (approximately 80–99.8%), and low index of refraction [1, 2]. Any material synthesized by the sol-gel method with a proper drying technology from organic or inorganic precursors can be termed as aerogel in which characteristics like 3D structures and highly porous networks are present. Such characteristics provided them to be efficient in processing various morphologies as well as sizes and having many applications [3].

In 1931, S. Kistler first coined the idea of aerogel after Kistler developed silica aerogel by extracting liquid from wet silica gels in a supercritical drying process. The obtained solid materials were of approximately the same dimensions as their original wet gel form but filled with air [4]. After many years, Teichner in 1968 and Pekala in 1989 introduced SiO_2-based aerogel and carbon-based aerogel, respectively [5]. The usage of precursors like tetraethyl orthosilicate (TEOS), tetramethyl orthosilicate (TMOS), resorcinol, and formaldehyde provided a remedy for high production cost, safety concerns, and time consumption [6]. Over the last decade, researchers have concentrated on synthesizing novel aerogels based on carbon nanotubes (CNTs) or graphene oxides for their extraordinary properties.

✉ Papita Das
papitasaha@gmail.com; papita.das@jadavpuruniversity.in

1 Department of Chemical Engineering, Jadavpur University, 188, Raja S. C. Mullick Road, Kolkata 700 032, West Bengal, India

2 School of Advanced Studies for Industrial Pollution Control Engineering, Jadavpur University, Kolkata 700032, West Bengal, India

3 University of Petroleum & Energy Studies, Dehradun, India

Published online: 10 May 2024

Biomass Conversion and Biorefinery
https://doi.org/10.1007/s13399-025-06776-2

ORIGINAL ARTICLE

Extraction of silica and biochar from biomass waste for the synthesis of aerogel and its application for the removal of dye

Ashmita Samanta[1] · Subhasis Ghosh[1,2] · Papita Das[1,2]

Received: 19 December 2024 / Revised: 4 March 2025 / Accepted: 13 March 2025

Abstract

Contamination o f wastewater is one of the rising global issues, and several studies are being conducted to perform efficient treatment processes with cost-effective methods. In this study, sugarcane bagasse was used as biomass to extract silica (Si) and biochar (BC) and was used further as fillers for aerogel formation with polyvinyl alcohol (PVA) polymer to eliminate Congo red dye from the solution. A batch study was conducted in each case, and the efficiency of dye removal, by different aerogel PVA, PVA-Si, and PVA-BC was studied. Experimental parameters were varied to analyze the effect of the various parameters in each case. The highest removal was 94.98% using PVA-Si aerogel at 300 min with 10 mg/L initial concentration of Congo red, pH 7, and temperature 30 ℃. The adsorption capacity of Congo red was 29.49 mg/g by PVA-Si aerogel. The characterization of the aerogel showed the occupancy of various functional groups, modification in crystallographic structure, and surface alteration of aerogels. The analysis for the study of kinetics exhibited that the process of adsorption fitted the pseudo-second-order reaction for all the aerogels and also the thermodynamics data demonstrated that the adsorption process was spontaneous and endothermic. Also, from the isotherm modeling, it was observed that the process best fitted with the Freundlich isotherm model.

Keywords Aerogel · Silica · Biochar · PVA · Congo red · Adsorption · Modeling · Sugarcane bagasse

1 Introduction

The rising concern of water contamination due to indiscriminate wastewater disposal has awakened global environmental problems. Wastewater disposal, which includes contaminants like heavy metals, soluble organic dyes, and toxic chemicals, is a constant threat to aquatic life and dangerous to consume. Several techniques for purifying wastewater have been created due to industrialization, which includes procedures like adsorption, precipitation, ion exchange, and reverse osmosis. Of these, adsorption is the most successful and economical method [1]. As hazardous chemicals are present in the discharged wastewater, they might act as carcinogens and mutagens, and their release from anthropogenic activities increases water contamination daily [2]. Waterbody pollutants seep into the bodies of small creatures, building up to bigger magnitudes and resulting in human health impacts such as skin cancer, hemolytic anemia, irritation, digestive issues, and anomalies of the central nervous system [3]. Upon scrutinizing at nano-gram and microgram-per-liter levels in effluents, persistent pollutants are detected which are very essential to remove as they can cause waterborne pandemic diseases [4]. Among several methods of treating wastewater, the most effective one is using adsorbent due to its high efficiency, relatively cost-effective, and lesser by-products that further cause less pollution. Several adsorbent materials are used which are categorized into, inorganic mineral adsorbent, synthetic polymer adsorbent, and natural organic adsorbent [5]. Inorganic and synthetic adsorbents are widely used, although synthetic adsorbents degrade very slowly compared to natural organic adsorbents. Natural organic adsorbents that are derived from biomaterials are highly considered due to their reasonable price, renewability, and biodegradability. The most common naturally obtained adsorbents that are investigated for the removal of

✉ Papita Das
papitasaha@gmail.com; papita.das@jadavpuruniversity.in

[1] Department of Chemical Engineering, Jadavpur University, 188, Raja S. C. Mullick Road, Kolkata 700 032, West Bengal, India

[2] School of Advanced Studies for Industrial Pollution Control Engineering, Jadavpur University, 188, Raja Subodh Chandra Mallick Rd, Jadavpur, Kolkata, West Bengal 700032, India

Published online: 20 March 2025

Biomass Conversion and Biorefinery
https://doi.org/10.1007/s13399-024-05616-z

ORIGINAL ARTICLE

Silica-coated cellulose using *Shorea robusta* sawdust biomass and its application for methylene blue dye removal from aqueous solution

Subhasis Ghosh[1,2] · Sampad Sarkar[1,2] · Sayan Mukherjee[1,2] · Sirsha Ganguly[1] · Papita Das[1,2]

Received: 8 January 2024 / Revised: 20 March 2024 / Accepted: 7 April 2024

Abstract

This study focuses on the synthesis of silica-cellulose composite and its utilization for methylene blue removal from aqueous solution. *Shorea robusta* sawdust was used for the extraction of cellulose using chemical pre-treatment method and the extracted cellulose was treated with tetraethoxysilane (TEOS) to prepare the composite. Batch study was conducted to compare the removal of methylene blue from aqueous solution by cellulose and silica-cellulose composite respectively. Different parameters, viz., contact time, pH, adsorbent dose, adsorbate concentration and temperature were varied to investigate the effect of mentioned parameters on methylene blue adsorption. From the characterization studies of adsorbents, the presence of different functional groups, change in crystallographic structure and surface modification was observed after TEOS treatment of adsorbent. From the observations of results derived in batch study, it can be stated that the silica-cellulose composite has a higher adsorption capability over cellulose. The highest removal achieved by the composite was 98.39% at 180 min while maintaining other parameters at pH 7, adsorbent dose 2 g/L, adsorbate concentration 10 mg/L and temperature at 30 °C. From the kinetic analysis of adsorption process, the observation was made that both the adsorbents are following pseudo-second-order reaction. Also, the data of thermodynamic analysis represented that the reaction is endothermic and simultaneous in nature for both the adsorbents. Isotherm study of this experiment showed that the pollutant performed a heterogenous distribution on the surface of the adsorbent cellulose as well as silica-cellulose composite. Reusability and selectivity study of the adsorbent was performed and from the data, it was interpreted that the adsorbent has a high reusability as well as high selectivity towards methylene blue.

Keywords Cellulose · Silica-cellulose composite · Methylene blue · Adsorption · Kinetics · Thermodynamics

1 Introduction

Over the last few decades, environmental issues are gaining attention at both the national and international platforms. With the development of civilization, technology and industrialization, the contamination of ground and surface water is increasing at a progressive rate and has become a global problem. Due to this problem worldwide, approximately 14,000 people die every day [1]. When pollution of the source is known or the pollutants are from an identifiable source, the source is considered as a point source of water pollution and recognized as the main threat to waterbodies in developed as well as developing countries [2].

There is different type of pollutants responsible for water contamination, though dyes are among the main pollutants derived from industrial activities. Different industries, viz., printing, cosmetics, pharmaceuticals, food and textile use synthetic dyes for various purposes [3]. Dyes contain unsaturated groups and conjugate chemical bonds with complex chemical structures. These complex structures cause difficulty to be removed from wastewater [4]. Any dye contains two different parts. One is chromophore that is responsible for the colour and another part is auxochrome, responsible for the increase of its affinity towards the fibres [5].

Generally, dyes are classified into three types: anionic, cationic and non-ionic [6]. According to the study, cationic dyes are toxic and cause allergies, skin irritation, mutation

✉ Papita Das
papitasaha@gmail.com

[1] Department of Chemical Engineering, Jadavpur University, 188, Raja S. C. Mullick Road, Kolkata 700032, West Bengal, India

[2] School of Advanced Studies for Industrial Pollution Control Engineering, Jadavpur University, Kolkata, West Bengal 700032, India

Published online: 12 April 2024

Sādhanā (2024)49:15
https://doi.org/10.1007/s12046-023-02388-6

Synthesis of rice husk-derived cellulose for efficacious removal of malachite green from aqueous solution

SANKET ROY[1], SAYAN MUKHERJEE[2], SUBHASIS GHOSH[2] and PAPITA DAS[1,2,*]

[1]Department of Chemical Engineering, Jadavpur University, 188, Raja S. C. Mullick Road, Kolkata, West Bengal 700032, India
[2]School of Advanced Studies for Industrial Pollution Control Engineering, Jadavpur University, Kolkata, West Bengal 700032, India
e-mail: sanket00100@gmail.com; sayan.mukherjee.mis@gmail.com; subhasisghosh1604@gmail.com; papita.das@jadavpuruniversity.in

MS received 22 June 2023; revised 25 October 2023; accepted 30 October 2023

Abstract. Malachite green (MG), a common dye composed of N-methylated diamino-triphenylmethane, is often released uncontrollably into wastewater by leather and textile manufacturing industries. The abundance of MG in the environment poses a severe threat to mankind and associated organisms. In this study, cellulose was synthesized from lignocellulosic biomass rice husk after pre-treatment with different concentration of sodium hydroxide with or without ultrasonication followed by its utilisation to develop a non-toxic, pocket-friendly adsorbent for treatment of wastewater. Understanding the role of process parameters along with calculation of the isotherm, kinetics and thermodynamic parameters were conducted in the experiment in order to elucidate the novel pre-treatment method. In this study, the highest MG removal of 97.9% was acquired using rice-husk-derived cellulose. The obtained data have suggested that the spontaneous endothermic process and Langmuir isotherm models.

Keywords. Agricultural waste; rice husk; cellulose; wastewater treatment; malachite green.

1. Introduction

As development progressed through industrialization, the waste production increased. Since then, effluents from various industries have polluted the very source of civilizations' survival. Coloured wastewater is generated due to industry dyeing and finishing processes, further ejected into natural streams, having negative repercussions on environmental ecosystem and anthropogenic health. More than 10,000 different synthetic dyes and colouring agents exist with an annual production of over 0.7 million tonnes [1]. Interestingly, over 20% of the total dye produced enters the industrial discharge signifying its existence pollute water bodies [2, 3].

One such commonly used dye of cationic nature is Malachite Green (MG). MG, while useful in various industrial applications, is also used in aquaculture industries as a fungicide, bactericide, and parasiticide. In solutions, malachite green (MG) produces two distinct ions: chromatic malachite green (cation) and carbinol base. This dye is chemically reduced to a leuco derivative [4] which is carcinogenic in nature.

Proper treatment of wastewater is one of the major concerns in recent times. Due to the high stability of the synthetic dyes, environmental exposure to heat, water, light, and the microbial attack becomes effectless [5, 6]. Although there are various traditional methods of dye removal is present but high operating costs, labour intensive and incomplete removal are some of the major disadvantages. In this dilemma, Adsorption has emerged as a cost-effective, easy-to-use and efficient alternative by which complete removal of the pollutant is possible even in diluted conditions. Usage of agricultural waste such as rice husk, sawdust, banana peel, orange peel, etc. has a significant edge due to the easy availability, cost-effectiveness, low toxicity and possibility of dye recovery [7].

Agricultural lignocellulosic wastes consist of a non-edible, sustainable supply of chemical components [8]. Rice being the staple food of most of the world's population, especially in South Asia and Africa, generates a massive amount of agricultural waste such as straw and husk. Recent developments have increased the processivity of rice straw into biofuels, fertilizers, paper and animal feed [9]. Burning of rice straw after harvesting is one of the major environmental concerns in countries like India [10, 11]. In order to break down rice husk and synthesize cellulose, the disintegration of the lignin-hemicellulose

*For correspondence
Published online: 08 January 2024

Discover Chemistry

Research

Removal of naphthalene utilizing synthesized silica doped PVA aerogel: removal, optimization and mechanism

Subhasis Ghosh[1,2] · Debojyoti Basak[1] · Suvendu Manna[3] · Avijit Bhowal[1] · Papita Das[1,2]

Received: 17 January 2025 / Accepted: 1 April 2025
Published online: 15 April 2025

Abstract
The focus of this study is the modification of (3-Aminopropyl) triethoxysilane (APTES) by hydrogen peroxide (H_2O_2) and its utilisation as a filler in Polyvinyl alcohol (PVA) aerogel preparation along with normal APTES and extracted silica (Si) to understand its effect on the removal of naphthalene from water solution. An increase in the peak of the –OH group was observed along with the presence of other groups, viz., C–O–C, Si–O, and CH_2. Along with the difference in characterization, a different adsorption efficiency was also found for all the adsorbents. In all the scenarios the PVA-modified APTES aerogel showed a higher removal compared to PVA-APTES and PVA-Si aerogel. The effect of different parameters, viz., pH, temperature, pollutant concentration, and aerogel dose on removal percentage were investigated. The highest removal of naphthalene was found to be 99.74% at 180 min at aerogel dose 1 g/L, pH 7, temperature 35 °C, and naphthalene concentration 5 mg/L. From the adsorption modelling it was observed that the adsorption process best fitted with Langmuir isotherm in the case of PVA-modified APTES and Freundlich isotherm for the rest of the adsorbents respectively. The kinetic analysis showed that all the adsorbents followed a pseudo- 2nd order reaction. In the pH_{pzc} analysis of PVA-modified APTES, it was observed that the point of zero charge was detected at 7.16. It was found that the main controlling mechanism of this process was dipole-induced dipole interaction and hydrogen bonding. The effect of naphthalene on *Lysinibacillus* sp. before and after adsorption was observed. A significant suppression in the growth curve occurred because of the contamination of naphthalene.

✉ Papita Das, papitasaha@gmail.com | [1]Department of Chemical Engineering, Jadavpur University, 188, Raja S. C. Mullick Road, Kolkata 700032, West Bengal, India. [2]School of Advanced Studies in Industrial Pollution Control Engineering, Jadavpur University, Kolkata 700032, West Bengal, India. [3]University of Petroleum and Energy Studies, Dehradun, India.

Biomass Conversion and Biorefinery
https://doi.org/10.1007/s13399-024-05855-0

ORIGINAL ARTICLE

Beyond waste: waste rice husk to value-added products using sonic waves and chemical treatment and principal component analysis of extraction

Subhasis Ghosh[1,2] · Sanket Roy[1] · Papita Das[1,2]

Received: 7 May 2024 / Revised: 4 June 2024 / Accepted: 10 June 2024

Abstract

This study mainly focussed on the chemical pre-treatment of waste rice husk using sodium hydroxide followed by sonication to extract cellulose, hemicellulose, and lignin. This paper also reported the production of bioethanol using *Aspergillus* sp. and *Saccharomyces* sp. The highest amount of ethanol production was observed from 4% NaOH pre-treated sonicated rice husk, that is, 30.40 mg/g. This study also estimated the xylan content in the hydrolysate after lignin extraction. The highest amount of xylan was estimated in 2% NaOH pre-treated non-sonicated hydrolysate, that is, 8.24%. Furfural was also produced from extracted cellulose and extraction of furfural was 15%, produced from 2% NaOH pre-treated non-sonicated rice husk. This paper also focused on the optimization and yield of the process to extract different value-added products utilizing rice husk as a raw material. By extracting various products in different steps of the process, this study deals with the zero-waste idea by minimizing the waste materials and contributing toward the generation of clean energy.

Keywords Rice husk · Chemical pre-treatment · Sonication · Bioethanol · Furfural · Xylan

1 Introduction

Rice husk (*Oryza sativa*) is a common bioproduct of rice cultivation. From 23% of total cultivated rice, 545 Mt of rice husk is being produced with 50% accounting for China and India being the second. Nowadays, most of the produced rice husk is burned to reduce the volume of the disposed material. This burnt rice husk contains a high amount of silica, contributing significantly to the pollution. The outer layer of rice husk contains a significant proportion of inorganic silica (2–5 wt%), and the interior layer is mostly made up of lignocellulose. Lignocellulose is a natural polymer that comprises cellulose (33%), hemicellulose (20%), lignin (28%), and moisture (7.5%) in the case of rice husk [1]. Because of the structural composition, rice husk has been identified as a viable precursor for the synthesis of various value-added products [2]. A high percentage of cellulose, crystalline structure, degree of lignification, and complex structure of cell wall are responsible for the high recalcitrance of rice husk [3]. To break down the structural integrity of the biomass and conduct an easier degradation, various pre-treatment methods are used. One of the most common methods for pre-treating lignocellulosic biomass is mechanical extrusion. In this process, a high temperature and constant shearing force are used which is responsible for the breakdown of the crystalline structure of the biomass and the shortening of fibre that increases overall carbohydrate availability [4]. Mechanical grinding, another method used for the mechanical pre-treatment, majorly integrates grinding, chipping, and milling techniques, respectively. This process also can break down the crystalline structure of biomass and reduce the size to 10–30 mm [5]. A study reported that planetary ball milling resulted in the most amount of glucose and galactose compared to other methods [6]. Though these methods are significantly effective, in many cases, they are not applicable on an industrial scale. To overcome this problem, other methods have been introduced and investigated. Microwave digestion is one of the simplest methods

✉ Papita Das
papitasaha@gmail.com; papita.das@jadavpuruniversity.in

[1] Department of Chemical Engineering, Jadavpur University, 188, Raja S. C. Mullick Road, Kolkata 700 032, West Bengal, India

[2] School of Advanced Studies for Industrial Pollution Control Engineering, Jadavpur University, Kolkata, West Bengal 700032, India

Published online: 15 June 2024

Patent filed copy

Office of the Controller General of Patents, Designs & Trade Marks
Department for Promotion of Industry and Internal Trade
Ministry of Commerce & Industry,
Government of India

INTELLECTUAL PROPERTY INDIA
PATENTS | DESIGNS | TRADE MARKS | GEOGRAPHICAL INDICATIONS

Application Details	
APPLICATION NUMBER	202411084055
APPLICATION TYPE	ORDINARY APPLICATION
DATE OF FILING	04/11/2024
APPLICANT NAME	**UNIVERSITY OF PETROLEUM AND ENERGY STUDIES, DEHRADUN**
TITLE OF INVENTION	A METHOD OF PREPARATION OF A MICROBE-DOPED POLYMERIC AEROGEL FOR WASTEWATER TREATMENT
FIELD OF INVENTION	CHEMICAL
E-MAIL (As Per Record)	kbipservices@gmail.com
ADDITIONAL-EMAIL (As Per Record)	
E-MAIL (UPDATED Online)	
PRIORITY DATE	
REQUEST FOR EXAMINATION DATE	05/11/2024
PUBLICATION DATE (U/S 11A)	15/11/2024

Application Status	
APPLICATION STATUS	Application Awaiting Examination

View Documents

Certificate of conference

The Institution of Engineers (India)

39th Indian Engineering Congress

Kolkata, 20-22 December 2024

This is to certify that the following Extended Abstract has been approved for presentation and was presented during the 39th Indian Engineering Congress, held at Hotel Novotel, Kolkata during 20 – 22 December 2024.

Preparation of Activated Biochar doped Polyvinyl Alcohol (PVA) Aerogel and its Application in Wastewater Treatment

Theme: Chemicals & Hydrocarbons

Authored by:

Subhasis Ghosh, *Department of Chemical Engineering, Jadavpur University*

Papita Das, *Department of Chemical Engineering, Jadavpur University*

Presented by:

Subhasis Ghosh

Dr. Raju Basak
Organising Secretary
39th Indian Engineering Congress
T2R2P3

Er. Sandip Kr. Deb
Chairman, Organising Committee
39th Indian Engineering Congress

Prof. (Dr.) Ajoy Kumar Ray
Chairman, Technical Committee
39th Indian Engineering Congress

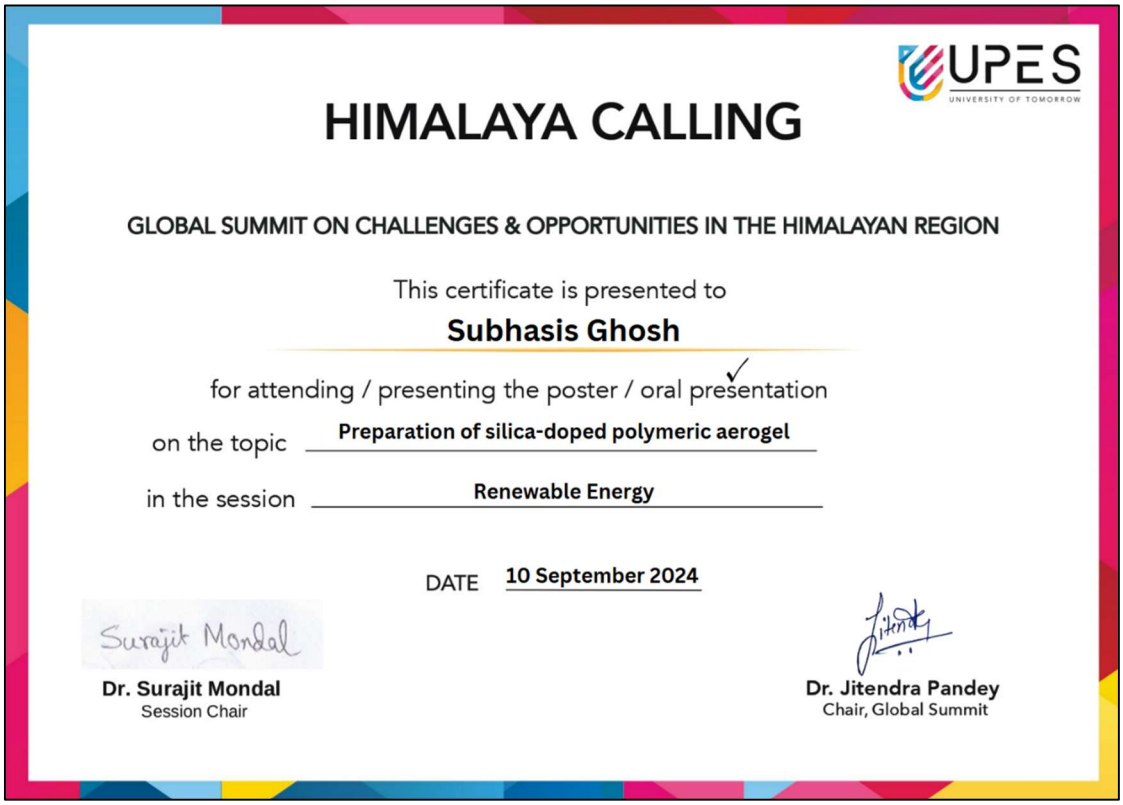

UPES
UNIVERSITY OF TOMORROW

HIMALAYA CALLING

GLOBAL SUMMIT ON CHALLENGES & OPPORTUNITIES IN THE HIMALAYAN REGION

This certificate is presented to

Subhasis Ghosh

for attending / presenting the poster / oral presentation ✓

on the topic **Preparation of silica-doped polymeric aerogel**

in the session **Renewable Energy**

DATE **10 September 2024**

Surajit Mondal

Dr. Surajit Mondal
Session Chair

Dr. Jitendra Pandey
Chair, Global Summit

CENTRE FOR ENVIRONMENTAL STUDIES (CES)
ANNA UNIVERSITY, CHENNAI - 600025

International Conference on
"SUSTAINABLE RESILIENT REMEDIATION"

CERTIFICATE OF PRESENTATION

This is to certify that Dr./Mr./Ms. **SUBHASIS GHOSH**

from **JADAVPUR UNIVERSITY, KOLKATA** has delivered an oral presentation of a research paper of significance entitled **PRODUCTION OF BIOCHAR FROM LIGNOCELLULOSIC BIOMASS AND ITS APPLICATION IN DYE REMOVAL** in the two day '***International Conference on Sustainable Resilient Remediation - (ICSRR'23)***' Organized by CES, Anna University, Chennai during 02nd and 03rd February, 2023.

CO-ORDINATOR
Dr. Saranya Kuppusamy
Scientist–D, CES
Anna University, Chennai

CONVENER
Dr. S. Kanmani
Professor & Director, CES
Anna University, Chennai

CERTIFICATE OF PARTICIPATION

International Conference on Chemical Engineering Innovations and Sustainability (ICEIS-2023)

Chemical Engineering Department, Jadavpur University

This is to certify that

Subhasis Ghosh

Jadavpur University, Kolkata, India

Orally presented technical paper entitled "Cellulose from acid pre-treated lignocellulosic biomass and its application in dye removal" in ICEIS-2023 held during 26th-27th February, 2023 at Jadavpur University, Kolkata, India

PROF. RAJAT CHAKRABORTY — Chairman, ICEIS 2023

PROF. RANJANA CHOWDHURY, PROF. KAJARI KARGUPTA, PROF. PAPITA DAS — Joint Conveners, ICEIS 2023

3rd International Conference on Water Technologies (ICWT - 2023)
AUA Academic Conference
December 4th -7th, 2023
Organized by
Water Innovation Center: Technology, Research & Education
In association with
Asian Universities Alliance
at
Indian Institute of Technology Bombay

Asian Universities Alliance

Presentation Certificate

This is to certify that
Subhasis Ghosh
has attended the 3rd ICWT-2023 AUA Academic conference
and presented titled
ICWT2023_PR001 – *Bacterial Bioremediation of Acenaphthene and Phenol using isolated Bacteria: A promising Technology for water treatment*
Subhasis Ghosh, and Papita Das

Shobha Shukla

Prof. Shobha Shukla
Conference Convenor
Professor-in-charge WICTRE
Indian Institute of Technology Bombay

Asian Universities Alliance · Department of Science & Technology · SPIE. Student Chapter · LASER SCIENCE · IOP Publishing · Springer

Platinum Jubilee Celebration
Of
Indian Institute of Chemical Engineers

An International Conference on
Energy Transition: Challenges and Opportunities

IIChE-CHEMCON 2023

December 27 - 30, 2023
Conference Venue: Heritage Institute of Technology, Kolkata

Organized by · *Co-sponsored by* AIChE · *In association with*

Certificate

This is to certify that Prof. / Dr. / Mr. / Ms. / Mrs. Subhasis Ghosh

has presented a paper (Oral / Poster) in IIChE-CHEMCON 2023, *held at Heritage Institute of Technology, Kolkata, during 27 - 30 December 2023.*

Title: Synthesis of ..... Containing Solution.
(Synthesis of Bilane Treated Aerogel for the Treatment of Napthalene Containing Solution.)

Co-authored by:

Ghosh

Prof. Anil Kumar Saroha
President, IIChE

Dhawal Saxena
Honorary Registrar, IIChE

Dr. Avijit Ghosh
Organizing Secretary, IIChE-CHEMCON 2023

ABSTRACT

With the development of civilisation, industrialisation is increa establishment of various industries, waste is also being g exponentially. Organic pollutants, like polyaromatic hydr petrochemical industries, dyes from textile industries, heav industries, and solid biotic wastes from agricultural sectors, l places are generating more concerns nowadays. Rather than usi waste, and treating the waste before disposal, in the age of circul and reusing waste materials of one sector as the raw material in a accepted approach.

The current study focuses on the extraction of cellulose, hemice sonochemical method from rice husk and sawdust, and the s bioethanol. Also, silica and biochar were produced from the biochar, cellulose, and silica were utilised to synthesise PVA treatment was investigated. Bacteria were also doped into the P to increase their efficiency, along with phytotoxicity stud

ABSTRACT

With the development of civilisation, industrialisation is increa establishment of various industries, waste is also being g exponentially. Organic pollutants, like polyaromatic hydr petrochemical industries, dyes from textile industries, heav industries, and solid biotic wastes from agricultural sectors, l places are generating more concerns nowadays. Rather than usi waste, and treating the waste before disposal, in the age of circula and reusing waste materials of one sector as the raw material in a accepted approach.

The current study focuses on the extraction of cellulose, hemice sonochemical method from rice husk and sawdust, and the s bioethanol. Also, silica and biochar were produced from the biochar, cellulose, and silica were utilised to synthesise PVA treatment was investigated. Bacteria were also doped into the P to increase their efficiency, along with phytotoxicity stud

ABSTRACT

With the development of civilisation, industrialisation is incre establishment of various industries, waste is also being g exponentially. Organic pollutants, like polyaromatic hydr petrochemical industries, dyes from textile industries, heav industries, and solid biotic wastes from agricultural sectors, l places are generating more concerns nowadays. Rather than usi waste, and treating the waste before disposal, in the age of circul and reusing waste materials of one sector as the raw material in a accepted approach.

The current study focuses on the extraction of cellulose, hemice sonochemical method from rice husk and sawdust, and the s bioethanol. Also, silica and biochar were produced from the biochar, cellulose, and silica were utilised to synthesise PVA treatment was investigated. Bacteria were also doped into the P to increase their efficiency, along with phytotoxicity stud

Subhasis final thesis.docx

ORIGINALITY REPORT

6%
SIMILARITY INDEX

PRIMARY SOURCES

1	uni-mate.hu Internet	519 words —	1%
2	www.mdpi.com Internet	199 words —	< 1%
3	Sandipan Bhattacharya, Papita Das, Avijit Bhowal, Abhijit Saha. "Thermal, Chemical and ultrasonic assisted synthesis of carbonized Biochar and its application for reducing Naproxen: Batch and Fixed bed study and subsequent optimization with response surface methodology (RSM) and artificial neural network (ANN)", Surfaces and Interfaces, 2021 Crossref	111 words —	< 1%
4	coek.info Internet	100 words —	< 1%
5	Rui-Feng Wang, Li-Gao Deng, Kai Li, Xue-Jing Fan, Wen Li, Hai-Qin Lu. "Fabrication and characterization of sugarcane bagasse–calcium carbonate composite for the efficient removal of crystal violet dye from wastewater", Ceramics International, 2020 Crossref	87 words —	< 1%
6	repository.sustech.edu Internet	87 words —	< 1%

7	www.researchgate.net Internet	87 words — < 1%
8	Elif Cerrahoğlu Kaçakgil, Deniz Bingöl. "Performance assessment and statistical modeling of modification and adsorptive properties of a lignocellulosic waste modified using reagent assisted mechanochemical process as a low-cost and high-performance method", Sustainable Chemistry and Pharmacy, 2020 Crossref	78 words — < 1%
9	Jadaa, Waleed. "Development of Photocatalytic Reactor System for Dye Degradation from Lab to Pilot Scale", The University of Western Ontario (Canada), 2024 ProQuest	72 words — < 1%
10	oaktrust.library.tamu.edu Internet	62 words — < 1%
11	mdpi-res.com Internet	53 words — < 1%
12	dns2.asia.edu.tw Internet	49 words — < 1%
13	Fei Gu, Jing Geng, Meiling Li, Jianmin Chang, Yong Cui. "Synthesis of Chitosan–Ignosulfonate Composite as an Adsorbent for Dyes and Metal Ions Removal from Wastewater", ACS Omega, 2019 Crossref	48 words — < 1%
14	Shamik Chowdhury. "Removal of safranin from aqueous solutions by NaOH-treated rice husk: thermodynamics, kinetics and isosteric heat of adsorption", Asia-Pacific Journal of Chemical Engineering, 03/2012 Crossref	45 words — < 1%

15	spectrum.library.concordia.ca Internet	43 words — < 1%
16	studentsrepo.um.edu.my Internet	43 words — < 1%
17	Zhu, Jin. "Effective Management Solutions for Biogenic Odour in Drinking Water.", University of New South Wales (Australia) ProQuest	42 words — < 1%
18	discovery.researcher.life Internet	42 words — < 1%
19	publicatio.bibl.u-szeged.hu Internet	42 words — < 1%
20	www.researchsquare.com Internet	42 words — < 1%
21	Yunfeng Tan, Shengqiang Ma, Nengsheng Liu, Xintao Wang et al. "Study on the adsorption mechanism of CL-20 in waste acid by silicic acid: adsorption model and DFT calculation", Environmental Research, 2025 Crossref	41 words — < 1%
22	Sanket Roy, Sayan Mukherjee, Subhasis Ghosh, Papita Das. "Synthesis of rice husk-derived cellulose for efficacious removal of malachite green from aqueous solution", Sādhanā, 2024 Crossref	40 words — < 1%
23	nopr.niscair.res.in Internet	40 words — < 1%
24	Jixiang Zhang, Qiuxiang Zhou, Lailiang Ou. "Kinetic, Isotherm, and Thermodynamic Studies	39 words — < 1%

of the Adsorption of Methyl Orange from Aqueous Solution by Chitosan/Alumina Composite", Journal of Chemical & Engineering Data, 2011
Crossref

25	www.tandfonline.com Internet	39 words — < 1%
26	vdocument.in Internet	37 words — < 1%
27	www.hindawi.com Internet	36 words — < 1%
28	ebin.pub Internet	34 words — < 1%
29	Shreen Adel Rashiq, Nour E. A. Abd El-Sattar, Hoda Abd Elhay abd Elhamid, Gharieb S. El-Sayyad et al. "Enhanced Bioadhesive and Antimicrobial Properties of PVA/Ascorbic Acid Composite with Tannic Acid Synthesized by Gamma Irradiation for Biomedical Applications", ACS Omega, 2025 Crossref	33 words — < 1%
30	"Biorefinery of Oil Producing Plants for Value-Added Products", Wiley, 2022 Crossref	32 words — < 1%
31	link.springer.com Internet	31 words — < 1%
32	Fatema Zahan, Md Masudul Karim, Tahmina Akter, Md Alamgir Hossain. "Screening of potato genotypes based on glucose and Asparagines content to minimize Acrylamide formation in potato chips and French fries", Research in Agriculture Livestock and Fisheries, 2016 Crossref	30 words — < 1%

33	depositonce.tu-berlin.de Internet	30 words — < 1%
34	Alain C. Pierre, Gérard M. Pajonk. "Chemistry of Aerogels and Their Applications", Chemical Reviews, 2002 Crossref	29 words — < 1%
35	bioresources.cnr.ncsu.edu Internet	28 words — < 1%
36	www.ijcr.info Internet	28 words — < 1%
37	Preetha Ganguly, Ashis Khan, Papita Das, Avijit Bhowal. "Cellulose from lignocellulose kitchen waste and its application for energy and environment: bioethanol production and dye removal", Indian Chemical Engineer, 2020 Crossref	27 words — < 1%
38	Dilwar Singh Parihar, Mahesh K Narang, Baldev Dogra, Apoorv Prakash, Akshay Mahadik. "Rice residue burning in Northern India: an assessment of environmental concerns and potential solutions – a review", Environmental Research Communications, 2023 Crossref	26 words — < 1%
39	akjournals.com Internet	26 words — < 1%
40	Hajar Maleki, Nicola Hüsing. "Aerogels as promising materials for environmental remediation—A broad insight into the environmental pollutants removal through adsorption and (photo)catalytic processes", Elsevier BV, 2018	25 words — < 1%

Crossref

41	gyan.iitg.ernet.in Internet	25 words — < 1%
42	jeelm.vgtu.lt Internet	24 words — < 1%
43	repositorio-aberto.up.pt Internet	24 words — < 1%
44	Jais, Farahin Mohd.. "Development of Sugarcane Bagasse-Based Adsorbents for Dye and Antibiotic Removal from Contaminated Water", University of Malaya (Malaysia) ProQuest	23 words — < 1%
45	ir.mu.ac.ke:8080 Internet	23 words — < 1%
46	edubirdie.com Internet	22 words — < 1%
47	Cristina E. Almeida-Naranjo, Fabián Santana-Romo, Elvia Gallegos-Castro, Cristina Alejandra Villamar-Ayala, Alexis Debut. "Triclosan removal from synthetic solution using corn cobs and their magnetic composites: Insights from batch adsorption and fixed-bed column studies", Industrial Crops and Products, 2025 Crossref	21 words — < 1%
48	da Silva Esperança Guimarães, Ana Cristina. "Inhibition of Fungal Growth and Mycotoxin Production by Lactic Acid Bacteria", Universidade do Minho (Portugal), 2024 ProQuest	21 words — < 1%

49	Alnaief, Mohammad Hussein Ali. "Process development for production of aerogels with controlled morphology as potential drug carrier systems", Technische Universität Harburg, 2011. Publications	20 words — < 1%
50	www2.mdpi.com Internet	18 words — < 1%
51	Henglong Tang, Mingyue Qian, Zhu Long, Dan Zhang, Chang Sun. "Design and preparation of non-porous amorphous PEI-based polymers and their adsorption properties for anionic dyes", Journal of Hazardous Materials, 2025 Crossref	17 words — < 1%
52	Jian Xu, Wei Song, Lili Ren, Nan Wu, Rui Zeng, Shuai Wang, Zeyu Wang, Qingzhu Zhang. "Reinforced hydrogel building via formation of alginate-chitosan double network with pH & salt-responsiveness and electric conductivity for soft actuators", International Journal of Biological Macromolecules, 2024 Crossref	17 words — < 1%
53	limsforum.com Internet	17 words — < 1%
54	Neha Mishra, Vikas Kumar, Jaspreet Kaur, Yogesh Gat, Ashwani Kumar, Basista Rabina Sharma, Garima Yadav. "Process optimisation for saccharification and fermentation of wheat straw for the production of single cell protein", International Journal of Environment and Waste Management, 2020 Crossref	16 words — < 1%
55	etd.aau.edu.et Internet	16 words — < 1%

56 Ali A. Abdulhameed, Mahir M. Hason, Amjad Ali K. Sharba, Ammar N. Hanoon, Mugahed Amran, Hassan M. Magbool, Yaser Gamil. "Experimental and environmental investigations of the impacts of wood sawdust on the performance of reinforced concrete composite beams", Case Studies in Construction Materials, 2023
Crossref
15 words — < 1%

57 Deblina Das, Raja Selvaraj, M. Ramananda Bhat. "Optimization of inulinase production by a newly isolated strain Aspergillus flavus var. flavus by solid state fermentation of Saccharum arundinaceum", Biocatalysis and Agricultural Biotechnology, 2019
Crossref
15 words — < 1%

58 Venkatramanan Varadharajan, Dilip Saravanan Senthilkumar, Kathiresan Senthilkumar, Venkatesa Prabhu Sundramurthy et al. "Process modeling and toxicological evaluation of adsorption of tetracycline onto the magnetized cotton dust biochar", Journal of Water Process Engineering, 2022
Crossref
15 words — < 1%

59 Shuaibing Gao, Yixin Sui, Anwar Mamat, Linlin Chai, Shawket Abliz. "Characterization and adsorption properties of nickel ion-imprinted composites using Silane-modified sand grains as carriers", Journal of Water Process Engineering, 2025
Crossref
14 words — < 1%

60 Tonni Agustiono Kurniawan, Wai hung Lo, Mika ET Sillanpää. "Treatment of Contaminated Water Laden with 4-Chlorophenol using Coconut Shell Waste-Based Activated Carbon Modified with Chemical Agents", Separation Science and Technology, 2011
Crossref
14 words — < 1%

61	docslib.org Internet	14 words — < 1%
62	espace.curtin.edu.au Internet	14 words — < 1%
63	gyan.iitg.ac.in Internet	14 words — < 1%
64	ijesm.co.in Internet	14 words — < 1%
65	"Rice Husk Biomass", Springer Science and Business Media LLC, 2025 Crossref	13 words — < 1%
66	Abiram Karanam Rathan Kumar, Kongkona Saikia, Gerard Neeraj, Hubert Cabana, Vaidyanathan Vinoth Kumar. "Remediation of bio-refinery wastewater containing organic and inorganic toxic pollutants by adsorption onto chitosan-based magnetic nanosorbent", Water Quality Research Journal, 2019 Crossref	13 words — < 1%
67	Das, Abhijit. "A Metabolic Approach to Investigate the Role of Amino Acids in Brain.", University of New South Wales (Australia) ProQuest	13 words — < 1%
68	George F.M. Ball. "Vitamins In Foods - Analysis, Bioavailability, and Stability", CRC Press, 2019 Publications	13 words — < 1%
69	Leo M.L. Nollet, Leen S. P. De Gelder. "Handbook of Water Analysis", CRC Press, 2019 Publications	13 words — < 1%

70	Yazan Ibrahim, Elham Abdulkarem, Vincenzo Naddeo, Fawzi Banat, Shadi W. Hasan. "Synthesis of super hydrophilic cellulose-alpha zirconium phosphate ion exchange membrane via surface coating for the removal of heavy metals from wastewater", Science of The Total Environment, 2019 Crossref	13 words — < 1%
71	archive.saulibrary.edu.bd:8080 Internet	13 words — < 1%
72	docnum.univ-lorraine.fr Internet	13 words — < 1%
73	etd.auburn.edu Internet	13 words — < 1%
74	journalskuwait.org Internet	13 words — < 1%
75	nms.usz.edu.pl Internet	13 words — < 1%
76	www.nature.com Internet	13 words — < 1%
77	www.scielo.br Internet	13 words — < 1%
78	www.thinkswap.com Internet	13 words — < 1%
79	"Biodegradable Waste Management in the Circular Economy", Wiley, 2022 Crossref	12 words — < 1%

80 "Cellulose-Based Superabsorbent Hydrogels", Springer Science and Business Media LLC, 2019 — 12 words — < 1%
Crossref

81 "Handbook of Graphene", Wiley, 2019 — 12 words — < 1%
Crossref

82 Fuyuan Ding, Ping Ren, Guannan Wang, Shuping Wu, Yumin Du, Xiaobo Zou. "Hollow cellulose-carbon nanotubes composite beads with aligned porous structure for fast methylene blue adsorption", International Journal of Biological Macromolecules, 2021 — 12 words — < 1%
Crossref

83 Kumar, Y.P.. "Removal of copper from aqueous solution using Ulva fasciata sp.-A marine green algae", Journal of Hazardous Materials, 20060901 — 12 words — < 1%
Crossref

84 Kun Liu, Haishun Du, Ting Zheng, Huayu Liu, Meng Zhang, Hongxiang Xie, Xinyu Zhang, Mingguo Ma, Chuanling Si. "Recent advances in cellulose and its derivatives for oilfield applications", Carbohydrate Polymers, 2021 — 12 words — < 1%
Crossref

85 Lopamudra Das, Niladri Saha, Antara Ganguli, Papita Das, Avijit Bhowal, Chiranjib Bhattacharjee. "Calcium alginate–bentonite/activated biochar composite beads for removal of dye and Biodegradation of dye-loaded composite after use: Synthesis, removal, mathematical modeling and biodegradation kinetics", Environmental Technology & Innovation, 2021 — 12 words — < 1%
Crossref

86 Nattawan Khiewsawai, Thitirat Rattanawongwiboon, Chonnipha Tangwongputti, — 12 words — < 1%

Sarute Ummartyotin. "Preparation of cellulose fiber derived from sugarcane bagasse and polyvinyl alcohol (PVA)-based hydrogel composite by gamma irradiation as a platform for colorimetric sensor", Emergent Materials, 2023
Crossref

87 Naznin Sultana, Sanchita Bandyopadhyay-Ghosh, Chin Fhong Soon. "Biomedical Materials and Biofabrication for Regenerative Medicine", CRC Press, 2025 — 12 words — < 1%
Publications

88 Uttam Kumar Sahu, Siba Sankar Mahapatra, Raj Kishore Patel. "Synthesis and characterization of an eco-friendly composite of jute fiber and Fe 2 O 3 nanoparticles and its application as an adsorbent for removal of As(V) from water", Journal of Molecular Liquids, 2017 — 12 words — < 1%
Crossref

89 Yuan-Qing Li, Yarjan Abdul Samad, Kyriaki Polychronopoulou, Saeed M. Alhassan, Kin Liao. "Carbon Aerogel from Winter Melon for Highly Efficient and Recyclable Oils and Organic Solvents Absorption", ACS Sustainable Chemistry & Engineering, 2014 — 12 words — < 1%
Crossref

90 Zhongqing Ma, Junhao Wang, Cong Li, Youyou Yang, Xiaohuan Liu, Chao Zhao, Dengyu Chen. "New sight on the lignin torrefaction pretreatment: Relevance between the evolution of chemical structure and the properties of torrefied gaseous, liquid, and solid products", Bioresource Technology, 2019 — 12 words — < 1%
Crossref

91 Zishan Aslam, Pervez Alam, Raisul Islam, Afzal Husain Khan, Hasara Samaraweera, Athar Hussain, Tasneem Imtiyaz Zargar. "Recent developments in moving bed biofilm reactor (MBBR) for the treatment of — 12 words — < 1%

phenolic wastewater -A review", Journal of the Taiwan Institute of Chemical Engineers, 2024
Crossref

92	de Oliveira, Maria João Quitoles. "NanoSers Microfluidics Platform for Rapid Screening for Infectious Diseases", Universidade NOVA de Lisboa (Portugal), 2024 ProQuest	12 words — < 1%
93	dergipark.org.tr Internet	12 words — < 1%
94	dokumen.pub Internet	12 words — < 1%
95	eaapublishing.org Internet	12 words — < 1%
96	ethesis.nitrkl.ac.in Internet	12 words — < 1%
97	html.pdfcookie.com Internet	12 words — < 1%
98	lurepository.lakeheadu.ca Internet	12 words — < 1%
99	nova.newcastle.edu.au Internet	12 words — < 1%
100	pdffox.com Internet	12 words — < 1%
101	qspace.qu.edu.qa Internet	12 words — < 1%

102	scholar.sun.ac.za Internet	12 words — < 1%
103	umpir.ump.edu.my Internet	12 words — < 1%
104	www.frontiersin.org Internet	12 words — < 1%

EXCLUDE QUOTES	OFF	EXCLUDE SOURCES	OFF
EXCLUDE BIBLIOGRAPHY	ON	EXCLUDE MATCHES	< 12 WORDS